Effect of formwork's parameters on surface properties of different concrete mix designs

Sayed Hashim Mohseni

UNIVERSITÉ DE STRASBOURG

ÉCOLE DOCTORALE 269 MATHEMATIQUES, SCIENCES DE L'INFORMATION ET DE L'INGENIEUR (MSII)

ICube UMR 7357

THÈSE

présentée par :

Sayed Hashim MOHSENI

Soutenance prévue le : **20 Juin 2022**

pour obtenir le grade de : **Docteur de l'Université de Strasbourg**

Discipline/ Spécialité : **Génie Civil**

Effect of Formwork's Parameters on Surface Properties of Different Concrete Mix Designs

THÈSE dirigée par :

[M. BIRINCI Fahri]	Professeur, Université d'Ondokuz Mayis (directeur)
[Mme FEUGEAS Françoise]	Professeur, INSA Strasbourg (Co-directrice)

RAPPORTEURS :

[Mme CURTIL Laurence]	Professeur, Université de Lyon1
[M. KARACA Zeki]	Professeur, Université d'Ondokuz Mayis

AUTRES MEMBRES DU JURY :

[M. KHELIDJ Abdelhafid]	Professeur, Université de Nantes
[M. CEMEK Bilal]	Professeur, Université d'Ondokuz Mayis
[M. OMARY Safiullah]	Maître de conférences, INSA Strasbourg

Dedicated

to

my beloved parents, sisters, brother, and wife

for their love, sacrifices and prayers

“In the name of God, the merciful”

ACKNOWLEDGMENTS

Those to who I should express my gratitude in the first place are my parents, my father Sayed Ahmad, and my mother Amena Nabizade, my dearest siblings, Fatima, Sayed Mahdi, Zeynab, Tahira, and Atifa, and my beloved wife Zohra Codabaccus. Indeed, without their support and motivation, it would become so much harder to finish this task.

I cannot begin to express my thanks to my thesis supervisors, Prof. Dr. Francoise FEUGEAS and Assis. Prof. Fahri BİRİNCİ whose care for me was unlimited from day one of my Ph.D. journey till I completed it. They supported me by all means, in terms of scientific knowledge, emotionally, and intellectually. They believed in me at the times I was hesitating and trying.

Doing my research with two supervisors was a great honor. Moreover, the opportunity of being a Ph.D. student at two universities, my first university, Ondokuz Mayis University in Turkiye, and the second university, Strasbourg University in France, gave me many beautiful experiences in terms of knowledge, culture and enriched my life skills. Also, I am thankful to all my colleagues at the ICUBE laboratory at INSA Strasbourg, the trainees’ Eng. Safiullah Sherzad, Eng. Aliakbar Ahmadi, and Eng. Rahimullah Hasanzai who worked with me and helped during my research.

I would like to extend my deepest gratitude to Dr. Safiullah OMARY, my friend in the first place, and then being my advisor, who was with me by all means. My presence in this project would not have been possible without his help and support. I cannot show my gratefulness in terms of words on this paper. Also, I would like to thank my dear friend and classmate Dr. Sifatullah Bahij, a person with a beautiful heart and personality, who supported me academically and emotionally. And, I am very grateful for having very good friends in Strasbourg and Samsun.

Finally, I am grateful to the Turkish Scholarship Program (YTB) for awarding me a doctoral scholarship and also to the ERGOFORM project for backing this work financially and technically.

Table of contents

List of Figures

List of Tables

General Introduction

1. General context

Globally, the building sector is growing fast. The global construction rate in the building sector will be 230 billion m^2 over the next forty years – it is like adding the equivalent of Paris to our planet every week. This rapid growth is going to have vast consequences [1]. As one of the leading used components, concrete plays a great functionality in the construction field. Concrete has been known for thousands of years [2], although it is characterized as a modern material. Since the time of the Romans, lime-based hydraulic cementitious materials (those set by chemical reaction with water) have been in use, and samples of ancient mortars (cement and aggregate) may still be found. Besides, scientific development and studies have dramatically changed concrete, materials, and functionality over the last century. The determinative factors such as cost-efficiency, expectations, and the usage category in the industry continue to influence design and construction methods, workmanship methods, materials used, and the standards associated with the construction and concrete structures. Nowadays, in the construction process, to manufacture the concrete in the desired form, the concrete at the fresh state is poured into the formwork to give the required shape.

During the Roman Empire, the first concrete slab samples were made. Even at that time, Roman engineers discovered a way to use concrete in structures. As a result, vaults, domes, and arches had to be used in the first concrete formwork examples (**Figure 1**). Moreover, engineers were able to effectively construct a mold that would allow them to monitor and manage the final appearance of the concrete structure. As the 16th and 17th centuries progressed, these designs became more and more popular to the point that nearly all buildings were planned in this manner. However, during this time, they began to use iron or metal-based slabs as nearby solutions to overcome the weakness of the formwork structure.

Figure 1 *The Colosseum; its material was of travertine limestone, tuff (volcanic rock), and brick-faced concrete. @wikipedia*

Moreover, Lumber formworks were the predominant types of formwork before the development of the plywood. Traditionally, the formworks used to be built on the construction site for one usage, and after the concrete member got the required strength, the formworks being removed, which costed very much due to the high labor cost and unrepeatability of the system. In order to minimize the cost and energy, the prefabrication, assembly in large units, the automation of formworks industry (replacing the formworks and holding them in place), and the repeatability in terms of usage of the same formwork were some of the established solutions [3]. Whether applied to complex or standard works, formwork is an essential element in the art of construction. Often essential and constantly improving, the formwork process remains imperfect, such as the difficulty of its implementation and the environmental impact associated with the use of release agents. The French metal formwork was invented in 1955, since then, its use has spread widely.

Although the cement and aggregate types, the uniformity issue in mixing, placing, concrete workability, casting time, temperature, and curing methods can affect the surface quality, the bad quality of the formwork surface is one of the major causes of a poor quality concrete surface, which subsequently leads to the deterioration of the concrete structures [16, 26].

Regarding the functionality of formworks, they can be found in different types and materials. Some of the most common types are wooden formworks, metal formworks, permanently insulated formworks, stay-in-place formworks, and flexible formworks in different geometrical shapes such as plane and circular (see **Figure 2**). The most common materials used to create formwork walls are wood and metal.

Figure 2*; a) Wooden formwork ©123rf.com, b) 3D printed Flexible Formwork ©Brian Peters, ACADIA 2014, c) metal formwork © Hussor.com, d) insulating concrete formwork © theconstructor.org*

For structures or elements of complex and non-repetitive shapes, mainly wooden formworks are used. Wood is preferred when the material's flexibility for the easy assembly and shaping of formwork parts is concerned. The disadvantage of wooden formwork is its limited re-use.

Indeed, these forms are more fragile and deteriorate more quickly than metal. This degradation of the formwork walls can damage the shape and appearance of the cast elements.

Moreover, to aim a very complicated geometrical shape with cementitious materials, the wood and metal cannot fulfill the need unless with a great effort and cost. Therefore, the silicone molds - the generation of molds that meets the requirement- come to fabricate these products. The concrete is cast in a flexible rubber which can be deformed in advance or afterward [6]. A counter-mold or lid is needed to prevent the concrete from flowing out of the mold, plus an exemplar control shape is required in order to guide the rubber mold into its final form. This method is used to prefabricate thin cladding panels with limited size. Silicon rubber molds and polyurethane rubber molds are used for small molding purposes.

The flexibility, chemical resistance against acids, solvents, oil, and water, resistance against the extreme high and low temperatures, economy (long service life), and easy production are the plus side of the silicon molds [7]. However, the high viscosity characteristics, the efflorescence (calcium carbonate microcrystals or microcrystalline products of silico-calc-alkaline composition in the case of alkali-aggregate reactions), and the need for the release agent to get an acceptable surface put the silicon mold not among the best options as formwork [8]. Therefore, based on mentioned informations, some reasons give the steel formworks a better position compared to other material types in the majority of works:

- It is solid which can be used for enormous dimension surface.
- It is resistant in terms of test repeatability.
- It gives a smoother finish to the cementitious surface compared to wooden formwork.
- It is waterproof and nonabsorbent.
- It can be used many times (service life).
- it can be installed and dismantled with greater ease, leading to less time and labor.
- No shrinkage or deformation of steel formwork occurs (due to the frame holding the plates) compared to the wooden framework, especially for the more extensive construction elements with large surfaces.

Furthermore, construction is continuously growing in the cities; hence, more efficient procedures are needed to save time and money and increase the reliability of the final products.

The economy is a significant concern since formwork and labor cost constitute from 35 up to 60 percent of the total cost of concrete work in a project [5,16,19,20] (**Figure 3**). The formwork's effect on the concrete surface is unavoidable during concrete pouring, setting, and demolding [21– 23].

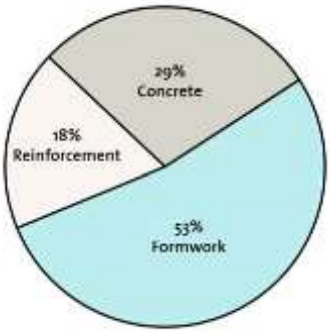

Figure 3 *cost parts in a typical construction work* [9] [10]

It must be mentioned that the formwork assembly is a heavy and hard job (**Figure 5**). Furthermore, formwork coating with oil (release agent) is necessary to prevent or reduce the concrete adherence to the formwork skin and protect the formwork surface from corrosion [14].

Moreover, as known fact, the concrete composition includes binders that hold the dry components together. The cementitious materials will cause the sticking of the components between themselves and the other materials that are in contact with them that can be called adhesion. Formworks regarding their categories might need to be removed and separated from the concrete. Release agents are the mediators that facilitate the demolding process. Most of these release agents' origins get back to either petroleum resources or biodegradables; besides, they are also being used unceasingly. In addition, oil utilization forms a significant proportion of this energy consumption (**Figure 4**); to overcome this specific problem, the private construction sectors are trying to play a more effective role in eliminating these unfavorable materials - oil - from the construction cycle.

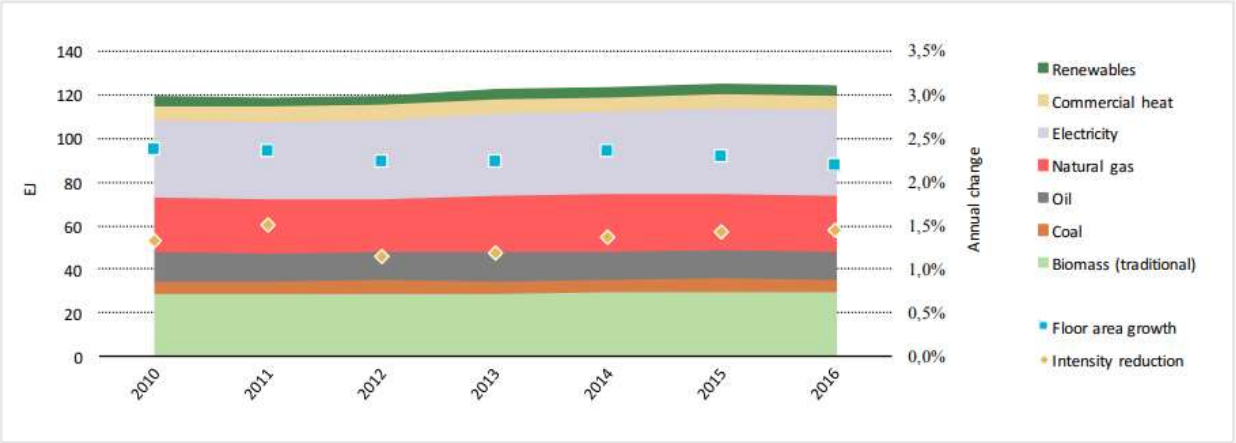

Figure 4 *Worldwide construction sector fuel type energy intake* [15]

It is now more than necessary to consider the environmental impact of each of our actions and act to limit their environmental impacts.

Generally, construction projects use different formworks such as wooden / timber, steel, plywood, and aluminum [4-6]. These various types of formworks present different characteristics which directly affect the surface in contact. For illustration, wooden formworks have a shorter service life due to the material's properties. Moreover, the formwork surface moisture would affect the final concrete quality; if the wooden formwork is dry, due to its material characteristics, it will absorb the concrete moist which might result in weakening the concrete surface, or in the opposite situation, the excessive moisture content will result in more surface defects and crazing (pattern cracking). Wooden materials are being applied in the construction industry, resulting in the depletion of wood resources as an essential environmental impact. Therefore, the formworks of the wood base material is being replaced by other materials such as plastics (polymeric materials), different metal types, and fabric materials [18]. Among these choices, steel formworks proved to be more efficient due to the repeatability, easy to clean, and more resistant to the corrosion and scratching forces received from concrete casting [19]. Moreover, various types of release agents are applied to the formwork skin to facilitate the separation of the concrete from the formwork by decreasing the adhesion forces present at the concrete/formwork interface. It also protects the formwork surface from corrosion and decreases the harmful cleaning process [20]. On the other hand, petroleum or herbal products are used as release agents on the formworks to prevent the formation of an adhesive force between concrete surface and formwork surface. As concrete is

the most used construction material [21] , oil products as release agents are also proportionally used in a large amount, contributing to significant environmental impact.

Cementitious surfaces are directly related to the mix design, placement methods, vibration methods, curing, demolding, and formwork type. Mainly the formwork type can be counted as a significant parameter which affect their properties such as durability, aesthetic appearance, and sustainability [16]. Although the selection of materials for a concrete mix design is a known challenge in the civil engineering field, the initial factors that should be considered are durability, sustainability, environmental impact, recyclability, the economic and health aspects which is related to the surface properties of cementitious materials [17].

2. Purpose

This work is carried out in the frame of ERGOFORM (Ergonomic Formwork) project which one of its objectives is to offer an alternative to used release agents by applying a polymer coating with high durability and low adhesion property to the formwork surfaces. In addition, this project aims to reduce to decrease the harsh working conditions, increase the efficiency of the work by automatization of the system. Including INSA Strasbour/ICube, four parteners are carried out the project. Hussor company, which produced the formworks. Lormac company, which specializes in the manufacture of special machines for the implementation of cylinders. A chemical laboratory, named LPIM, from university of Mulhouse focused on proposition of polymeric coating materials as an alternative to release agents. Finally the laboratory of ICube/INSA Strasbourg, as a scientific partener, studied the durability of proposed polymeric coating materials in terms of reusage and its effect on the surface of cementitious material in different scales of mesearments (micro to macro scales).

This study aims to understand the effect of formwork surface properties on the cementitious surface from the macro-scale to the micro-scale and focus on the possibility of a sustainable and environmental friendly alternative solution instead of used release agents as sub-product of petroleum which presents harmful impact to the environment and human life [11- 12]. Besides, this research work will develop the effect of mix design components by varying the w/c ratio and cement type against various types of release agent, and formwork coatings on adhesion or demolding force between concrete and formwork. In addition, the cement surface are analyzed through microstructure analysis of Interferometry Microscopy (IM), Scanning Electron Microscopic (SEM) and X-ray Diffractometry (XRD) analysis.

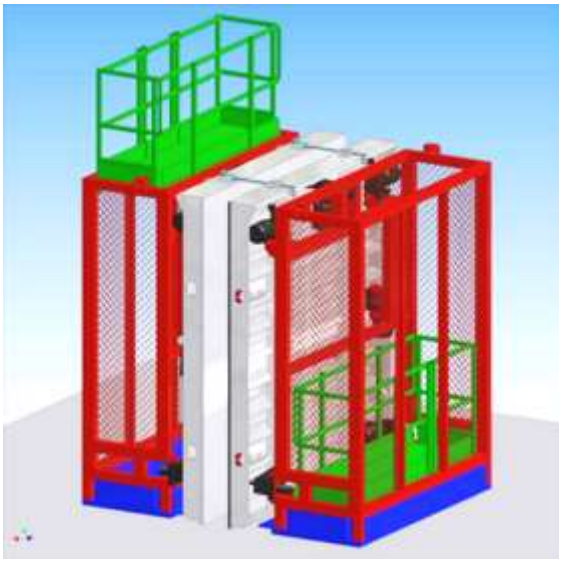

Figure 5 *Steel Formwork, @www.fibres-energivie.eu/fr/ergoform*

The document is arranged in 4 chapters:

- **Chapter 1**: The first chapter is focused on literature review synthesis of the previous work on adhesion between concrete/release agent/formwork and concrete/formwork surfaces and to understand the effect of various parameters on this phenomenon.
- **Chapter 2**: In this part, the materials and methods utilized in the experiments are presented. Moreover, the methods and tests for specifying the characterization of the material that is used in this work are described. Using the Environmental Scanning Electron Microscopy (SEM), X-ray Diffractometry (XRD) and laser Granulometry, cementitious materials' chemical and physical properties are studied. Also, an original procedure, pull-off demolding test for concrete samples in modes I and II of fracture, and pre-crack demolding test on cement samples in fracture mode I are presented.
- **Chapter 3**: The third chapter covers the results of materials characterization to ensure their quality in accordance with the standards. Firstly, cement is characterized by laser granulometry, density, specific gravity, modulus of fineness, and setting times. Following that the physical properties of fine and coarse aggregates are studied.
- **Chapter 4**: The chapeter four presents the obtained data through the experimental procedure on cement paste and concrete samples. In first step, the effect of various parameters such as, cement type, w/c ratio, and coating, are analyzed on the cement paste samples by pre-crack demolding test. Thereafter, in microscopic scale, the surface morphology of cement samples are analyzed through Interferometry Microscopy (IM),

Scanning Electron Microscopic (SEM) and X-ray Diffractometry (XRD) analysis. A detailed discussion is carried-out on effect of such parameters on demolding force and adhesion. In the second step, in a macro scale, the chapter presents the adhesion between mentioned formworks and concrete through the pull-off demolding test. The effect of various parameters on demolding force are analyzed. Finally, the effect of such parameters on visual aspect are studied.

It should be mentioned that a Turkish version of this thesis work with entitled: "KALIP YÜZEY PARAMETRELERİNİN BETONUN YÜZEYİ, DAVRANIŞLARI VE ÖZELLİKLERİ ÜZERİNE ETKİLERİ" has been submitted to the Ondokuz Mayis University in Turkiye.

The purpose of this chapter is to establish a state of art concerning the effect of various parameters on adhesion force and on the surface characteristics of cementitious materials.
As previously mentioned that the adhesion phenomena is related to type of formwork, release agents and mix design components which affect the final surface characteristics of cementitious materials. Therefore, in this chapter, different studies have been cited to describe the effect of various parameters on adhesion force between concrete and formwork. Moreover, the effect of these parameters on the surface characteristics of cementitious materials which present the first barrier to the environmental impacts has been analyzed.

1. Adhesion

Adhesion is the attraction of two different materials or the tendency of dissimilar particles or surfaces to cling to one another [119, 120]. In contrast with adhesion, cohesion is referred to the attraction within one body that keeps it together (**Figure 6**). Moreover, the adhesion phenomenon forms from a combination of two or more different factors such as mechanical interlocking related to surface morphology, capillary forces, physical and chemical (surfaces reactions) forces together [30, 31, 121].

In terms of strengths, four different forces exist: two of them are the interatomic forces (between neutrons, electrons, and protons) which have a very short action range of less than 10^{-5} nm. Furthermore, two other forces are the electromagnetic and gravitational interactions that can happen either between atoms or/and molecules. The effective range of these forces differs from subatomic to infinite distance. An example can be the forces that keep and govern the properties of solids, liquids, and gases [29].

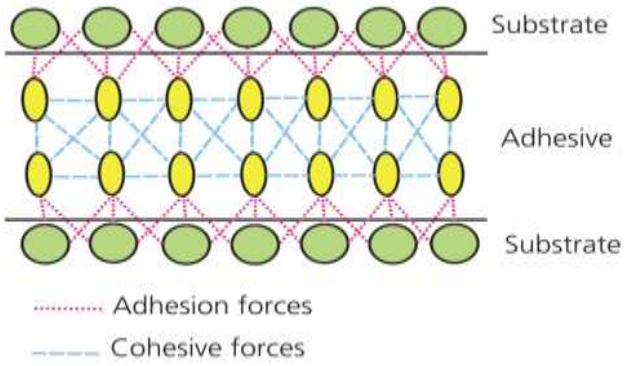

Figure 6 *adhesion force between two substrates. @www.adhesives.org*

1.1.Mechanism of adhesion

As mentioned, the adhesion phenomena between formwork and cementitious material is related to the types of used materials. For each particular material, the adhesion mechanism accurse in a particular way. In general, these particular mechanisms are as follows:

1.1.1. Mechanical adhesion

An adhesive connection between an adhesive and a smooth surface adherent will generate a mechanically weak if there is nothing other than van der Waals forces at interfaces. Since van der Waals interactions are the only force holding the two surfaces together, the work required to break the bond of these two surfaces will be minimal. In this case, the interfacial crack, in the application of a force at the edge of the interface, will rapidly propagate between the two surfaces.

Whether harsh or soft, all materials contain numerous voids and pores on their surfaces to an extent [119, 122]. The adhesive materials fill these pores and voids and maintain them together by interlocking. In the formwork/concrete interface, on one side, semi-liquid cementitious material (at the hydration period) will function as adhesive, and on the other side, a porous surface, like wood, steel, aluminum, plywood, etc. as a substrate (**Figure 7**) [42, 120, 123]. The fracture energy needed to separate or break two materials will be several kJ/m2, referred to as practical adhesion. Besides, the mechanical breaking energy depends on the adherent surface energy and the pore size on a microscale or less [30].

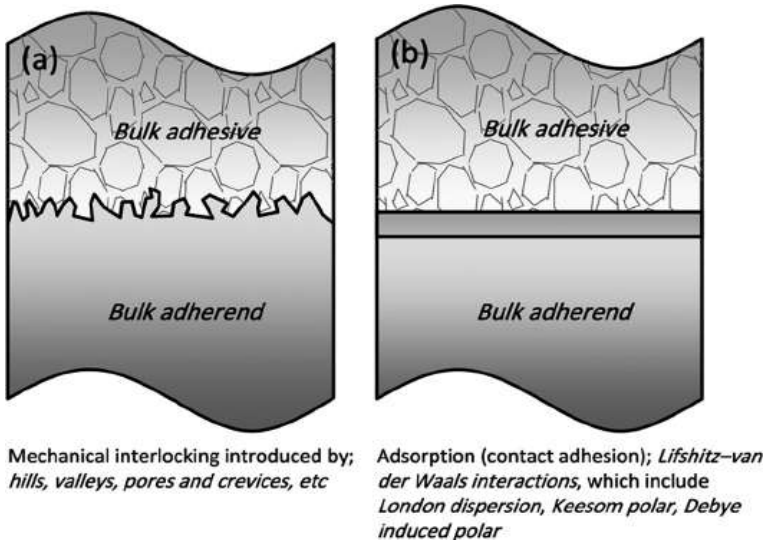

Figure 7 *Schematic view of the representative adhesive bonding interphase; (a) mechanical interlocking, (b) contact adhesion* [33]

1.1.2. Chemical bonding

In this type of adhesion, two materials form a compound at their contact surface after substrates contact each other. The bonding can happen by sharing the electrons of atoms, which is called ionic bonding or covalent bonding. This connection is a strong type of bonding. However, the bonding of the hydrogen atoms of a molecule with the nitrogen, oxygen, or fluorine atoms of another molecule is weak. Some of the bonding types and their bond energies are shown in **Figure 8**. Briefly, the bondages of ionic, covalent, or hydrogen bonds are all included in the chemical bond category. The effectiveness of these bonds is at a nanometric distance and on a molecular scale [32].

Adhesive forces

Type	Bond length in nm	Bond energy in kJ/mol
Chemical bonds		
• Covalent	0.1–0.2	150–950
• Metallic	0.3–0.5	100–400
• Ionic	0.2–0.3	400–800
Intermolecular interactions		
• Van der Waal forces	0.4–0.5	2–15
• Hydrogen bonds	0.2	20–30

Figure 8 *Adhesion force for types of bondings @www.adhesives.org*

1.1.3. Dispersive adhesion

In this kind of adhesion, the van der Waals forces of attraction hold two materials together. Because the molecules exhibit localized positive and negative charges, they are classified as polar by the average density charge. These positive and negative charges in a molecule may be permanent (Keesom force); however, they can also be a temporary effect that occurs in any molecule. Random electron movement inside molecules can result in an ephemeral condensation of electrons in an area (London forces).

1.1.4. Electrostatic adhesion

Some conducting materials may pass electrons to form a difference in electrical charge at the joint. Results in a structure similar to a capacitor create an attractive electrostatic force between the materials.

1.1.5. Capillary forces

The capillary forces depend on the surface properties -hydrophilicity/hydrophobicity, surface morphology- of the surfaces which are brought into contact. Indeed, the surface properties of bodies, and in particular the surface energy, are modified by their contact. Also, there is a variation in interfacial energy in interfacial energy which is linked to capillary forces. Capillary forces are also created by intermolecular interactions and occur when water or other liquids are present between two parallel smooth surfaces that are close to each other.

1.1.6. Hydrogen bond

The original structure of concrete creates many hydroxyls (–OH) –free groups after starting to interact with water. After adding water to the concrete cement, it starts interacting and creates hydroxyl (-OH) bonds between the concrete and steel surfaces (rebar or metal formwork). This bond is made between hydroxyl groups and the iron atoms present in steel (**Figure 9**). However, these adhesive forces are small, nevertheless [34].

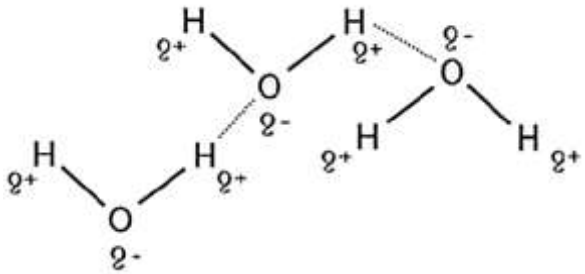

Figure 9 *Hydrogen bonding of water molecules.* [34]

However, capillary forces develop in the water that is not absorbed by concrete and gathers close to the interface between formwork and concrete.

1.2.Influential factors on adhesion between formwork and concrete

In the new form of designs and developments, formworks are the systems for keeping the concrete in its fresh state to obtain the required size and shape and control the element's alignment and position. However, the formwork is not only attributed to the mold's functionality, besides, it must hold temporary the weight of; concrete structure at the fresh state, the workman load, other materials, and the equipment (all the dead and live loads). Through the literature, it can be seen that some formworks are more usefull and durable in terms of large dimension of required concrete structure element and reusage [14-15].

Moreover, there are certain parameters that define the adhesion between concrete and formworks such as surface roughness, type and materials of formwork, curing condition, friction, compaction method and as well the concrete composition. These parameters have a direct impact on the surface roughness, surface porosity, hydration quality, and surface durability of cementitious materials. Thus, the surface and final physical and mechanical properties of cementitious structural elements are influenced by the demolding or adhesion force [33, 34, 32]. A figurative picture of the most influential factors in terms of concrete-formwork adhesion is presented in **Figure 10**.

Cementitious surfaces are directly related to the mix design, placement methods, vibration methods, curing, demolding, and formwork type. Mainly the formwork type can be counted as a significant parameter which affect their properties such as durability, aesthetic appearance, and sustainability [16]. Although the selection of materials for a concrete mix design is a known challenge in the civil engineering field, the initial factors that should be considered are durability, sustainability, environmental impact, recyclability, the economic and health aspects which is related to the surface properties of cementitious materials [17].

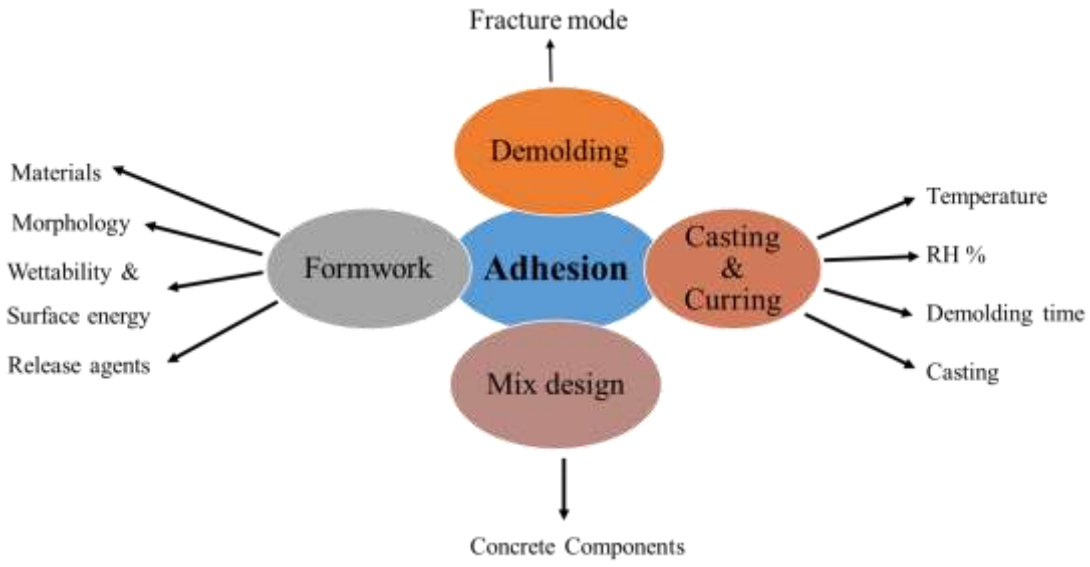

Figure 10 *effective and involved factors in concrete-formwork adhesion phenomenon*

Some experimental studies that have focused on the influncial parameters on adhesion between formwork-concrete are summarized in ***Table 1***. Scientific studies are mainly interested in the concrete thrust phenomenon, formwork/concrete abrasion, and the concept of facing quality [5, 35, 36, 37, 38, 39] based on variation of w/c ratio and formworks. Few studies are invistegated the cement type.

Table 1 *the interactions in formwork-concrete interface studies*

Year	Studied properties and methods	Type of formwork	Materials		w/c	Authors
1999	Surface finish, surface strength, freezing and thawing, surface porosity,	Permeable formwork	Concrete	-	0.45-0.60	P.G. Malone [44]
2003	determination of autogenous shrinkage, temperature and setting kinetics, porosity	Metal	Cement paste	CEM II/B	0.30 0.36 0.45	Andriamanantsilavo et al. [45]
2010	surface hardness, pull-off strength, carbonation, chloride penetration, absorptivity, and abrasion resistance	Permeable (geotextile) formwork with drainage holes	Concrete	CEM I	0.6	Metin Arslan [46]
2013	Chemical interactions and friction stress at the concrete/oil/formwork interface	Mineral oil and vegetable oil on the steel formwork	Concrete class: C28, C30, C32, C34, and C36	CEM I	0.57	S. Bouharoun [16]
2016	Concrete facing quality, friction coefficient	Metal plate with vegetable oil coating	Self-consolidating concrete	CEM I	0.35	C. Djelal et al. [40]
2018	Evolution of the concrete/formwork interface at a very early age by friction stress study	Slipforming	Mortar	CEM I	0.3	T. Craipeau et al. [31]
2018	Formwork surface quality effect on the concrete sticking via topographical, chemical, and mechanical characterization of formwork surfaces	Steel and polymeric formwork	-	-	-	N. Spitz et al. [18]
2020	Effect of formwork on the voids, bleeding, segregation, and insufficient self-consolidation	Plywood, PVC, steel, and permeable formworks	Concrete	High early strength Portland cement (HE) and white cement (FW)	0.41	Megid and Khayat [47]
2021	Formwork surface topography and wear investigation through interferometry, tribology test, and friction force measurement	Metallic and polymeric coated	Concrete: without additives and with SP	CEM I	0.57 0.37	N. Spitz et al. [48]
2021	Adhesion in the concrete/formwork interface, surface morphology	Polished metal, mineral oil coated, polymer coating	Cement paste	CEM II/B-S	0.4	Chadfeau *et al*. [11]

1.2.1. Formworks' materials and morphology effect on adhesion of formwork/concrete

The formwork determines whether the finished surface is smooth, profiled, or patterned. Therefore, it is essential to consider the choice of formwork material thoroughly. Depending on the material, the formwork surface will react with the fresh concrete either physically and/or chemically [3]. These interactions are capable of causing damage to the concrete surface. The fresh concrete will take shape, and the formwork pattern will reflect it after hardening.

Regarding to the materials, various formworks are used in literature such as wooden / timber, steel, plywood, and aluminum, with various characteristics which affect the surface in contact [4-6]. Moreover, the formwork surface moisture would affect the final concrete quality. For example, the wooden formworks present shorter service life due to the material's properties and if the wooden formwork used in dry state, it will absorb the concrete moist which might result in weakness of the concrete surface, due to its material characteristics. In the opposite situation, the excessive moisture content will result in more surface defects as crazing (cracking pattern). It must be highlighted that the usage of such formworks resulting in the depletion of wood resources as an essential environmental impact. Based on these reasons other materials such as plastics (polymeric materials), different metal types, and fabric materials can be counted as alternative solution to replace the wooden formworks [18]. Due to the repeatability, easy to clean, resistance to the corrosion and durability to scratching forces through concrete casting the steel formworks can be used [19].

F. K. Yuksel [49] was experimented to analyse the effect of formwork type on the concrete surfaces properties. To see the effect of different formworks (metal, wooden, and plastic) on the concrete surface, capillary water absorption, water absorption, Karsten tube test, and vapor diffusion resistance factor monitoring were conducted. The samples, prepared in wooden formwork, showed a lower capillary coefficient and water absorption than metal and plastic ones. Due to its material properties related to its porosity structure, the wooden formwork absorbs the water, which results in lower water content at the contact surface. Therefore, the capillary tube diameter in the concrete was reduced and caused the lower water absorption properties of the wooden formworks.

Moreover, beside the chemical and physical properties, the morphological characteristics of the formwork will have an impact on the concrete's facing. It can be seen in the literature that the

selection of one type of formwork over another is partially based on the morphological nature of the formwork surface parameters due to the print of the formwork surface and shape on the concrete facing [50].

Some studies are shown that the adhesion between formwork and concrete are related to the morphological parameters of used formworks. Libessart *et al.* [38] measured the used 3 steel formworks (same materials) with various morphological parameters, the authors indicate that the adhesion/demolding force between these tow surfaces are related to the high roughness parameters of formworks, it means that the higher demolding force are recorded for the rougher fromworks. In the same context, an experimental study was conducted to explore the relation between formwork surface roughness and the demolding force. The objective was to investigate how the adhesion between concrete and formworks is affected by various morphological and thermodynamic surface properties of formwork. The formworks with 3 different surface textures were considered: a) steel formwork with and without a demolding agent, b) polished stainless-steel formwork, and c) polymeric coated surfaces. Overall, the surface texture and surface energy were analyzed by interferometry and contact angle measurement, respectively. The outcomes from interferometry analysis showed that the surface area in contact with the cement is reduced for the polished surfaces and this value decreases with the increase of polishing. The adhesion improved for the formworks with a less rough surface due to the reduced physical interlocking [11]. Besides, research considered three different types of formworks: new, used, and polished, with various surface roughness, in order to investigate the effect of formwork's roughness on adhesion force. The outcomes indicate a direct correlation between the adhesion formwork surface parameters; the higher demolding force was the consequence of a rougher formwork surface [14].

Moreover, N. Spites *et al.* [17] studied the effect of various types of formwork against different concrete mix designs. Their work focused on the adherence between these two surfaces by developing an original pull-off test procedure at the laboratory scale. The selected material for the formwork surface was two types of polymer, steel formwork and a Zn/Al alloy coated steel plate with various surface parameters. The authors conclude that the surface properties of formwork have a significant influence on the adherence mechanism as a result of the trapping of cement particles in the metal surface of formwork (mechanical reaction). Moreover, in the case of Zn/Al coated steel a chemical reaction between the cement particles and the formwork surface material

was observed. Finally, the lower demolding force was recorded for the concrete against polymeric coated formwork surfaces with lowest roughness parameters.

Moreover, numerous experimental research works were conducted to verify the effect of various formwork roughness on adhesion force between formwork and concrete [10, 23, 62–65].

1.2.2. Surface energy and wettability

The contact angle method can highlight the information regarding the hydrophilicity or hydrophobicity of material's surface. These information can be meseared by depositing a drop of liquid on the surface, which the smaller contact angle present the hydrophilicity of the material as shown in **Figure 11**. Furthermore, the relationship between contact angle and molecular interactions, as well as the thermodynamic approach to interfacial phenomena via the work of adhesion, has generated much interest, with the goal of using contact angle measurements to determine absolute values of the excess free energy associated with solid surfaces, called surface energy [55].

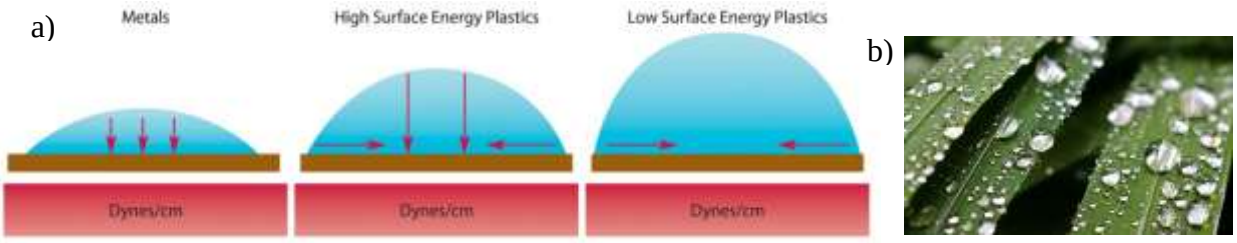

Figure 11 *a) Surface energy of materials due to their contact angles, b) Material with low surface energy @http://www.vmnameplate.com*

The work of adhesion or cohesion in vacuum is defined as the variations of free energy necessary to separate units of area from two surfaces or media which are in infinite contact with vacuum [55]. When discussing a system and the need to uncover its properties to know about its stability and capacity for work, one of the fundamental properties is its energy. The energy between two different surfaces can be called work of adhesion W_{12} while for two identical surfaces, it is called work of cohesion W_{11}. It must be noted that the energy between concrete and formwork, two different surfaces in terms physical, mechanical and chemical properties, is work of adhesion W_{12}.

Surface energy, or surface tension, is the energy required to create one unit of surface area and is equal to the energy required to separate two half units of area [55]. It can be caluculated as following equation :

$$\gamma_1 = \frac{1}{2} W_{11} \qquad \textit{Eq. 1}$$

For solids, the unit of surface energy, often denoted $\boldsymbol{\gamma_s}$, is $mJ.m^{-2}$. For liquids, the unit surface energy, called surface tension, is indicated as $\boldsymbol{\gamma_l}$ and expressed in $mN.m^{-1}$. Moreover, the free energy developed on to extend the interfacial area of a unit between two immiscible and contacting liquids 1 and 2 is called interfacial energy or interfacial tension. It is defined according to equation [55]:

$$\gamma_{12} = \frac{1}{2} W_{11} + \frac{1}{2} W_{12} - W_{12} = \gamma_1 + \gamma_2 - W_{12} \qquad \textit{Eq. 2}$$

The wettability of a surface can be assessed by observing the behavior of a drop of liquid deposited on this surface. This deposit causes a reorganization of the chemical and physical structure of the surfaces under the action of interaction forces. Depending on the chemical and physical properties of these two surfaces, the drop arrangement on the surface, called the contact angle generated by the drop, is the result of the balance of energy at the three interfaces: solid/liquid $\boldsymbol{\gamma_{SL}}$, liquid/vapor $\boldsymbol{\gamma_{LV}}$, and solid/vapor $\boldsymbol{\gamma_{SV}}$ (**Figure 12**).

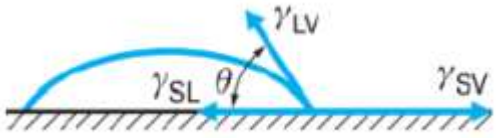

Figure 12 *Contact angle observation on a surface*

When a drop of chemically defined liquid is dropped on a non-porous surface, the contact angle between the drop and the surface may be observed, allowing the wettability of the solid to be determined. Either it is hydrophilic or hydrophobic.

Various methods exist to define the surface energy of solid materials. Based different liquids' contact angles to mechanical tests on polymers that only contain Carbon, Hydrogen, Nitrogen and

Oxygen, various methods are being used to try to find the surface energy [55][56] [57] [58] [59]. These methods depending on the various factors such as; temperature and roughness of the surface. The outcome is that there is no accuracy in the values to be used for computing adhesion or interfacial energy. The contact angles of various liquids on the different solids maybe a more relevant alternative for determining surfaces' behavior. There are different approaches to contact angle measuring, which lead to surface energy determination.

Young's Equation

To analyze the nature of interfacial behavior, it consider a solid-liquid-gas contact. This relationship is illustrated in Young's equation [56] [60]:

$$\gamma_{LV} \cos\theta = \gamma_{SV} - \gamma_{SL} \qquad \textbf{Eq. 3}$$

In this formula, γ_{SV} , is the free energy of the interfaces between the solid (***S***), liquid (***L***), and vapor (***V***) phases. It may be pointed out that γ_{SV} is related to the surface energy of the solid γ_S (supposedly in contact with vacuum) by the spreading pressure of molecules adsorbed from the vapor.

The Owens-Wendt Approach

From the measurement of the contact angle, different models are developed such as the Owens-Wendt model [61].This model is based on Young's equation and allows to evaluate the surface energy of solids. The equilibrium of the drop of liquid on the solid is created by the action of interaction forces which can be polar and non-polar. The model considers the action of these polar and nonpolar (dispersed) components of the surface energy of the solid and the surface tension of the liquid in defining the position of thermodynamic equilibrium. The application of this method is described by standard NF EN 828 [62]. The roughness and the chemical heterogeneity of the surface of the solid are not integrated as parameters in the Owens-Wendt model, even if their impact on the energy calculation surface is recognized by the standard. This model is notably applied to evaluate the surface energies of formwork surfaces [17] [38].

In this study the Owens-Wendt method is used to meseared the surface energy of used formworks due to the allowance of evaluating the surface energy of solids.

Berry's Representation

Berry (1960) [63] found that by plotting the locus of equilibrium points, the equilibrium curve that depends on the solid geometry and toughness, obtained from the part of domain Q-q between stress intensity factor, KI(*l*) < KIc , toughness, which is bounded by the curve Γ in the length l, and the loading curve, it is possible to get a geometric interpretation of the various energies that are consumed (**Figure 13**):

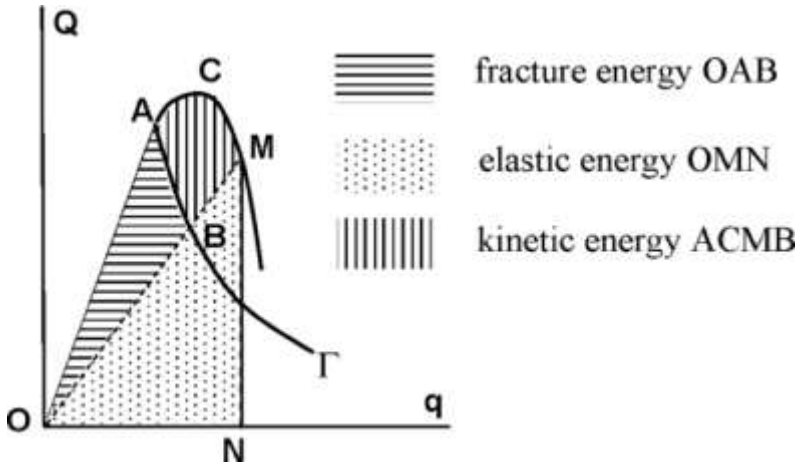

Figure 13 *Berry's diagram* [63]

In the diagram:

- OACMN is the total energy provided by the external load,
- OMN is the stored elastic energy by the cracked system with the crack length l(B),
- OABO is the total Griffith surface energy

There is an elastic solid that cracked with the length of l in a 1 D loading direction. The load-displacement coordinate Q-q system is quasi-static. As long as KI(*l*) < KIc, the Q-q slope is constant. The equilibrium curve, which depends on the solid's geometry and toughness, is obtained from the part of domain Q-q between KI(*l*) < KIc, which is bounded by the curve Γ in the length l. The increase in the crack length is inversely related to the Q/q slope (***Figure 13***). The surface energy for an elastic material is equal to the area between the loading curve and the equilibrium curve [63].

Effect of surface energy on adhesion

The surface energy of used formworks affect the adhesion or demolding force. research work was conducted to investigate the adhesion between concrete and formwork. The authors considered three different types of formworks: new, used, and polished, in order to invistegate the relationship between surface energy of formwork and demolding force. The outcomes the higher demolding force was the consequence of higher surface energy with rougher formwork surface [14] [38].
The same approaches were illustrated through the study by C. Chadfeau [39]. In the same context, Libessart *et al.* [38] measured the contact angle of 3 steel formworks (new steel plate, used steel plate, and mirror polished with the P1200 abrasive paper) with various surface roughness. The outcomes indicate that the demolding force or adhesion is related to the surface energy of used formworks.

1.2.3. Release agents effect on adhesion between formwork and concrete

A release agent or demolding agent is a product that facilitates the release of concrete elements by reducing the adhesion between the concrete and the formwork [64]. In addition, these products make it possible to treat molds against corrosion and facilitate their cleaning. According to the manufacturer's instructions, the release agent must be applied in a thin and even layer. Moreover, these release agents are usually used produce a concrete surface with good aesthetic qualities. In the case of a rough surface, the release agent will help with the adhesion reduction. However, for a very smooth surface (glass surface), it has the opposite effect [59, 60]. It must be noted that The release agent is harmful to the health and would cause problems in the long term surface [16-18].

Besides, the selection of the release agents depends on the formwork type, working condition, and the expected requirements [38, 39, 67].

The criteria for the selection and application of the release agent according to NF EN 13670 CN [71] are:

- The formwork release products must be selected and applied not to harm the concrete, steel at reinforced concrete, prestressing steel, formwork, or permanent structure.
- The form release products must not have any unwanted effect on the color, the quality of the facing of the permanent structure, or on the subsequent coatings planned.

As per SYNAD classification [72] , release agents, considering their composition, flammability level, and biodegradability, are classified into five groups: -vegetable, vegetable-based, synthetic, synthetic based, and recycled and recycled emulsion. However, this classification does not constitute a regulation in the production sector. For example, release agents based on their composition are mineral-based and vegetable-based release agents.

The release agents are heavily applied to produce a better barrier to the concrete surface. However, on the other side, it increases staining or bughole's defections on the concrete surface. They form beads and go in the fresh cement paste, as they are not compatible with water. An optimum and homogeneous application will result in more accessible and cleaner demolding, much fewer bugholes and stains, preserve the form, prevent parts damage, and significantly save costs [64]. The oils depending on their composition, act differently. For example, in the vegetable oils, the fatty acid and the esters form a soap layer which by stabilizing the emulsion results in reducing the friction between interfaces. However, the mineral oil creates a physical barrier between the interfaces [10, 39].

In this context, numerous research studies are performed to analyze the effect of surface texture of formwork, release agent, and other parameters on the demolding force between concrete and formwork. Libessart *et al.* [14] [38] research work was conducted to investigate the adhesion between oil release agents and formwork. The authors considered three different types of formworks with various roughness and two types of release agents: mineral oil and vegetable ones. The authors find out that the higher demolding force was the consequence of a rougher formwork surface which decreases by using the demolding agents. As a comparison, the vegetable oil had appropriate interfacial properties for demolding. While mineral oil did not demonstrate appropriate adhesion energy because of the lower contribution from their surface tension [14] [38].
In the same manner, specific tests were carried-out to evaluate the replacement of vegetable-based release agents with conventional mineral oils. The variable parameters were hydration process, adhesion force, concrete facing, and surface porosity. The findings point-out that the vegetable-based release agent equals or even surpasses the mineral oil in terms of adhesion performance [73]. Similarly, an experimental study was carried out to explore the impact of release agents and concrete composition on the final surface quality with the help of imaging analysis and mechanical tests. The results demonstrate that the type of release agent (ethyl-alcohol and biodegradable-oil-

based) decrease the adhesion between concrete and formwork [12]. Moreover, numerous experimental research works were conducted to verify the effect of various release agents on adhesion force formworks in contact with cementitious material [6, 10, 23, 62–65].
Samir Bouharoun [74] worked on the mechanisms in the formwork-concrete interface and checked the influence of release agent type on contact between these two surfaces. The authors used two types of vegetable-based and mineral-based release agents, and curried out a series of tribology tests on the concrete surface. The obtained results showed that the release agent implementation helps to reduce the friction at the formwork-concrete interface. Moreover, taking in account the combination of roughness and release agent, it was proven that the adhesion force decreased with the usage of release agent. In addition, the demolding force decreased with the reduction of surface texture. This reduction was more significant for the formworks having mineral oils and mirror-like formworks compared to others [11].

In literature, less studies can be seen regarding to the usage of other materials such as polymers as demolding agent. In this context, N. Spites *et al.* [17] studied two types of polymer (PTFE and a polymer with an unknown composition), steel formwork and a Zn/Al alloy coated steel plate. The authors indicate that the demolding force decreases through the usage of polymeric materials as a demolding agent. The adhesion is much lower and comparable to those from oil coated formworks.

1.2.4. Cement and w/c ratio effects effect on adhesion of formwork/concrete

The cement definition given by EN 197-1 [75] European standard is as follows: Cement is a hydraulic binder, which is defined as a finely powdered inorganic material that, when mixed with water, forms a paste that sets and hardens through hydration reactions and processes, retaining its strength and stability even when submerged.

Solid phases in a porous material such as cement paste are one of the major components of its microstructure. Moreover, these phases 'formation depends on many factors, including the crystal structure, the mechanism of formation, w/c ratio, compositions, temperature, the space available for the phase to form, and particularly the parameters of the formwork. Indeed, it can be highlighted that the microstructure of cementitious materials strongly depends on the casting process that affects their final properties. This bond depends on many factors, primarily the formwork material and release agent. In addition to that, the roughness of the formwork surface,

type of concrete, the pouring procedure, compaction and time of curing conditions, the temperature of the environment, and additives used in mix design [36].

According to the percentage of each of the constituents, five types of common cement are listed by the standard. Each one has a notation relative to this composition. Clinker, slag, silica fume, fly ash, and limestone, as well as up to 5% additives, are the major ingredients of cements, depending on the type. The classification and the main compositions of the common cements available are brought in [75].

According to the European Cement Association, the consumption of cements according to their types in France is presented in **Table 2**. Because CEM I and CEM II account for almost 90% of all cement usage during this period, two types of cement, CEM I and CEM II/B-S, were chosen for the current study.

Table 2 *Cement consumption from 1990-2008 in France, according to the cement type @ https://cembureau.eu*

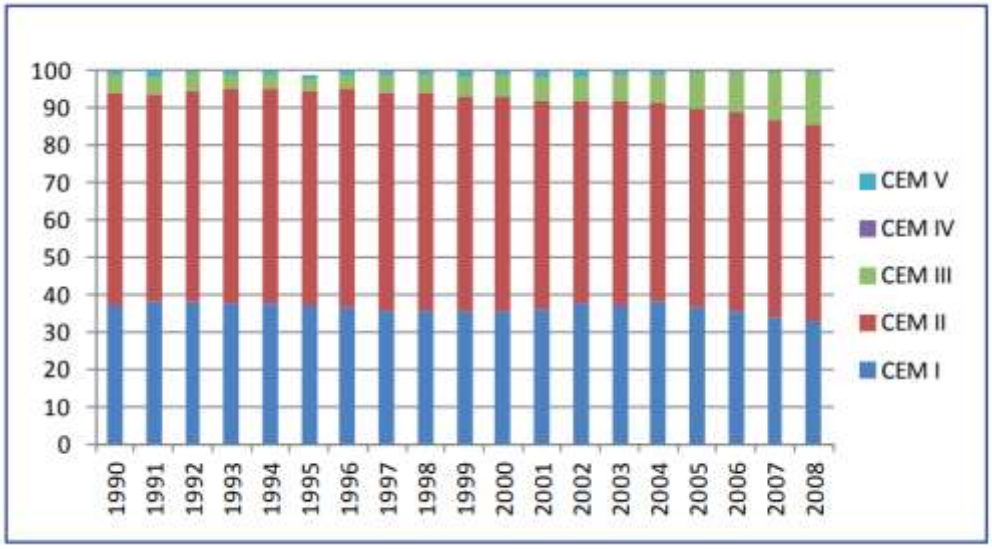

The water-cement (w/c) ratio defines the proportion of water's weight to the cement's weight in the concrete. The high w/c ratio in a mix design presents the hign amount of water in the process of cement hydration per unit weight of cement. In the presence of more water, the gel-like products of hydration get washed away with the water from the cement surface [76]. However, in the case of a low w/c ratio, the voids after the hydration process will be so less. The formed gel does not have enough space to move, and it fills the voids. The space limits the growth of crystals, so they

remain smaller in size. Subsequently, as per the size effect law, the smaller gels have greater strength than those formed in the high w/c ratio.

Samir Bouharoun [74] worked on the mechanisms in the formwork-concrete interface and checked the influence of paste volume. For the friction of fine aggregates of fresh concrete on the formwork surface, the authors prepared two types of cement pastes with 0.28 and 0.34 w/c ratios. The obtained results showed that the cement grains and water-cement ratio directly affect the friction between these two surfaces. As the w/c ratio increase, the contact pressure increases.

Cement hydration

Hydration is the chemical reaction between water and cement. Depending on water availability, it starts at the beginning of the mixing process and lasts for months or even years. During hydration, the anhydrous phases of cement react with water to set. The hydration of cement is a complex process, the mechanisms of which have been the subject of numerous studies. Different phenomena take place in synergy during this process: dissolution of mineral phases until the solution is supersaturated in ions inducing the germination and growth of different hydrates. The equilibrium between ionic solution and solid crystals evolves with time, which explains the hardening phenomenon that can last long after setting [75, 76, 77, 78].

Hydration development occurs in the early stages of hydration. Studies on the mechanisms of hydration showed that hydrates could be observed on the surface of alite or any anhydrous clinker in the first minutes and hours of hydration [77, 84, 191, 192]. These first minutes and hours correspond to the mixing and pouring times of the fresh slurry in the formwork and the first curing times. Anhydrous or partially hydrated phases can thus be in contact with the formwork surface. Furthermore, the growth of hydrates not only depends on the surface state of the anhydrous, the composition of the paste - the components present in the solution - but also on the quantity of available water and the space [82]. Moreover, the C3S, which is the most critical factor in cement strength growth for the first month of hydration, starts reacting with water within 3-24 hours. Also, it has about 30% of the cement contributes to C-S-H formation. In fact, the C-S-H growth is more related to the ettringite formation rather than developing from C3S, directly [75, 193, 192, 194]. The C3S in the clinker, while C2S develops slowly for the further impact to the long-term strength of cement [86].

Cement hydration is the source of adhesion. It initially causes water consumption, resulting in suction and the development of hydrates, which may attach to the surface. The overall chronology of the hydration process in the first 24 hours is known. This can be followed using various techniques such as electron microscopy or heat release monitoring by isothermal calorimetry. The hydration mechanisms can be different depending on the cement formulation with the presence of various secondary constituents and the development of new additive materials such as nano-particles that impact the characteristics and properties of cements [79, 80].

- ***Hydration mechanics:***

The kinetic mechanism of hydration in cementitious materials is a matter of interest in academic and practical engineering. The chemical and microstructure characterization of the cement hydration are complex resulting in difficulty resolving the mechanisms individually. Therefore, it requires more fundamental studies to overcome the scientific challenges through experimental techniques and methods. In a practical position, to obtain more sustainable materials with better functionality, there is a need to introduce secondary mineral additions, leading to more complex mix designs. To offer a rational basis for mixture proportioning, as well as the design and selection of chemical admixtures, a better understanding of basic kinetic principles of hydration is required. Several studies have been carried out on the hydration mechanism and its effect on the chemical and mechanical properties of cement and concrete [81, 82, 83, 84].

The nature of the process determines the chemical reactions that make up cement hydration and the condition of the system, combined. These reactions are included in one of the following categories:

- *Dissolution* consists of the detachment of molecular units from the surface of a solid in contact with water [92].
- *Diffusion is* caused by solution components being transported through the pore volume of cement paste [93].
- *Growth* involves the surface attachment, the process of molecular units being incorporated into the structure of a crystalline or amorphous solid within its self-absorption layer [94].

- *Nucleation* occurs due to the Szilard process, which involves continuously attaching and detaching single molecules (monomers) to and from clusters. It starts the sedimentation of particles on solid surfaces in a heterogeneous or homogenous manner [95].

The inability to separate and investigate each phase in detail makes it difficult to study these processes in cement hydration [90]. The $Ca_3 SiO_5$ or C_3S (alite) constitutes 50-70 % of the Portland cement (PC). C_3S is responsible for the early hydration and the setting and the development of early strength by forming the calcium silicate hydrate gel (C–S–H), the main hydrate product in PC [96].

The following are the principal hydration processes of PC, from the most reactive hydrate to the least reactive hydrate:

a) Simple hydrates or hydroxides:
   - Portlandite (calcium hydroxide): $Ca(OH)_2$
   - Aluminum hydroxide: 2 $Al(OH)_3$ or AH_3
   - Silicic acid (or hydrated silica): $Si(OH)_4$ or SH_2

b) Binary hydrated compounds:
   - Calcium silicate hydrates: C-S-H
   - Hydrated Calcium Aluminates:
     - C_4AH_{13}: tetra calcium alumina hydrate
     - C_2AH_8: bi calcium alumina hydrate
     - C_3AH_6: tri calcium alumina hydrate

c) Ternary hydrated compounds:
   - Hydrated gehlenite (or hydrated alumina-calcium silicate): C2ASH8; It is the only known ternary hydrate C-A-S-H.
   - Hydrated calcium sulphoaluminates:
     - Ettringite: C_3A, $3CaSO_4$, $32H_2O$
     - Calcium monosulfoaluminate hydrate: C_3A, $CaSO_4$, $12H_2O$

- ***Hydration phases:***

The cement hydration is mainly the study of the basis of the reactions occurring for certain phases of clinker and Portland Cement (PC) in particular. In general, for PC, five stages can be distinguished:

Stage I: the contact between cement and water bring a temperature peak. Ettringite is formed when aluminate (C_3A) interacts with H_2O (calcium and sulfate ions) [91]. The initial peak is caused by the release of energy from these processes.

Stage II: The dissolution of ions continues to reach supersaturation in the interstitial solution. The reactions of this period are the subject of various hypotheses, particularly on the formation of CSH. During the induction period, Ca++ dissolves in the solution with slow kinetics and is controlled by the diffusion of ions through the protective layer formed at the very beginning. Any other activity is considered negligible. The interstitial solution becomes very rich in calcium ions. The end of the induction period comes when the portlandite ($Ca(OH)_2$ or CH) starts to precipitate, inside or outside the layer. This precipitation process weakens the coating, which is torn apart in places. This period lasts, generally, from 2 to 3 hours, during which the heat release is weak and the pH increases. To be specific, it ends with an initial set of concrete.

At the same time, there is a growth of ettringite needles in the matrix. Both phenomena make that the layer is gradually destroyed. The theory of delayed nucleation proposes another mechanism. To achieve the precipitation of portlandite, Ca++, and OH- must reach a particular concentration in the interstitial solution. During the dormant period, they will dissolve slowly, and once the solution is saturated, the precipitation phenomenon is made possible. This is a chemical trigger effect, accelerating the precipitation of hydrates [97].

Stage III: In this phase, the supersaturation of the interstitial solution accelerates the consumption of C3S. The CSH develops and the portlandite precipitate. The CSH creation greatly influences the concrete strength during this stage. Moreover, with the formation of portlandite, cement setting occurs, which consequently results in workability loss. Formwork removal can take place during this period when the threshold mechanical strengths are reached. The second heat peak appears on the isothermal calorimetric curve (**Figure 14**) [97].

Stage IV: Mono-sulfo aluminate compounds formation followed by dissolution of ettringite. This precipitation can be seen as a slight peak on the heat tracking curve (**Figure 14**). Nevertheless, it is a period of a slow evolution of hydration. This slowing down would be the translation of the hydration by diffusion through a layer of hydrates initially developed on the surface of the anhydrous grains. During this period, the hardening of the paste appears [97].

Stage V: This last period is considered quasi-stable. The slowing down of the reaction, due to the diffusive character of the hydration reaction, can last for months or years. This period is critical from the point of view of the development of mechanical resistance because it starts very early, after one day of hydration, and persists long afterward.

The hydration reactions are slowed down but do not stop. The hydrous microstructure grows slowly without the anhydrous being fully hydrated. The formwork is often removed at this time, and the concrete will now continue the hydration process and reach final strengths over time (which can take weeks or months) [98].

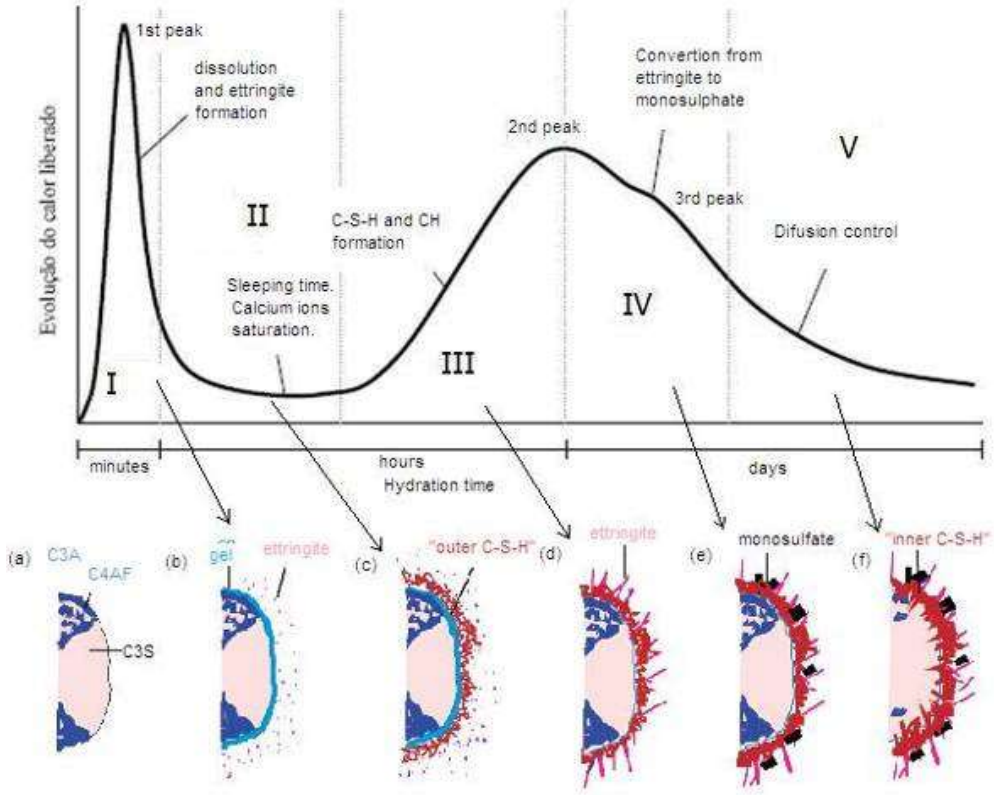

Figure 14 *Isothermal calorimetry curve and hydration stages of typical Portland cement; a) Un-hydrated section of poly-mineral grain, b) some C_3A react with Calcium Sulfate in solution. Amorphous, aluminate rich gel forms on the surface and short Aft rods nucleate at the edge of gel and in solution, c)reaction of C_3S to produce outer product C-S-H on Aft rod network, d)secondary hydration of C_3A producing long rods of Aft. C-S-H inner product starts to form inside the shell from continuing hydration of C_3S, e)C_3A reacts with any Aft inside shell forming hexagonal plates of AFm. Ongoing formation of inner product reduces separation of anhydrous grain and hydrated shell. f) sufficient inner C-S-H has formed to fill the space between grain and shell. The outer C-S-H has become more fibrous.* [98] [99]

1.2.5. Casting and curring effect on adhesion of formwork/concrete

The hardening rate of the concrete is influenced by many factors such as w/c ratio, cement type, and concrete grades, concrete member size, curing, temperature etc… [21]. The demolding time is related to the type of structural element, for example, the flexural members require a longer time because these members will encounter the self-load and the live load. The possible problems in the case of early demolding can be such as collapse or deflection of the structural member or physical damage during the removal. The member is designed based on the considered design loads at its performing period. To optimize the time consumption, Harrison (1995) suggests the removal time of the formwork can be calculated by the following formula (***Eq. 4***) [100]:

$$\text{The required maturity of the structure at the demolding time} = \frac{\text{Dead load} + \text{Construction load}}{\text{Total design load}} \times \text{grade of concrete} \qquad \textit{Eq. 4}$$

The other method to determine the removal time is possible by conducting non-destructive tests on the members. If nothing is suggested in the technical documents, a concrete strength equal to 5 MPa must be achieved to remove formwork to resist tearing due to stripping, according to NF EN 13670 CN [71].

Moreover, the time for which formwork stripping is possible can be determined by monitoring the pressures of the concrete [31]. The evaluation of concrete thrust considers the rheology of the concrete, the height of the formwork, the rate of filling, and the vibration. The NF P93-350 [101] standard for the formwork dimension specifies that the formwork must resist the pressures due to the placement of ordinary concrete in the elastic range. For the pressure calculation, it is considered hydrostatic [102].

The first 24-48 hours after casting is an important period for concrete, because, after 48h, the porosity and color change on the surface becomes less noticeable. It must be noted that the components of concrete mix design affect directly the surface color of cementitious structural elements [103].

1.2.6. Fracture mechanics effect on adhesion of formwork/concrete

The theory of elasticity is used to predict and analyze failure in a crack-free solid [104]. However, when solids include flows or cracks, the elasticity theory loses effectiveness because it ignores the singularity of stress. Therefore, it becomes necessary to implement the principles of fracture mechanics to predict the failure of structural element. Due to the dislocation of the microstructure, inclusions, grain size, and microstructure phases, the role of the microstructure of the material is significantly undeniable in the fracture process.

By applying force, which results in stress, separating a material or object into two or more parts is called fracture [63]. As earlier reviewed, the concrete-formwork surface is the field of physio-chemical interactions. After pouring the fresh concrete into formworks, cement starts to react with water chemically. Following that, the curing process starts, but we cannot keep the concrete inside the formwork for a long time. So, in the demolding of the concrete-formwork surface, a separation between materials occurs. Fracture mechanics can describe this phenomenon. Fracture strength which is also called the breaking strength, demonstrates the stress at which the fracture of system happens.

- ***Failure theory***

The failure of engineering materials put under uniaxial tension shows four different stages. By seeing **Figure 15**, in the beginning, linear elastic (0-1), second, strain hardening (1-3), continues with perfectly elastic (3-4), and in the end, strain-softening stages (4-5). The contribution of the different stages can vary with the material being tested. For example, in steel material subjected to uniaxial traction, after linear elastic range, the perfect plasticity occurs then strain hardening. The strain-softening stage is represented with a vertical drop in the strain-stress diagram that is not significant at point (5).

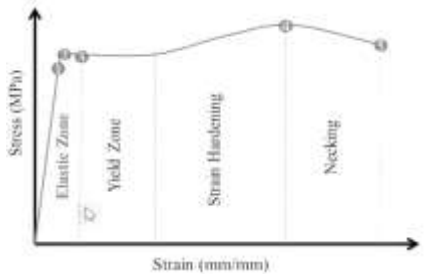

Figure 15 *Steel strain-stress diagram,1- proportional limit, 2- elastic limit, 3- yield point s_y, 4-ultimate strength s_u , 5-rupture stress s_r* [105]

However, in some materials, the failure does not happen in the same order as mentioned previously. Indeed, the elongation will not be noticeable when failure happens. These materials do not have a clear yield point and strain hardening. Therefore, the ultimate strength and fracture strength of these materials are the same [105].

- ***Brittle fracture***

Typically, when the fracture involves low energy absorption, the brittle fracture happens (high speed), and there is no plastic deformation that can be seen (**Figure 16**). In materials such as concrete, carbon fiber, and glass, the fracture occurs by division following a tensile stress acting perpendicular to the cleavage plane.

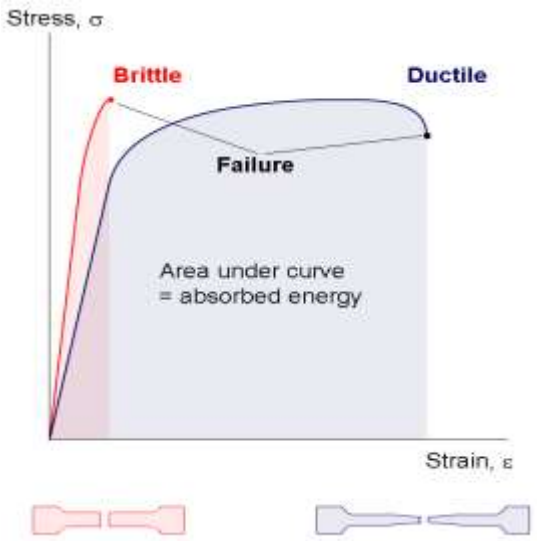

Figure 16 *Ductile and Brittle fracture behavior (stress-strain diagram) resulting from low carbon steel and high carbon steel traction.*

- ***Griffith's crack theory***

Fracture stress depends on the crack size and the material's properties. The first person who established a quantitative relationship between fracture stress and the quantities such as crack size and stiffness was Griffith, who did it on brittle solids.

Let us consider a solid (**Figure 17**) with a sharp crack inside it with the width of 2a, solid thickness of B, and which is introduced to a nominal stress s. When the stress doesn't reach the critical value,

the fracture will not happen. At the time of crack propagation, due to strain energy and external work done, the mechanical energy of the system will decrease [106].

The change in mechanical energy due to the introduction of the crack can be shown as:

$$\Delta U_M = U_a - U_o = -\frac{\pi \sigma^2 a^2 B}{E} \qquad \textbf{Eq. 5}$$

Which still cannot be the total force for the propagation of cracks.

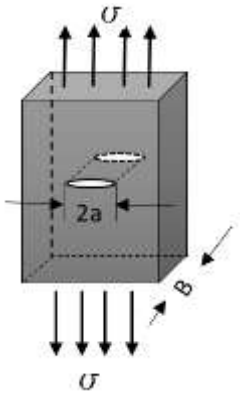

Figure 17 *a central crack of length 2a material*

As the crack starts to propagate, two new free surfaces of the crack are created; this was introduced by Griffith (1921) to analyze fracture that also brings into account another energy change component related to the surface.

With the crack propagation, two surfaces are created with a total area of 2aB:

$$\Delta U_S = 2 \times 2aB \times \gamma \qquad \textbf{Eq. 6}$$

So, due to crack, there is an increase in the energy equal to:

$$\Delta U_S = +4aB\gamma \qquad \textbf{Eq. 7}$$

γ- Surface energy per unit area of the fracture surface.

The total change in the energy due to crack propagation:

$$\Delta U_T = \Delta U_M - \Delta U_S = -\frac{\pi \sigma^2 a^2 B}{E} + 4aB\gamma \qquad \textbf{Eq. 8}$$

The total potential energy of the stressed solid body is related to the release of stored energy and the work done by the external loads.

If we try to plot the total energy change in the system, we will see that the crack length magnitude is at maximum (a_C) at a point.

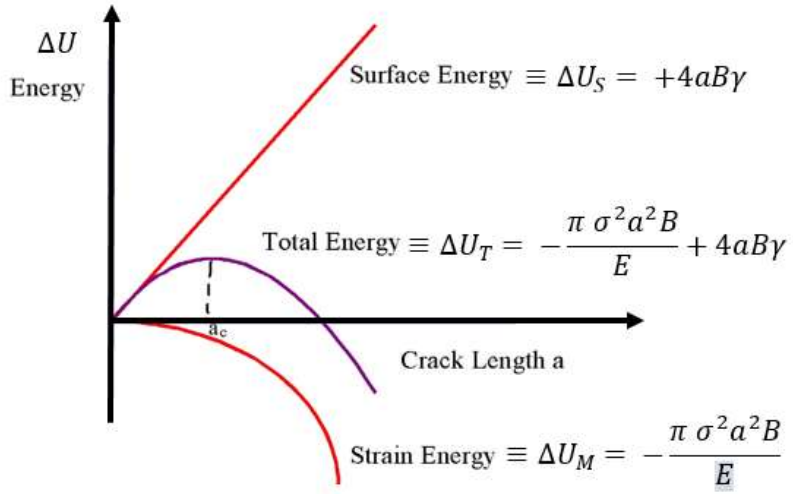

Figure 18 *change in energy of the system due to crack propagation*

Results can be extracted from the plotted figure:

- If the crack length is less than a_c and growing, the system's energy will increase, so cracks with a $<a_c$ will not grow.
- If the crack length is more significant than a_c and growing, the system's energy will decrease, so cracks with a > a_c will not grow.

The value of critical crack length a_c can be obtained from:

The system energy has the maximum magnitude at a_c, so:

$$\left.\frac{\partial \Delta U_T}{\partial a}\right|_{a=a_c} = 0$$

$$\Rightarrow \frac{\partial}{\partial a}\left(\frac{\pi \sigma^2 a^2 B}{E}\right) + \frac{\partial}{\partial a}(4aB\gamma) = 0 \qquad \textbf{Eq. 9}$$

After solving the differential equation, the critical crack size is obtained in terms of the elastic properties of the material, the surface energy, and the mechanical stress applied:

$$a_c = \frac{2E\gamma}{\pi\sigma^2} \qquad \textit{Eq. 10}$$

Now, let us see at what critical stress the member will fracture. The critical stress value can be extracted from the upper formula, which is called the Griffith equation/criteria:

$$\sigma_f = \sqrt{\frac{2E\gamma}{\pi a}} \qquad \textit{Eq. 11}$$

- ***Ductile fracture***

When the material under stress shows a tendency of significant plastic deformation (irreversible strain) before rupture, it is called a ductile material [107], and the phenomenon is happening is called a ductile fracture. Compared with brittle fracture, the ductile fracture involves a very high energy absorption (high energy dissipation) related to a large amount of plastic deformation before the member's failure (**Figure 16**).

- ***Loading modes***

When visualizing a solid body with a crack that is submitted to a constant and progressively increasing loading mode, the crack growth is stable until the stress in the system reaches the critical level ($s \rightarrow s_c$), in the beginning. The next stage starts when the $s > s_c$ and the crack grow rapidly, resulting in the system's failure. There are three modes of fracture [137–139] (**Figure 19**).

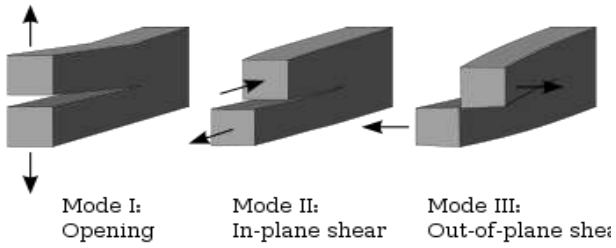

Figure 19 *Fracture modes*

- **Mode I**: if displacement develops perpendicular to the surfaces, it is called a normal crack.

- **Mode II**: sliding mode, a shear stress parallel to the crack plane but perpendicular to the crack front.
- **Mode III**: out of plane shear, the shear stress parallel to the crack front and crack plane.

A solid's fracture is usually caused by forming a displacement discontinuity of surfaces within the solid. If a displacement develops perpendicular to the surface of displacement, it is called a normal tensile crack or simply a crack; if a displacement develops tangentially to the displacement surface, it is called a shear crack, slip band, or dislocation.

We consider metallic materials for describing some experimental evidence at the basis of the plasticity theory. Elasticity law holds for the magnitude of stress or strain below some threshold value called the yield stress s_0.

For greater values of stress, one observes a plastic deformation ε_P.

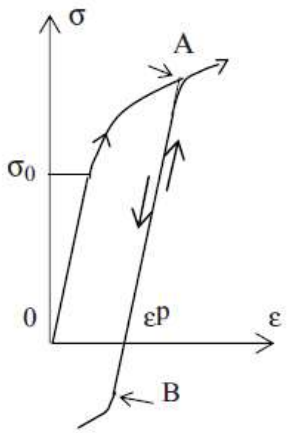

Figure 20 *Stress-strain curve in uniaxial loadings* [111]

Figure 20 describes the loading process. Unloading at ***A*** is elastic and reloading at ***A*** is plastic with the same strain rates $\partial\varepsilon^P/\partial t$ as before unloading. Models are described by H. D. Bui [111].

- ***A mechanical model***

There is a spring with stiffness *k* attached to a piston. The piston is moving inside a fixed tube with the length l (**Figure 21**). The piston displacement is y, and the resistance force τ is taken proportional to the frictional contact zone (l-y). The spring displacement:

$$x - y = \tau/k = \alpha\,(l-y)/k \qquad \textit{Eq. 12}$$

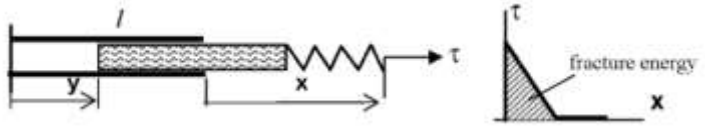

Figure 21 *A mechanical model of fracture shows a spring attached to a piston moving with fraction inside the fixed hollow tube*

The force-displacement curve parameters are defined by $\tau = \alpha\,(\tau - y)$ and $x = y + \alpha\,(l - y)/k$. The resulting curve is a straight line with a negative slope for $0 < x < l$. Beyond this length, the piston will go out of the cylinder. Moreover, after $x \geq l$, force becomes 0. This simple model of fracture, consisting of the separation of the spring from the hollow cylinder, makes it possible to analyze the energy dissipated by friction in the process zone inside the tube.

The adhesive tape on a rigid substrate; another type of fracture model, which is a ductile model, is pulled out of a normal scotch tape. The cohesive force comes from the glue layer, whose long molecules act similarly to the piston inside hollow cylinders but at a molecular scale.

The force between surfaces of solid and liquid; imagine a spherical ball put on a rigid surface in contact with a liquid which forms a concave meniscus of radius ***R***. The surface tension α is the reason behind the pulling back of the spherical ball to the substrate surface, $-p = \alpha/R$. An example of this action can be seen on the beach, which results in the cohesion of sand particles to each other.

The atomic force; this force is at an atomic scale which at a very short distance is repelling but after that distance attracts each other. From all types of primary and secondary bonds, most of which exist chemically, the Van der Waals forces of attraction describe the adhesion between two solids. This attractive force is weak [112].

- ***Fracture force***

The parameters in mode II of fracture are calculated from the maximum force point of the load-displacement curve by taking the first peak force Fc of the curve (**Figure 22**), because, during the experiments, most of the specimens exhibited similar saw-toothed load-displacement behavior due

to applied lateral force on the specimen, making it difficult to accurately determine critical energy release rates from the curves [142, 143, 144].

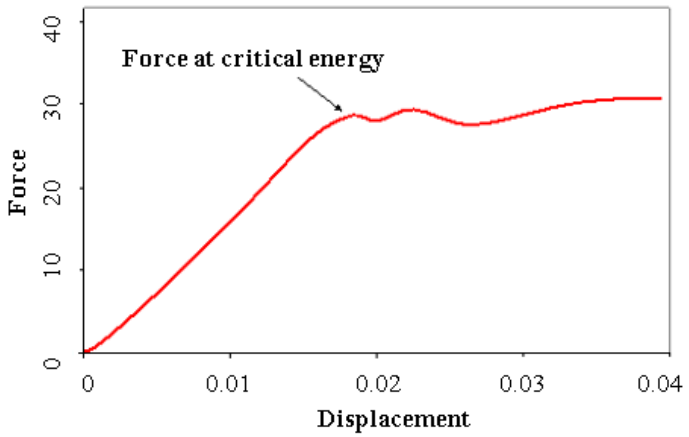

Figure 22 *Typical Load Displacement Curve for Determination of the Mode II Interlaminar Fracture @ Energy. www.sharcnet.ca*

In most failure theories, the material is assumed to be entirely homogeneous, isotropic, and without any defects such as cracks, voids, and mechanical discontinuities. The analysis goes based on these assumptions. The fracture occurs when the externally applied stress level attains a critical level (s -> s_c) [104].

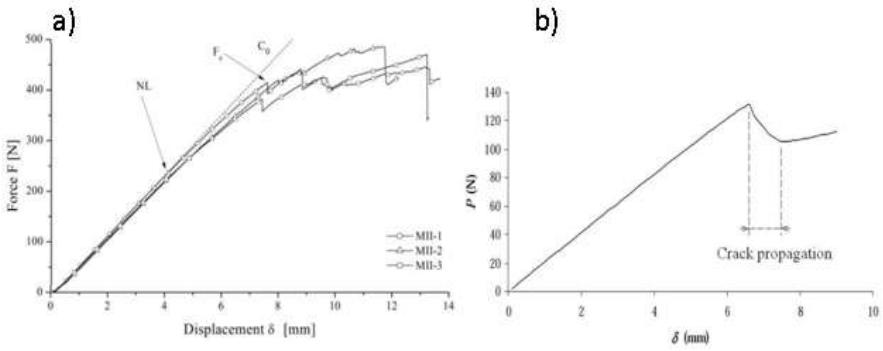

Figure 23 *a) unstable crack growth, b) Stable crack growth [104]*

2. Discussion and selection of parameters

The adhesion phenomenon between formwork and concrete is related to various parameters such as formwork, conception of mix design, curring and casting of concrete and the fracture mode. Moreover, it can be seen that these parameters are also related to each other.

Based on industrial demand and requirement of ERGOFORM project, some of these parameters are studied and some other are mentained constant. The studied parameters are as follows:

- Formwork's morphology
- Surface energy and wettability of formworks
- Release agent : oil coated and polymeric coated formworks
- Cement type: two types of most used cement are studied
- w/c ratio : three variation of w/c ratio used (0.3, 0.4 and 0.5)
- Fracture mode

It must be noted that same type of steel formwork is used. There is no usage of filler or additive materials. Finally, the curing and casting procedure mentained constant for all mix designs and tests.

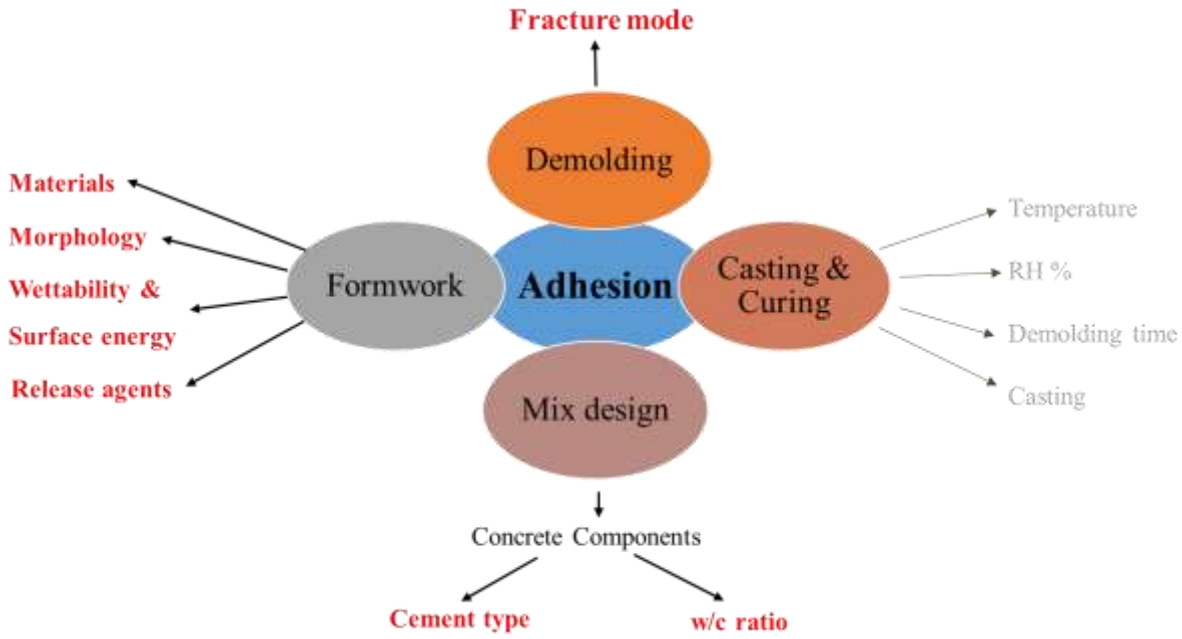

Figure 24 : Selection of parameters among influential parameters of adhesion

3. Characterization of surface in contact

In this part of chapter the discussion will focus on the effect of mentioned parameters (formwork, release agent, cement type and w/c ratio) on the surface of cementitious materials in contact. It must be mentioned that some of these parameters are well experimented in literature, however, some others such as; cement type, w/c ratio and polymeric materials as a demolding agent, are less studied in literature.

Libessart *et al.* [14] [38] find out the existent of a direct correlation between the adhesion energy of various release agents and the final surface esthetics. Similarly, an experimental study was carried out to explore the impact of release agents and concrete composition on the final surface quality with the help of imaging analysis and mechanical tests. The results demonstrate that the type of release agent (ethyl-alcohol and biodegradable-oil-based) did not have a significant effect on the concrete final appearance [12].

In connection with these evidences, L. Libessart *et al.* [70] and L. Courard *et al.* [65] studied the effect release agent's effect on surface quality and appearance of the concrete surface. The vegetable oil and mineral oil were tested, their surface energy was studied. The authors highlight that the vegetable oil gives a better surface finish than mineral oil.

Moreover, numerous experimental research works were conducted to verify the effect of various release agents and formwork roughness on final facing of cementitious material [6, 10, 23, 62–65].

3.1.Surface characteristics

At the surface of concrete, there is a concentration of cement paste, presenting morphology and complex inorganic solid phases. This layer which is exposed to the environment is called concrete skin, which consists of three layers: first a 100 µm of the binder with water and possible additives, then a 5 mm of mortar in case of sand diameter less than 5mm, and the third layer is the concrete skin about 30 mm thick [116] (**Figure 25**).

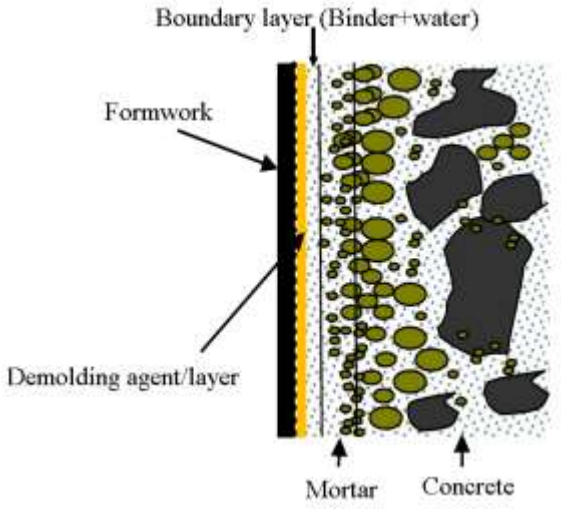

Figure 25 *Schematic representation of the formation of a boundary layer in the vicinity of the formwork* [74]

During the first phases of concrete hydration, it is in contact with the formwork. The chemical and physical properties of formwork materials and their morphological characteristics will have an impact on the concrete's facing. There is a lack of research on the relation between concrete and formwork right after demolding that shows their effects on each other, particularly on the adhesion between concrete – formwork surface at micron and sub-micron scales. The works are done, and results are not further than optical observation, compressive strength tests, and surface chemical composition. In recent work, C. Chadfeau [39] studied the interaction between the cementitious material and different types of formwork surfaces (metallic with different surface roughness, polymer, and release agents) at the early stripping age (24 h of hydration). The surface roughness, surface energy, and the analyses of the thermodynamic aspects of the surfaces lead to the result that the surfaces with lower roughness and surface energy (calculated from contact angle measurement) help to a better stripping. A very polished smooth steel formwork surface (Sa= 16±8 nm, Sq= 32±15 nm) showed the best functionality, but still, implementing this method on a live scale can be challenging. The morphological and chemical analyses of rough cement surfaces at 24 hours of hydration at microscopic and submicroscopic scales confirm the effect of the formwork on the quality of the facing.

3.2.Roughness parameters

In the process of pouring concrete into the formwork, after the concrete gets the required shape and strength, the formwork should get separated/demolded from the concrete with the least effort and defection of the concrete surface. The surface roughness has a direct impact on the demolding force and the surface thermodynamic characteristics (wettability) [30, 104, 105, 106, 107]. The rougher surface will negatively affect the demolding process unless the rough surface is desired [106, 107]. Surface roughness is a parameter of the surface's texture measurement. It is obtained from the vertical deviation of the real surface from its ideal surface. As the deviation value increases, the surface is identified as a rough surface, on the other hand, it becomes smoother as it decreases. There are different ways to measure the roughness values, such as; optical profilometer and contacting profilometer, i.e., Atomic Force Microscopy (AFM) and 3D Stylus profilometers.

In the context of the formwork surface topography effect on demolding process,

Some pronounced roughness parameters that used traditionally in literature can be explained as following:

3.2.1. Profile roughness parameters

The average absolute deviation from the mean line over one sampling length $\boldsymbol{R_a}$, which is one of the most used parameters in literature, is the value of the average of several consecutive length measurements (**Figure 26**). This parameter of roughness can be calculated according to the standard NF EN ISO 4287 [121], as follows:

$$R_a = \frac{1}{l}\int_0^l |z(x)|\,dx \qquad \textbf{Eq. 13}$$

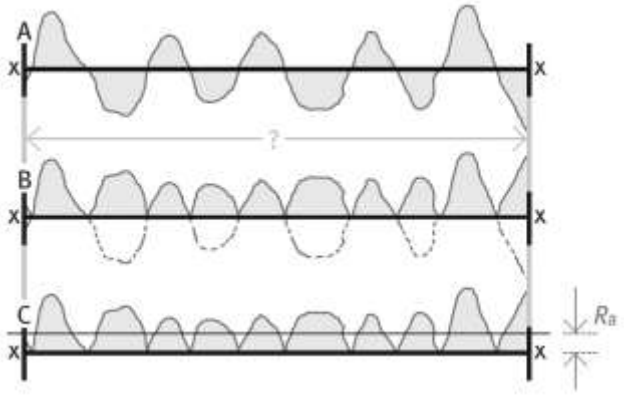

Figure 26 *Measurement of average roughness (Ra)* [122]

As second roughness parameter $\boldsymbol{R_q}$, equals the root mean square deviation of the profile means along the sampling length. Based on mentioned standard [121], this parameter can be calculated using the following formula:

$$Rq = \frac{1}{l}\int_0^l z^2(x)\,dx \qquad \textbf{Eq. 14}$$

Two other profile parameters, the height of the highest peak from the mean line ($\boldsymbol{R_p}$) and the depth of the deepest valley from the mean line ($\boldsymbol{R_v}$), both defined on the sampling length, can also provide important information.

If the surface is perfectly smooth, then $R_a = 0$. However, there are profiles with different R_a values depending on which profile will be studied (**Figure 27a &b**).

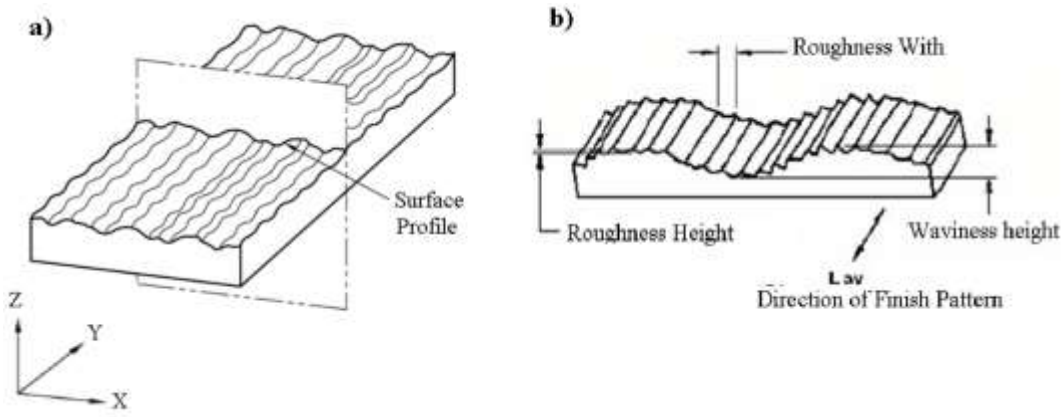

Figure 27 *Surface Characterizations; a) surface profile, b) profile detail* [122]

Profiles perpendicular to the X-axis in **Figure 27 b** will give identical R_a values, which will be different compared to profiles perpendicular to Y-axis. Plus, different types of surfaces can have similar R_a values, leading to a wrong conclusion (**Figure 28**).

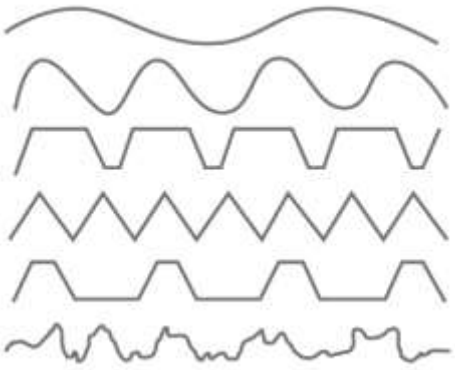

Figure 28 *different profiles with the same Ra value* [122]

The profile parameters do not provide much detail to avoid misinterpretation of the surface [122], therefore, in this study, the surface parameters can be take in account for the morphological analysis of cementitious surface.

3.2.2. Surface roughness parameters

In the research domain, when talking about the surface, they aim to determine the physical and chemical properties of the discontinuity zone between a solid and another medium and to study the phenomena that occur there. Also, the NF EN ISO 4287 [121] standard describes the surface finish: Profile method Terms, definitions, and surface finish parameters in detail. In an ideal condition, depending on the observation scale, a surface still has a degree of unevenness or roughness (**Figure 29**). There are certain specified parameters that can assist in better describing the characteristics of the surface. The arithmetical mean height of the line (***S_a***) – the difference in the height of each point compared to the arithmetical mean of the observed surface area – which indicates the roughness closer to reality, is one of the most commonly used parameters.

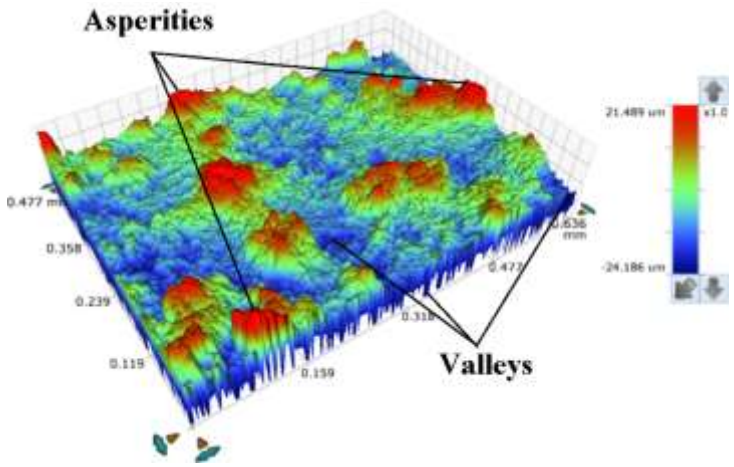

Figure 29 *cement paste surface texture (valleys and asperities/peaks) under Interpherometric microscope*

According to the NF EN ISO 2517-2 [123] can be calculated with the following formula:

$$Sa = \frac{1}{A}\iint_A |z(x,y)|dxdy \qquad \textbf{Eq. 15}$$

Sq represents the root mean square value of ordinate values within the observed area. It is equivalent to the standard deviation of heights. Moreover, the value can be obtained using the following formula:

$$Sq = \left(\frac{1}{A}\iint_A |z(x,y)|dxdy\right)^{1/2} \qquad \textbf{Eq. 16}$$

A rough surface leads to a stronger bonding [124], [125] due to:

- The rougher area exposed additional surface area, with which the binder can make contact during the formation of a bond.
- Additional mechanical interlocking
- Irregularities of the rougher surface possibly mitigate the proliferation of the cracks, leading to stronger, fatigue-resistant bonds.

3.3.Esthetic appearance

In the past, concrete was used for its functional properties, i.e., mainly bearing loads. At this time, as concrete is the most used construction material globally, appearance plays a significant role. It is appraised as a kind of artwork. Building Surface has a definite impression from a close distance ~0-10 meters. In the case of having a good mix design and skilled workers, concrete can serve the needs with little or no maintenance in its lifetime (**Figure 30**).

Figure 30 *a) Concrete exterior finishing © Michael Compensis, b) Villa Saitan © Koichi Torimura*

In the facing phenomena, two distinct elements come to the front: formwork and concrete. The formwork is a temporary structure keeping the fresh concrete (a liquid plastic material) for enough time to get the necessary strength to hold its weight. These two materials in their contacting interface interact and show specific physiochemical mechanisms, which are discussed in detail in another section. Even with the same work condition and mix design, the formwork selection dramatically affects the concrete appearance (**Figure 31**).

Figure 31 *Two surfaces made with an identical concrete composition and casting procedure, but different formwork* [126]

Once the concrete is hardened, the formwork should be removed. In the case of the absence of the anti-adhesive material (release agent), depending on the many factors such as formwork surface material (porosity, texture, staining ability, retarding ability), workmanship, and mix design, bonding develops between two surfaces. Furthermore, removing the formwork will cause alteration of both the concrete and the formwork's surfaces. Consequently, the aesthetics of the concrete face is under question.

Conclusions

The conducted literature review investigated different parameters involving the concrete-formwork adhesion phenomenon. Different types of formworks are being used in the construction industry, such as flexible formworks, self-supporting formworks, and stay-in-place formworks based on various types of materials. The concrete is poured into the formwork in a fresh state through the casting process. The hydration process take place while the water reaches the cement (binding components in the mix design).

Moreover, the concrete is in direct contact with the formwork surface. A big part of the hydration happens in the first hours of mixing inside the formwork (first 24 hours of hydration) [91]. Various treatments are utilized to prevent concrete from adhering to the formwork surface. The release agents improve the releasing functionality by creating a physical barrier or a chemical separating layer. However, at the same time, release agents affect the esthetics of the concrete surface and create hazardous problems for the users and the environment. In addition, after each usage, the formwork surface needs to be cleaned and covered with the release agent again.

There are parameters affecting the concrete-formwork adhesion phenomenon. Surface roughness, formwork surface material, concrete mix design (cement type, w/c ratio, and fillers), and demolding technique are being researched. The roughness and the material of the formwork surface are among the most influencing parameters that affect the concrete's adhesion and finishing skin [35, 120].

The cement bonding process with the materials in contact starts after it is poured into the formwork. The adhesion between concrete and formwork is adhesion between two solids that form due to the setting and hardening of cement paste/concrete mix. Furthermore, the preparation technology, adhesion performance, and external conditions, particularly humidity, influence the sticking of the cementitious materials to the formwork. There are forces occurring in the phenomenon of adhesion between concrete and formwork. These forces depend on the structural properties of molecules and external conditions.

Through the literature review, it was illustrated that researchers had considered some of the affecting parameters. However, their focus did not cover all the involved factors. Regarding the

scale of the work, the studies considered either macroscopic or microscopic characterizations. This study is carried out in form of ERGOFORM porjet in order to answer some industriel demands. Moreover, this work attempts to cover some existent gaps in literature and the aspects affecting the phenomena of adhesion through different scales.

CHAPTER # 2 : Materials and experimental methods

This chapter mainly focuses on the materials used for the elaboration of cement paste and concrete, as well as the testing procedures for materials characterization, cement paste and concrete samples. Firstly, the used materials for the preparation of cement paste and concrete mix design are introduced in detail. In the second part, the experimental methods for material characterization are discussed.

Bulk density test, size distribution, and specific gravity tests are carried out to characterize the aggregates. Additionally, laser granulometry experiment are performed to determine the particle size description for the various types of cement.

Thereafter, the experimental methods for mix design, mixing procedure, casting, and curing of cementitious mixtures are explained. Besides, environmental scanning electron microscopy (SEM) and interferometry microscopy (IM) are used to investigate microscale information about surface topography of cementitious samples. Furthermore, the chemical composition of the cement powder and cement samples on the surface are determined using X-ray Diffractometry.

Finally, experimental methods for evaluation of demolding force are described. Two type of tests, the first one named "Pre-crack demolding test" for cement samples and the second one named "Pull-off demolding test" on concrete samples are presented.

1. Materials

1.1. Cement

Two types of Portland Cement (PC) of CEM I 52.5 N and CEM II B-S 42,5 N CE CP1 NF produced by HEMING according to the standard NF EN 197-1/A1 [75] was used for the preparation of specimens. The specific characteristics and chemical composition of both types of cement are shown in **Table 3.**

Table 3: *Chemical and physical characteristics of CEM I and CEM II/B [145, 146]*

CEM I 52,5 N CE CP2 NF	physical charactristics													
	Mass (g/cm3)		Mass area (cm2/g)		setting start time (min)									
	3.18		4310		155									
	Chemical charatristics													
	PAF	INS	SiO2	Al2O3	Fe2O3	CaO	MgO	SO3	K20	Na2O	S--	Cl-	CO2	free CaO	active eq Na2O
	0.8	0.2	20	4.8	3.1	61.3	4.9	3.7	1.12	0.26	0.03	0.07	0.7	1.6	1
	Composition													
	Constituantes (%)									Setting regulator		Aditives		
	Clinker						Secondary constituants			Anhydrate		Grinding agent CXN2		
	95						5			5.2		0.05		
	Clinker composition													
	C3A		C3S		C4AF									
	7		63		10									

CEM II/B-S 42,5 N CE CP1 NF	physical charactristics													
	Mass (g/cm3)		Mass area (cm2/g)		setting start time (min)									
	3.04		4040		206									
	Chemical charatristics													
	PAF	INS	SiO2	Al2O3	Fe2O3	CaO	MgO	SO3	K20	Na2O	S--	Cl-	CO2	free CaO	active eq Na2O
	1,2	0,5	23,9	6,1	2,4	54,8	5,6	3	0,9	0,31	0,28	0,07	0,9	1,5	0,74
	Composition													
	Constituantes (%)									Setting regulator		Aditives		
	Clinker		Blast Furnace Slag (S)				Secondary constituants			Anhydrate		Grinding agent CXN2		
	67		31				2			4.3		0.05		
	Clinker composition													
	C3A		C3S		C4AF									
	7		63		10									

1.2. Aggregates

Three fractions of natural river aggregates are used to provide concrete samples. Fine aggregates (sand) had the size of (0-4) mm, and coarse aggregates containing two types; *a)* fine coarse aggregates (4-8) mm and *b)* coarse aggregates (8-16) mm as shown in **Table 4.**

The aggregates classification was carried out by the sieve size. Grading of the aggregates used in the concrete mix design meets the EN 933-1[129] standard requirements.

***Table 4**: Aggregates used in this work*

Aggregates	Symbol	Size (mm)	Picture
Course	CA	8-16	
Fine course	CA	4-8	
Fine	FA	0-4	

1.3. Water

Tap water available inside laboratories was used for mixing and curing of cement and concrete specimens. The outcomes shows that the pH regular tap water is equal to 7.2±0.2.

1.4. Superplasticizer

A superplasticizer certified by EN 934-2 [130] was used to improve the workability of concrete and keep the workability S4 for all mix designs. The superplasticizer was purchased from a local provider (SIKA) in France. The superplasticizer's physical and chemical characteristics are shown in **Table 5** based on product's technical report.

***Table 5:** SIKA superplasticizer properties*

Superplasticizer SIKA	Properties
Colour	Dark brown
State	Liquid
Density (kg/L)	1.15 ± 0.03
pH	7.5 ± 1.0
Chloride content (%)	≤ 0.1

Dosage (L/m^3 of concrete)	5

1.5. Demolding agents

In this work, to facilitate the demolding process and to decrease the adhesion between concrete and used formwork, as well as to compare these properties with those of polymeric coated formworks, two types of release agents were utilized: 1) mineral oil and 2) vegetable oil. The characteristics of these release agents, as provided by the producers, are summarized in **Table 6**.

Table 6: *Release agents' characteristics*

Release agent	**Commercial name**	**Viscosity**	**Biodegradability**	
Mineral Oil **Qty = 1 L/40 m^2**	SIKA® DECOFFRE MINERAL [131]	▪ ≈ 23 mPa.s à + 20 °C ▪ ≈ 49 mPa.s à + 5 ° C	15-35 %	
Vegetable Oil **Qty = 1 L/60 m^2**	Vegetable oil, 357 LANKODEM VEG, [132]	29 ± 3 mm^2/S (20° C)	62 % at 28 days NF EN 9408-OCDE 301 F	

1.6. Formwork

In the framework of the ERGOFORM project, several coating solutions have been developed. The solutions chosen have been implemented on steel plates by the partner laboratory **LPIM** before being transmitted to the ICube laboratory.

The used steel plate specifications correspond to NF A35 and NF-EN- 10088-2 [133]. The dimensions of the plate provided by Hussor Company, are 160×94×5 mm^3 (**Figure 32**).

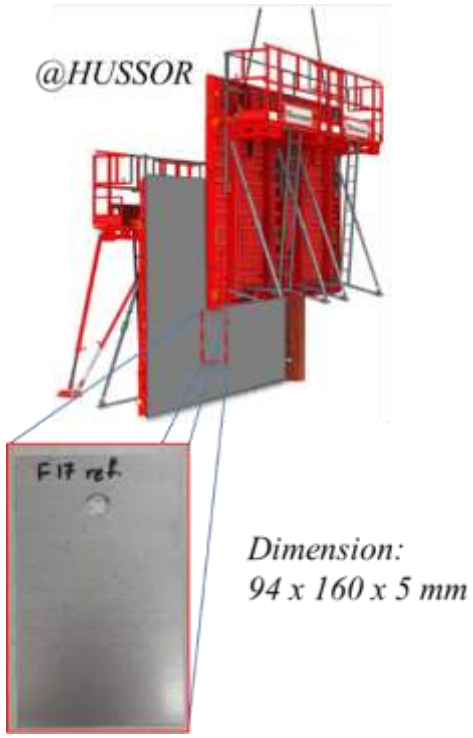

Figure 32: *Formwork plate*

The chemical composition of the ERGOFORM formwork plates is shown in **Table 7**.

Table 7: *ERGOFORM formwork plates' characterization.*

Elements	**C**	**Si**	**Mn**	**Cr**
Percentage	0,05	0,35	0,40	16,5

In this work, five types of formworks surfaces were considered for the further experiment:

- ***Reference formwork (F17-Ref)***

Formwork plates of stainless steel provided by Hussor Company were considered as reference formwork for the experiments. The latter was used without any surface treatment or coating as shown in **Figure 33**. Surface roughness and contact angle measurements were carried out on the sample plate.

Figure 33 *: Reference formwork plates (F17-Ref)*

- ***Formwork coated with release agents (F17-MO & F17-VO)***

A thin layer of release agent (according to the product's technical report) was applied to the formwork surface using a paintbrush. The formwork coated with mineral oil (MO) and the one covered with vegetable oil (VO) is called F17-MO and F17-VO, respectively.

- ***Formwork coated polyethylene terephthalate (PET)***

As a type of formwork coating, a polyethylene terephthalate (PET) film was procured from the market. PET is the product of heating the ethylene glycol and terephthalic acid together, which causes the chemical polymerization of monomers to produce a chain-like transparent product. The following is a diagram of the general reaction that leads to PET production (**Figure 34**).

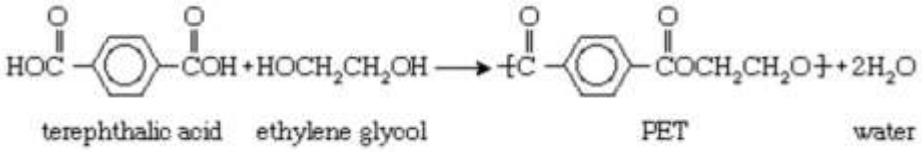

Figure 34*: Diagram of the general reaction for the production of PET*

In our experiments, a PET film with a thickness of 190 µm was placed on the F17-Ref plate. A skinny layer of adhesive glue (t≈ 100 µm) ensured the proper sticking of the PET to the plate surface.

- ***C20C27***

A polymeric coating solution produced by LPIM Laboratory – an ERGOFORM project partner - was used in the experiments. The development of this solution is described in the research work of Agnès Rannée [134]. This coating consists of two layers: 1) C20, a commercial resin polymer

solution is the bottom layer deposited on the formwork plate. It was chosen due to its adhesive properties to metal, and 2) C27, the top acrylate resin layer was selected due to its moisture resistance. This layer acted as a demolding agent to ensure the aesthetics and durability of the concrete surface. The photo-polymerization process was used to place layers on the formwork plates. The total thickness of this layer is 100 – 200 µm [134] (**Figure 36**).

Figure 35*: PET, and C20C27 formwork plates*

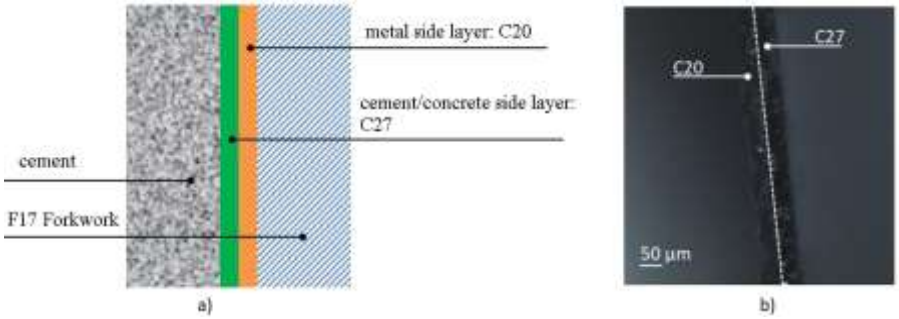

Figure 36: *Structure of the double-layer polymer solution applied on the F17 formwork: a) diagram of the F17 formwork coated with the C20C27 polymer solution, b) C20C27 double-layer coating observed with an optical lens* [39]

2. Characterization of cement paste and concrete components

This part includes the testing procedures for characterizing the cement paste/concrete components.

2.1. Cement characterization

For the characterization of cement, the following properties are investigated.

2.2. Specific gravity and bulk density

Specific gravity is the property of materials to compare densities of a particular material to the water at a specified temperature. Specific gravity is calculating whether the material is able to sink or float on water.

On the other hand, bulk density is the behavior of materials which is defined as the mass divided by the total occupied volume. The total volume is equal to the volume of particles, the volume of inter-particles, and the volume of internal pores.

Besides, the specific gravity and bulk density of cement were conducted according to the ASTM C188-17 [135] standard considerations.

2.3. Normal consistency and setting times (initial and final setting time)

The normal consistency of cement represents the percentage of required water for the cement paste at which the viscosity of cement paste becomes that vacant plunger penetrates to a depth of (6 ± 1) mm from the bottom of the mold. The time at which cement begins hardening and completely loses its plasticity is called the initial setting time of cement. The time required for the cement to achieve its complete strength is called the final setting time. These behaviors of cement were measured in compliance with the EN NF 196-3 [136] standard considerations.

2.4. Laser Granulometry

Cement's size and particle distribution significantly affect hydration, setting, hardening [137], microstructure development, and material strength [138]. This highlights the importance of knowing about this material's characteristics. For measuring and controlling the particle size distribution and surface area of cement, many techniques can be used such as; sieve analysis, air permeability, etc., but laser diffraction is the most popular and accurate method. Because the laser diffraction method is quick, easy, and provides a complete picture of the full-size distribution [139]. In this method, a laser beam passes through spread particles of the sample, and angular variation in the intensity of scattered light is calculated. For large particles, the relative angle of the light scattering is smaller compared to small particles. Such data for angular scattering intensity is then analyzed to measure the size of particles, which is reported as a volume equivalent to sphere diameter.

Using the Mastersizer 3000E, it was possible to measure particle size range from 10 nm up to 3.5 mm using a single optical measurement path (**Figure 37**). Ten samples of cement were examined. The tested samples, equivalent of one tea spoon, present a mix of cement powder taken from different depths of the cement bag.

Figure 37: *Laser granulometry*

2.5. Aggregates characterization

The aggregates were characterized based on the following properties.

2.6. Specific gravity, bulk density, and water absorption

The specific gravity, bulk density, and water absorption of aggregates are important properties for the preparation of concrete with a proper mix design. Specific gravity is the ratio between the masses of material and an equal volume of water at a specified temperature. Since aggregates have water permeable voids, therefore, it is necessary to measure two types of specific gravity: bulk specific gravity and apparent specific gravity.

Bulk density is the mass of aggregates needed to fill the cylinder of a unit volume after aggregates are batched according to the volume. Moreover, water absorption is defined as the difference in weights of aggregate samples at oven-dried and saturated conditions. Thus, these properties were measured according to the NF EN 1097-6 [140] standard considerations.

Three samples for each type of aggregates were tested, the specific gravities, apparent specific gravity, and water absorption were calculated throughout the following equations.

$$\text{Specific gravity} = \frac{W_4}{W_3 - (W_1 - W_2)}$$

$$\text{Apparent specific gravity} = \frac{W_4}{W_4 - (W_1 - W_2)}$$

$$\text{Water absorption} = \frac{W_3 - W_4}{W_4} \times 100$$

Where,

W_1: weight of aggregates + water + pycnometer.

W_2: weight of pycnometer + water.

W_3: weight of surface dried aggregates after 24 hours immersed in water.

W_4: weight of oven-dried aggregates.

Furthermore, the bulk densities was obtained throughout the following formulas:

$$\text{Loose bulk density} = \frac{W_2 - W_1}{V}$$

$$\text{Compacted bulk density} = \frac{W_3 - W_1}{V}$$

Where,

W_1: weight of the empty cylinder.

V: volume of the selected cylinder.

W_2: weight of cylinder and aggregates.

W_3: weight of the cylinder and rodded aggregates in three layers.

2.7. Size distribution

Grading or size distribution states the process to determine the particle size distribution of a typical sample of aggregates. This property was measured based on NF EN 933-1 [160] standard considerations.

After taking the weights of retained aggregates in each sieve, a curve of aggregate grading is plotted, where the x-axis represents the size of aggregates, and the y-axis indicates the percentage of passing.

2.8. pH value of water characterization

Tap water available inside the laboratory was used for the production of mixtures. The pH test was performed using PHM 210 standard pH meter to analyze the acidity of water. The pH value was measured as an average of 3 samples.

2.9. Preparation of molds for cement paste and concrete samples

To cast a specific amount of cement paste on the formwork plate and have a desired condition for the demolding pre-crack test, molds were prepared from a slender PVC pipe (Ø = 2.54 cm). The PVC pipe was cut in 2.7 cm length. Both ends of the mold were polished with sandpaper to obtain

smooth edges and prevent the cement paste's loss from the molds. To adjust a point for inserting the load (F) during the test, a hole was drilled 5 mm below the upper edge of the molds. A bolt was fixed in the hole, acting as an anchor point (**Figure 38**).

Figure 38: *PVC mold preparation*

The 10×10×10 cm^3 standard stainless steel molds were used for casting the concrete cube samples (**Figure 39**).

Figure 39: *10×10×10 cm^3 steel mold*

3. Experimental methods for cement paste and concrete

3.1. Mix design and mixing procedure

Based on two types of cement (CEM I and CEM II/B), different types of mixtures were prepared.

3.2. Cement paste

The cement paste was prepared in accordance with NF EN 196-3 [136], using a standardized mixing machine as shown in **Figure 40**.

Figure 40: *Standard cement paste preparation mixer*

3.3. Concrete

Concrete mix designs were prepared using three W/C ratios and two types of cement (CEM I and CEM II/B). The concrete mixtures were provided according the French standard NF P18-404 [141].

It must be noted that the gravels were previously dried in the oven at 105 ± 5° C for 24 h, and all the gravels and cement were weighed with the accuracy of ± 1 g.

The components of all mix designs are presented in **Table 8**. The superplasticizer was used to maintain the concrete consistency class S4 = 160-210 mm for all mix designs.

Table 8: *Concrete mix components according to different w/c ratios for 1 m^3 of concrete*

w/c ratio	Components	Weight (kg)	w/c ratio	Components	Weight (kg)
0.4	cement	370	**0.5**	cement	370
	Coarse Aggregate 8-16 mm	595.2		Coarse Aggregate 8-16 mm	595.2
	Coarse Aggregate 4-8 mm	396.8		Coarse Aggregate 4-8 mm	396.8
	Sand 0-4 mm	772.7		Sand 0-4 mm	772.7
	Water	1480		Water	185
	Superplasticizer*	3%		Superplasticizer*	1%
0.6	Cement	370			
	Coarse Aggregate 8-16 mm	595.2			

Coarse Aggregate 4-8 mm	396.8
Sand 0-4 mm	772.7
Water	222
Superplasticizer*	0.5%

***: the superplasticizer was measured and added according to the cement weight.**

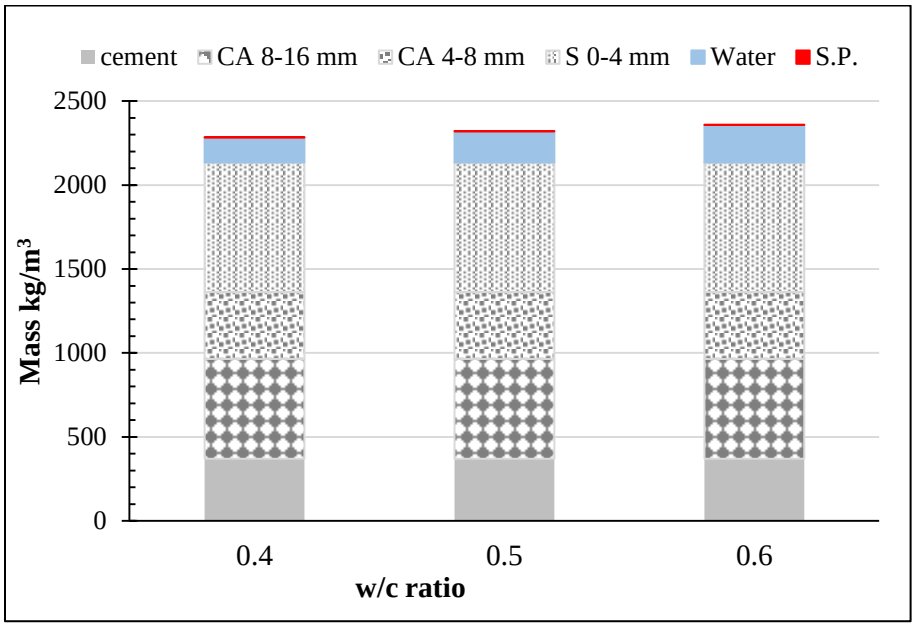

Figure 41: *Proportion of constituents for ordinary concrete in 1 m^3 of concrete*

3.4. Casting and curing

3.5. Cement paste samples

The plate surface was washed with normal water then dried with tissue paper. Two molds were placed on each plate with a minimum 2 cm distance between them. During the filling, we held the mold with one hand to prevent the leakage of cement paste from the bottom of the mold as shown in **Figure 42**.

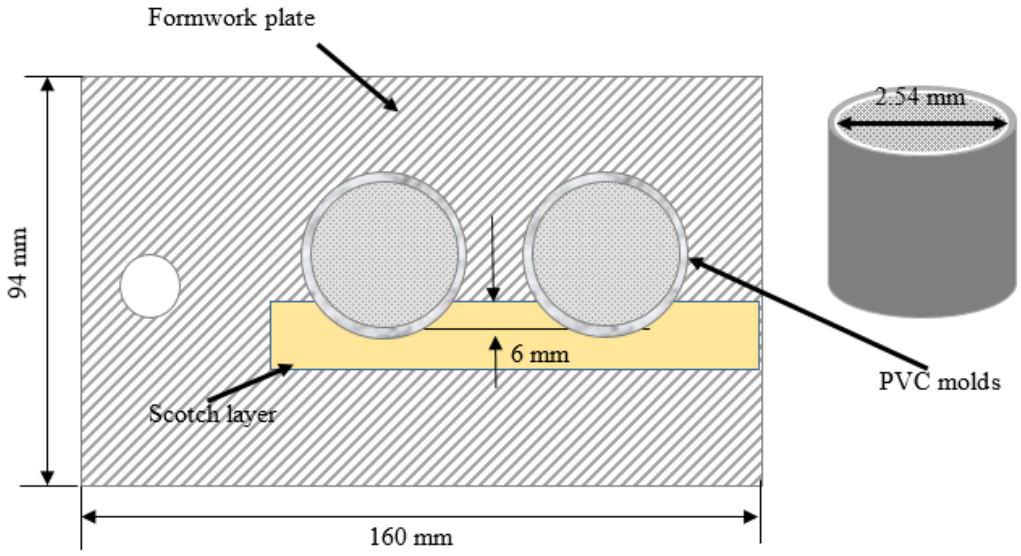

***Figure 42**: Sample preparation for cement paste*

Here, the cement paste was filled for a specific 8 ml volume in each mold to eliminate the cement weight factor and obtain the exact size of samples. By a small handmade vibrator, each cement paste was vibrated for 30 seconds to remove the possible air bubbles. The used vibrator is shown in **Figure 43**.

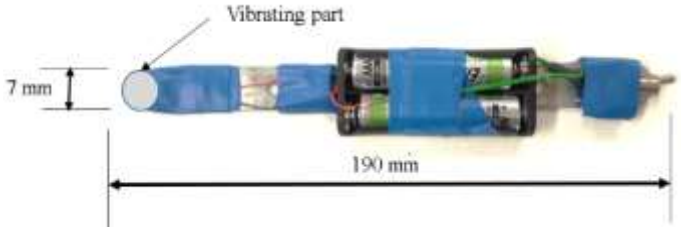

***Figure 43:** Vibrator to remove air bubbles in cement paste*

Finally, the samples were moved into a curing chamber and kept for 24 h under standard conditions with a temperature of 20 ± 2°C, and the humidity not less than 90% (***Figure 44***).

Figure 44: *Curing of the cement paste samples in the chamber*

3.6. Concrete samples

Metal molds were cleaned and the surfaces were coated with mineral oil lightly. Then, formwork plates were placed in the molds face-to-face in a direction that the coated surface of plates locate in front of each other (**Figure 45**).

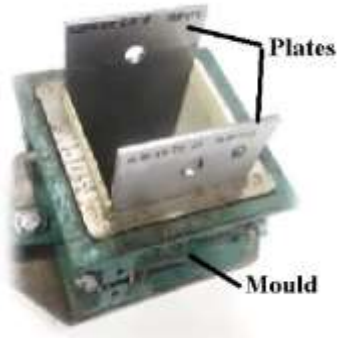

Figure 45: *Placing of plates in the mold*

The molds were filled in two layers (≈ 5 cm) and each layer was compacted by 25 times impact using a non-sticky metal scoop. After casting, all the samples were stored in a curing chamber under standard conditions of T= 20 ± 2 C° and RH ≥ 90 % according to standard EN 206-1 [142].

3.7. Fresh properties

3.8. Slump test

The test is carried out according to NF EN 12350-2 [143]. According to the mentioned norm, the slump must not collapse or shear. In the case of an undamaged and symmetrical concrete shape, the measured slump is acceptable. For all concrete mix designs the slump class S4 was expected.

3.9. Mechanical properties

3.10. Compressive strength

For all concrete samples with different cement types and w/c ratios, the compressive strength test was conducted following EN 12390-3 [144]. Three samples of $10^{x}\,10^{x}\,10$ cm^3 from each mix design variation were prepared to perform the test (**Figure 46**).

Figure 46: *Compressive test machine*

In addition, the loading rate was 0.5 MPa/s, and the recording stopped when the compressive force dropped to 20 % of maximum strength.

3.11. Stopping hydration

In the existence of water, the cement hydration continues even for years [91, 92]. To understand the effect of formwork on the surface of cement paste and characterize the cement surface right after demolding at the 24 hours of casting, therefore, the hydration process should be stopped [145].

There are different ways to stop the hydration process of cement at an early age: freeze-drying, solvent exchange [94, 95], microwave ,and drying at 105° C for 24 h [146].

Zhang *et al.* [148] investigated the drying technics' effects on the microstructure and compositions of cement paste. Besides, the authors studied that application of different drying technics results in water phase transitions, shown in **Figure 47**.

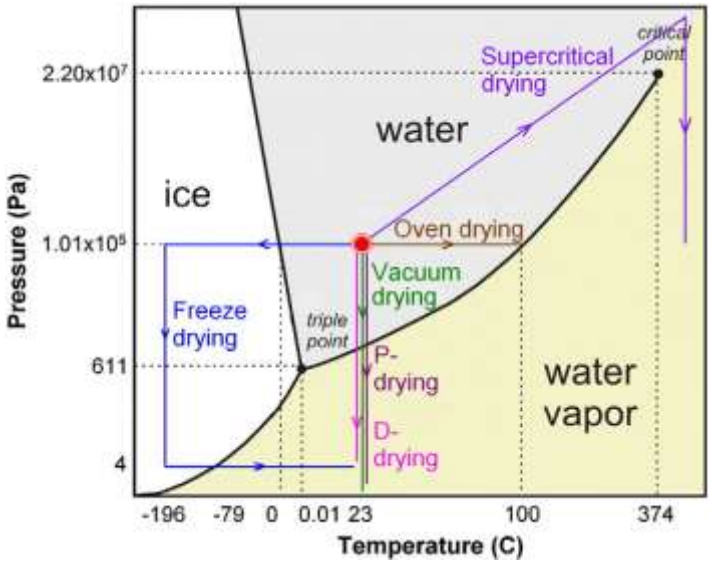

Figure 47 *The phase diagram of water. The transitions between the phases are shown using the diagram for the processes of freeze-drying, oven drying, D-drying, P-drying, vacuum drying, and supercritical drying. The red point is the initial state of water in the sample at atmosphere pressure and room temperature. The arrows indicate the paths followed during the drying process.* [148]

Some common drying techniques for extracting water from the cement paste are described below:

- ***D drying method***

The machine used for the D drying method is a sealed container connected to a vacuum machine at a specific condition (T= −79° C). This method is efficient in completely removing the non-bound water, and it will not cause any damage to the microstructure of the sample. The drying time in this technique is very long; depending on the requirements, it can take 12 hours up to many days [97, 94].

- ***Freeze-drying method***

In this method, the sample is submerged in nitrogen liquid (-196° C) for a short time (5 minutes). The water in the sample freezes immediately after immersion in the liquid nitrogen. Then, with the help of a desiccator, the ice water will be removed, and this will not cause any damage to the pores' structures [146].

- ***Oven drying method***

The oven which is used in this method should be ventilated with programmable system of temperature. The sample is placed into the oven at a temperature of 105±1°C. The duration of drying is 24 h in most works. This method is proved to be the most efficient one in removing the non-bound water and the most damaging to the microstructure of the sample[97, 98], which will not be suitable in case of analysis of the surface of the sample.

- ***Solvent exchange method***

In this method, the non-bound water of the paste (the pore solutions) is replaced with an organic liquid such as isopropanol, methanol, ethanol, and acetone, among others. The liquid must be replaced many times, and it lasts from hours to days, depending on the requirements and the microstructure tests [145]. Then, the solvent is removed by evaporation at the ambient temperature or at a low temperature in the oven.

- ***Solvent to sample ratio***

It is a topic on which researchers suggest different ratios, e. g. Aligizaki [151] gives a 100: 1 ratio of solution to sample volume; Day and Marsh [152] give a different ratio of 500:1 according to solvent to pore water ratio; Beaudoin *et al.* [153] applied the 100: 0.003 for the solvent to solid ratio. As seen, the solvent to sample ratio is very high, but if the solvent is changed regularly, a lower ratio of solvent to sample can be used [148].

- ***Influence of drying methods on the cement microstructures***

In order to study the effect of drying techniques on the microstructure of the cement paste, several works have been performed. In all of these studies, researchers compared drying processes and checked the effect of these dehydration techniques on the pore structure of the samples. Summarized literature on these techniques has been presented here separately.

- ***Oven-drying***

The oven-drying method shows that it causes changes to the pore structure of cement [150]. Galle says that the oven drying method affects the pore diameter and causes the overestimation of capillary porosity [154]. This method is inappropriate for analyses with techniques such as XRD, TGA and NMR, because of carbonation risk since the exposure of samples to higher temperatures (105° C) dehydrates ettringite, Afm and C-S-H partially [151].

The research in the field of the stopping hydration effect on the cement shows that each method has different results and effects on the sample's property. Regarding references, methods and their effect are assessed in **Table 9** briefly.

Table 9 *Assessment of drying techniques on the cement samples at the early age*

Technique	**process**	**duration**	**effect**	**Stops hydration**	**analyses**
D drying	vacuum	12 h	+ Removes the unbound water and preserves the microstructure [155]		
Freeze drying	Submerge in nitrogen liquid (-196° C)				
Oven drying	Heat evaporates the water content	24 h	−affects the pores' structure [150] + Preserves the composition	fast	
Solvent exchange	**Solvent replaces the water**	**12 – 48 h**	**−More pit on the surface compared to freeze-drying**		**SEM, XRD, and interferometry**
Vacuum drying		24 h	−Slow water removal		
Microwave drying	Electromagnetic radiation to heat the sample	< 1 h	−Removes the bound water	fastest	

In the current work the solvent exchange technique was used for stopping the hydration of the cement paste samples. The acetone was the solvent to be replaced with distilled water [156].

Each plastic bottle was filled with 100 ml of acetone, and a cement paste sample was put in the bottle. The volume ratio of cement to acetone was 1:25. Then, the bottles were shaken for 2 minutes. The bottles were positioned, with their lids open (for acetone to evaporate), in a fume hood for 4 hours. To maximize the effect of the solvent replaced with water in the cement pastes, the remaining acetone was emptied. The exchange cycle was repeated two more times for each

sample. After the third time, the acetone was changed for the last time, and the cement paste was kept in the solvent (**Figure 48**). Three samples of each cement paste variation were taken for stopping hydration.

Figure 48 *Cement paste sample in the acetone*

Since acetone can irritate the breathing system and skin if exposed to it even for a short time, using chemical safety goggles and face shield is recommended.

3.12. Contact angle and surface energy

The contact angle measurement and surface energy calculation were performed per NF EN 828: 2013 [62]. The measurement was carried out with the DROP SHAPE ANALYSER – DSA30 equipped with an ALLIED vision technology camera (**Figure 49**).

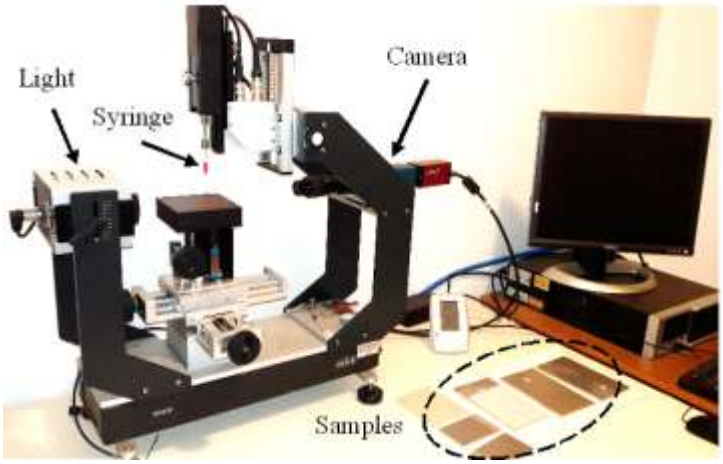

Figure 49 *Drop shape analyzer*

The standard liquids selected for measuring the contact angle required to calculate surface energy and their characteristics are presented in **Table 10**.

Table 10: *Contact angle test liquid's parameters* [62]

Test liquid	Surface tension (mN/m)	Disperse proportion (mN/m)	Polar proportion (mN/m)
Distilled water	72.80	21.80	51.00
Glycerol	63.40	37.00	26.40
Ethylene glycol	47.70	30.90	16.80

- ***Sample preparation***

All formwork, cement, or concrete samples were given an ultrasonic bath to remove all potential dust or foreign particles from the plates' surfaces before the contact angle and surface energy tests. Firstly, the ultrasonic bath container was filled with a solution of 50% distilled water and 50% ethanol. Afterward, the samples were placed in the solution of the ultrasonic bath container for 5 minutes. Finally, the samples' surfaces were dried with a blow dryer (**Figure 50**).

Figure 50: *Ultrasonic bath apparatus containing a solution of 50% distilled water + 50% ethanol.*

- ***Measurement of angle***

To measure the contact angle, a series of steps were carried out and recorded as follows:

- The temperature was recorded.
- The measuring surface was adjusted horizontally, at the same level as the camera and light source.
- The light, the optical device, and the analyzing system were switched on. By zooming in and out and calibrating the brightness, a clear image of the syringe's needle, droplet, and the surface in the monitor was obtained.

- The ideal scale was that the drop covers 2/3 of the image width (L). The dosing needles and the drop position are shown in **Figure 51**. Afterward, the focus was on obtaining a clear drop image.

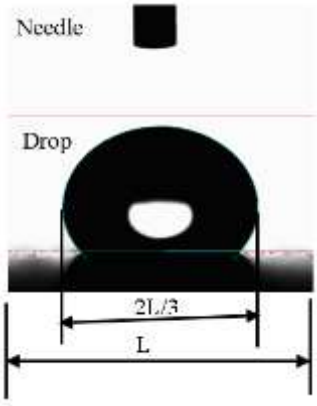

Figure 51: *The drop and needle position in the image scale*

- The plane surface of the sample was positioned horizontally in the lower half of the image.
- The syringe was filled with the specific liquid. It was verified that the syringe would not be contaminated.
- The drop size was between 2-6 µl depending on the viscosity of the liquid.
- Adjustment of the baseline was so that it intersects the triple point of the drop (**Figure 52**).

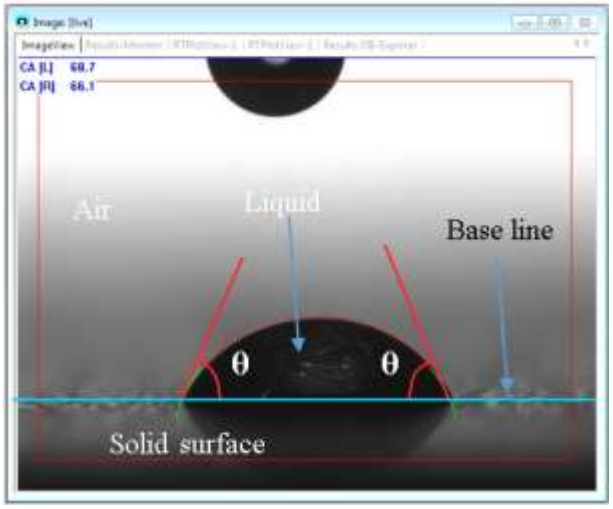

Figure 52: *Adjusting the baseline on the droplet*

- The time between placing the drop on the surface and measurement of the contact angle should not exceed 15 s. The dosing liquid should not get into reaction with the measuring surface. The recommendation for the measurement is twenty measurements, at one second gap between.
- To be sure of the homogeneity of the sample, ten drops of each liquid were measured on different areas of the surface (**Figure 53**).

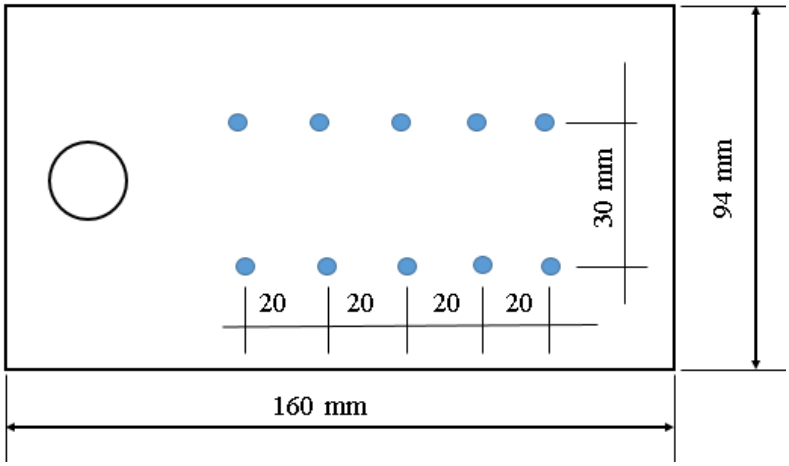

Figure 53: *The liquid drops' position (in blue color) on the formwork surfaces*

3.13. Microstructure analysis

3.14. Interferometric microscopy (IM)

The effect of contacting surfaces and their reciprocal influence can be determined by studying the 3D metrology of the cement paste surface. Interferometry microscope provides a non-contacting method for studying the surface. Interferometry is based on the study of the path of a single light beam divided into two identical beams, one of which impacts a surface to be analyzed. The difference in optical paths between the two beams, which are recombined, creates a phase difference. These interferences allow the reconstruction of the topography of a surface under study (**Figure 54**).

The Bruker® Contour GT-K interferometer is used for the surface roughness measurement. It has three objectives: two interferometric objectives – of magnifications 5 X and 50 X- and an optical objective, of magnification 10 X. Moreover, for each objective, three magnifications are available

through the system's lenses: 0.55 X, 1.0 X and 2.0 X; and it allows to work in monochromatic polychromatic light (white or green light respectively for the Bruker® Contour GT-K).

The characterization of surface roughness depends on the observation scale and the device used. However, it is necessary to determine the measuring parameters to obtain and observe the consistency in the measuring results. This is why a non-standardized procedure for deciding a measuring scale is planned.

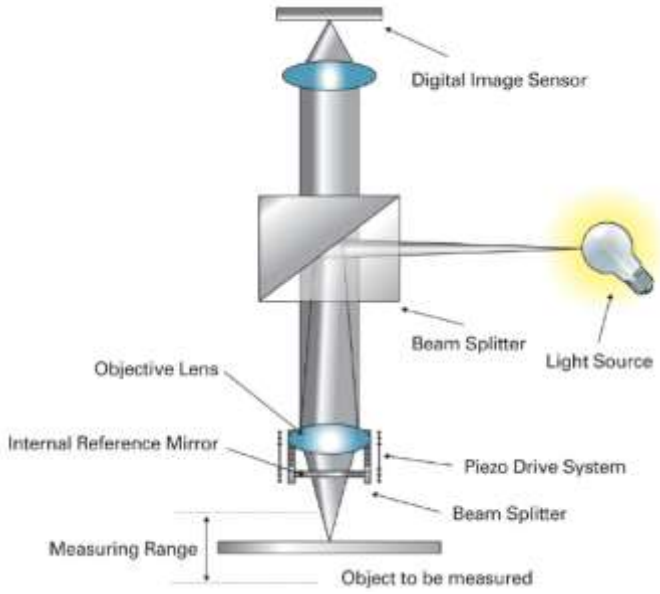

Figure 54: *An interferometer design* [157]

- ***Stitching method***

The arithmetic mean of the point surface parameters (Sa_1, Sa_2...) and the value of the same parameter (Sa_{stitch}) are compared. Besides, this last parameter (Sa_{stitch}) obtained from the point parameters following the adhering procedure for which an overlap is considered. The measurements of consecutive points with a 10% overlap zone are stitched together in this technique to provide practical information on the surface morphology.

For all cement paste samples and formworks, a 5×5 mm^2 of area, 130 points measurement/area, was measured at the middle of the sample (**Figure 55**).

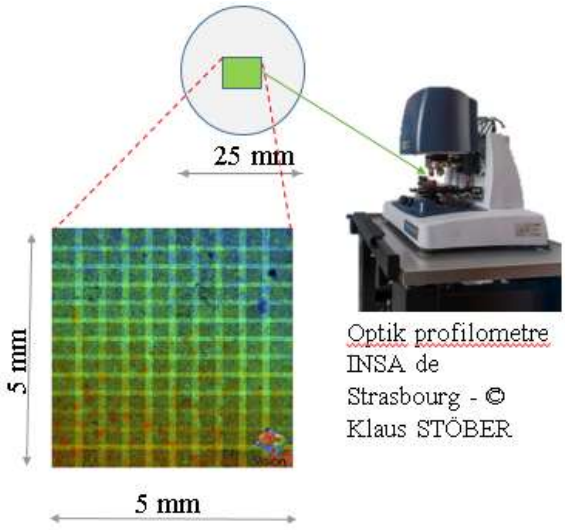

Figure 55: *Sampling, stiching method*

3.15. Scanning Electron Microscopy (SEM)

SEM microstructure analyses were carried out using the XL30 E-SEM Philips brand in backscattered electron mode (BSE) at a voltage of the order of 20.0 KV (**Figure 56**). The spot magnification was at 5. The images are obtained in slow scan mode of 3.36 ms. During measurement, the vacuum in the chamber was kept at 4-5 mbar.

Cement samples were taken out of acetone one hour before putting them in the microscope chamber. No touching of the surface of the sample was allowed. In every measurement, three cement samples with a diameter of 2.55 cm were placed in the chamber beside each other. The samples were adorned with a black scotch at the edge of each for easier identification from one another. 5 zones were studied on each sample; pictures were taken in different scales: 100, 250, 500, 800, 1000, 1500, 2000, and 2500 times.

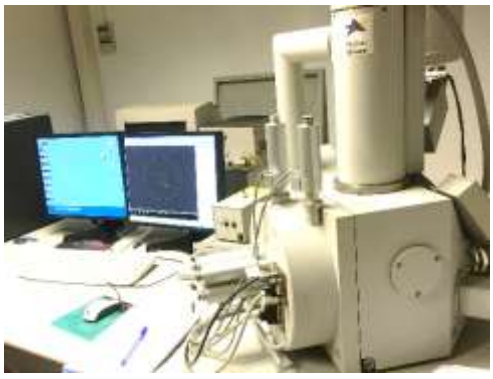

Figure 56: *E-SEM Equipment*

3.16. X-ray Diffractometry analysis (XRD)

For XRD analysis, D8 Advance Bruker® X ray diffractometer has been used in order to identify the solid phases of studied cement paste. The test mainly carried-out according to the Bragg–Brentano system, where the sample rotates at a diffraction angle ¨θ¨, and the detector rotates at the angle ¨2θ¨. All samples have been analyzed with a basic configuration and a Cu ceramic 2.2 kW X-ray tube and equipped with a Peltier detector and normal optic, with an angular range of 2θ = 10-70 degrees, at a radiation of λ=1,54182 Å, voltage of 25 kV and intensity of 25 mA (**Figure 57**). The measurement parameters are summarized in **Table 11**.

Table 11: *XRD measurement parameters*

	Type	Start position	End position	Steps	Step Operations
Parameters	Locked Coupled	10°	69.995°	0.017°	X Offset -0.175

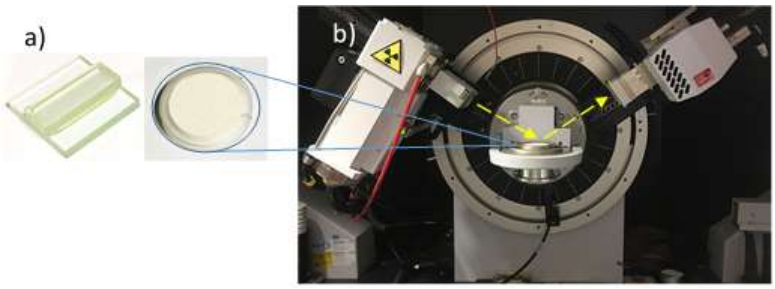

Figure 57 *a) Sample b) Bruker D8 Advance XRD machine in INSA Strasbourg*

3.17. Demolding tests

The demolding process was to be carried out only when the concrete gained sufficient strength, and this strength was to be at least two times more than the stress subjected to the concrete at the time of demolding [4]. To study the effect of various mentioned parameters (cement type, W/C ratio, formwork and coating materials) on adhesion between concrete and formwork, two types of tests were realized:

- Pre-crack demolding test on cement cylindrical samples with Ø = 2.54 cm.
- Pull-off demolding test on concrete cubic samples with a dimension of 10×10×10 cm^3

3.18. Pre-crack demolding test on cement paste samples

To realize the fracture mode I in the desired direction and the edge, a preconditioning crack growth environment was prepared as follows:

- The middle of the formwork plate was taped with scotch tape along its length.
- Then, the edge of the molds was placed 6 mm forward on the scotch tape (**Figure 58**).

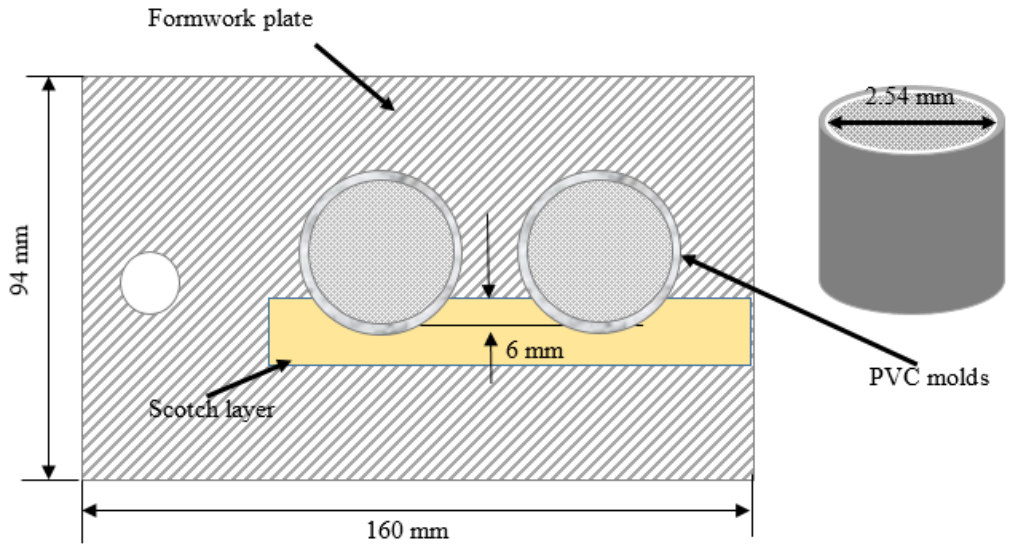

Figure 58: *Cement paste samples' preparation*

After 24 hours, the samples were ready for the demolding test. The test was conducted in mode I of fracture. The formwork plate was fixed to the Universal test bench- BED 100, test machine, at both edges to the table. The traction force was applied through a steel wire connected to the traction arm and anchor bolt on the sample. The sample placement and the traction force application are shown in **Figure 59**.

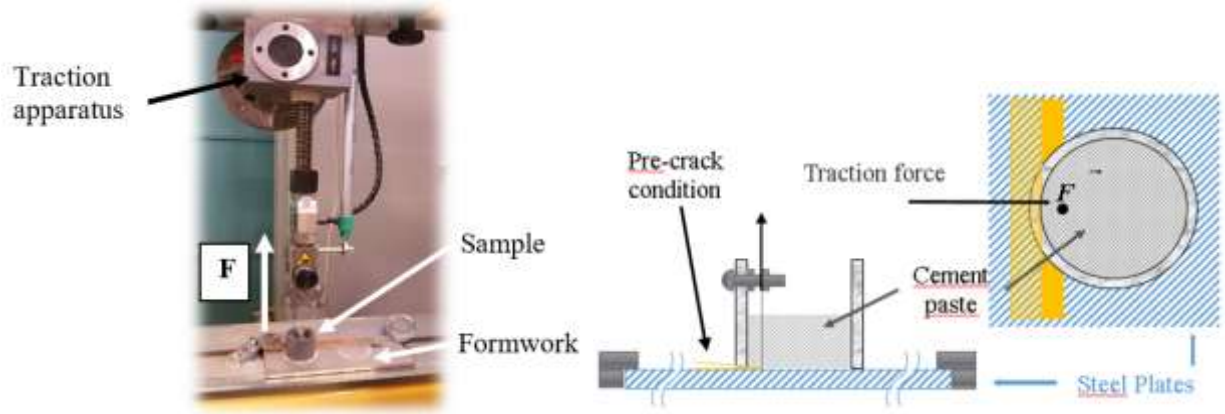

Figure 59 *Demolding pre-crack test set-up* [39]

The setting parameters of the test were as follows:

- The load application = 0.1 mm/s
- The maximum displacement (D_{max}) = 90mm

Temperature and humidity were recorded every time. The traction force was applied to the sample through the steel wire till the mold was demolded. The test result was plotted in a force-displacement graph, and the evolution of the force-displacement values was recorded in an excel sheet at the same time.

Following the demolding test, the cement paste samples were carefully removed from the PVC molds (by fastening the mold and pressing the cement paste with a plastic stick) for further dehydration, quantitative examination of its component material properties, and surface microscopic analysis.

3.19. Pull-off demolding test on concrete samples

This experiment focuses on the behavior of the formwork against concrete. The stainless steel formwork (F17) was used for the current study. The pull-off demolding test aims to show how different formworks behave in contact with different concrete mix designs. The following results are to be analyzed:

- The amount of the mechanical force to separate the formwork from the concrete
- The porosity and crack development on the concrete surface
- The scratches on both concrete and formwork surfaces
- The usage repeatability of the formwork after each treatment

Besides, the variable parameters were w/c ratio, cement type, formworks and release agents and two other polymeric barriers.

This original experimental device aims to measure the forces developed during formwork removal. The test scale and size were optimized for lab conditions.

This test was performed in the SHIMADZU multi-purpose testing machine. The concrete samples were placed and fixed on the SHIMADZU machine with four long nuts and bolts. Then, a lateral force was applied (**Figure 60**) to the back of the steel plates with the help of a steel clamp to:

- Create the fracture condition consisting of mixed fracture modes I and II.

- Get a more simultaneous demolding process.

The lateral force was optimized with our scale of work equal to 2 KN. The amount of lateral force was measured thanks to a load cell/dynamometer (Model: H3-C3-1.5t-3B, Capacity: 1.5t).

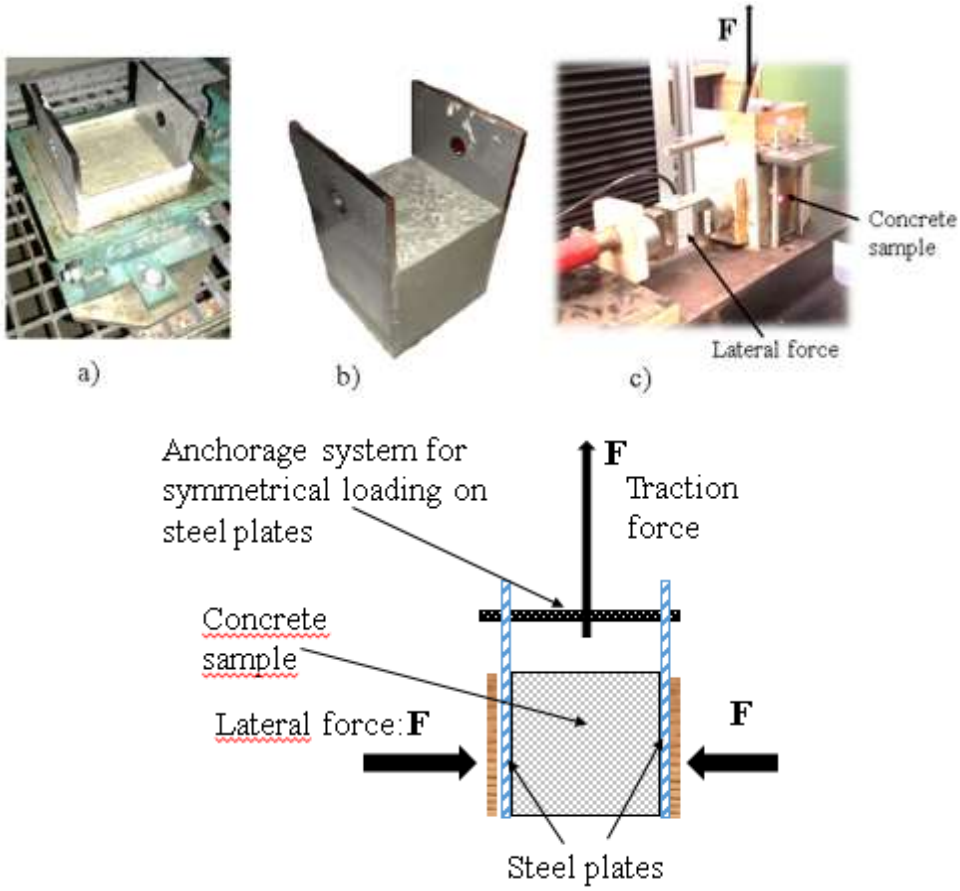

Figure 60: *a) Concrete sample after casting, b) concrete sample ready for test, c) Demolding test setup*

Conclusion

The experimental methods carried out as part of this work have been grouped together in **Table 12**. The used methods for the characterization of materials, cement paste, and concrete were conducted in accordance with the standards. The adhesion properties between the cementitious materials and the formwork were measured with procedures developed especially for the ERGOFORM project.

Table 12 *Conducted tests and their methods*

Type of property			**Standard/equipment**
Materials characterization	Cement	Specific gravity	ASTM C188-17 [158]
		Bulk density	
		Laser granulometry	Mastersizer 3000E
		Normal consistency and setting times	NF EN 196-3 [159]
		SEM and EDs analysis	E-SEM based Philips XL30
	Aggregates	Bulk density	NF EN 1097-6 [160]
		Specific gravity and water absorption	
		Size distribution	NF EN 933-1 [161]
	Water	pH value	pHM210
Concrete	Fresh properties	Workability	EN 1015-3 [162]
		Fresh density	EN 1015-6/A1 [163]
	Mechanical properties	Compressive strength	EN 1015-11 [164] EN 12390-6 [165]
Microstructure analysis	Surface energy	Contact angle and surface energy	DROP SHAPE ANALYSER – DSA30 equipped with an ALLIED camera
	Surface roughness	Interferometric microscopy (IM)	Bruker® Contour GT-K interferometer
	Surface microstructure	Scanning Electron Microscopy (SEM)	E-SEM based Philips XL30
	Crystalline phases	X-ray Diffractometry analysis (XRD)	D8 Advance Bruker®
Adhesion or demolding force	Demolding force	Pre-crack demolding test	Universal test bench- BED 100
		Pull-off demolding test	Shimadzu 100 kN machine

CHAPTER # 3 : Characterization of cement paste/concrete components

This chapter describes the results for the characterization of cement, sand, fine coarse and coarse aggregates, and water.

The first part of this chapter present the cement characterization through bulk density, specific gravity, modulus of fineness, normal consistency and setting times. Moreover, the scanning electronic microscopy (SEM), and laser granulometry were used in order to evaluate the microstructure of cement powder.

The second part of this chapter is focused on the results through the bulk density, specific gravity, water absorption and size distribution analysis of three fractions of aggregates (fine, fine coarse and coarse aggregates). The pH value of water used for the preparation and curing of cement paste/concrete specimens is checked to ensure their quality.

1. Characterization of cement

Two types of Portland Cement (PC) of CEM I 52.5 N and CEM II/B-S 42,5 N CE CP1 NF produced by HEMING according to the standard NF EN 197-1/A1 [75] was used for the preparation of cementitious specimens. The following tests were carried out to characterize the behaviors of cement.

1.1. Laser granulometry

To measure the surface area and particle size of the used cement, from each cement five samples were tested using laser granulometry apparatus. The surface area of both CEM I and CEM II/B are 4509±157 (cm^2/gr) and 4054± 182 (cm^2/gr), respectively. The surface area and particle size distribution of both types of cement are identical. As it is seen, the results are in accordance with the NF EN 197-1/A1 [75], Besides, the obtained surface area of cements are in accordance with the technical form of the producer company, HEMING [166] and is in good accordance with the literature [167]. The Portland Cement Association (PCA), and ASO cement which recommends the usage of cement with the surface area of > 2500 cm^2/gr. Furthermore, **Figure 61** shows that laser granulometry analysis of particle size distribution reveals that both cements have the same grinding quality and sizes.

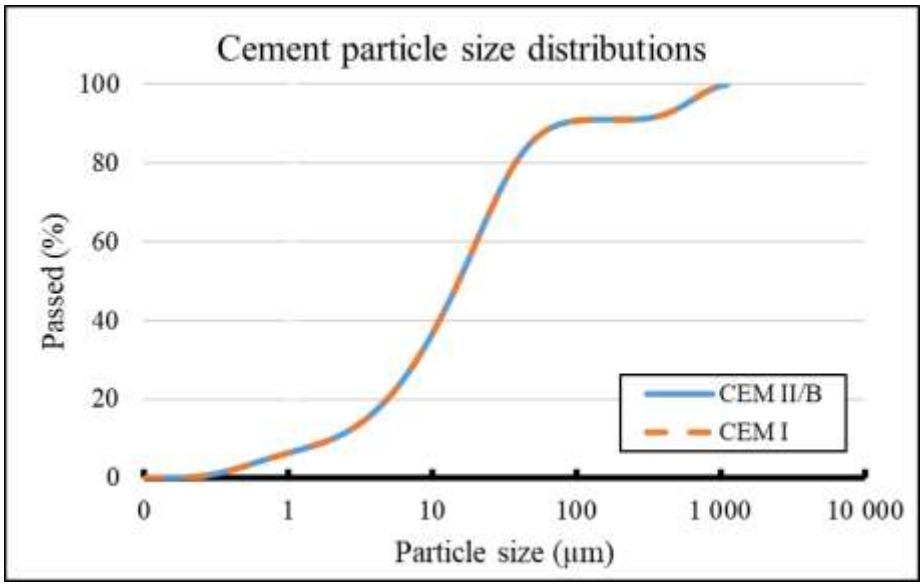

Figure 61: *Size distribution of CEM I and CEM II/B*

In addition, SEM image analysis was conducted on CEM I 52.5 N and CEM II/B cements, in order to analyze the microstructure of cement particles. The images were shown in **Figure 62** reveal that both types of Portland present the same grinding quality, However, some of grains of CEM II/B are greater than CEM I.

CEM I

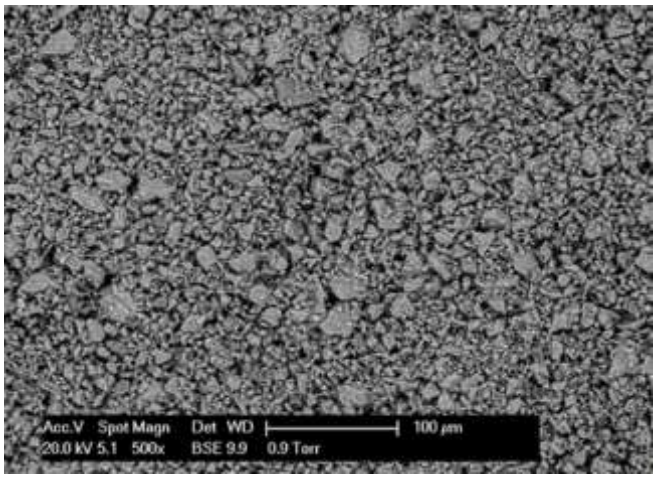

CEM II/B

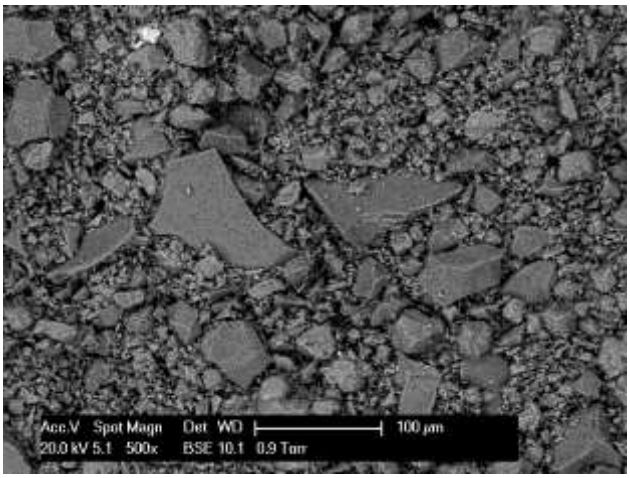

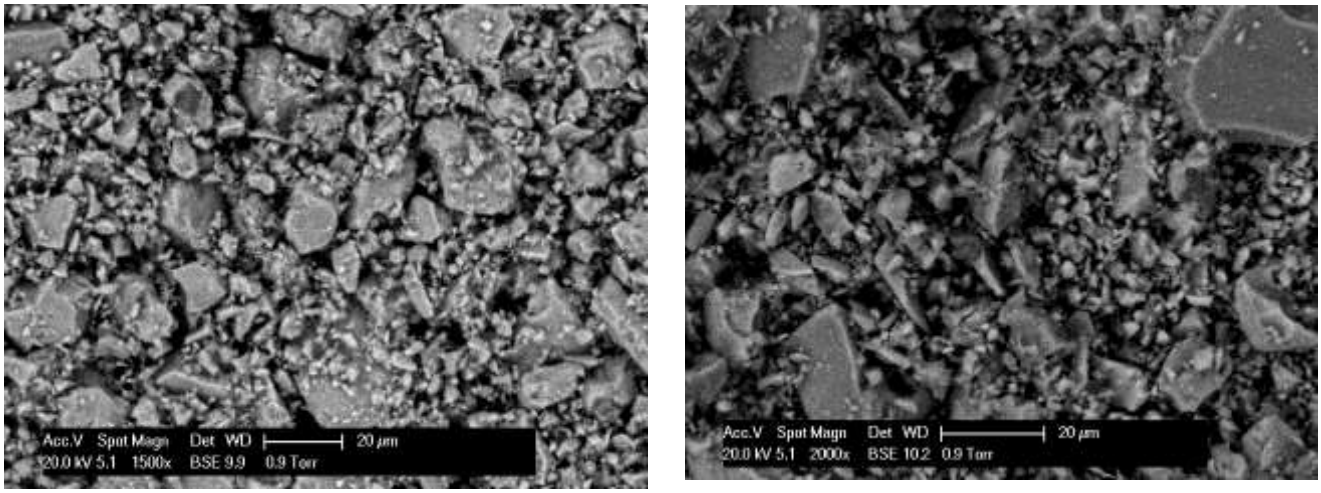

a b

Figure 62: *SEM observations of a) CEM I 52.5 N b) CEM II/B*

1.2.Specific gravity and bulk density

In order to measure the specific gravity and bulk density of cements, 3 samples of each cement, CEM I 52.5 N and CEM II/B, were tested. The obtained results are presented in **Table 13**.

Table 13: *Specific gravities and bulk densities of both type of cement*

Cement type	**Specific gravity**	Bulk density (gr/cm^3)
CEM I	3.169 ±0.015	3.110 ±0.010
CEM II/B	3.105 ±0.027	2.985 ±0.012

The average specific gravities of CEM I and CEM II/B are 3.167 and 3.105, respectively. It can be seen that the CEM II/B presents slightly lower specific gravity than the CEM I. Moreover, the same trend was observed for the bulk density, whereas, the CEM I present a higher bulk density than CEM II/B one. It can be explained through the lower detected surface area of CEM II/B. Moreover, the specific gravity and bulk density of Portland Cement ranges from 3.10 to 3.25 as per Portland Cement Association [168]. Therefore, the CEM I and CEMII/B answer properly to the recommendation proposed by PCA [168].

1.3.Normal consistency and setting times

In order to observe the normal consistency of cement, the test has been repeated on the cement paste containing various amounts of water until the paste found viscosity that vacant plunger penetrates to a depth of 6 ±1 mm from the bottom of the mold according to EN 196-3 standard [136]. The tests were realized in two different labs, but the temperature was maintained according

to the requirement of the mentioned standard (20 ±2 °C) and the relative humidity was about 40%. The results of normal consistency on cement paste for both CEM I 52.5 N and CEM II/B cement are shown in **Table 14**.

Table 14: *water/cement ratio for normal consistency of CEM I 52.5 N and CEM II/B cement paste*

Cement type	w/c ratio	Plunger Penetration (mm)
CEM I	0.330	6.1
CEM II/B	0.321	6.0

As shown in **Table 14** that the CEM I answer to the normal consistency with a slightly higher w/c ratio compared to the CEM II/B one. The lower amount of mixing water needed by CEM II/B for the normal consistency can be attributed to its coarser ground fineness. Besides, the normal consistency of CEM I and CEM II/B are in accordance with the literature [167].

After finding the normal consistency, the initial and final setting times were measured and their results are shown in **Table 15**.

Table 15: *Setting times of CEM I 52.5 N and CEM II/B cement*

Sample	CEM I 52.5 N		CEM II/B	
	Initial (min)	**Final (min)**	**Initial (min)**	**Final (min)**
Average	**131 ±2.9**	**275 ±3.8**	**124 ±4.5**	**258 ±6.8**

The obtained results present that the initial setting time for CEM I and CEM II/B cement is 127 and 124 minutes. Besides, the final setting time of CEM I and CEM II/B cement is 275 and 258 minutes, respectively. These values were confirmed by previous studies which reveal that the initial setting time of Portland cement should not be earlier than 45 min and the final setting time should not exceed 6.5 hours [169]. On the other hand, a slight difference was observed between the outcomes of setting times of both types cements. This can be attributed to the coarser behaviors of CEM II/B cement compared to the CEM I.

It must be noted that both types of used cement fulfil the recommendations and requirements of international standards.

2. Characterization of aggregates

Three different sizes of aggregates were used as fine and coarse aggregates. The following tests were performed to characterize the behaviors of both fine and coarse aggregates.

2.1.Size distribution

The results of the sieve analysis and distribution curves of aggregates are shown in **Figure 63**.

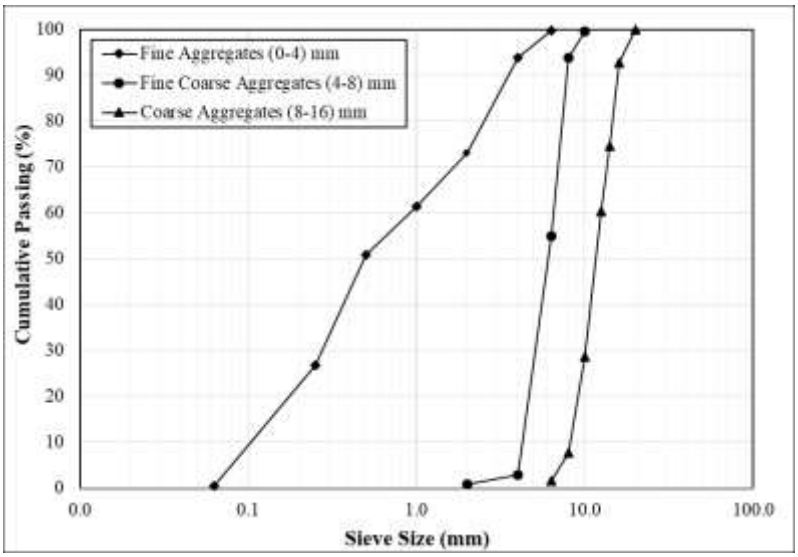

Figure 63: *Size distribution curve for fine and coarse aggregates*

The obtained results of sieve analysis of aggregates clearly present that the curves are uniform and no gaps were seen. In addition, this phenomenon was confirmed by the ASTM C33 [170] standards as shown in **Figure 64**. It can be confirmed that three fractions of used aggregates can be used for the production of concrete.

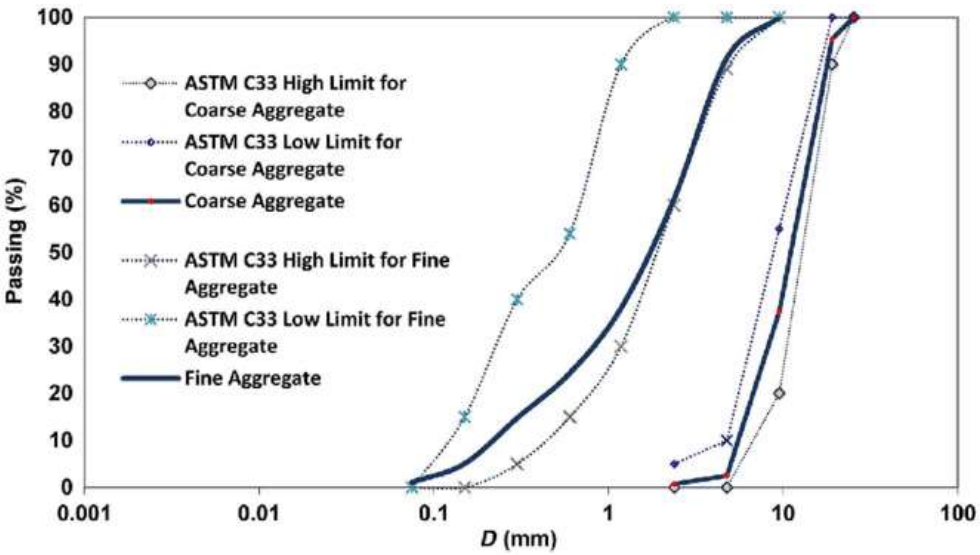

Figure 64: *Standard size distribution curve* [170]

2.2.Specific gravity and water absorption

The specific gravity and water absorption of aggregates are measured based on three samples for each fraction of aggregate. Experimentally obtained results are summarized in **Table 16**.

Table 16: *Specific gravity and water absorption (WA) values of fine aggregates, fine coarse aggregates, and coarse aggregates*

Aggregates	Specific gravity	Apparent specific gravity	WA (%)
Fine aggregates (0-4 mm)	2.589±0.004	2.660±0.014	1.07±0.20
Fine coarse aggregates (4-8 mm)	2.504±0.004	2.617±0.008	1.72±0.15
Coarse aggregates (8-16 mm)	2.566±0.015	2.639±0.012	1.09±0.01

The aggregates used in France were calcareous limestone with round surfaces, but the aggregates utilized in Afghanistan were calcareous crushed stone. In addition, the aggregates used in Afghanistan had slightly higher specific gravity compared to the ones in France. On the other hand, both types of aggregates present almost the similar coefficient of water absorption.

2.3.Bulk density

The bulk density of three fractions of aggregates are conducted according to standard NF EN 1097-6 [140]. The experimental results are an average of three samples for each fraction of aggregates. The results are summarized in **Table 17.**

Table 17 *Bulk and compacted bulk densities of fine aggregates, of fine aggregates, fine coarse aggregates, and coarse aggregates*

Aggregates	Bulk density (kg/m^3)	Compacted bulk density (kg/m^3)
Fine aggregates (0-4 mm)	1735±12	1821±7
Fine coarse aggregates (4-8 mm)	1495±21	1574±2
Coarse aggregates (8-16 mm)	1516±2	1612±1

The obtained results reveal that there is a difference between the bulk densities of aggregates used in both laboratories. The aggregates used in Afghanistan have lower bulk densities compared to the ones used in France. This is due to the microstructure, maximum sizes, and size distribution of aggregates.

3. Characterization of water

Tap water available inside the laboratory of INSA Strasbourg was used for the preparation and curing of samples. Three samples were tested to find the pH value of water and the recorded results are shown in **Table 18**.

Table 18: *pH value of water*

Sample #	pH value
1	7.24
2	7.21
3	7.23
Average	7.23 ±0.012

The pH values of water indicate that water is neither acidic and nor alkaline. Thus the pH of the water complies with the standard and could be used for both preparation and curing of cement paste and concrete samples.

Conclusions

Overall, the results of material characterization present that cements, aggregates, and water used meet the required standards and are suitable for having proper mix designs. However, some slight difference were seen for both types of cements.

- The CEM II/B is slightly coarser (with a surface area of 4509±157 cm^2/gr) than CEM I 52.5 (with a surface area of 4054± 182 cm^2/gr). It explains the amount of water used for the normal consistency of CEM II/B cement that is slightly less compared to CEM I 52.5.
- The physical and mechanical properties of sand and aggregates used for concrete elaboration are in well accordance with the aforementioned standards.
- The results of fineness modulus for fine aggregates (sand) are according to the EN 12620+A1 [171] standard with the range of (2.4 - 4.0).

Finally, it can be concluded that the characterized material can be used for the production of cement paste and concrete mix design of this study.

CHAPTER # 4 : Characterization of cement paste samples and concrete

A combination of experiments was conducted to understand the functionality of formwork and its physiochemical characteristics on the demolding procedure. Five dissimilar types of formwork were used for the surface material coating and its functionality: F17-Ref reference formwork, PET and C20C27 polymeric coatings, mineral oil and vegetable oil as release agents (F17-MO and F17-VO). In terms of mix design, the w/c ratio and cement type were changed to analyze the effect of these variation on demolding force.

Furthermore, microscopic examinations were performed. The surface morphology of formworks and cement pastes was studied via interferometry. Besides, the crystallography and chemical composition of the cement paste samples at the early stage of hydration (24 hours) was observed under environmental scanning electron microscopy (SEM) and X-ray diffractometry (XRD).

The nomenclatures of formwork plates, cement paste, and concrete samples against all the formworks used in the experiments are presented in **Table 19**.

Table 19: *nomenclature of the formworks, cement paste, and concrete samples*

Variations	**Formwork** 	**Cement paste samples** 	**Concrete samples** 
Reference plate	F17-Ref	Cem-Ref	Con-Ref
Mineral oil coated	F17-MO	Cem-MO	Con-MO
Vegetable oil coated	F17-VO	Cem-VO	Con-VO
PET coated	PET	Cem-PET	Con-PET
C20C27 coated (LPIM)	C20C27	Cem-C20C27	Con-C20C27

1. Characterization of the formwork surface and its effect on the demolding force

1.1.Morphological characterization of used formworks

The formwork plates provided by the project partner named Hussor were considered as reference formwork (F17-Ref). Besides, no coating or preliminary treatment was performed on reference formwork during experimental procedure, these formworks used in initial state. For the surface characterization, two surface parameters, S_a (arithmetic mean height) and S_q (root mean square height) were measured. As the interferometry microscope (*IM*) functions by the interference of waves (light, radio, or sound waves) to measure the surface roughness parameters, therefore, the material's transparency is an obstacle. However, due to the transparency of both PET and C20C27 coatings, both layers were surface-metalized prior to morphological analysis to alleviate the problem. The metallization thickness is between 5 to 10 nm, which is ignored in the analyses of IM.

The obtained results of formwork surfaces roughness are summarized in ***Table 20***. The outcomes reveal that the roughest surface is recorded for reference formwork (F17-Ref), (S_a = 4.56 ± 0.39 µm, S_q = 5.663 ± 0.467 µm). It must be noted that there was no surface treatment applied to the reference plates. Moreover, to compare the polymeric coated formwork's surface, the PET layer had the lower roughness value comparing to C20C27 of S_a = 0.11 ± 0.02 µm, S_q = 0.14 ± 0.03 µm, and S_a = 0.93 ± 0.23 µm, S_q = 1.17 ± 0.37 µm, respectively. Roughness values of S_a and Sq for reference formwork and polymer-coated ones and their interferometric 2D and 3D images are summarized in ***Table 20*** and ***Figure 65***.

Table 20: *Obtained roughness parameters of formworks through Interferometry microscopy*

Formwork surface	**S_a (nm)**	**S_q (nm)**	**Remarks**
F17-Ref	4563 ± 389	5663 ± 467	No treatment
C20C27	931 ± 235	1176 ± 370	Metalized (gold)
PET	108 ± 21	141 ± 30	Metalized (gold)

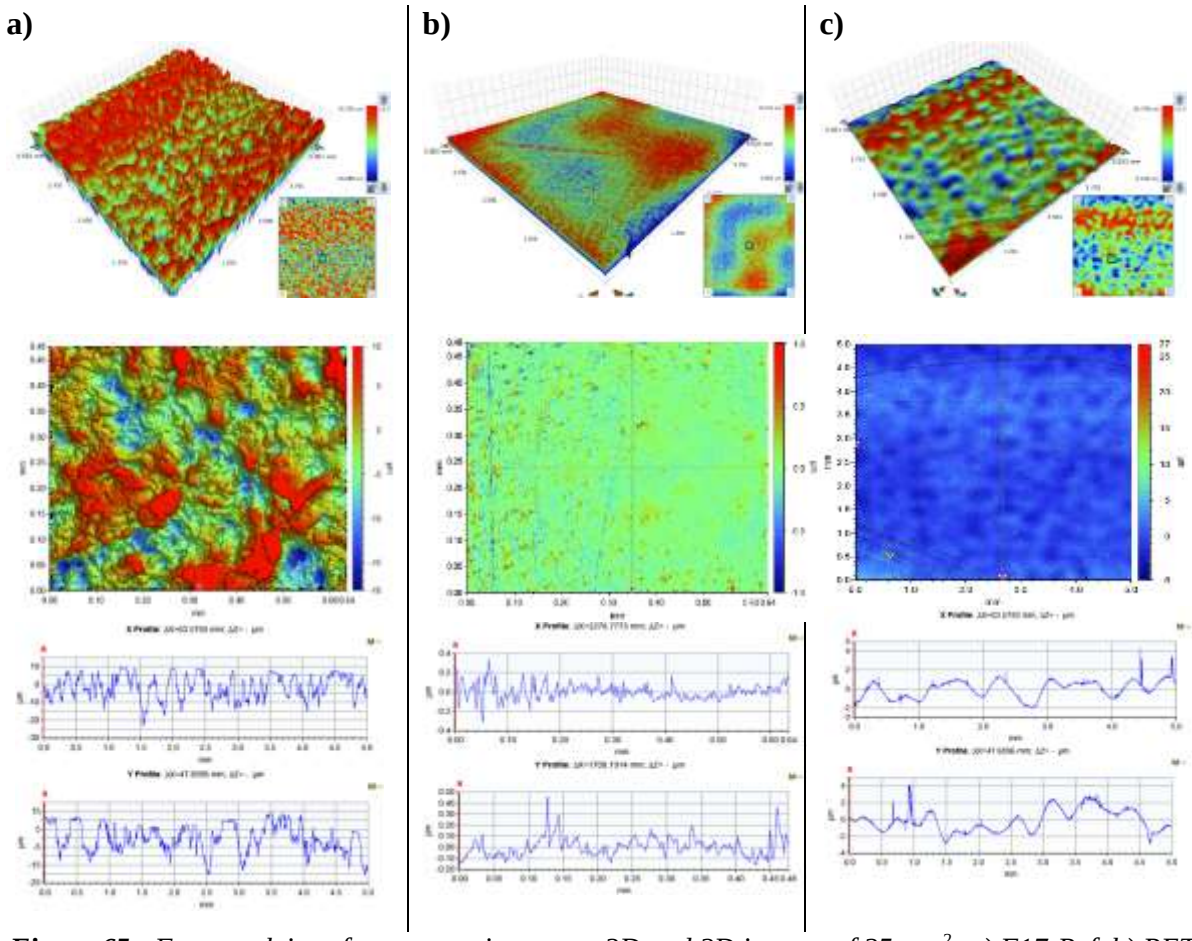

Figure 65 : *Formwork interferometry microscopy 3D and 2D images of 25 mm²; a) F17-Ref, b) PET & c) C20C27*

The obtained results for polymeric coated surface are in well accordance to the literature. Spitz *et al*. [17] measured surface parameters on polymer coated forms. The authors investigated two types of polymeric coated surface: polypropylene PP and polytetrafluoroethylene PTFE. The values of S_a and S_q parameters were estimated to be: 0.8 ± 0.1 µm and 1.0 ± 0.1 µm for PP coating, respectively, which compared to 108 ± 21 nm, 141 ± 30 nm for PET and 931 ± 235 nm, 1176 ± 370 nm for C20C27 (***Table 20***).

1.2.Demolding force

A series of mechanical demolding experiments were conducted to determine the demolding force value at the time of removing the formwork from the cement paste or concrete sample.

1.2.1. Pre-crack demolding test on cement paste

The formworks F17-Ref, PET, C20C27, F17-MO, and F17-VO demolding functionality was investigated. Moreover, to analyze the effect of cement type and W/C ratio on demolding force, two types of cement (CEM I and CEM II/B) and three variation of W/C ratio (0.3, 0.4 and 0.5) were applied. **Figure 66** summarizes all of the variants that were chosen for this test series.

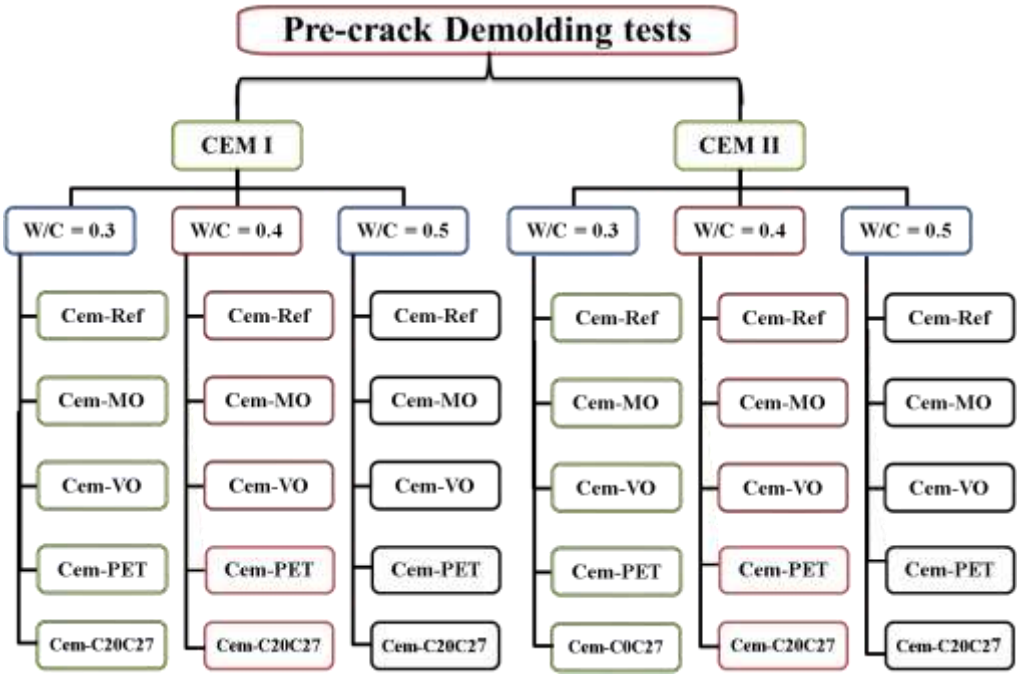

Figure 66 *Pre-crack demolding test variables*

The demolding force, named F_d, was obtained through force-displacement diagram of pre-crack demolding test on cement paste samples. One of force-displacement recorded diagram for CEM I with a W/C ratio = 0.5 is presented in **Figure 67**.

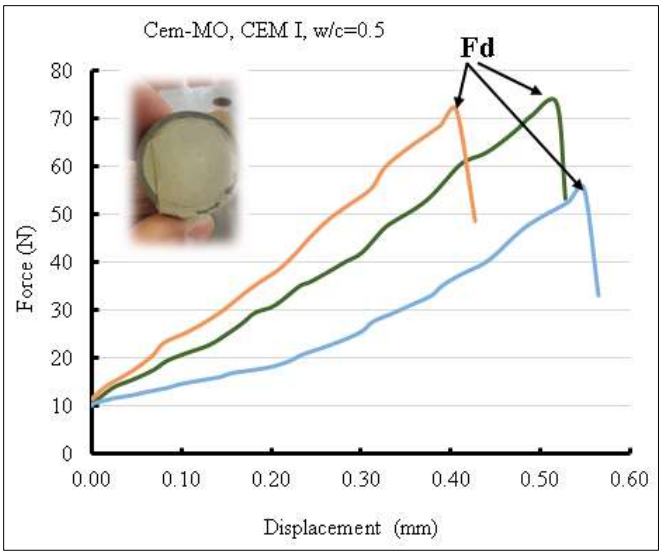

Figure 67: *Force-displacement diagram of the pre-crack demolding test; F_d - the force at the moment of demolding*

It must be noted that for each mentioned variation (cement type or W/C ratio), 10 tests were carried out. Moreover, in the analysis, the traction data from the samples that had cohesive failure were not taken into account. This can be explained that generally the demolding force is attributed separation of formwork from cement paste but in this case the fracture of cement paste is included to the demolding force as well. **Figure 68** shows a sample of demolding of cement samples with adhesive failure (a) and cohesive failure (b).

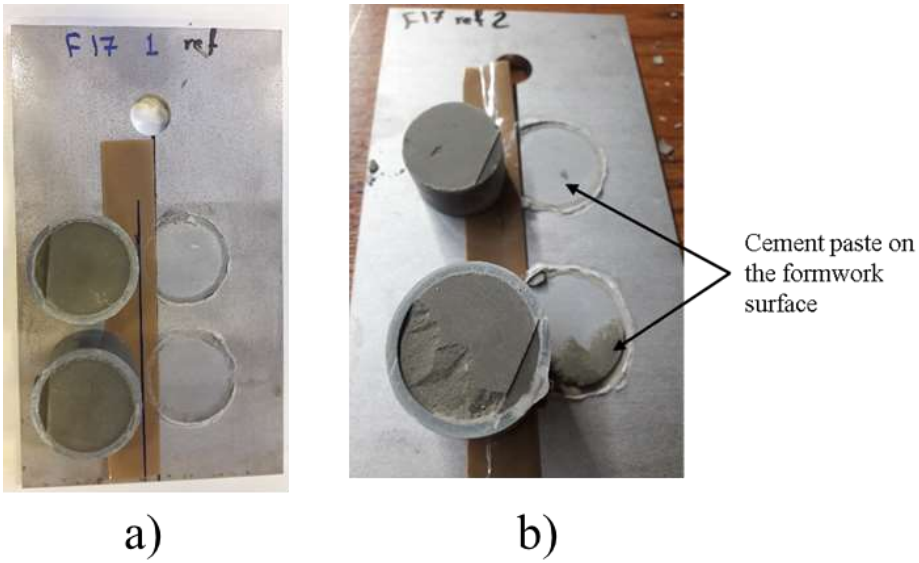

Figure 68: *a) adhesion failure, b) cohesion failure*

- ***Effect of cement type***

For well understanding of the various parameters, the obtained experimental result through pre-crack demolding are separated according to different W/C ratios. The average results for demolding force are presented in **Table 21**.

Table 21: *Adhesion forces of cement pastes*

Sample	**Cement type**	**F_d (N) with its corresponding w/c ratio**		
		0.3	**0.4**	**0.5**
Cem-Ref	CEM I	122.70 ± 18.18	124.31 ± 26.71	103.39 ± 12.53
	CEM II/B	133.64 ± 20.73	122.67 ± 16.86	136.97 ± 38.68
Cem-C20C27	CEM I	101.25 ± 2.30	107.25 ± 23.30	60.50 ± 8.85
	CEM II/B	71.00 ± 13.49	71.25 ± 12.45	48.50 ± 17.54
Cem-PET	CEM I	50.00 ± 15.60	36.75 ± 4.03	29.00 ±4.24
	CEM II/B	59.75 ± 11.90	9.27 ± 1.54	27.50 ±3.32
Cem-MO	CEM I	17.20 ± 4.05	35.22 ± 5.99	35.28 ±6.72
	CEM II/B	31.65 ± 22.97	36.33 ± 5.92	32.86 ±8.58
Cem-VO	CEM I	**F_d < 10 N**	**F_d < 10 N**	**F_d < 10 N**
	CEM II/B	**F_d < 10 N**	**F_d < 10 N**	**F_d < 10 N**

In addition, the outcomes were presented in the following figures:

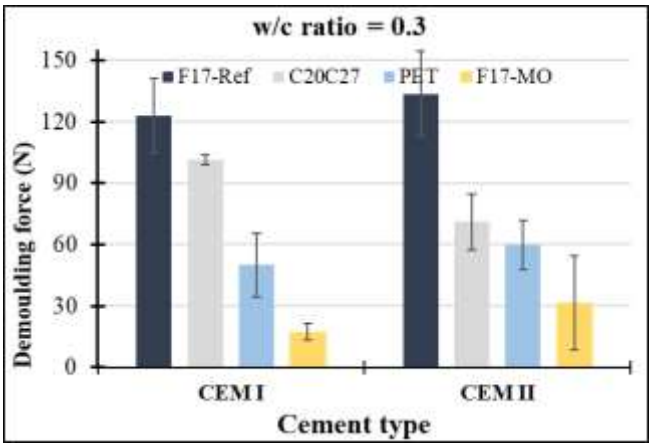

a)

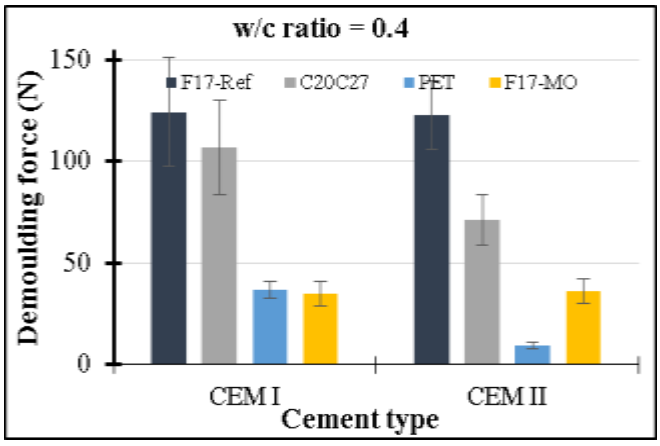

b)

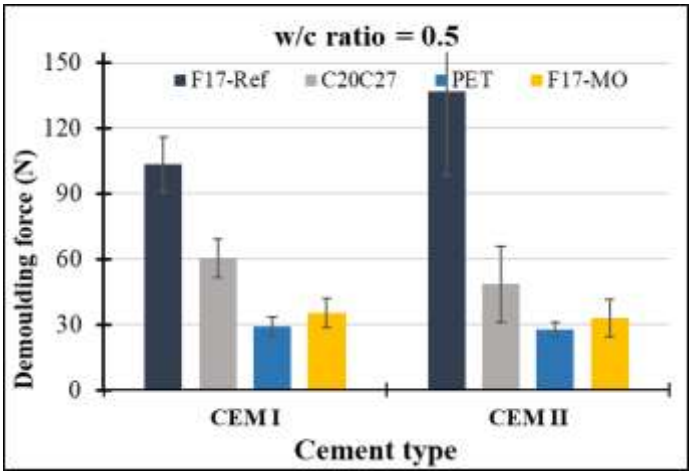

c)

Figure 69 *Pre-crack demolding test results categorized according to different the w/c ratio: a)w/c = 0.3, b) w/c = 0.4, and c) w/c = 0.5*

In **Figure 69** and **Table 21**, regarding to the effect of cement type, it can be seen that the maximum F_d belongs to the F17-Ref (F_d = 133.64 ± 20.73 N) with CEM II/B compared to CEM I. Moreover, the same trend can be seen for the cement paste against C20C27. Nevertheless, for w/c of 0.3 and 0.5 the cement type doesn't present any effect on demolding force of cement paste sample against PET coated formwork (**Figure 69a** and **Figure 69c**), however, the the demolding force decreases by changing the CEM I by CEM II for a w/c ratio of 0.4 (**Figure 69b**). In addition, it reveals that there is no effect of cement type on the demolding force of cement samples against F17-MO and F17-VO. It must be noted that F_d for F17-VO were not considered because of its small value (F_d < 10N), which was not recorded by the test apparatus.

- ***Effect of the w/c ratio***

In this section the effect of w/c ratio on demolding force of cement paste samples against various type of coated formwork are presented. The demolding force for different w/c ratios for both types of cement are graphically illustrated in **Figure 70**:

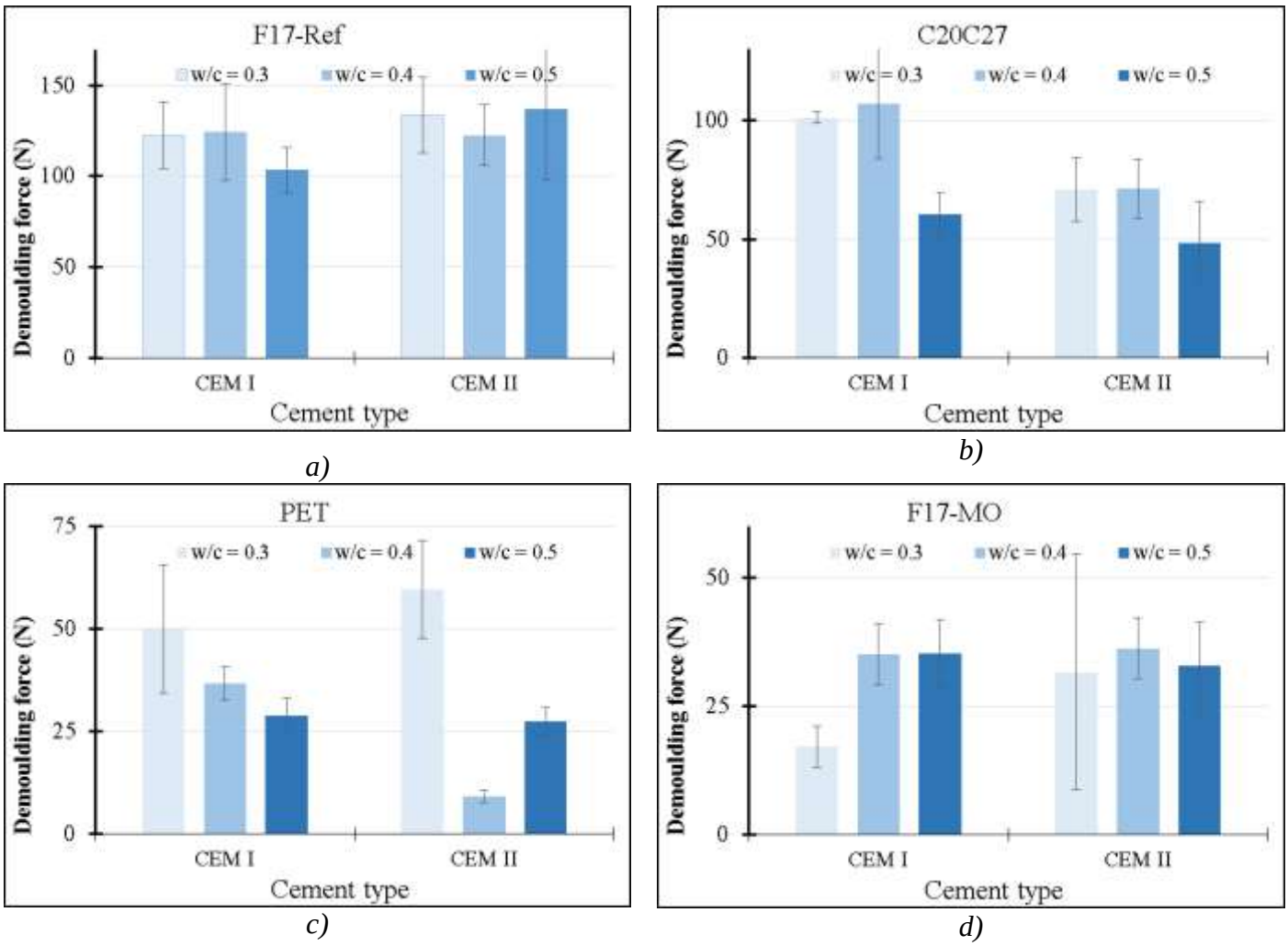

Figure 70: *Pre-crack demolding test results as per formwork type and cement: a) F17-Ref, b) C20C27, c) PET, and d) F17-MO*

The obtained results in **Figure 70a** indicate that the w/c ratio don't present any effect on demolding force of cement paste against reference formwork (F17-Ref without any treatment and coating) because of the large values of standard deviations. Conversely, for the C20C27 the demolding force with w/c = 0.3, 0.4 are recorded 101.25 ± 2.30 N and 107.25 ± 23.30 N respectively. However, when the w/c ratio increased to 0.5, the F_d was decreased by 40 % (60.50 ± 8.85 N). Moreover, this 40% reduction in F_d was noticed in PET (w/c ratio = 0.4) (**Figure 70**). The lower F_d is recorded for the CEM I again mineral oil coated formwork, whereas, the w/c ratio in CEM II doesn't affect the demolding force. At the work of C. Chadfeau [39], the separation force (w/c ratio = 0.4, CEM II/B) obtained from the F17-Ref was 145 ± 47 N, and for C20C27, 98 ± 24 N, which had the same experiment condition, were ≈ 20% and 28% higher, respectively. It can be concluded that effect w/c ratio is dependent of the type of formwork, wheareas, the demolding

force doesn't change for cement samples against F-17, however, it can be seen that the F_d decreases proportionally with increase of water content for CEM I against PET formwork.

- ***Effect of release agent***

The obtained experimental results with all variation (two cement type, three w/c ratios and five different formwork) reveal that the demolding or adhesion force decreases significantly by interoducing the release agents. It can be explained that the application of release agents on the formwork surface causes a surface roughness modification [66]; it fills the cavities on the formwork surface, resulting low demolding force compare to those without release agents. However, on a smooth surface, the effect of the release agent is different, it creates a barrier of variable thickness between the formwork and the concrete, which increases the micro-roughness of the formwork surface and, therefore, the concrete surface.

Moreover, in terms of difference in release agents, the obtained results indicate that the vegetable release agent ensures better demolding in terms of low demolding force compared to the mineral release agent. The experimental results are in well accordance with those of literature [14, 38, 39, 40, 67]

It must be noted that in all tests the F_d for the cement paste samples against F17-VO formwork were very small (F_d < 10N), which could not be recorded by the test apparatus.

The average results for demolding force are presented in **Table 22**.

Table 22: *Adhesion forces of cement pastes*

Sample	**Cement type**	**F_d (N) with its corresponding w/c ratio**		
		0.3	**0.4**	**0.5**
Cem-Ref	CEM I	122.70 ± 18.18	124.31 ± 26.71	103.39 ± 12.53
	CEM II/B	133.64 ± 20.73	122.67 ± 16.86	136.97 ± 38.68
Cem-C20C27	CEM I	101.25 ± 2.30	107.25 ± 23.30	60.50 ± 8.85
	CEM II/B	71.00 ± 13.49	71.25 ± 12.45	48.50 ± 17.54
Cem-PET	CEM I	50.00 ± 15.60	36.75 ± 4.03	29.00 ±4.24
	CEM II/B	59.75 ± 11.90	9.27 ± 1.54	27.50 ±3.32
Cem-MO	CEM I	17.20 ± 4.05	35.22 ± 5.99	35.28 ±6.72
	CEM II/B	31.65 ± 22.97	36.33 ± 5.92	32.86 ±8.58
Cem-VO	CEM I	**F_d < 10 N**	**F_d < 10 N**	**F_d < 10 N**
	CEM II/B	**F_d < 10 N**	**F_d < 10 N**	**F_d < 10 N**

The obtained results are in well accordance to those of literature. Mazkewitsch and Jaworski [172], studied the adhesion of concrete to formwork in vertical bond strength after one day and three days. The authors selected various types of formworks: Steel without a release agent, steel with a release agent, glass fiber reinforced plastic, Textolit, multilayered compressed paper, flour plastic, and weneer with a layer. It should be mentioned that the values of the steel roughness parameters were not specified. The workability class of their prepared concrete was kept to 4-6 cm. the temperature was 16-18 °C and RH = 80-90 %. The obtained stress magnitude for their formworks presented in **Table 23**. The obtained demolding stresses from one day casted samples reached 0.185 MPa for formwork without a release agent, 0.047 MPa for formwork with a release agent, 0.021 MPa for a glass fibers reinforced plastic formwork, and 0.009 MPa for a plastic formwork containing fluorine. Their stress values obtained without a release agent are of the same order of magnitude as the experimentally obtained stresses of this study for the reference formwork F17-Ref and C20C27. In addition, the reduction of demolding stresses for the use of formwork with a release agent were confirmed by authors and the outcomes in their study relatively close to those of this work (0.09 ± 0.04 MPa). Finally, it must be noted that the demolding stresses increase with time, particularly, for those against steel formworks with or without release agents.

Table 23: *Bonding strength in mode 1 of fracture according to different formwork types* [172]

Formwork type	**Bond strength (MPa . 10^{-3})**	
	1 day	**3 days**
steel without release agent	185	489
steel with release agent	47	142
glass fiber reinforced plastic	21	26
Textolit	9	10
multilayered compressed paper	18	18
flour plastic	9	10
Weneer with a layer	31	43

- ***Formwork polymer coating performance in terms of demolding***

The C20C27 polymer and PET releasing property/removability were studied. Comparable demolding force figures for both CEM I and CEM II/B are presented in **Figure 71**.

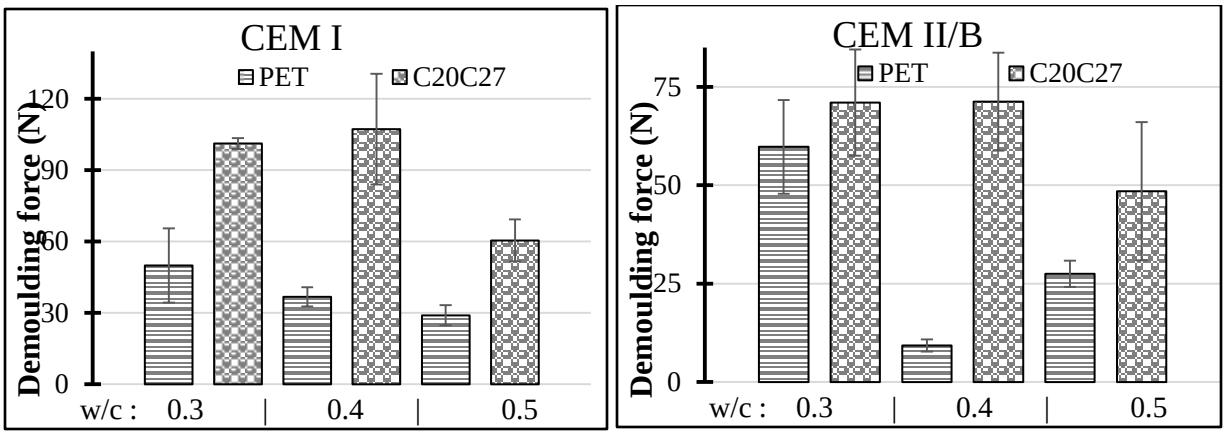

a) *b)*

Figure 71: *C20C27 and PET releasing layer performance against cement paste adhesion with different w/c ratios: a) CEM I and b) CEM II/B*

The experimental results indicate that the F_d for the cement paste samples against formwork coated by PET with CEM I exhibited better performance compared to C20C27 for the three variations of w/c ratio. Moreover, the same tendency was recorded for cement paste samples with CEM II/B, whereas, the F_d decrease 66% and 52% for w/c ratio = 0.4 and 0.5, respectively, for PET compared to the C2027 ones. In literature, less studies can be found out regarding to the usage of polymeric materials as release agent. However, the effect of polymeric coating materials are in well accordance with those of N. Spites *et al.* [17].

2. Cement paste surface early age (24 hours) hydration

After the demolding procedure, three samples of cement paste for each variation were followed by the process of stopping hydration process for further microstructure analyses (**Figure 72**). In order to understand the surface roughness, microstructure and hydration phases, three types of microscopic analyses were performed as follows:

- Interferometry microscopy (IM) as a non-contact method to measure the morphology and texture of the cementitious surface
- Scanning Electron Microscopy (E-SEM) to evaluate the surface feature and crystallization by imaging of the cement paste surface at an early age (24 hrs) of hydration
- X-Ray Defractometry as non-destructive test method for analyzing the crystallization structure of cement paste surface

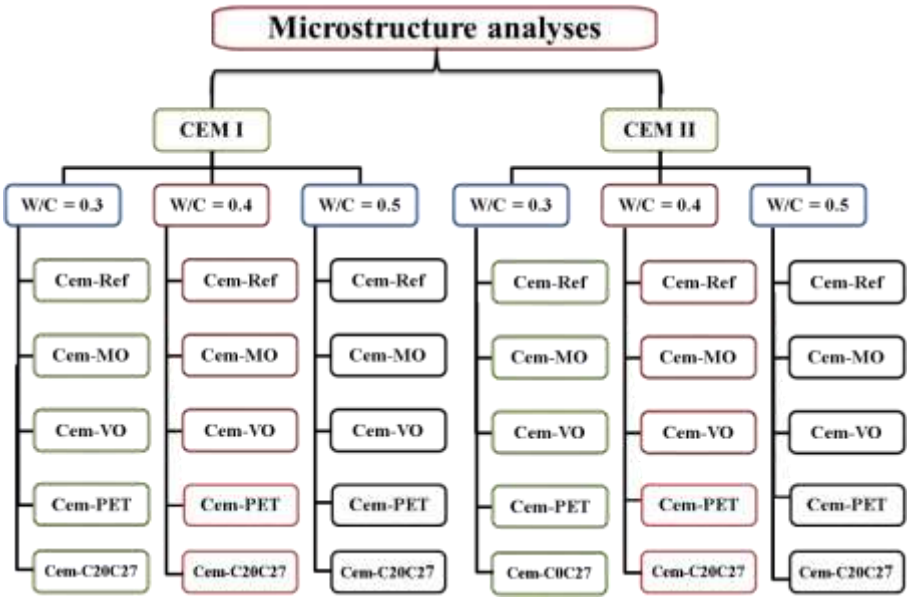

Figure 72: *Cement paste sample variations for microscopic analyses*

2.1. Cement paste surface morphology analysis via Interferometry microscopy (IM) and scanning electron microscopy (SEM)

The adhesion phenomena at the concrete-formwork interface is related to various factors during casting of cementitious materials in formwork. The morphology of the formwork surface is one of the significant factor. Therefore, to understand the effect of formwork on the cement surface, different types of cement paste (cement type and w/c ratio) against various used formwork were investigated. It must be mentioned that the cement paste samples were analyzed at initial state and no treatment was conducted before the mentioned microstructure tests.

The Interferometry microscopy (IM) as a non-contact method analysis was conducted on the cement paste sample having a cylindrical shape with Ø = 25 mm, A = 490 mm^2. The IM analysis were carried out through stitched method on a square shape area of 5×5 mm^2 in the middle of the sample (**Figure 73**). Each measurement presents a total of 130 point and each point had an area of = 0.60×0.48 μm^2, with 10% of overlapping. The surface roughness parameters S_a and S_q were considered for these analyses.

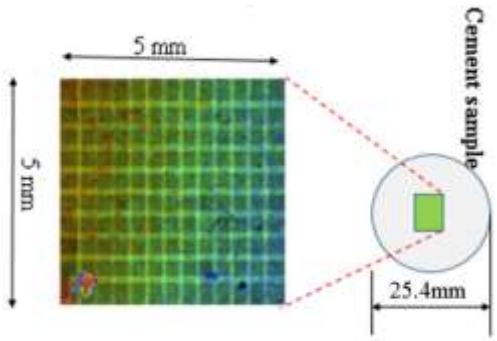

Figure 73: *Stitching area for roughness measurement*

The SEM analysis were conducted minimum on 10 zones of each cement samples for all variants. It must be noted that for each variation 2 samples were examined. These analysis are conducted at the initial state of cement surface (without surface treatment or preparation) for all specimens with different magnitudes under low vacuum. Moreover, the semi quantitive chemical analysis were realized through the EDS spectra.

2.1.1. Effect of various coated formwork on cement samples' surface roughness parameters

The Cem-Ref referred to the cement paste that was cast in the F17-Ref plate. The 2D and 3D images of cement paste via interferometry microscopy analysis at 24 hours of hydrate are shown below:

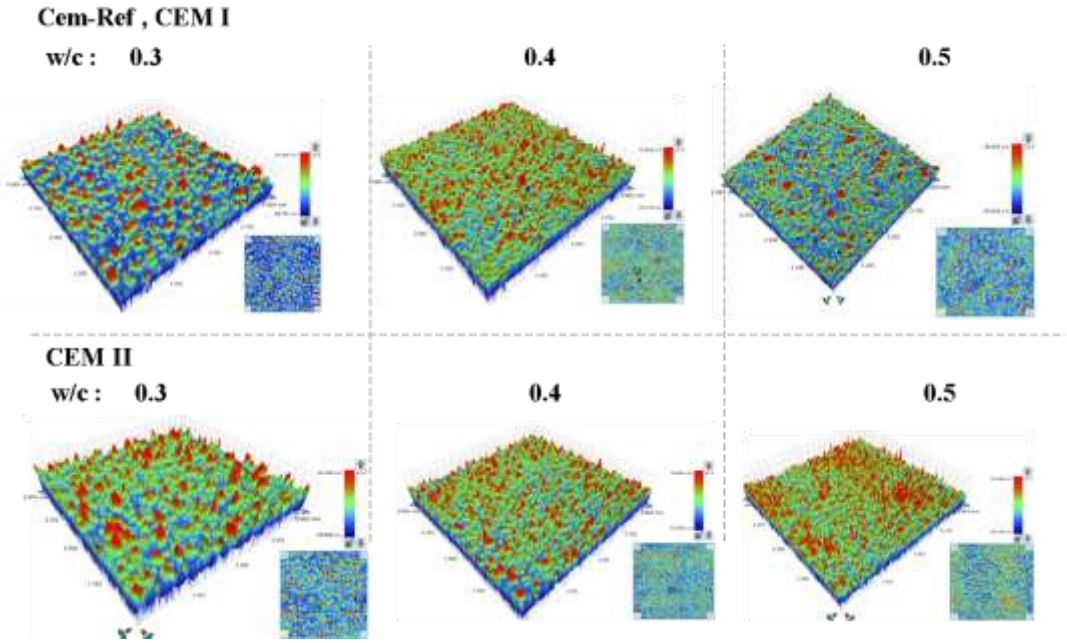

Figure 74: *Cem-Ref 2D and 3D images of surface texture with w/c ratios= 0.3, 0.4, and 0.5 and cement type: CEM I and CEM II/B by interferometry microscopy*

The results of IM for cement samples against reference formwork (Cem-Ref) are summarized **Table 24**. For both cement types, CEM I and CEM II/B, the roughness parameters of Cem-Ref with w/c = 0.3 showed slightly higher values comparing to Cem-Ref with higher w/c ratios (0.4 and 0.5). On the other hand, the results indicate that the obtained roughness parameters are similar for both types of cement with w/c ratio of 0.4 and 0.5. In addition, the obtained demolding force for cement samples against reference formwork by pre-crack demolding test showed that there is no measurable effect of cement type and/or w/c ratio on demolding force (F_d). It must be noted that the highest roughness parameters were observed for the reference formworks without any surface treatment before test.

***Table 24** : Surface roughness Development or reduction in surface roughness parameters*

w/c ratio	**0.3**		**0.4**		**0.5**	
Parameters	S_a (nm)	S_q (nm)	S_a (nm)	S_q (nm)	S_a (nm)	S_q (nm)
Cement past samples by CEM I against F17-Ref	5385 ± 837	7062 ± 766	4871 ± 745	6239 ± 980	4774 ± 523	6399 ± 607
Cement past samples by CEM II against F17-Ref	6086 ± 509	7742 ± 485	3795 ± 154	4962 ± 258	4759 ± 302	6019 ± 425
Formwork surface	**S_a (nm) = 4563 ± 389**			**S_q (nm) = 5663 ± 467**		

For better understanding of the cement samples' surface the same specimens are analyzed through the Scanning Electron Microscopy (SEM) to evaluate the surface feature by imaging. It must be noted that for each specimens 10 zones were observed under SEM and the same aspects were observed. **Figure 75** present an example of SEM image with a magnification of 2000 x of each cement sample. The darker areas represent the pores on the surface of the cement paste. Confirming the interferometry images results, as it can be seen that the pore size, number of cavities, and surface roughness of the cement paste samples are similar for the cement samples against reference formwork (F17-Ref). On the other hand, as known fact the interne porosity of cementitious materials increases with the increase of w/c ratio [173] [174] [175] while in case of experimentally obtained results, no significant difference are observed through SEM images.

Indeed, some tests such as; water penetration, capillarity and surface porosity by mercure need to be carried out.

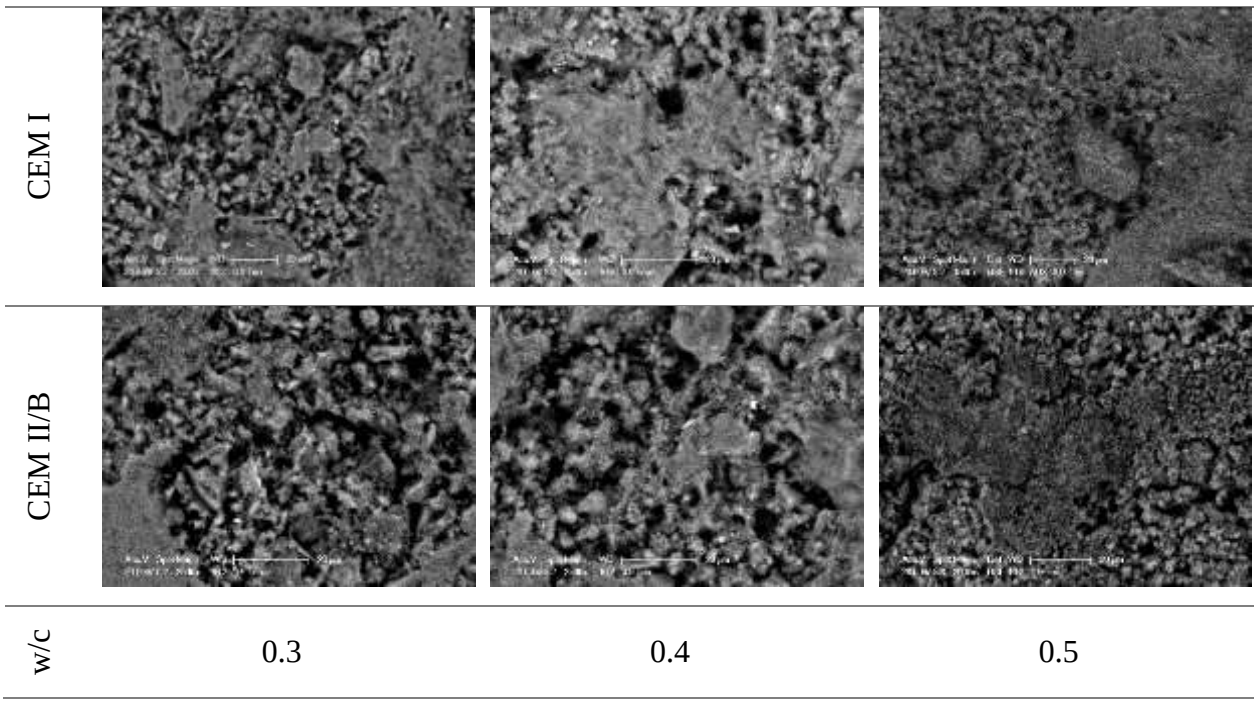

Figure 75: *Cem-Ref with different w/c ratios and cement types*

Moreover, compare to the Cem-Ref, the effect of polymeric coated materials on surface roughness of cement samples were analyzed. The roughness of cement samples against polymeric coated formworks, PET and C20C27, for CEM I are presented in **Table 25**. The outcomes indicate that roughness of cement samples' surface against polymeric coated formworks are significantly lower than those of Cem-Ref. The results show that roughness ratio betwenn Cem-Ref/ Cem-C20C27 and Cem-Ref/ Cem-PET are 4 and 10 times, respectively, for all variations of w/c ratio of CEM I. In addition, the Cem-PET samples presents lower surface roughness compared to the Cem-C20C27.

The w/c ratio doesn't effect the surface roughness, it can be seen that the surface of Cem-C20C27 and Cem-PET are similar for three variations of w/c ratios, by taking into account the standard deviations. However, the demolding forces were decreasing with the increase of w/c ratio through the pre-crack demolding test.

Table 25*: Surface roughness Development or reduction in surface roughness parameters for CEM I*

w/c ratio	Formwork	0.3	0.4	0.5

Parameters	S_a (nm)	S_q (nm)	S_a (nm)	S_q (nm)	S_a (nm)	S_q (nm)	S_a (nm)	S_q (nm)
Cem-Ref	$4563^{\pm389}$	$5663^{\pm467}$	$5385^{\pm837}$	$7062^{\pm766}$	$4871^{\pm745}$	$6239^{\pm980}$	$4774^{\pm523}$	$6399^{\pm607}$
Cem-C20C27	$931^{\pm235}$	$1176^{\pm370}$	$1453^{\pm288}$	$2802^{\pm885}$	$1739^{\pm210}$	$2616^{\pm326}$	$1722^{\pm213}$	$2519^{\pm168}$
Cem-PET	$108^{\pm21}$	$141^{\pm30}$	$531^{\pm126}$	$1570^{\pm213}$	$400^{\pm62}$	$942^{\pm577}$	$546^{\pm75}$	$1476^{\pm38}$

Moreover, by taking in account the roughness of used formwork, it can be seen that the rougher formwork give the rougher cement paste surface. The highest roughness is recorded for the reference formwork and cement samples against the F17-Ref and it is followed by the C20C27. In addition, the PET coated formwork with low roughness results in low roughness parameter of cement paste surface. The results are in accordance with the literature that the selection of one type of formwork over another is partially based on the morphological nature of the formwork surface parameters due to the print of the formwork surface and shape on the concrete facing [50].

The 3D and 2D interferometry images of Cem-Ref, Cem-C20C27 and Cem-PET, with CEM I with a w/c ratio of 0.3, are illustrated in **Figure 76**. It can be seen that cavities and microstructure on the surface of cement paste sample against reference formwork is much visible compare to those of polymeric coated ones.

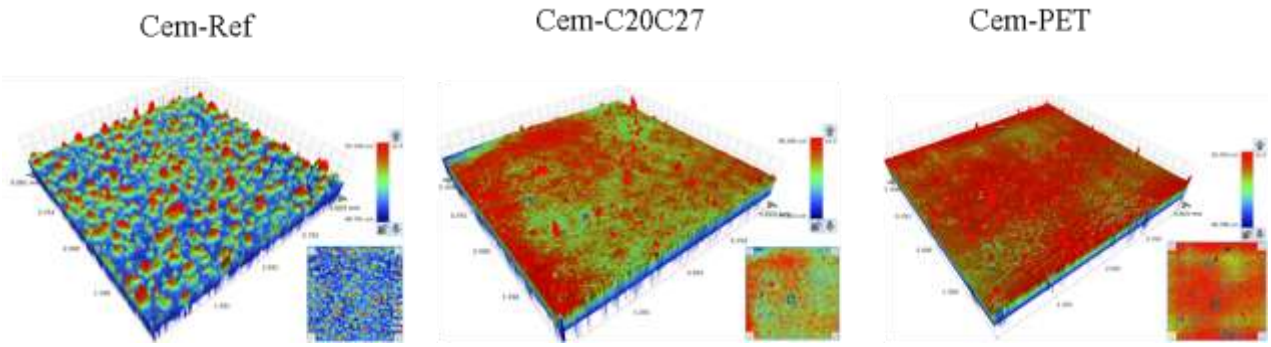

Figure 76: 2D and 3D images of cement paste surfaces with different formwork types (CEM I, w/c = 0.3)

For example, **Figure 77** presents the SEM images Cem-Ref, Cem-C20C27 and Cem-PET, with CEM I and w/c ratio of 0.3. It can be seen that the same images confirm the obtained results by IM analysis. The cement surfaces against polymeric coated fromworks are smoother than those against F17-REF. Finally, it must be noted that the same chemical composition are observed for all cement surfaces againt F17-Ref, C20C27 and PET.

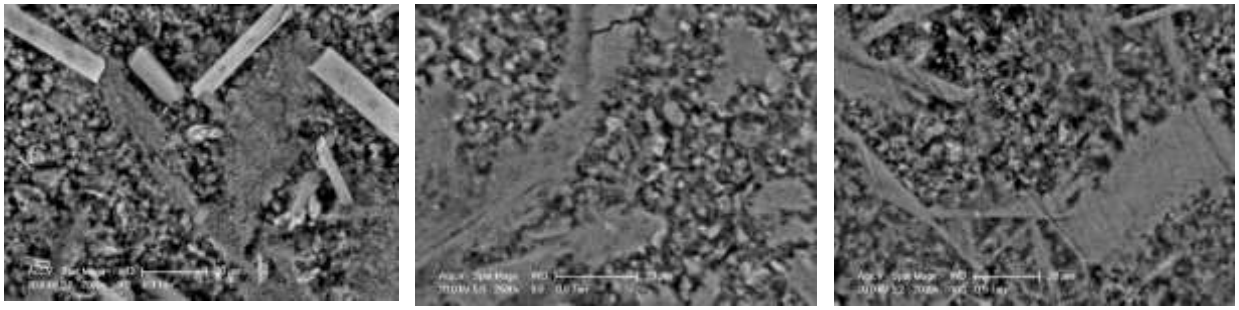

Cem-Ref Cem-C20C27 Cem-PET

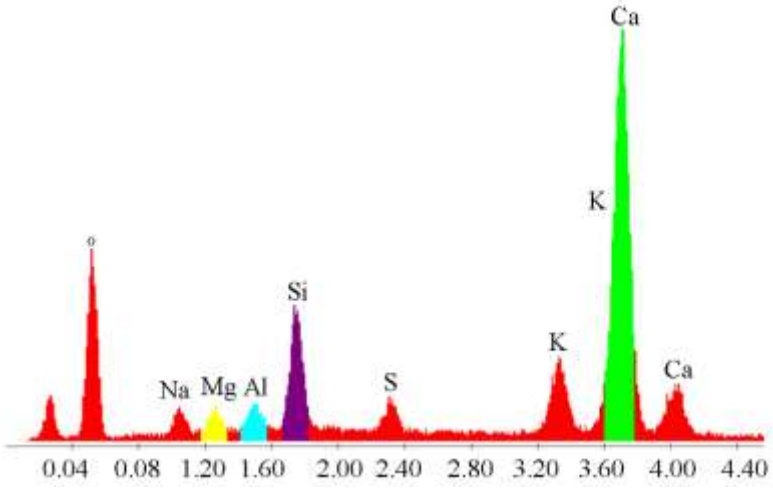

EDS Spectra, analysis of Cem-C20C27

Figure 77 *images of cement paste surfaces with polymeric coating formwork types, magnification: 2000 and EDS Spectra analysis of Cem-C20C27 (CEM I , w/c = 0.3)*

Coming to the effect of used release agents compare to the reference cement paste samples, **Table 26** summarize the experimental results.

The outcomes indicate that roughness of cement samples' surface against oil coated formworks are slightly lower than those of Cem-Ref. In addition, all cement sample surfaces present the same roughness whatever the w/c ration, it seems that it does'nt affect the surface roughness of cement samples against oil coated formwork. It can be seen that the surface of Cem-MO and Cem-VO are similar, by taking into account the standard deviations, except with the w/c ratio of 0.5, where the Cem-MO Sa and Sq values are significantly lower than those of Cem-VO. Beside, through the pre-crack demolding test, the lowest demolding force was observed for the cement samples against oil coated formwork, particularly for those against vegetable oil coated formworks (Fd < 10 N).

***Table 26** : Surface roughness Development or reduction in surface roughness parameters for CEM I*

w/c ratio	**0.3**		**0.4**		**0.5**	
Parameters	S_a (nm)	S_q (nm)	S_a (nm)	S_q (nm)	S_a (nm)	S_q (nm)
Cem-Ref	5385 ± 837	7062 ± 766	4871 ± 745	6239 ± 980	4774 ± 523	6399 ± 607
Cem-MO	4307 ± 475	5751 ± 280	4346 ± 242	5462 ± 323	2467 ±420	3707 ± 1028
Cem-VO	4008 ± 887	5852 ± 1529	4528 ± 314	5661 ± 168	5013 ± 160	6825 ± 361

The 3D and 2D images of Cem-MO and Cem-VO are presented in **Figure 78**. The presence of mineral and vegetable release agents did not result in smoothening the cement paste surfaces, neither did the increase of w/c. Furthermore, unhydrated cement particles (20-30 µm) were identified on the cement paste surfaces (**Figure 79**). It can be explained that the release agent creates a barrier of variable thickness between the formwork and the cement or concrete, which increases the micro-roughness of the formwork surface and, therefore, the cementitious surface [66] (**Figure 79**).

The SEM analysis reveal that the pore size, number of cavities, and surface roughness of the cement paste samples against mineral and vegetable oil coated fromwork are similar to those against reference formwork. However, the unhydrated cement particles are more visible on the surface of cement paste samples against oil coated formwork for all variated w/c ratio. It must be noted that the interne porosity of cementitious materials increases with the increase of w/c ratio [173] [174] [175] while in case of experimentally obtained results, no significant difference are observed through SEM images. As mentioned before, for well understanding of the subject some tests need to carried out such as; water penetration, capillarity and surface porosity by mercure.

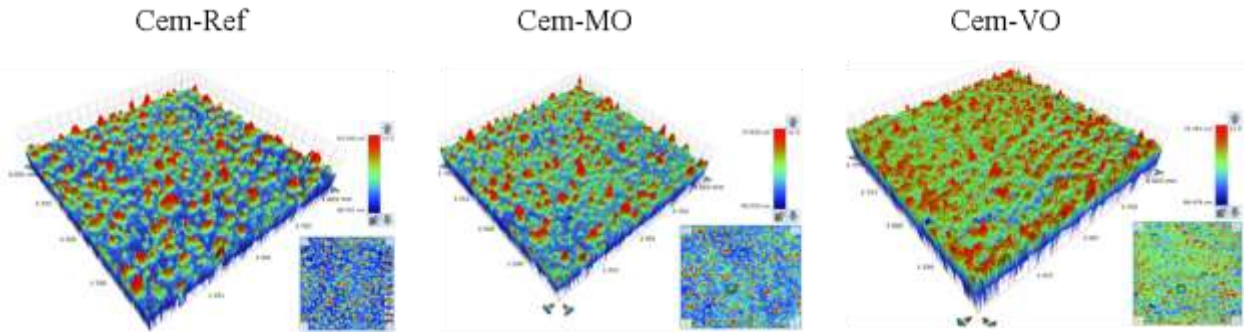

***Figure 78** 2D and 3D images of cement paste surfaces obtained from F17-MO and F17-VO formwork (CEM I, w/c = 0.3)*

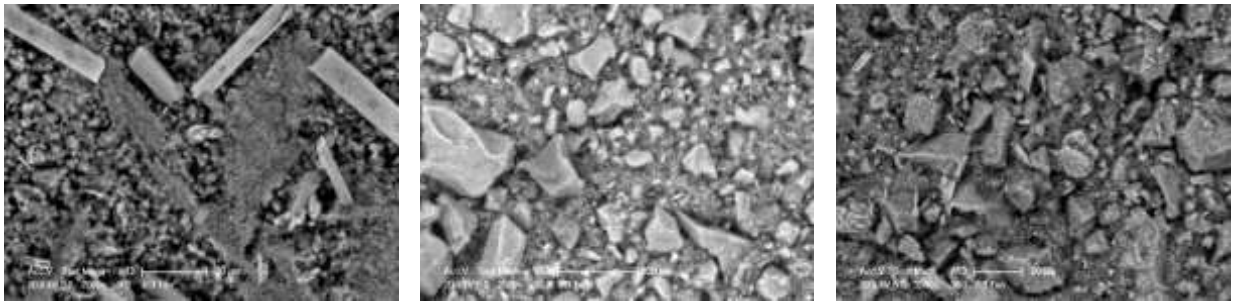

Cem-Ref | Cem-MO | Cem-VO

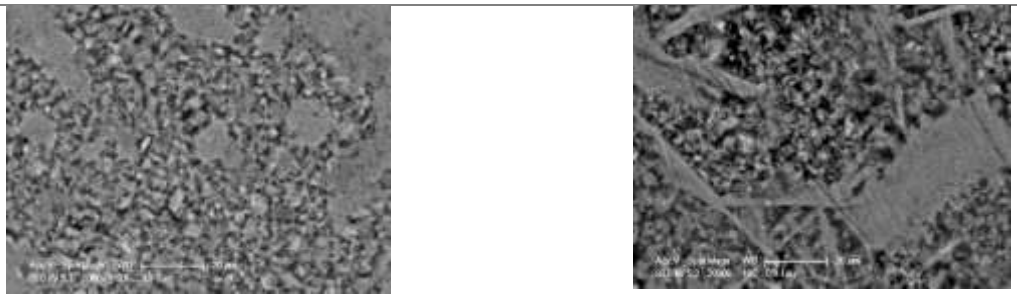

Cem-C20C27 | Cem-PET

Figure 79 *images of cement paste surfaces obtained from F17-MO and F17-VO formwork, magnification: 2000 (CEM I , w/c = 0.3)*

The experimental results obtained from Interferometry microscopic analysis for two types of cement and all w/c ratio variation against 5 types of formworks are summarized in **Table 27**.

Table 27 *cement pastes' surface roughness (**S_a** and **S_q**) with their dispersion values obtained through interferometry microscopy*

Cement type / Parameters		CEM I (nm)		CEM II	
		S_a (nm)	**S_q (nm)**	**S_a (nm)**	**S_q (nm)**
w/c = 0.3	Cem-Ref	5385 ± 837	7062 ± 766	6086 ± 509	7742 ± 485
	Cem-MO	4307 ± 475	5751 ± 280	4686 ± 202	6543 ± 344
	Cem-VO	4008 ± 887	5852 ± 1529	4139 ± 241	3247 ± 3698
	Cem-C20C27	1453 ± 288	2802 ± 1185	1111 ± 127	2014 ± 66
	Cem-PET	531 ± 126	1570 ± 213	468 ± 123	1416 ± 427
w/c = 0.4	Cem-Ref	4871 ± 745	6239 ± 980	3795 ± 154	4962 ± 258
	Cem-MO	4346 ± 242	5462 ± 323	3152 ± 917	4187 ± 1136
	Cem-VO	4528 ± 314	5661 ± 168	6284 ± 115	8080 ± 226
	Cem-C20C28	1739 ± 210	2616 ± 326	2570 ± 1739	3505 ± 1973
	Cem-PET	400 ± 62	942 ± 577	1456 ± 346	2447 ± 259
w/c = 0.5	Cem-Ref	4774 ± 523	6399 ± 607	4759 ± 302	6019 ± 425
	Cem-MO	2467 ±420	3707 ± 1028	2790 ± 167	3766 ± 186

Cem-VO	5013 ± 160	6825 ± 361	4465 ± 434	5925 ± 548
Cem-C20C29	1722 ± 213	2519 ± 168	1229 ± 107	2055 ± 325
Cem-PET	546 ± 75	1476 ± 38	499 ± 34	1218 ± 158

The used formworks in this work possessed different properties in terms of wettability, coating layer, releasing agent and morphology of the surface. The casting procedure included pouring the cement paste into the molds and vibrating it for optimum compaction and placement, which causes a direct contact between paste and formwork. Furthermore, as the paste hydrates and begins to harden, the cement hydration phase's formation on the formwork surface causes the concrete/cement-formwork adhesion phenomenon. The effect of formwork on the surface morphology of cement paste was investigated via interferometry microscopy.

The highest surface roughness belonged to those cement paste samples against F17-Ref, F17-VO and F17-MO formworks, respectively. Besides, Cem-C20C27 and Cem-PET cement paste samples had lower surface roughness parameters.

C. Chadfeau [39] observed the surface morphology of the cement pastes obtained against different formworks. Some of the studied formworks present the same roughness and characteristics compare to this experimental datas. It can be concluded that the similar outcomes find out in both studies. Moreover, in recent work, S. Gzarnecki and L. Sadowski [176] studied the effect of different formwork types on the surface of cement pastes prepared with CEM I, w/c = 0.35 and 0.5. The selected formworks were: wood, oriented strand board (OSB), steel, and plastic. Moreover, all formworks were coated with petroleum-based oil release agents. The studied parameters (Sa and Sq) were obtained by a 3D laser scanning method. The very rough pattern of OSB was visible on the cement paste surface (**Figure 80 b**); on the contrary, the use of steel and plastic formworks resulted in very smooth cement paste surfaces (**Figure 80 c** and **d**). The roughness parameters for the w/c = 0.5 are shown in **Table 28**. It should be stated that no information regarding the formwork surface morphology was provided in their work. The OSB samples had the biggest roughness parameters (Sa = 0.11 ± 0.02 mm and Sq = 0.14 ± 0.02 mm) which in contrast samples prepared in steel and plastic formworks had smoother surface, Sa = 0.07 ± 0.01 mm and Sq = 0.10 ± 0.015 mm, Sa = 0.07 ± 0.015 mm and Sq = 0.10 ± 0.04 mm, respectively) (**Table 28**).

Table 28 *The average values of the height parameters for cement skin surfaces as a result of formwork disassembling* [176], *- the values were transformed into digits from a clustered column chart of S. Gzarnecki and L. Sadowski*

cement type	**w/c = 0.5**		**w/c = 0.35**	
	S_a (mm)	***S_q (mm)***	***S_a (mm)***	***S_q (mm)***
Wood	0.08 ± 0.02	0.10 ± 0.03		
OSB	0.11 ± 0.02	0.14 ± 0.02		
Steel	0.068 ± 0.002	0.082 ± 0.008	0.75 ± 0.005	0.11 ± 0.03
Plastic	0.07 ± 0.015	0.10 ± 0.04		

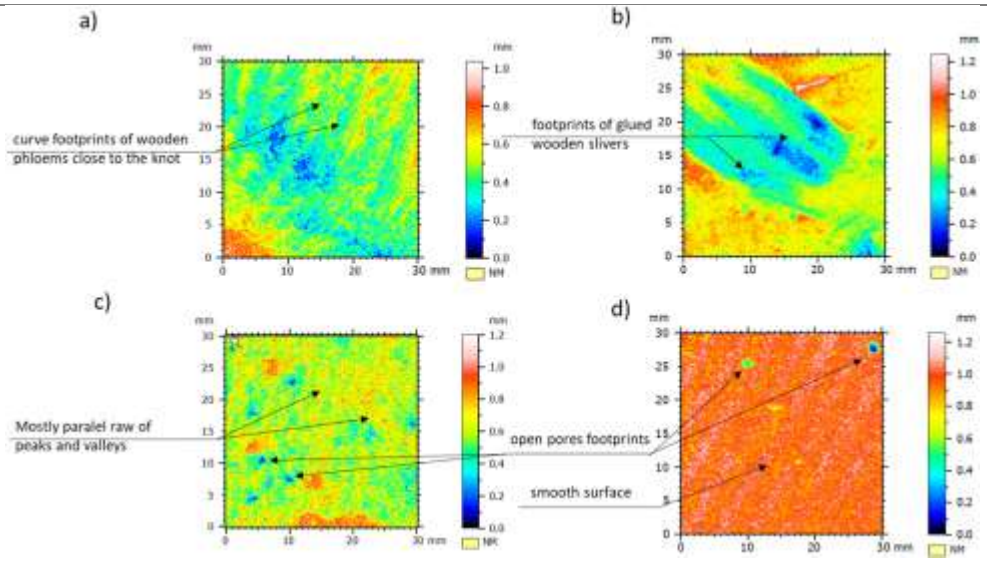

Figure 80 *The 3D isometric views of the cement surfaces prepared using different types of formworks: a) wood, b) oriented strand boards, c)steel and d)plastic*[176]

2.1.2. Effect of cement type and w/c ratio on cement samples' surface roughness parameters

A comparison in terms of roughness evaluation in percentage was performed. The formula for this comparison is shown below:

$$\text{Roughness variation} = 100 - (CI \times 100 / CII)$$

Where,

- *CI, CEM I roughness parameter in unit*
- *CII, CEM II/B roughness parameter in unit*

Table 29 presents the influence of cement change on the cement paste surface roughness parameters from CEM I to CEM II/B.

Table 29 *Roughness reduction by CEM I / CEM II/B (%)*

Roughness variation by CEM I/CEM II/B (%)

Parameters	0.3		0.4		0.5	
	Sa	**Sq**	**Sa**	**Sq**	**Sa**	**Sq**
Cem-Ref	11.5	8.8	−28.3	−25.7	0.3	−6.3
Cem-MO	8.1	12.1	−37.9	−30.5	11.6	1.6
Cem-VO	3.2	−80.2	27.9	29.9	−12.3	−15.2
Cem-C20C27	−30.8	−39.1	32.3	25.4	−40.1	−22.6
Cem-PET	−13.5	−10.9	72.5	61.5	−9.4	−21.2

- *Positive value (+): roughness increases/CEMI*
- *Negative value (−): roughness decreases/CEMI*

The calculation of roughness variation indicates that the roughness for the Cem-Ref (S_a and S_q) values decrease at w/c = 0.3 (11.5 % and 8.8 %) but with the water content increase to 0.4, a decline was observed by 28.3 % and 25.7 %, respectively, for S_a and S_q. This trend were not continued by w/c ratio equal to 0.5. It should be mentioned that similar results were observed for Cem-MO.

An extreme change in S_a and S_q was observed for Cem-C20C27s; by changing the CEM I to CEM II/B type of cement for w/c = 0.3, the roughness decreased by −30.8 and − 39.1 %, respectively. The same results were obtained for the cement samples with w/c=0.5 against F17-C20C27. However, this roughness reduction was not followed by changing the w/c ratio to 0.4; a roughness increase was observed, which was, respectively, 32.3 % and 25.4 % for S_a and S_q. It is worth mentioning that similar patterns were observed for Cem-PETs, as well, whereas, the change of cement, CEM I by CEM II/B, the roughness, S_a and S_q, increase by 72.5 % and 61.5 %, respectively. Finally, it can be seen that the effect of cement type is more pronounceable for the w/c ratio equal to 0.4, particularly for the surfaces against polymeric coated formworks (**Table 28**).

To discover the effect of water content change on surface morphology parameters (S_a and S_q) of cement samples against various coated formwork, the roughness reduction calculated using the following formula:

Roughness reduction = $100 - (n \times 100 / m)$

Where,

- n: roughness parameter of the sample with w/c = n
- m: roughness parameter of samples with w/c = m

Three variation of w/c was calculated for the roughness reduction factor ; 1) 0.3/0.4, 2) 0.4/0.5 and 3) 0.3/0.5. The calculated values of roughness reduction via w/c modification of cement paste samples are graphically illustrated in **Figure 81**.

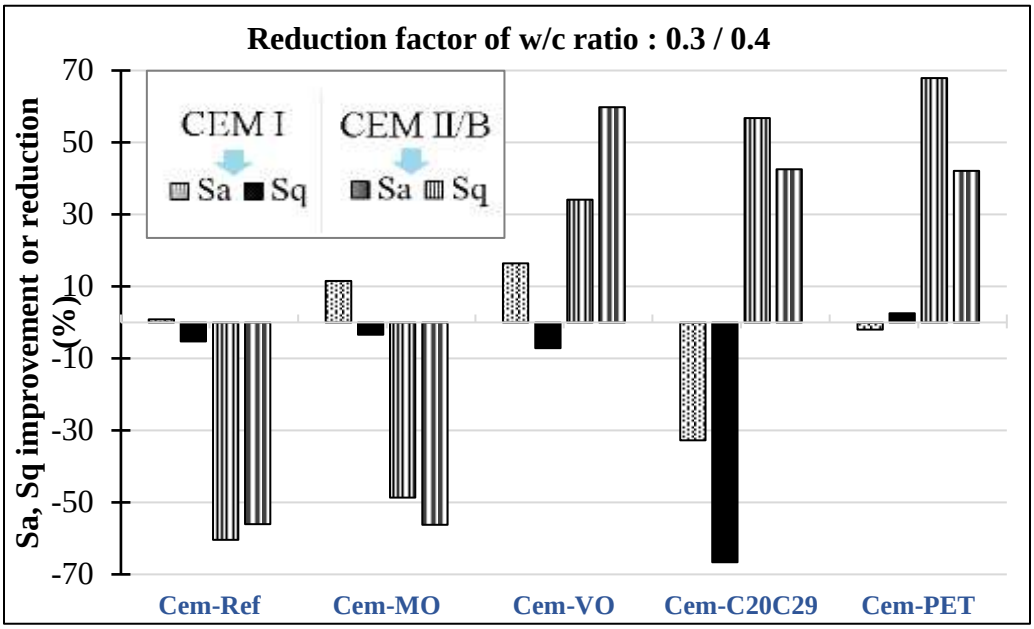

a)

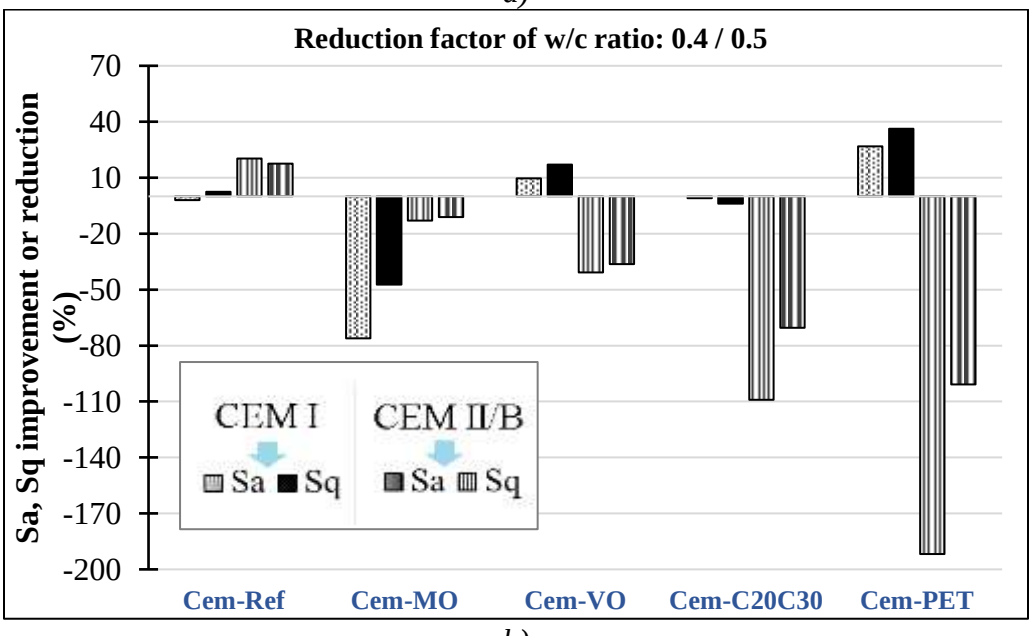

b)

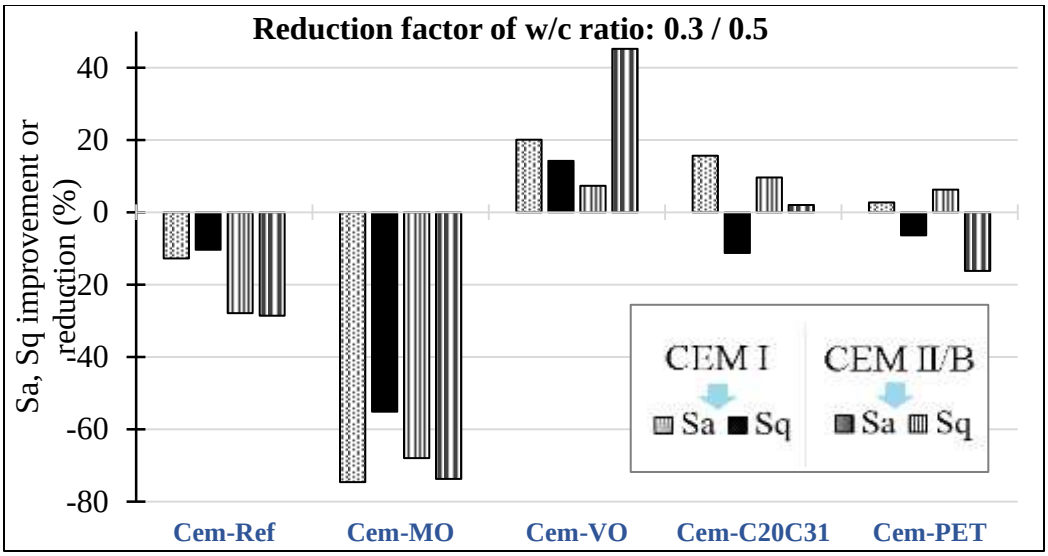

c)

Figure 81 *the effect of w/c ratio modification on Sa and Sq drop; a) w/c ratio: 0.3/0.4, b) w/c ratio: 0.4/0.5, and c) w/c ratio: 0.3/0.5*

The w/c ratio change from 0.3 to 0.4 in CEM I cement type affected the roughness morphology of Cem-Ref, Cem-MO, Cem-VO, and Cem-PET between ≈ 0 ± 10 %. However, the S_a and S_q of Cem-C20C27 for the same group were decreased −32.8 % and –66.7 %, respectively. Furthermore, the roughness of Cem-Ref and Cem-MO was reduced in a range of 48 to 60 % in samples produced with CEM II/B. In addition, the roughness characteristics of Cem-VO, Cem-C20C27, and Cem-PET increased in a range of 34 to 60% (**Figure 81 a**).

The w/c ratio effect on the obtained cement paste surfaces morphology was studied by S. Gzarnecki and L. Sadowski [176]. The authors studied the effect of different formwork types on the surface of cement pastes morphologies (S_a and S_q) prepared with CEM I and two different w/c ratios: 0.35 and 0.5. Although S. Gzarnecki and L. Sadowski used different types of formworks, they applied mineral release agents to all of the formwork types, and their results can be compared to those results of Cem-MO experimentally obtained in this study. In this case, the w/c ratio modification from 0.35 to 0.5 affected the cement surface roughness S_a and S_q by a decrease of ≈ 10.3 % and ≈ 34.1 %, respectively (**Table 28**). Therefore, it can be concluded that the water content present an effect on cementitious surface parameters. But there is no direct correlation between the increase of w/c ratio and the surface morphology of the samples, whatever the quality of the formwork surface.

2.1.3. Effect of coating on cement samples' surface roughness parameters

By observing **Table 30**, except Cem-VO/Cem-Ref of CEM II/B, w/c = 0.4, very nearly all the cement paste samples that were prepared with different formwork types were resulting in a smoother surface compared to the reference formwork, F19-Ref. The best results were witnessed for PET coating formworks (Cem-PET/Cem-Ref) by > 90% decrease of roughness, regardless of cement type and w/c ratios. The Cem-C20C27s had also smoother surfaces comparing to Cem-Ref which were dropped from ≈ 32 % for CEM II/B, w/c = 0.4 to 73 % for CEM I, w/c = 0.3 (**Table 30**). It clearly appears that it is the PET film which allows the greatest reduction in roughness compared to the raw surface of the metal formwork. On the other hand, it is not this type of coating that gives the best results in terms of stripping strength, the classification of stripping surfaces from the least effective to the most effective is: F17, C20C27, PET, MO, VO for the majority w/c ratios and the two cements. With regard to the roughness of cement paste samples against various formworks, the classification from the highest to the lowest roughness of the formwork surfaces is F17, MO, VO, C20C27, PET and for each variation of w/c ratio the order of roughness is summarized in **Table 30**.

Table 30 *Roughness parameters Sa and Sq drop according to formwork surface type (%)*

Roughness parameters Sa and Sq drop according to formwork surface type (%)

w/c		CEM I		CEM II/B	
		Sa	**Sq**	**Sa**	**Sq**
0.3	Cem-MO/Cem-Ref	20.0	18.6	23.0	15.5
	Cem-VO/Cem-Ref	25.6	17.1	32.0	58.1
	Cem-C20C27/Cem-Ref	73.0	60.3	81.7	74.0
	Cem-PET/Cem-Ref	90.1	77.8	92.3	81.7
0.4	Cem-MO/Cem-Ref	10.8	12.5	16.9	15.6
	Cem-VO/Cem-Ref	7.0	9.3	−65.6	-62.8
	Cem-C20C27/Cem-Ref	64.3	58.1	32.3	29.4
	Cem-PET/Cem-Ref	91.8	84.9	61.6	50.7
0.5	Cem-MO/Cem-Ref	48.3	42.1	41.4	37.4
	Cem-VO/Cem-Ref	−5.0	−6.7	6.2	1.6
	Cem-C20C27/Cem-Ref	63.9	60.6	74.2	65.9
	Cem-PET/Cem-Ref	88.6	76.9	89.5	79.8

The SEM imaging analysis are conducted minimum on 10 zones of each cement samples. It must be noted that for each variation 2 samples were scaned. The example of SEM images for all specimens are illustrated in **Figure 84** with two different magnitudes of 2000ˣand 500ˣ. Moreover, the semi quantitive chemical analysis were realized through the EDS spectra. One example of EDS analysis is presented **Figure 82**. The EDS spectra of all cement paste samples show the same chemical elements, there is no changes in spectra peaks by changing the cement type or w/c ratio.

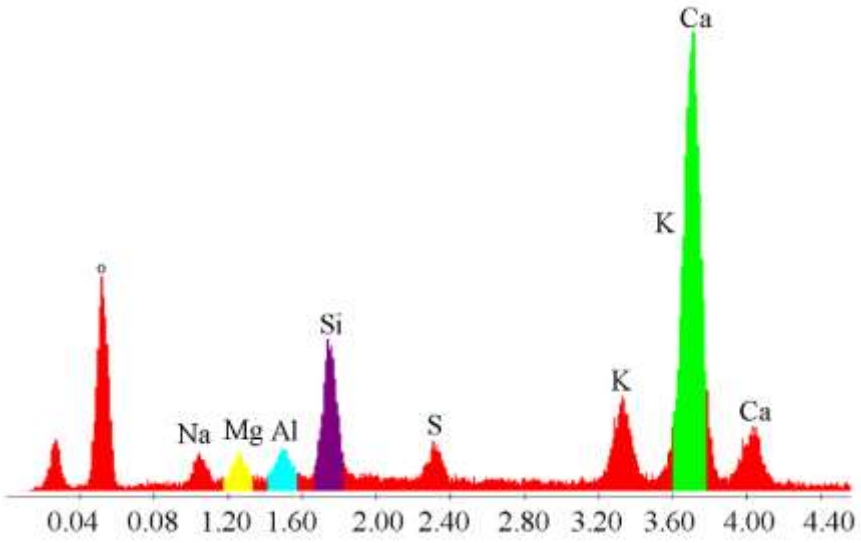

Figure 82 *EDS Spectra, analysis of Cem-C20C27 (CEM I , w/c = 0.3)*

Figure 84, the SEM images reveal that the Cem-Ref samples had a more porous surface compared to others, where the dark color areas signify the pores on the surface. The SEM pictures show a percentage of hydrated products on the surface of Cem-Ref samples, while the unhydrated cement particles can identified by comparing to cement powder at the initial state. Moreover, the Cem-VO cement paste surfaces appear similarly porous to reference ones, however, the Cem-VO cement paste surfaces had lower hydrated compared to reference ones due to the presence of numerous unhydrated particles on the surface. The E-SEM results are in good agreement with the experimental outcomes of the surface roughness from interferometry analyzes. Besides, the cement paste surfaces subjected to the PET and C20C27 polymeric-coated formworks were smoother and less porous compared to others. It indicates that the hydration process on the surfaces is well advanced for such cement paste samples compared to Cem-Ref and Cem-VO. Therefore, it can be explained by the hydrophobicity behavior of polymeric-based substrate which results in the formation of a water layer between cement paste and formwork surface during the hydration

process as shown in **Figure 108** [177]. Finally, the E-SEM analyzes reveal that the hydration in the cement paste surface of Cem-MO is almost similar to the polymeric-coated formworks.

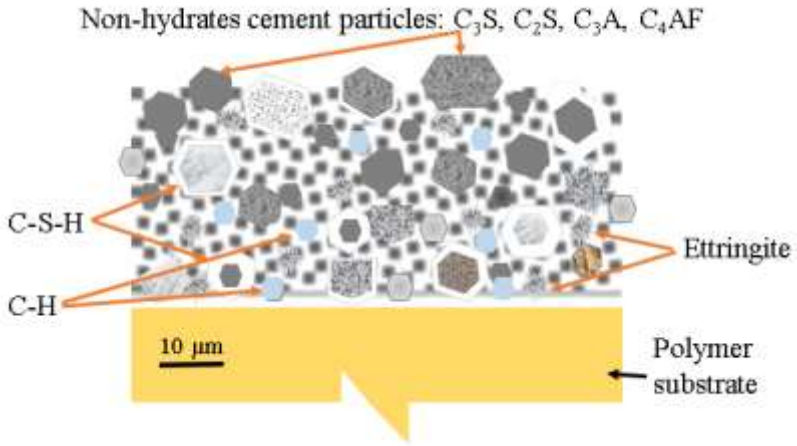

Figure 83 *Accumulation of water layer at the polymeric substrate-cementitious materials*

The comparison of the SEM images resulted in the following conclusions:

- Both mineral oil and vegetable oil caused the hydration at the surface of the samples to slow down, resulting in more unhydrated particles on the surface. Furthermore, the Cem-MO and Cem-VO surfaces had larger crystals than the reference surfaces.
- Compared to Cem-Refs and samples manufactured in release agent coated formwork plates, the Cem-PET and Cem-C20C27 samples' pictures revealed an elevated hydration level.

The SEM analysis of cement samples' surfaces confirms the outcomes of roughness parameters through Interferometry microscopic analysis.

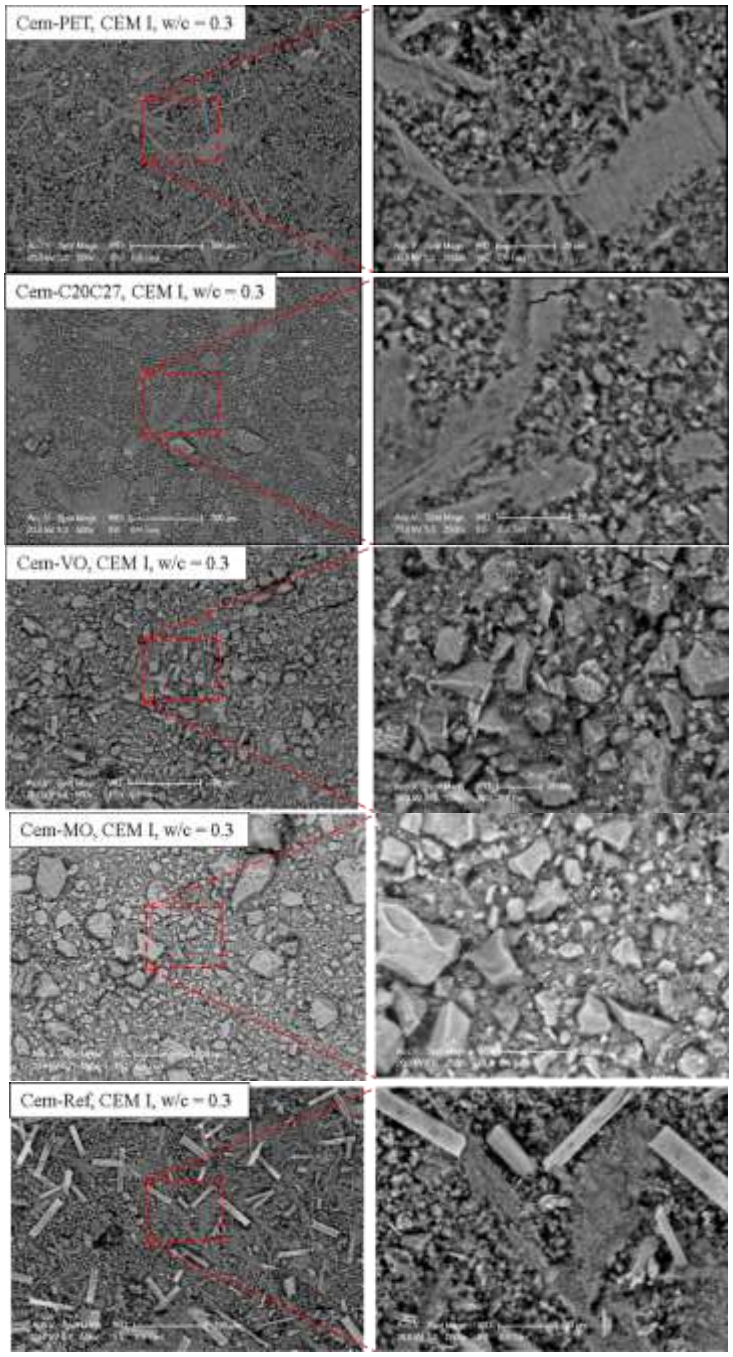
Cem-PET, CEM I, w/c = 0.3
Cem-C20C27, CEM I, w/c = 0.3
Cem-VO, CEM I, w/c = 0.3
Cem-MO, CEM I, w/c = 0.3
Cem-Ref, CEM I, w/c = 0.3

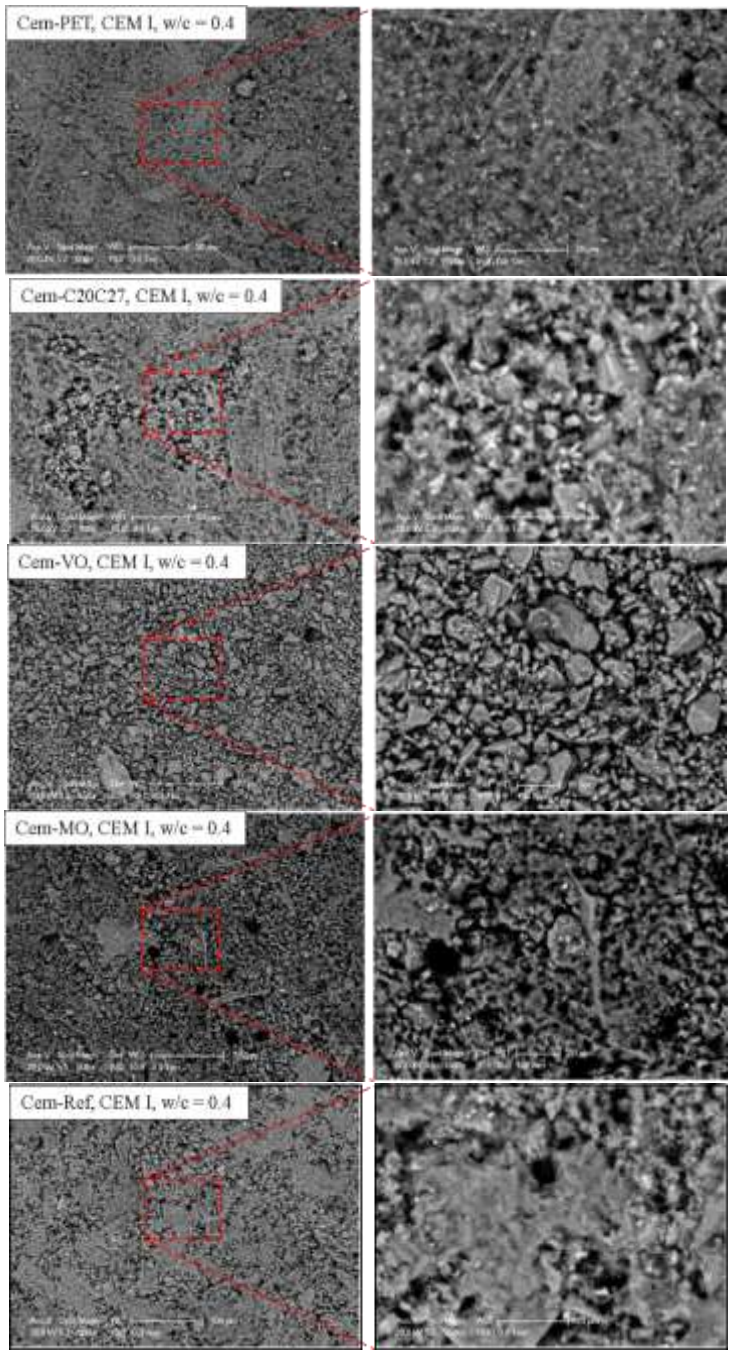
Cem-PET, CEM I, w/c = 0.4
Cem-C20C27, CEM I, w/c = 0.4
Cem-VO, CEM I, w/c = 0.4
Cem-MO, CEM I, w/c = 0.4
Cem-Ref, CEM I, w/c = 0.4

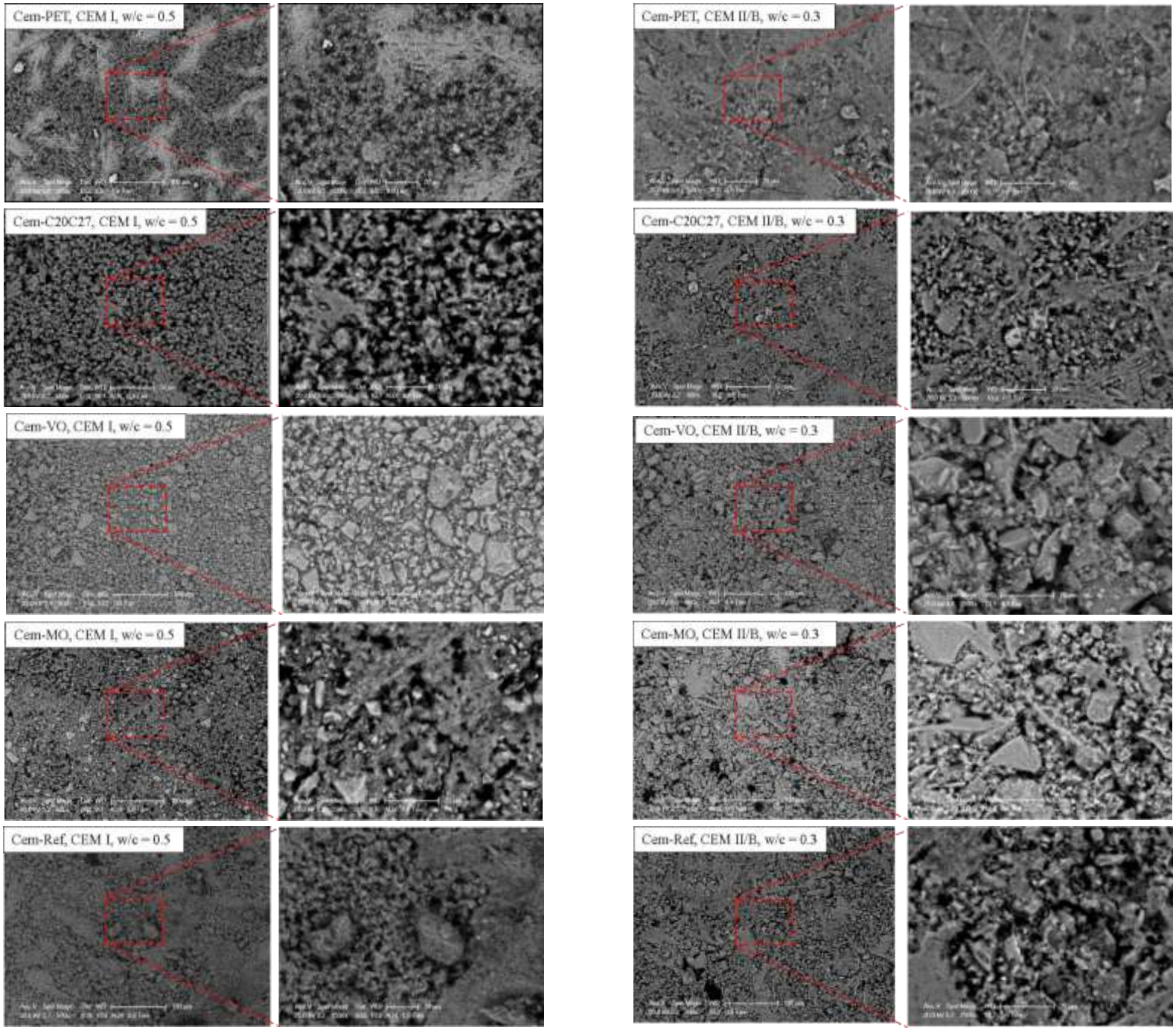
Cem-PET, CEM I, w/c = 0.5
Cem-PET, CEM II/B, w/c = 0.3
Cem-C20C27, CEM I, w/c = 0.5
Cem-C20C27, CEM II/B, w/c = 0.3
Cem-VO, CEM I, w/c = 0.5
Cem-VO, CEM II/B, w/c = 0.3
Cem-MO, CEM I, w/c = 0.5
Cem-MO, CEM II/B, w/c = 0.3
Cem-Ref, CEM I, w/c = 0.5
Cem-Ref, CEM II/B, w/c = 0.3

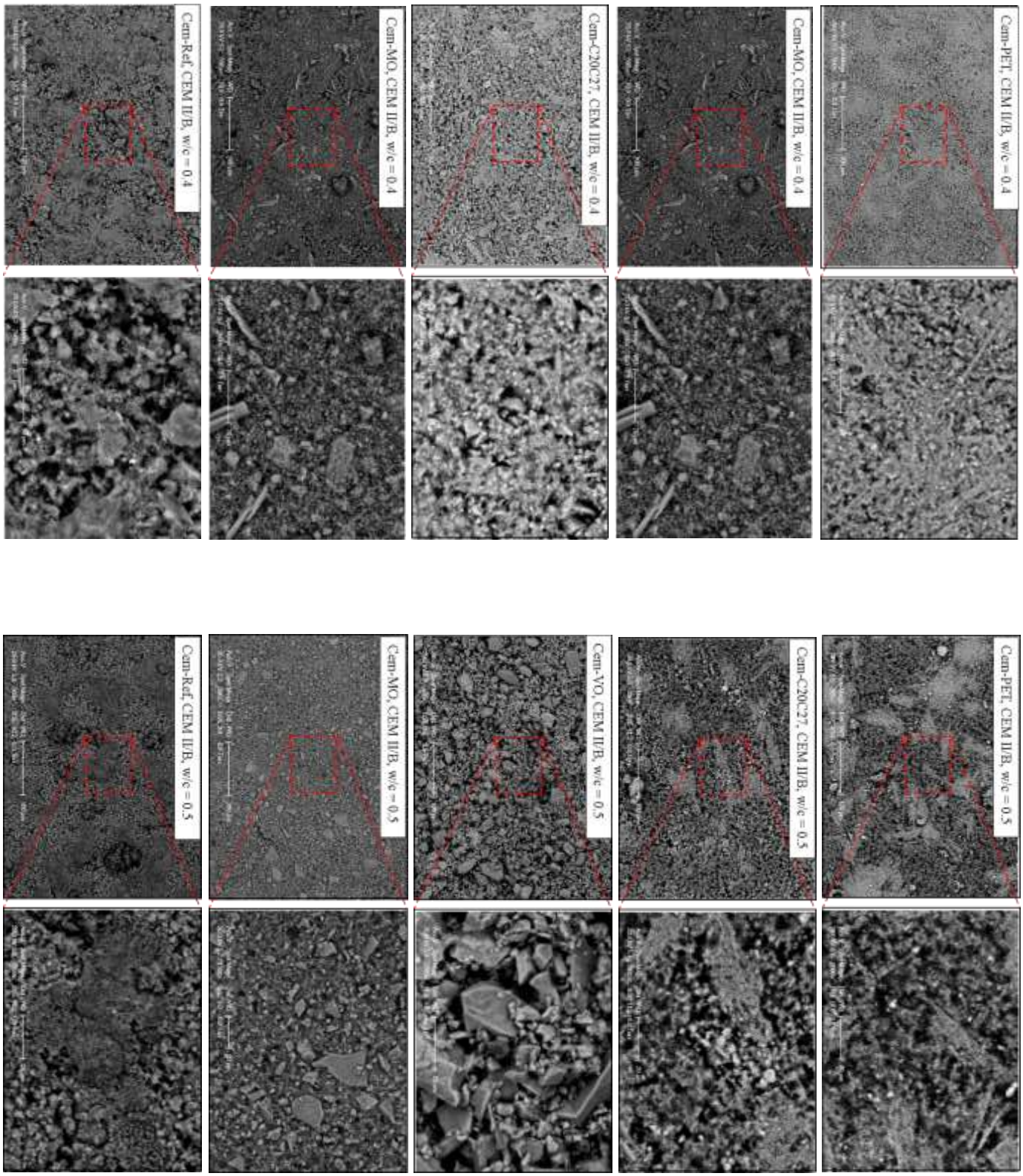

Figure 84 *SEM analysis of all cement paste samples variations after pre-crack demolding test at 24 h of hydration*

The total analysis of all cement type and w/c ratios against the various formworks are presented in ***Annex 2***.

For comparison, in the work of Hartmann and Plank [178], they studied the CEM I hydration – w/c = 0.55, 90% of RH / 35 °C – at the early age (1 day) of hydration till day 14th . The SEM images (**Figure 85**) of cement paste at one day of aging with 90% of RH / 35 °C condition and also 8 hrs of hydration showed the formation of nanoscale ettringite needles on the cement surface.

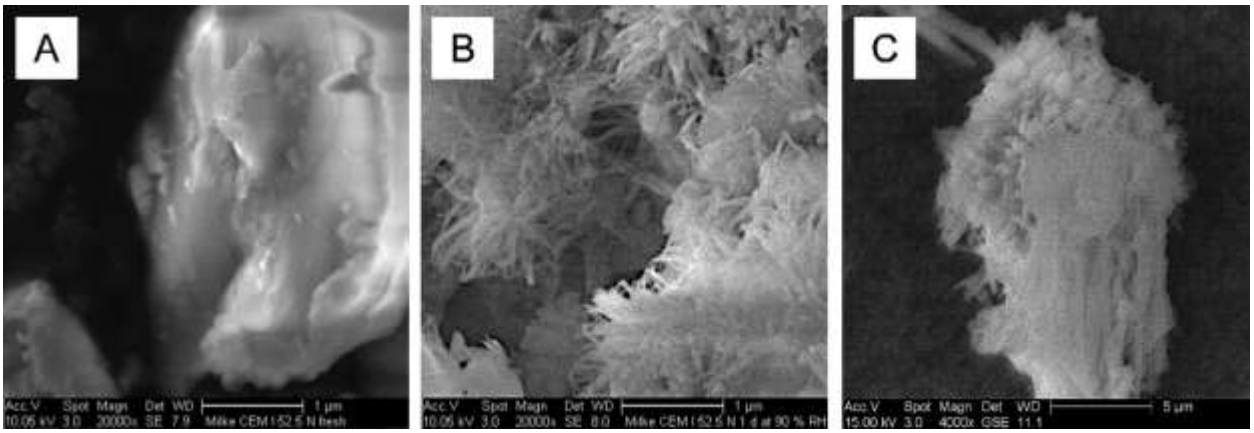

Figure 85 *SEM images of CEM I 52.5 N sample: A) before and B) after aging for 1 day (at 90 % RH / 35 °C), and C) SEM image after 8 h of hydration at w/c = 0.55, magnification: 20000 (SEM); 4000 (SEM)* [178]

Also, in the work of A. Peled *et al.* [179] they examined the mortar surface at the age of 1, 2 and 7 days to distinguish between the hydrated CSH and CH particles and unhydrated particles using AFM and SEM. The backscattered mode with high vacuum condition was applied. It should be mentioned that their samples were polished and coated with a thin layer of palladium.

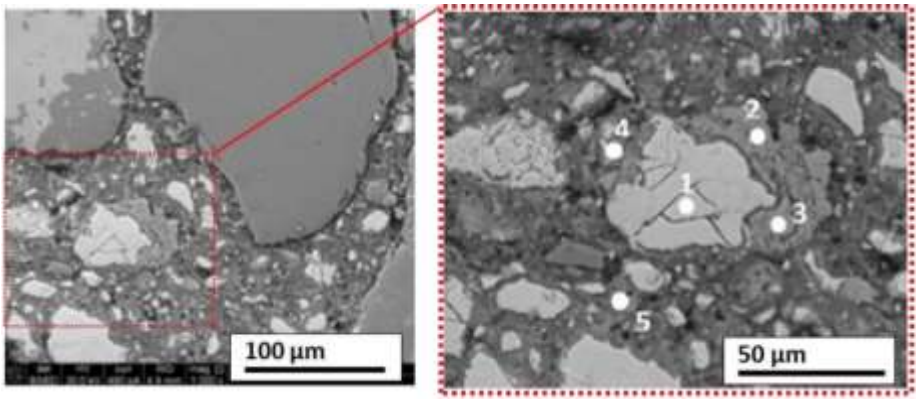

Figure 86 *SEM images: (a) entire observed area, and (b) area with different elements: 1 un-hydrated cement particle, 2 and 3 CH, and 4 and 5 CSH* [179]

2.2. XRD analyses

The non-destructive test method XRD was used to examine the structure [39] [180] and the hydration progression of cement pastes [181] [182] [183] made with various cements and in different formwork types. The detected phases on the surface of cement paste at the early age of hydration were categorized into two: hydrated and unhydrated phases. The mentioned phases are presented in **Table 31**.

Table 31 *Hydrated and unhydrated phases of cement pastes at the early age (24 hrs) of hydration*

Non-hydrated phases	**Hydrated phases**
○ Alite C_3S / Larnite C_2S	○ Portlandite $Ca(OH)_2$
○ Calcium Magnesium Aluminium Silicate	○ Calcite $CaCO_3$
○ Calcium Aluminoferrite C_4AF	○ Vaterite $CaCO_3$
○ Ankerite, $Ca(Mg,Fe)(CO_3)_2$	○ CSH : not detected due to very small cristals [184]
○ Gypsum/Calcium Sulfate $CaSO_4$	

The observed phases on the cement pastes (CEM I and CEM II/B, w/c = 0.3) at 24h are presented in **Figure 87**. The formation of Portlandite and calcite at the early age of hydration is well documented [39] [185] [186] [187]. Ettringite was not detected by XRD on the surface of these cement pastes. According to Baroghel-Bouny, it is mainly present in a finely crystallised form disseminated in the mass of hydrates, especially in the middle of the C-S-H gel. Ettringite can only develop on the surface of the samples under certain conditions [184].

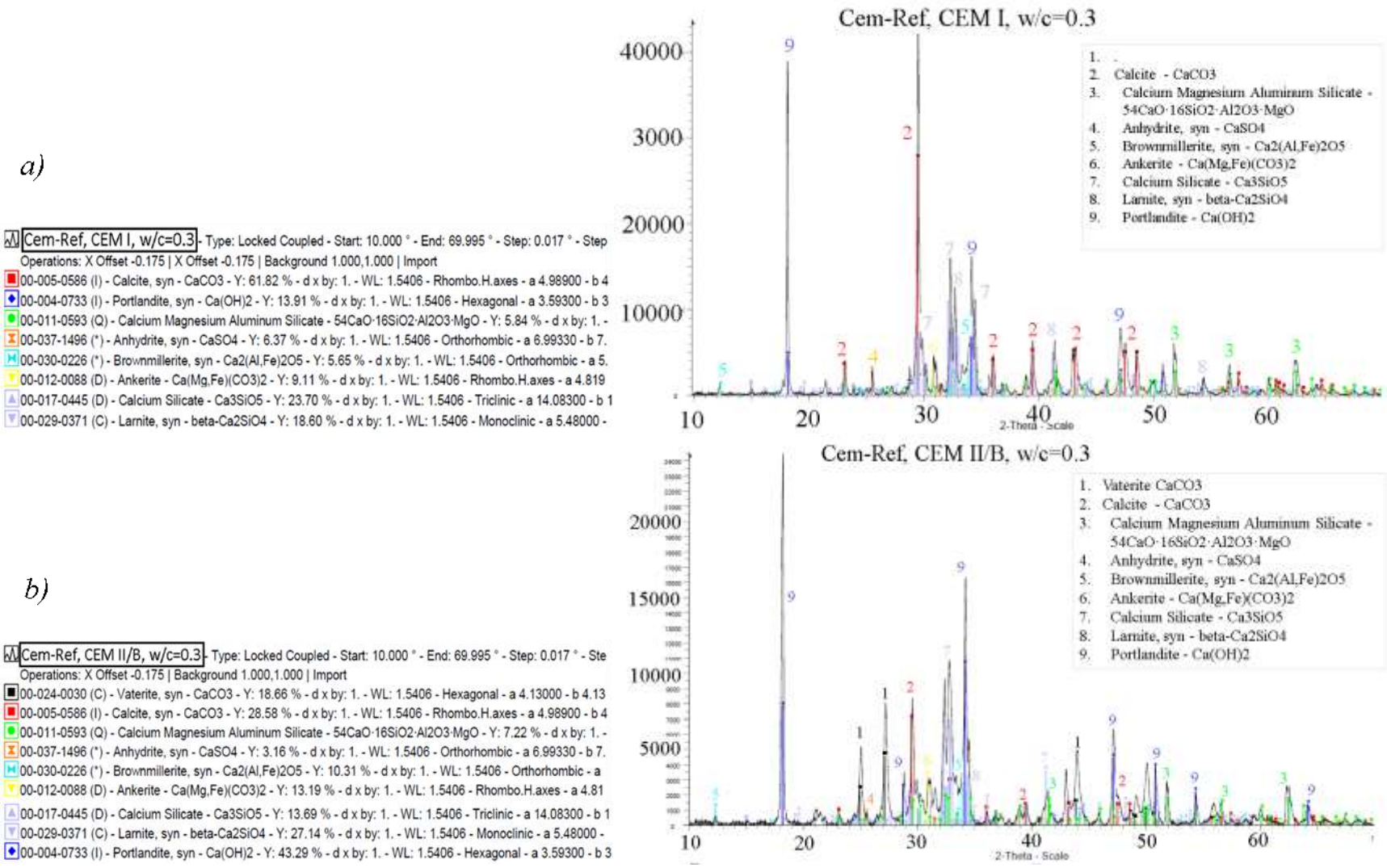

Figure 87 *X-ray difractometry analysis of reference cement paste sample with w/c = 0.3 at the early age of hydration (24 h); a) with CEM I and b) with CEM II/B*

The XRD results are presented in **Figure 88** according to the different w/c ratios,cement types and formwork at 24h.

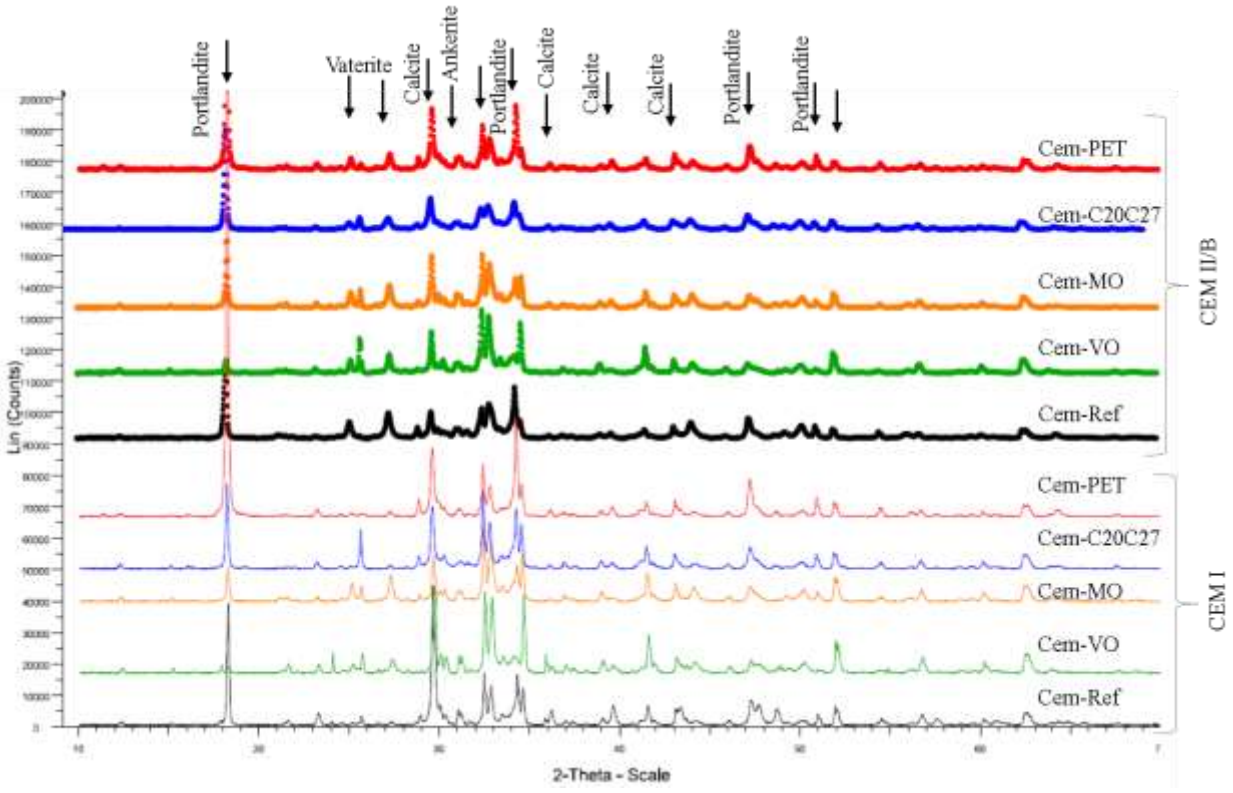
Portlandite
Vaterite
Calcite
Ankerite
Portlandite
Calcite
Calcite
Calcite
Portlandite
Portlandite
Cem-PET
Cem-C20C27
Cem-MO
Cem-VO
Cem-Ref
CEM II/B
Cem-PET
Cem-C20C27
Cem-MO
Cem-VO
Cem-Ref
CEM I
Lin (Counts)
2-Theta - Scale

a)

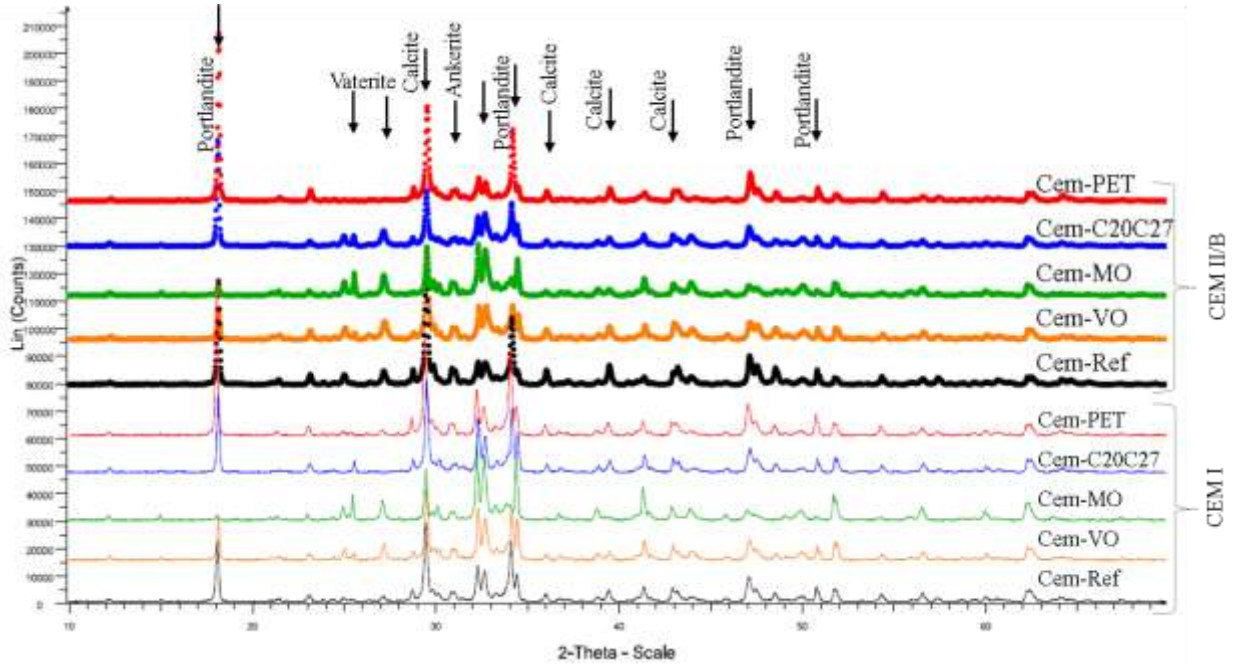
Portlandite
Vaterite
Calcite
Ankerite
Portlandite
Calcite
Calcite
Calcite
Portlandite
Portlandite
Cem-PET
Cem-C20C27
Cem-MO
Cem-VO
Cem-Ref
CEM II/B
Cem-PET
Cem-C20C27
Cem-MO
Cem-VO
Cem-Ref
CEM I
Lin (Counts)
2-Theta - Scale

b)

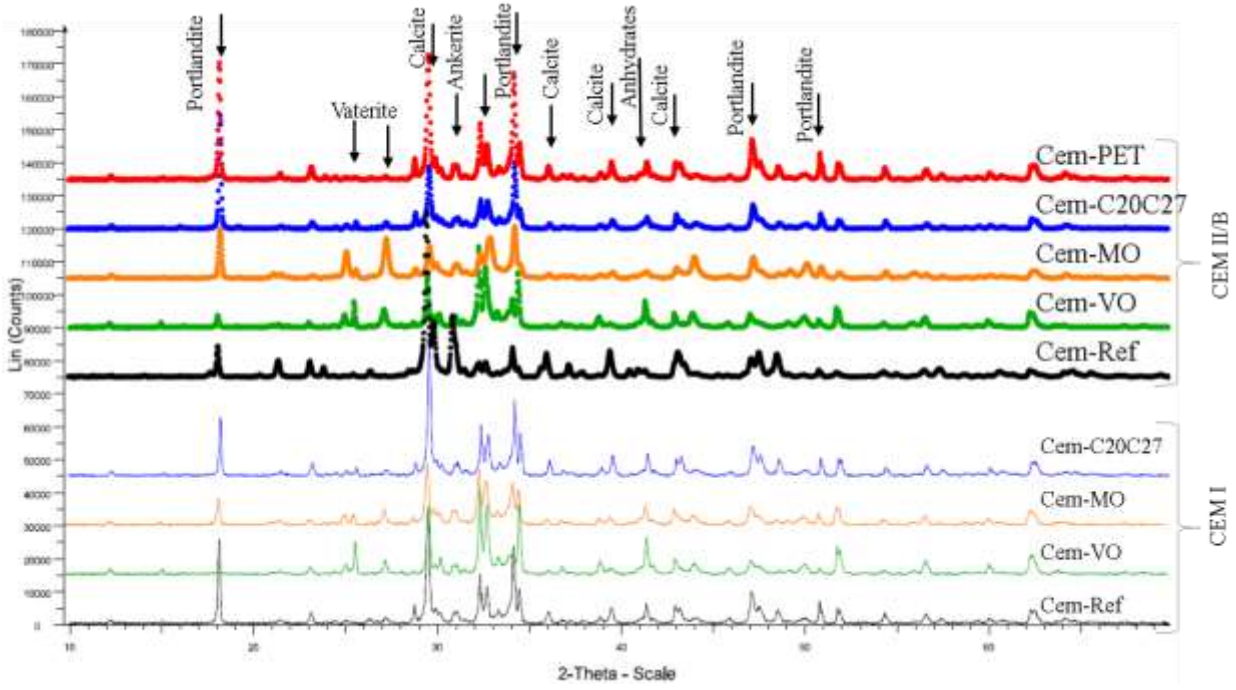

c)

Figure 88 *XRD diffractometry spectroscopy results categorised according to different w/c ratios: a)0.3, b)0.4, and c)0.5*

The used experimental program facilitate the identification of hydrated and non-hydrated phases. To findings through the nomination of peaks confirm through the same angle of diffraction analysis in literature [193,198]

The XRD test was conducted on the cement paste samples after 24 hours of standard curing conditions. The results indicate that the CSH gel was not detected because the crystals in CSH gel are very small compared to portlandite and surface carbonation explaining the calcite and vaterite and forming a superficial layer hiding the other crystalline forms of the hydrated cement.

The XRD experiments on cement samples with two cement type and w/c ratio against different coated formworks reveal that hydrated, non-hydrated and carbonated phases of cement for both types of cements were observed at 24 hrs of hydration. For the reference cement pastes Portlandite, calcite and vaterite (a hexagonal crystal version of calcite) were detected, regardless of cement type and w/c ratio. However, the presence of release agents blunts the hydration process. The mineral oil and vegetable release agents while being in contact with water form a soap layer which later functions as a separating layer [10, 218, 221, 222].

Regarding to the cement samples against polymeric coated surface, non-absorbent polymeric layers, C20C27 and PET, result in the formation of a thin water layer, which provides the later water for further hydration. As a result, in comparison to PET and C20C27, the hydration process was detected less in the F17-MO and F17-VO. Besides, among these two coating layers, the cement pastes prepared in F17-PET showed higher hydration comparing to C20C27. It must be noted that obtained XRD results confirm the relationship between hydration levels and roughness of cementitious surfaces and the approaches via the SEM images.

The total analysis of all cement type and w/c ratio against the various formworks are presented in ***Annex 2***.

2.3. Contact angle

F17-Ref, and polymeric coated formworks' (PET, and C20C27) thermodynamic characterization through contact angle ($Ø_{SL}$) measurements were carried out. For this purpose, three standard liquids with specified characteristics, distilled water, glycerol, and ethylene glycol, were selected. The measured contact angle and the corresponding surface energy were calculated via the Owens-Wendt model in accordance with NF EN 828: 2013 [62].

Table 32: *Formwork surface contact angle measurement using reference liquids*

Formwork surface	Contact angle (°)			Surface energy (mN/m)
	Water	Glycerol	Ethylene glycol	
F17-Ref	74.2 ± 2.8	65.4 ± 1.3	49.9 ± 2.2	31.74 ± 2.3
PET	113.8 ± 1.1	102.8 ± 0.7	57.7 ± 1.7	28.56 ± 0.8
C20C27	76.5 ± 2.4	75.2 ± 1.1	55.2 ± 1.9	27.60 ± 1.5

The environment RH and temperature were recorded at the time of measurement: 22 ± 2 °C and 52 %. Besides, the F17-Ref has not undergone any surface treatment before the test.

Table 32 presented the drop angle measurement with distilled water, glycerol, and ethylene glycol. The border to characterize the wettability of the surface is Ø = 90 °; if the contact angle is smaller than 90 °, the surface is characterized as hydrophilic, and when bigger than 90 °, it is counted as a hydrophobic surface [192]. In this context, the PET layer with distilled water, glycerol, and

ethylene glycol had contact angles of 113.8 ± 1.1°, 102.8 ± 0.7 °, and 57.7 ± 1.7 °, respectively. The contact angles of the F17-Ref and C20C27 were practically identical.

It should be noted that for steel surfaces, especially stainless steel, the contact angle values get affected by various factors such as the nature of the steel, the environmental conditions of measurement (RH %, Temp) [193], the type of treatment applied to the surface (e.g., polishing, heat treatment), prior cleaning of the surface, as well as the time between the time of treatment/cleaning and the time of measurement [202- 203].

The surface energy of F17-Ref, C20C27, and PET via the Owens-Wendt model was calculated. The results are illustrated in the figure below (**Figure 89**):

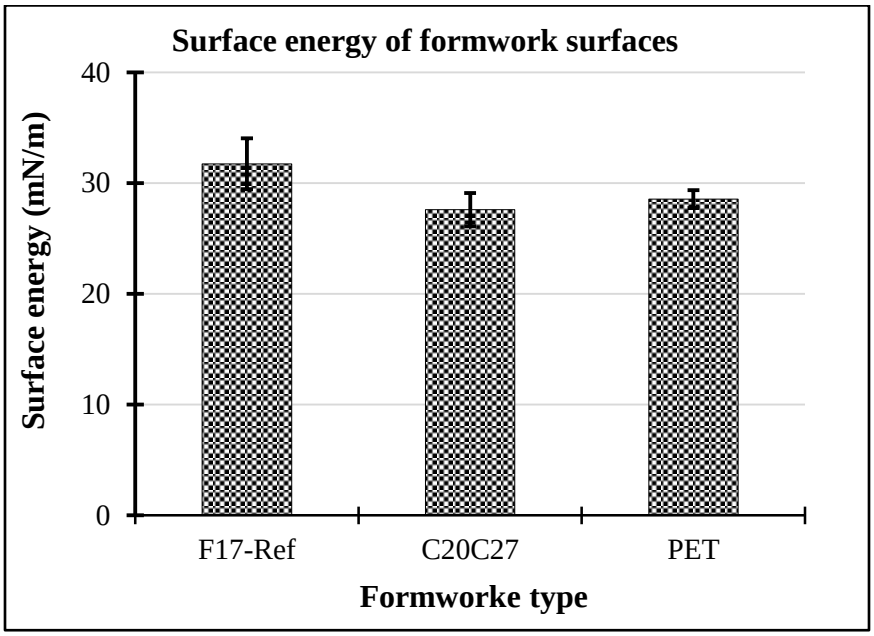

Figure 89 *Surface energy calculated for F17-Ref, C20C27 coating, and PET coating surface types*

The surface energy measured for the F17 R formwork, at 31.74 ± 2.3 mN/m, has a significant standard deviation, not allowing for observing any difference with the other formwork surfaces. The measurement in work of C. Chadfeau [39] for F17 R, F17 I, and F17 M were recorded at 27.7 ± 5.1 mN/m, 24.1 ± 3.6 mN/m, and 33.4 ± 3.8 mN/m, respectively, which for the reference formwork the obtained surface energy value was smaller compared to our calculation. Besides, the surface energy for C20C27 (27.60 ± 1.5 mN/m) was lower than F17-Ref (31.74 ± 2.3 mN/m). However, the PET surface energy (28.56 ± 0.8 mN/m, lower standard deviation) was between F17-

Ref and C20C27. **Figure 90** illustrates the contact angle value of F17-Ref, C20C27, and PET formworks and their corresponding surface energy values.

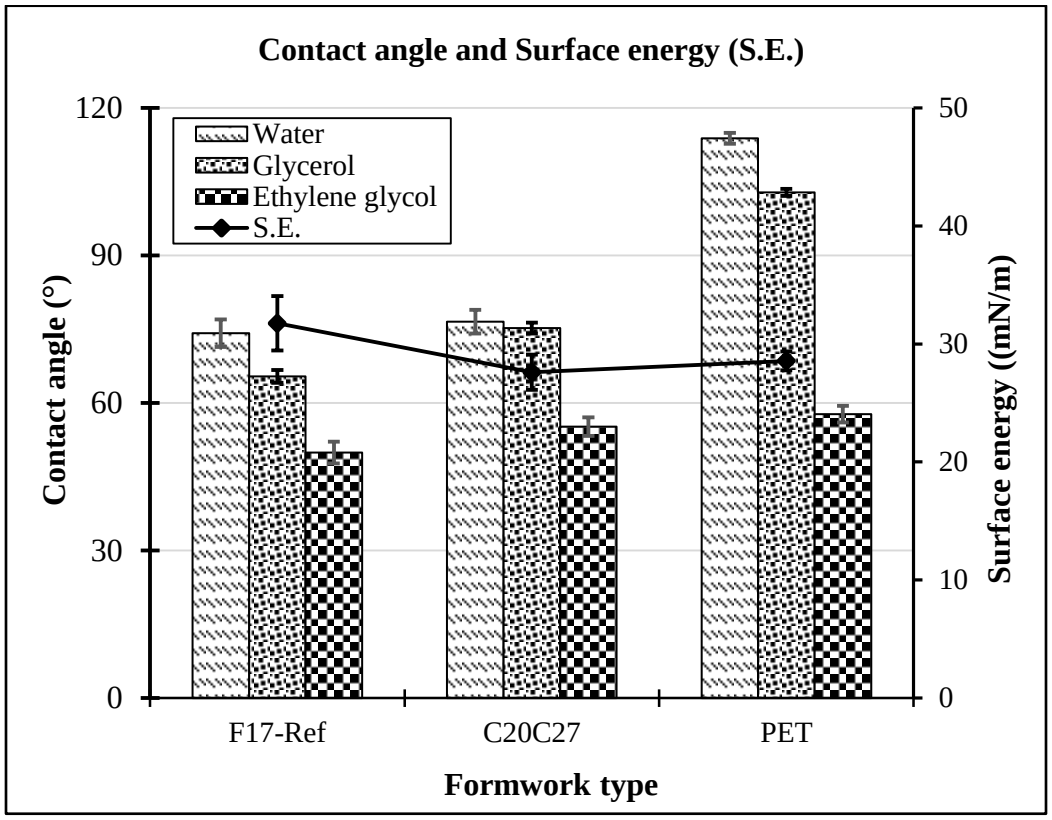

Figure 90 *contact angle of formworks with different standard liquids and theier corresponding surface energy*

The thermodynamic surface states of these formworks are relatively close, as indicated by the analysis of the results. F17-Ref has the highest surface roughness parameters (S_a = 4.56 ± 0.39 µm, S_q = 5.663 ± 0.467 µm), corresponding to a higher surface energy value (31.74 ± 2.3 mN/m) than C20C27 (27.6 ± 1.5 mN/m) and PET (28.56 ± 0.8 mN/m). Nonetheless, as compared to PET, the surface energy of C20C27 with a rougher surface is lower (**Figure 91**).

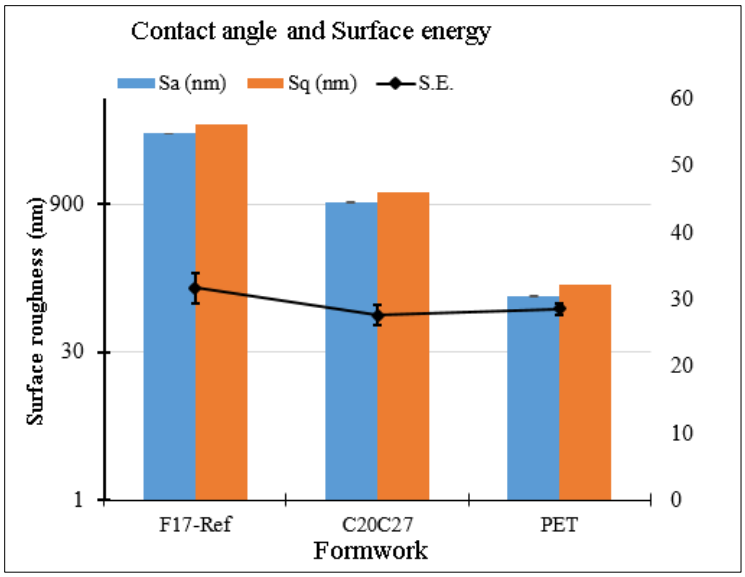

Figure 91 *Correlation of surface texture parameters Sa and Sq and surface energy of formworks*

Similar conclusions were observed by C. Chadfeau [39]; the reference formwork, C20C27, and F17 intermediate polished, had relatively close thermodynamic surface states except the mirror polished showing higher wettability and surface energy.

Based on these experimental results, there is no correlation between thermodynamic state of the formwork and its surface morphology. That is in agreement with the literature and confirms that Owen Wendt model is certainly the more often used but not the most accurate one to take the influence of roughness in account for the evaluation of surface energy based on contact angle values.

Synthesis of results and discussion

During concrete placement, the fresh semi viscos liquid hardens in the formwork and gets embedded in the smallest asperities, thus obtaining the formwork surface pattern. This pouring of fresh concrete generates a circulation of the fresh paste at the formwork surface which is dependent on the formwork surface's morphology [5, 204]. During the casting procedure, various types of formworks can be used, such as wooden / timber, steel, plywood, and aluminum [4- 6]. The different characteristics of used formwork on construction site affect the surface of cementitious materials in contact [5-6]. Due to the low durability, the wooden formworks have been replaced

by other materials such as plastics (polymeric materials), different metal types, and fabric materials [18]. Among all of these choices, steel formworks proved to be more efficient due to the repeatability, easy to clean, and are more resistant to the corrosion and impacts received from concrete casting [19]. Moreover, various types of release agents are applied to the formwork skin to facilitate the separation of the concrete from the formwork by decreasing the adhesion forces present at the concrete/formwork interface. It also protects the formwork surface from corrosion and decreases the harmful process of cleaning [6-10]. Release agents are applied to the formwork surfaces to have a lower adhesion force, smoother concrete surface and avoid sticking the concrete to the formwork.

The experimental results of this section confirm that the demolding force, named $\boldsymbol{F_d}$, is significantly high for the cement samples against reference formwork (F17-Ref) without any coating. The demolding force decreases remarkably through the usage of release agents. The lowest demolding force was recorded for the cement samples against vegetable oil coated formworks followed by the mineral oil and PET.

The decrease of demolding force through usage of release agents can be explained that the application of release agents on the formwork surface causes a surface roughness modification [66]; it fills the cavities on the formwork surface, resulting in better demolding. However, on a smooth surface, the effect of the release agent is different, it creates a barrier of variable thickness between the formwork and the concrete, which increases the micro-roughness of the formwork surface which impact cementitious surface. The difference between mineral oil and vegetable oil can be explained through their different chemical characteristics that affect the demolding force [38]. The experimental results are in well accordance with those of literature C. Chadfeau's work [39] and Mazkewitsch and Jaworski [172]. Moreover, the polymeric coated surfaces showed a better functionality as a release agent through a presentation of a low adhesion compared to the samples against the reference formworks.

As mentioned, the surface characteristics of a cementitious are related to the type of used formworks and release agents [6-10]. It can be seen that the cement samples against F17-Ref had the roughest surface, followed by release agents coated formwork and the C20C27 polymer

coating. It must be noted that the smoothest surface with a low surface roughness parameters belonged to the cement samples against PET coating layer.

In terms of changing the cement type from CEM I to CEM II/B, the roughness does not necessarily correlate with the w/c ratio change proportionately. For example, the S_a and S_q values in reference samples declined at w/c = 0.3 (11.5 % and 8.8 %, respectively), but when the w/c ratio was changed to 0.4, a smoothness loss was found by - 28.3 % and - 25.7 %, respectively. However, this tendency was not maintained by the other w/c ratio increase. It should be mentioned that the formworks coated with mineral oil had a similar effect on the prepared cement paste surface morphology.

The highest roughness change (S_a and S_q) was observed for Cem-C20C27 through the variation of cement type (CEM I by CEM II/B) at w/c = 0.3 by $-$ 30.8 and $-$ 39.1 %, respectively. Conversely, with w/c ratio equal to 0.4, an increase of roughness parameters, S_a and S_q, by 32.3 % and 25.4 % were observed. Thereafter, with w/c = 0.5 the S_a and S_q were increased back by $-$ 40.1 % and $-$ 22.6 %, respectively. It is worth mentioning that similar patterns were observed for Cem-PETs and Cem-VO, as well.

The w/c ratio modification from 0.3 to 0.4 with CEM I modified the roughness morphology of Cem-Ref, Cem-MO, Cem-VO, and Cem-PET $\approx 0 \pm 10$ %. The S_a and S_q of Cem-C20C27 for the same group were decreased $-$ 32.8 % and – 66.7 %, respectively. Moreover, in the same context, the roughness of Cem-Ref and Cem-MO was reduced by 48 to 60 % in samples produced with CEM II/B. On the other hand, the roughness characteristics of Cem-VO, Cem-C20C27, and Cem-PET, increased by 34 to 60% (**Figure 81 a**).

The Cem-MO and Cem-VO surface roughness have bigger compared to other cement surfaces.This change is observed due to the release agent being applied unevenly over the formwork surface. Therefore it creates a barrier of variable thickness between the formwork and the cement or concrete, which increases the micro-roughness of the formwork surface and, therefore, the concrete surface [66].

To establish if there is a correlation between demolding forces, surface roughness of formworks, cement type and w/c ratio, **Figure 92** graphically presents the surface roughness influence on the

demolding quality of the formworks in the pre-crack demolding test. It should be mentioned that the results were categorized according to the w/c ratio.

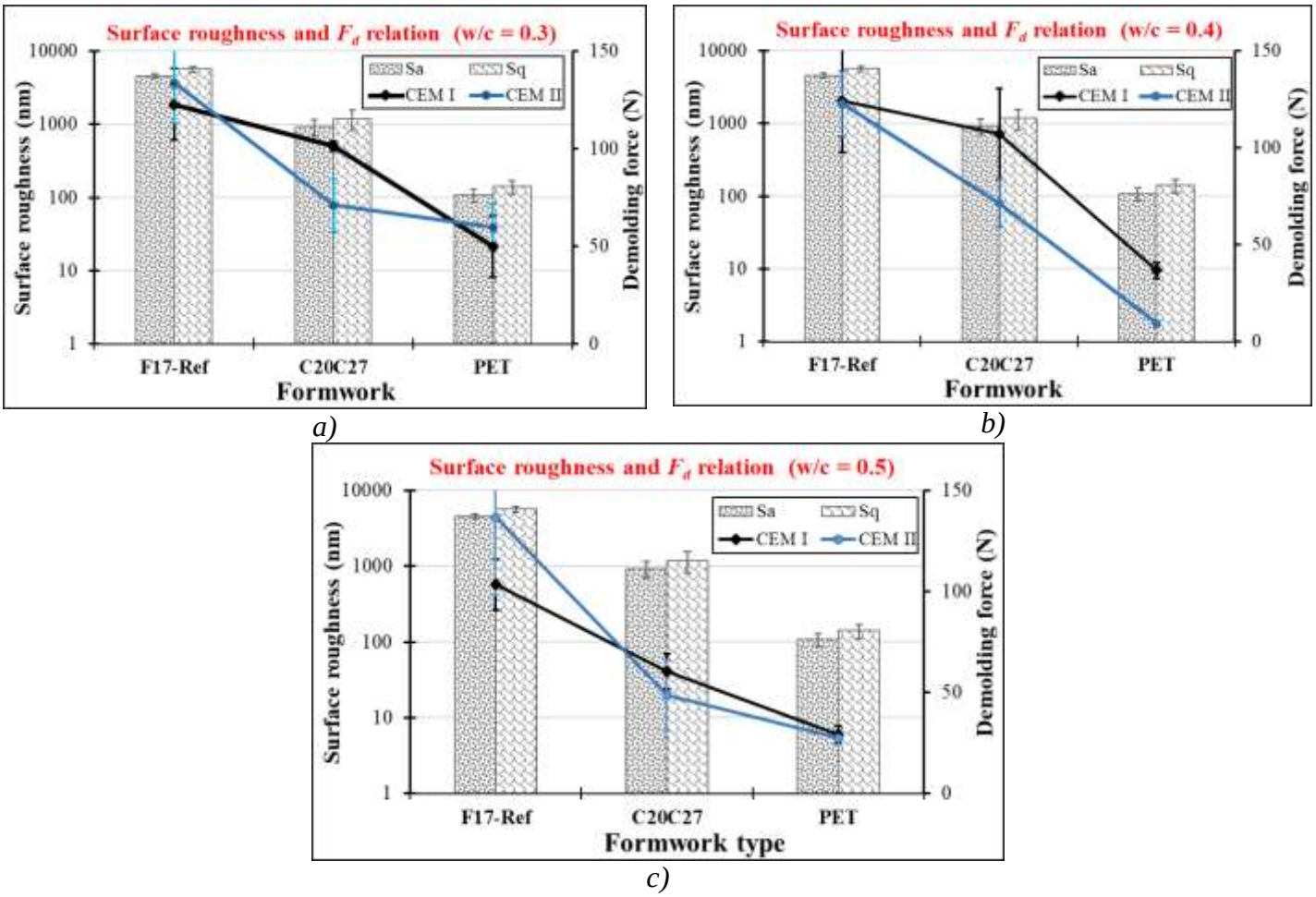

Figure 92 *Formwork surface roughness parameters (Sa and Sq) influence on the demolding force (Fd) at fracture mode I with cement pastes: a)w/c = 0.3, b) w/c = 0.4, and c) w/c = 0.5*

As it was mentioned that, the highest roughness parameter values belonged to F17-Ref (S_a = 4563 ± 389 nm, S_q = 5663 ± 467 nm) which followed by C20C27 (S_a = 931 ± 235 nm, S_q = 1176 ± 370 nm) and the smoothest roughness parameters were recorded for PET (S_a = 108 ± 21 nm, S_q = 141 ± 30 nm) (**Table 33**). Consequently, the reduction of roughness parameters S_a and S_q from F17-Ref, C20C27 and PET were followed by the F_d lessening in all w/c ratios (0.3, 0.4, and 0.5) (**Figure 92)**. To better understand the demolding force reduction improvement by using different formworks, **Table 33** shows the F_d reduction in percentage and it was calculated based on the average F_d. In cement paste with CEM I, the C20C27 compared to F17-Ref improved the stripping

force by 17.2 %, 13.7%, and 41.5% at w/c ratios 0.3, 0.4, and 0.5, respectively, which were the least improvement. The F_d for PET/F17-Ref exhibited the best improvement by 59.2%, 70.4%, and 72% with CEM I and 55.3%, 92.4%, and 79.9% with CEM II/B, for w/c ratio of 0.3, 0.4, and 0.5, respectively. Similarly, in the polymer coating evaluation of PET/C20C27, the stripping quality improvement was noticed (**Table 33**).

***Table 33 F_d** improvement by comparing the formworks demolding force average values*

	Average F_d reduction development (%)					
Cement type	**CEM I**			**CEM II/B**		
w/c ratio / Formwork	0.3	0.4	0.5	0.3	0.4	0.5
C20C27/F17-Ref	17.2	13.7	41.5	46.8	42	664.5
PET/F17-Ref	59.2	70.4	72	55.3	92.4	79.9
PET/C20C27	50.6	65.7	52	15.8	87	43.3

The formwork surface is put in contact with a fresh cementitious paste comprising anhydrous and hydrating phases. The dimensions of these phases are variable: from a few nanometers to a hundred micrometers [77, 191]. The arrangement of these cementitious structures is also variable: particulate organization (in the form of globular aggregates), crystals. The shape and dimensions will be compatible or not with the morphology of the formwork surface. This compatibility of structure corresponds to mechanical anchoring. In contrast to what was observed with C20C27 and PET, the finding of F17-Ref emphasizes the importance of mechanical anchoring at the concrete-formwork interface. In proportion to the volume of these surface cavities, hydrated and anhydrate cement particles take place in the cavities on the surface of plates, which can either enhance the mechanical bonding or decline it.

The findings on the effect of formwork surface roughness on the cement paste conform to the literature review. Fresh concrete spreads throughout the formwork and embeds itself in even the tiniest asperities, replicating the formwork surface [66]. As a result, the smoother the concrete surface is, the smoother the formwork surface will be. The literature review does not often provide information on the influence of the release agent on the surface roughness. The experimental results show that when the formwork surface is smooth, using a release agent will increase the micro-roughness of the concrete surface [66]. The release agent creates a physical fluid barrier at

the concrete-formwork interface; it is difficult to verify its application as perfectly uniform. Therefore, there are differences in the thickness of the release agent layer, which results in different thicknesses of the release agent layer across the formwork surface. It can be concluded that when the formwork surface is smooth, the use of a release agent will increase the micro-roughness of the formwork surface and thus of the concrete surface (**Figure 93 a**). When the formwork surface is rough, the release agent will reduce the roughness of the surface and thus the roughness of the concrete surface (**Figure 93 b**).

Figure 93 *Effect of release agent using on : a) smooth formwork on the micro-roughness of the surface of the cement paste, b) rough formwork on the microroughness of the surface of the paste*

In comparison, C. Chadfeau [39] investigated the surface roughness effect on the demolding force. She selected stainless steel formwork plate and polished the plates to two different levels, naming medium polished (F17 I) and mirror-polished (F17 M). The surface roughness parameters and the values she obtained are presented in **Table 34**.

Table 34 *Values of the surface parameters at stripping depending on the type of polishing using Interferometry microscopy, Chadfeau* [39]

Formwork surface	S_a (nm)	S_q (nm)	Sdr (%)	Vvc ($nm^3.nm^{-2}$)	Vvv ($nm^3.nm^{-2}$)
F17 mirror	16 ± 8	32 ± 15	0,01 ± 0,01	18 ± 9	5 ± 3
F17 intermediate	111 ± 11	153 ± 33	0,63 ± 0,09	152 ± 14	22 ± 5
F17 reference	4064 ± 488	4920 ± 593	11,08 ± 1,70	4994 ± 893	647 ± 105
C20C27	264 ± 60	328 ± 72	0,01 ± 0,01	388 ± 90	37 ± 12

As presented in **Table 34**, the S_a and S_q parameters for F17 M were 16 ± 8 nm and 32 ± 15 nm, and for F17 I, 111 ± 11 nm and 153 ± 33 nm, respectively. Moreover, the C20C27 coating in her work had a lower roughness parameter than this work. Regarding these parameters values, the Fd for F17 R, F17 I, and F17 M were 145 ± 47 N, 108 ± 22 N, and 25 ± 20 N, respectively. The

Surface roughness decrease resulted in a decrease in demolding force, which were on the same way as our outcomes.

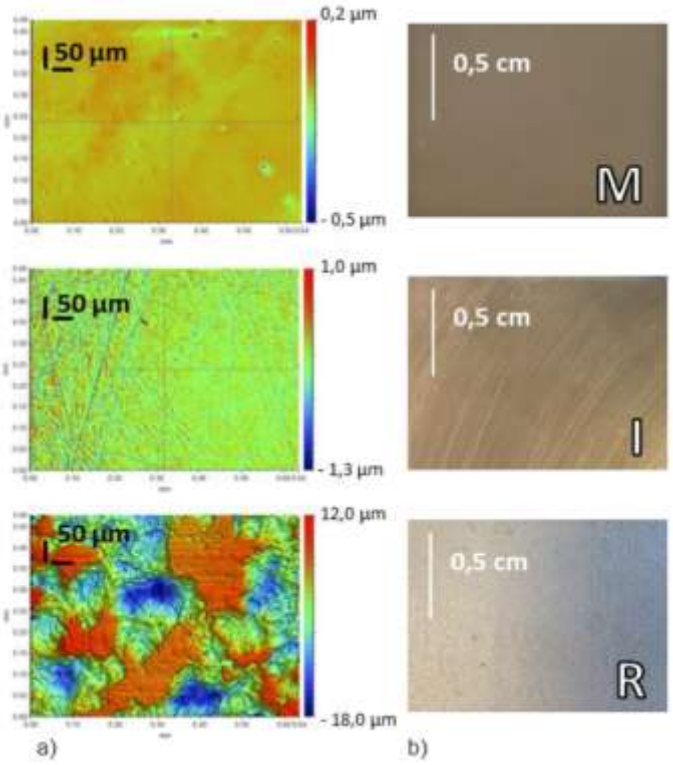

Figure 94 *States of polished and reference steel surfaces: a) Interferometric mapping of surface states for mirror polishing (M), intermediate (I), and reference surface (R), b) Surface aspects - macroscopic scale: mirror polishing (M), intermediate (I) and reference* [39]

3. Pull-off demolding test on concrete

A series of tests using concrete samples were conducted to understand the adhesion phenomena between formwork concrete in a macro scale. Therefore, the pull-off demolding test was conducted in mixed fracture modes I and II. All the formwork types with their corresponding changing factors are presented in **Figure 95**. Due to lack of provided C20C27 coated plates, to accomplish the requirement of ERGOFORM project, the experiment was performed for CEM II/B, w/c = 0.5, only.

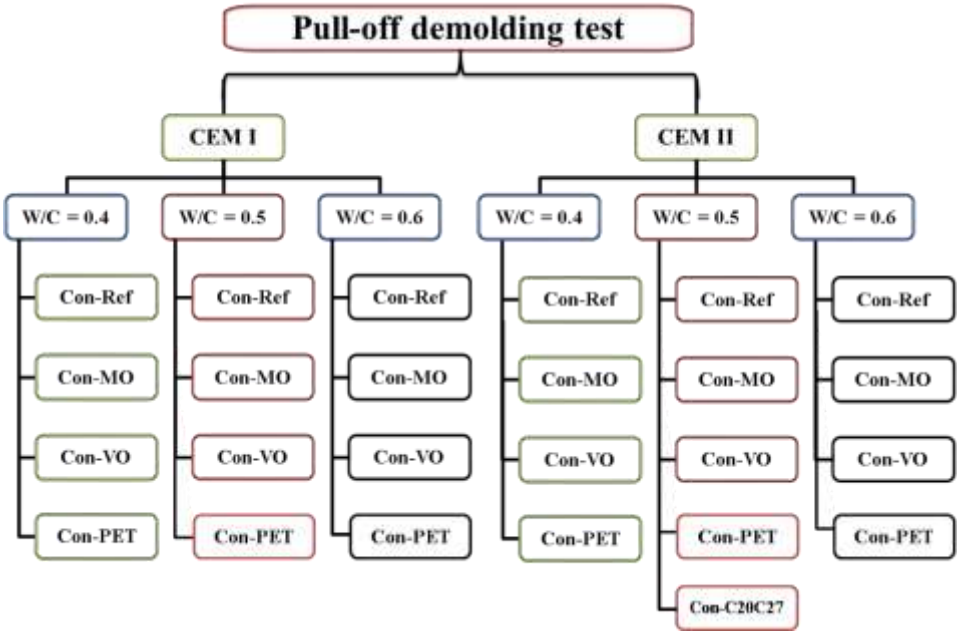

Figure 95 *Pull-off demolding experiment for all the concrete variations and formwork types*

The demolding test was performed in the SHIMADZU. The concrete samples were placed and fixed by nuts and bolts. Then, a lateral force was applied to insure the simultaneous demolding process (**Figure 96**):

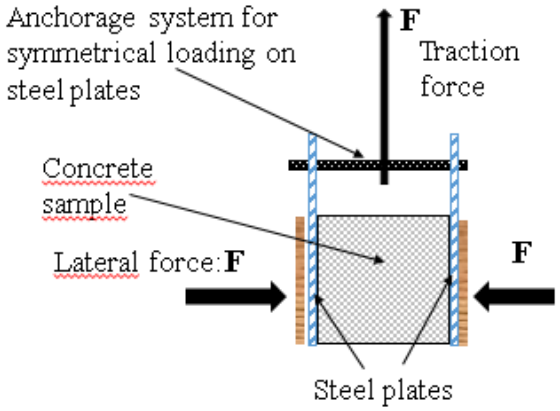

Figure 96 *: Pull-off demolding test on concrete samples*

The demolding force for concrete, also named F_d, was obtained through force-displacement diagram of pull-off demolding test on concrete samples against various type of coated formworks. An example of force-displacement curve is presented in **Figure 97**. The maximum demolding force was recorded as first peak force of force-displacement curve (F_d).

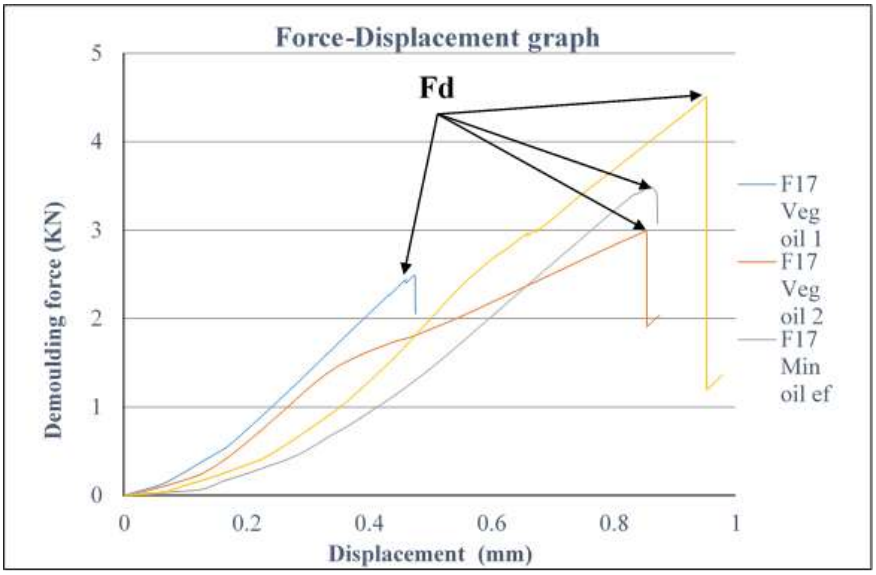

Figure 97 *Force-displacement graph of pull-off demolding test*

Each variation (cement type, w/c ratio, formwork surface caotting) can be discussed as following:

3.1. Effect of cement type on the concrete demolding force through pull-off demolding test

As mentioned two types of cement, CEM I and CEM II/B, are used for the elaboration of concrete mix design.

The pull-off demolding force results were plotted graphically in **Figure 98** by w/c ratio order (0.4, 0.5 and 0.6). The maximum adhesion between concrete and formwork is recorded for F17-Ref (14.26±2.21 kN) which is 5 times more than that of coated surfaces. Moreover, the lowest adhesion performance was underlined for the Con-PET and Con-VO samples as 2.75±0.33 kN and 2.68±0.31 kN, respectively. Whereas, the Con-MO samples present an increase of 25% in demolding force compared to the Con-PET ones. Besides, Con-C20C27 formworks had almost 2 times higher demolding force (5.04±1.36 kN) compared to the Con-PET one.

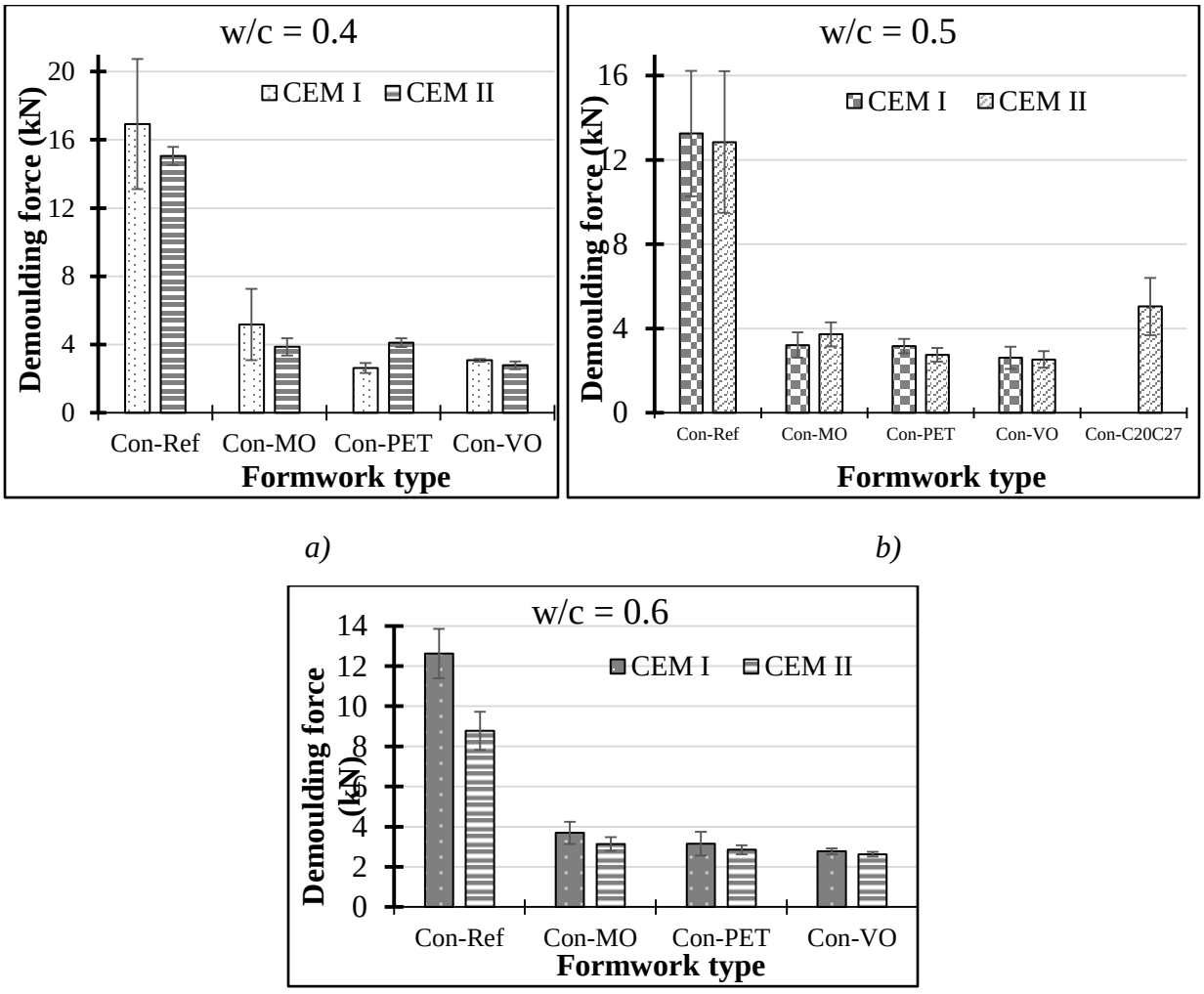

Figure 98 *Pull-off demolding average force, obtained from different formworks via changing the w/c ratio and cement type: a) w/c = 0.4, b) w/c = 0.5, and c) w/c = 0.6*

The results of demolding test on concrete against various coated formworks are in accordance with those of C. Chadfeau's work [39] and Mazkewitsch and Jaworski's work [172]. Considering the result dispersion range into account, it can be seen that both types of cement showed similar

adhesion degrees. It must be noted that the obtained results of pull-off demolding test on concretes confirms those obtained by the pre-crack demolding test on cement past samples.

3.2. Effect of w/c ratio on the concrete demolding force through pull-off demolding test

The F_d for all formworks by cement type were plotted in **Figure 99**. The demolding force, F_d, of concrete samples against reference formworks (Con-Ref) with w/c = 0.4 for CEM I and CEM II/B were recorded as highest value, which is 16927 ± 3817 N and 15055 ± 539 N, respectively. Because of the lack of C20C27 coating plates, it was only for one variation of cement type and w/c ratio the test was carried out. The result showed that the second highest F_d was recorded for Con-C20C27 with w/c = 0.5, CEM II/B (5043 ± 1358 N). The Con-MO for all w/c ratios (from lowest w/c ratio to highest: CEM I: 5171 ± 2088 N, 3212 ± 604 N, and 3696 ± 552 N, for CEM II/B: 3864 ± 506 N, 3724 ± 574 N, and 3133 ± 339 N) displayed higher demolding force comparing to Con-VO and Con-PET. Besides, the difference in the demolding force for the reference sample to the second one (Con-MO) was 70 - 75% reduction. Only in reference samples (F17-Ref) was detected that an increase in the w/c ratio resulted in a decrease in F_d. It should be noted that a consistent association was not established for the Con-MO, Con-VO, Con-PET, and Con-C20C27. The strong adhesion of concrete to the F17-Ref can be described physio-chemically phenomena [205-206], which in terms of concrete-steel chemical bonding, it was previously invesitaged by Y. Song *et al.* [199].

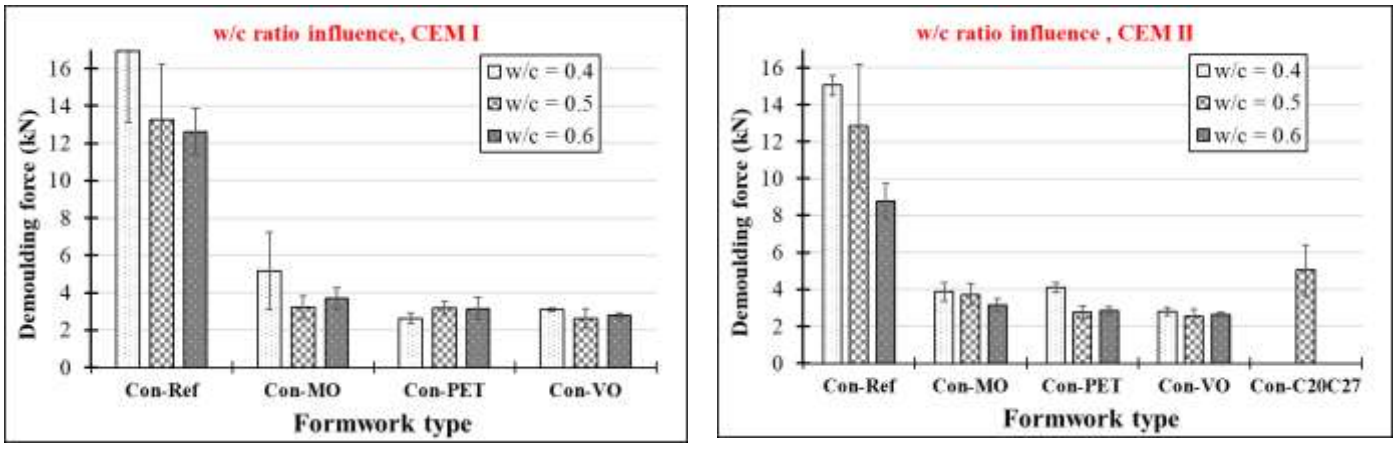

a) *b)*

Figure 99 *Pull-off demolding experiment results, effect of w/c ratio: a) Fd with CEM I, b) Fd with CEM II/B*

In order to check the compressive strength of concretes used versus various coated formworks, the test was performed after 28 days of standardized curing. The results from the compressive strength tests are presented in **Table 35**. It must be noted that no difference was observed for concrete samples against different coated formworks. In accordance with the literature, the compressive strength of concretes decreases with increase of w/c ratio.

Table 35 *Concrete samples compressive strength test results after 28 days of standard curing*

w/c ratio	Cement type	Compressive strength (28 days, MPa)
		f_{cm} (MPa)
0.4	CEM I	56.73 ±1.08
	CEM II/B	68.81 ±0.54
0.5	CEM I	54.07 ±0.34
	CEM II/B	60.89 ±0.57
0.6	CEM I	39.31 ±2.14
	CEM II/B	48.30 ±0.40

3.3. Coating effect on the concrete demolding force through pull-off demolding test

The graphs below were created using the results of the demolding tests. To avoid the result scattering, all of the results are presented in **Figure 100**.

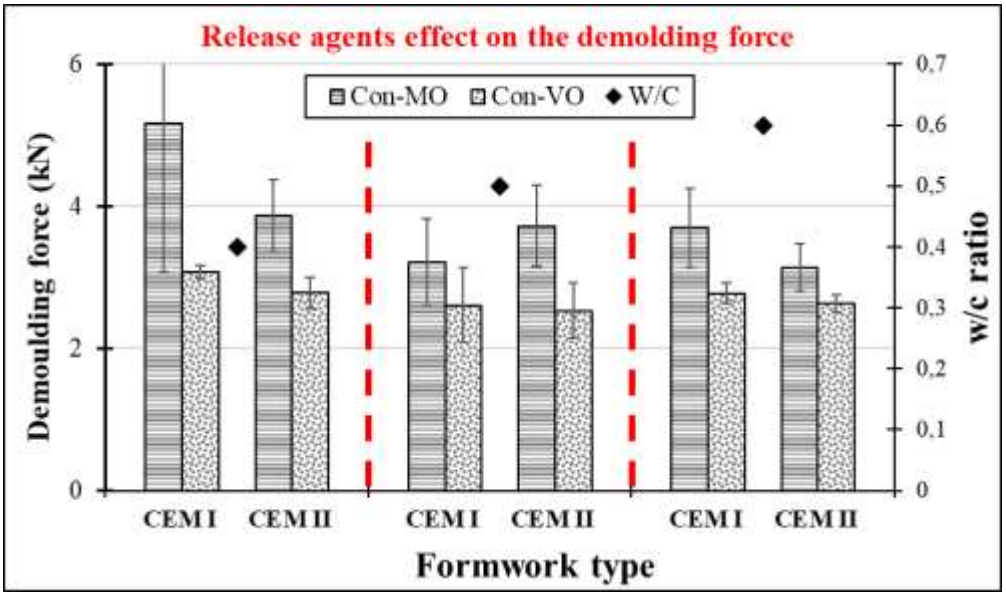

Figure 100 *Mineral oil and vegetable oil effect on the demolding force in pull-off demolding test*

The performance of the vegetable oil than mineral oil was recorded through pull-off demolding test on concrete. The F_d value high dispersion was recorded for Con-MO with CEM I, w/c = 0.4, which can be related to the thickness of oil coating [200].

In terms of polymeric coated materials as a release agent, both PET and C20C27 were utilized for the demolding/adhesion performance (CEM II/B, w/c = 0.5) and the results are shown in **Figure 101**. C20C27 and PET demolding forces were 5044 ± 1358 N and 2749 ± 331N, respectively. The result exposed the better demolding property of PET than C20C27. The PET/C20C27 demolding force decreased by 45.5 %, which was comparable to the obtained results by C. Chadfeau [39].

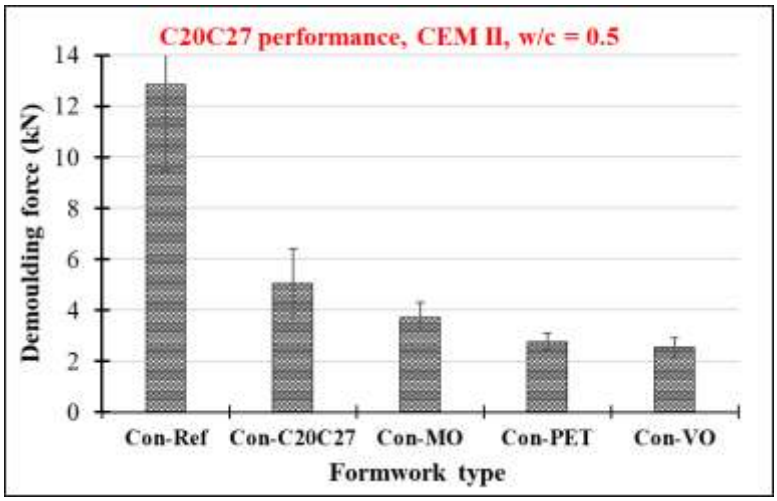

Figure 101 *Polymer coated formwork demolding/adhesion functionality*

4. The durability of C20C27 and PET polymer coatings

Coating durability was evaluated by repeating the experiment on the same coating multiple times. The procedure was that after each demolding pull-off test, the formwork plates with C20C27 and PET were rinsed with tape water and then air dried to be ready for the next test.

The durability of four pairs of C20C27 was tested. The results are presented in **Figure 102**. Besides, **Figure 103** shows the progression of demolding force for C20C27 coatings. The coatings were assessed visually by looking for signs of ripping and separation of the coating from the steel plate.

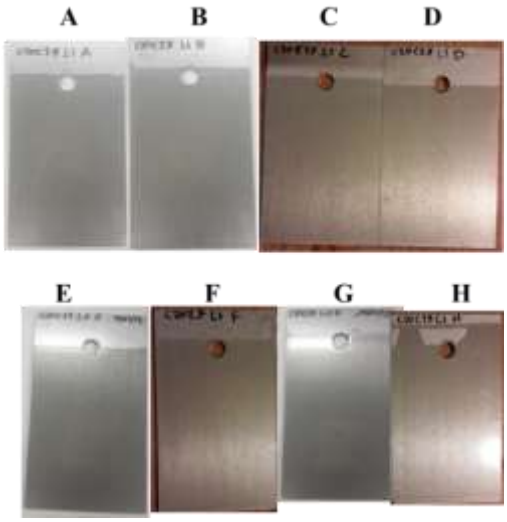

Figure 102 *C20C27 plates before utilization*

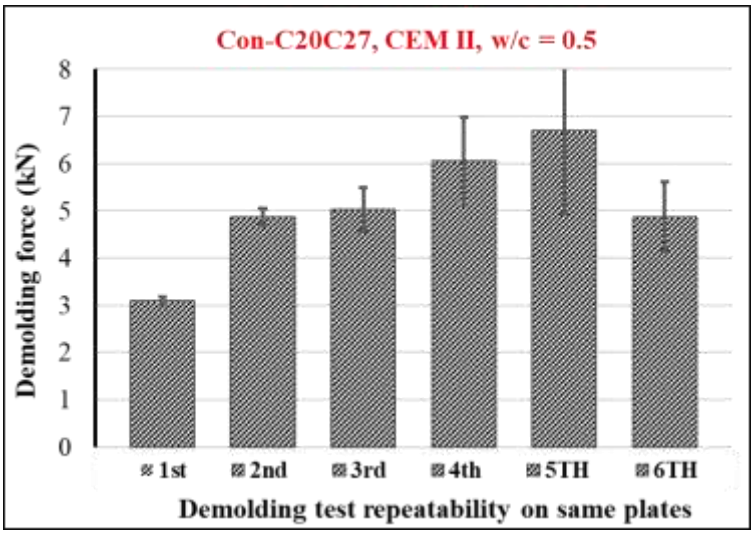

Figure 103 *Durability of the C20C27 formwork via demolding test repetition*

The evolution of the demolding force showed a roughly corresponding increase in F_d, which was again followed by a value drop at sixth utilization. **Table 36** shows the number of times each plate could be used.

Table 36 *The number of repetitions of each C20C27 plate*

C20C27 plates repetition								
plate name	A	B	C	D	E	F	G	H
usage number or repeatibility	3	3	5	4	4	4	1	6

It is worth mentioning that the releasing qualities of C20C27 were questioned since concrete particles remained after each demolding on some of the coatings, which were later removed by scratching **Figure 104**.

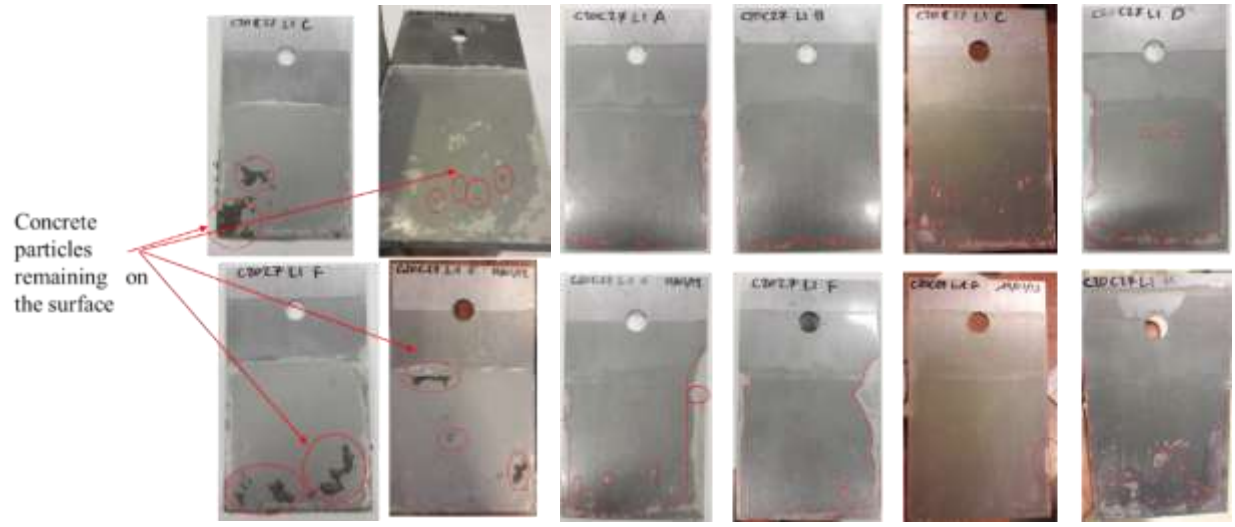

Figure 104 *concrete particle remainings on C20C27 plates and the detachment and tearing of the coating layer specified with a red line*

In a work by C. Chadfeau [39], the durability of the C20C27 layer was investigated through repetition of pre-crack demolding test with cement paste. She analyzed the demolding force result and concluded that after 10 times utilization, the plate's surface gets altered, but the demolding force does not change noticeably. The F_d at 1st and 10th utilization were 92 ± 20 N and 98 ± 54 N, respectively. The average stripping force for all 10 experiments was 98 ± 24 N. Whereas the behavior of the same coated formwork against concrete shows defaults after 6 utilizations.

The PET durability test, which involved repeating the demolding test, yielded a better result than C20C27. Six pairs of PET plates were utilized more than one time, but due to a time constraint, they were only used 13 times. The demolding force evolution and surface quality are given in **Figure 105**.

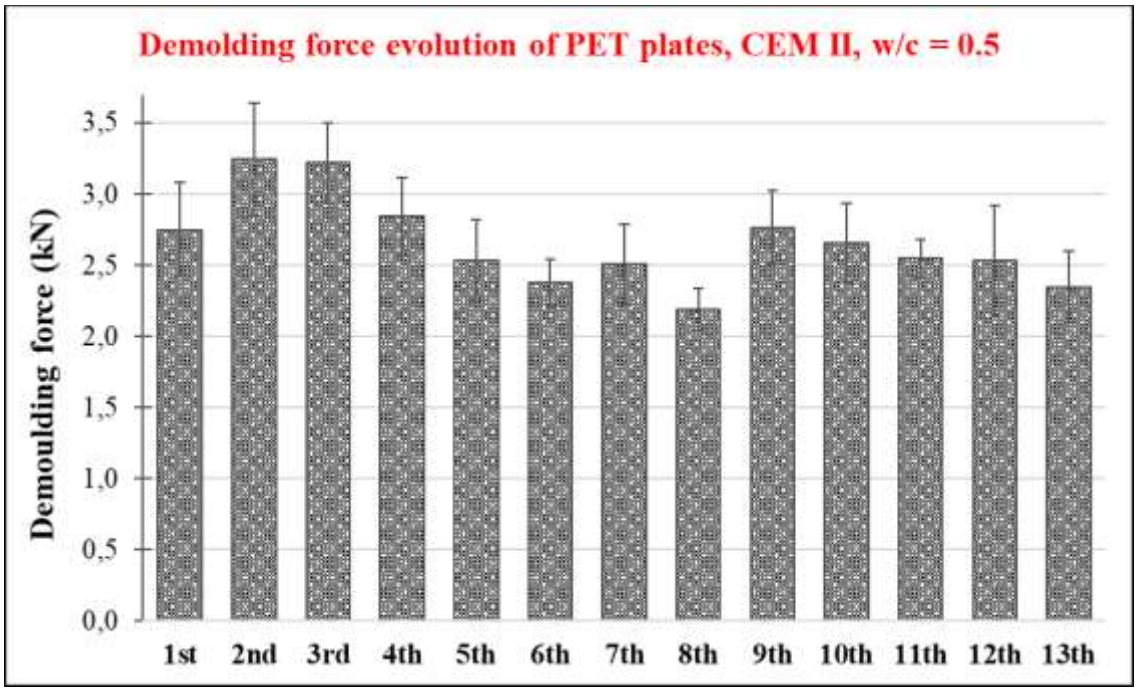

Figure 105 *PET durability test via pull-off demolding examination*

In the evolution of demolding force, no order was discernible. The F_d at the last usage (13^{th}), 2.3 ± 0.28 kN, was quite similar to the Fd at the first use, 2.7 ± 0.4 kN. In addition, the demolding test was carried out in both mixed fracture mode I and II, and the 2 kN lateral force behind the plates were the reason behind the high F_d value (F_d > 2 kN) for all samples.

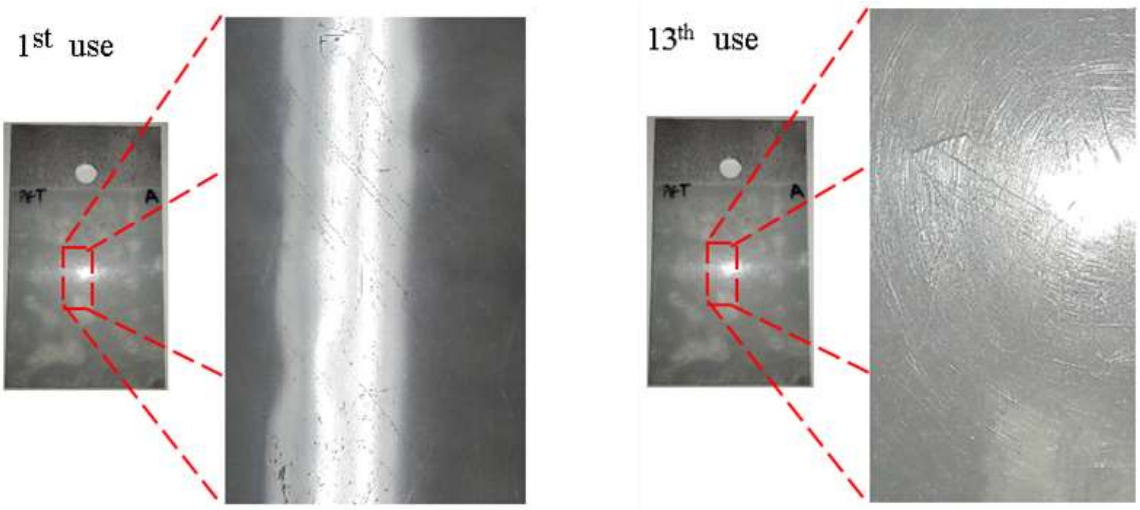

a) *b)*

Figure 106 *PET coating surface in action: a) PET surface after 1^{st} utilization, b) PET surface after 13^{th} utilization*

Figure 106 displays the effect of multiple utilization of PET coatings. Some micrometric scratches were observed after 1st utilization. After each subsequent utilization, the micrometric scratches number was increased. The surface status of PET after 13 times of utilization is shown in **Figure 106 b**.

Synthesis of results and discussion

The release agent depending on its physiochemical characteristics and the applying method [201], affects the concrete final surface properties and the releasing properties differently [4, 24, 39, 218, 219]. Leon-Martinez *et al.* [200] visually investigated the performance of biodegradable release agents and mineral oils at the formwork-concrete interface. It was indicated that all vegetable oils showed better performance than mineral oils. To observe the adhering properties of release agents, they performed a shear adhesion strength test. Release agent thickness was 26 to 58 µm, and the experiment condition: was 25 ± 2 °C and 53 % relative humidity. The higher affinity of glycerol esters of vegetable oils on the steel surface and higher intermolecular interactions were explained as their better performance causes. The polar groups in vegetable oil (ester molecules) adsorb favorably to the metal surface of formwork, and the calcium carboxylates position themselves to the hydrophilic concrete (**Figure 107 b**) [218, 220]. Moreover, the fatty free acids react with the cement hydration products and produce an organic salt at the metal and concrete surface [10, 218]. In addition, the mineral oil, due to its high hydrophobicity characteristics, forms a physical barrier and prevents direct contact at the concrete-formwork interface.

The thickness of this layer affects the quality of demolding [189]. The formation of micelles between carboxylates and hydrocarbons molecules at the concrete-formwork interface was explained as a result (**Figure 107 a**) or, in other words, the hydrocarbon compound was the boundary layer [10, 218, 221, 222]. Besides, it is worth mentioning that the amphiphilic nature of the triglycerides contributes to this barrier's stability via van der Waals cohesion forces [218, 223].

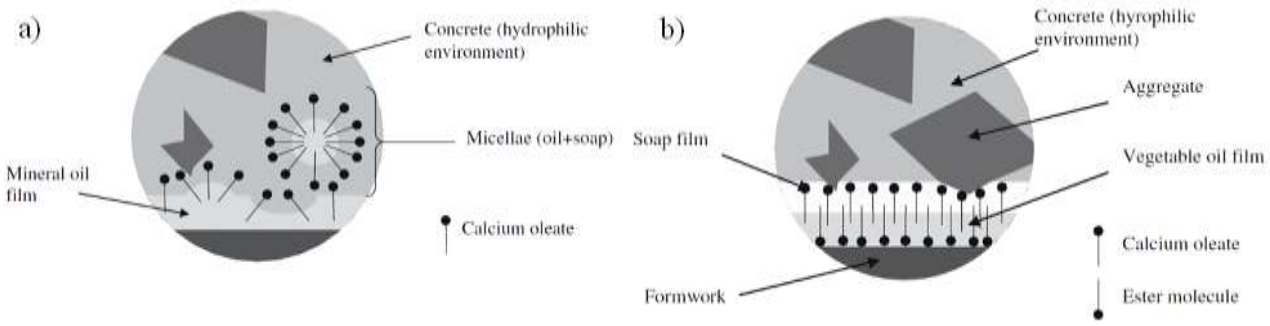

Figure 107 *Demolding mechanism of release agents: a) Solubilization of the mineral film by the soap micelle, b) Organization of a soap film in vegetable oil at the concrete/formwork interface* [189]

Both C20C27 and PET layers have non-absorbent characteristics. Besides, due to the water concentration at the concrete-formwork interface, the micrometric cavities on the formwork surface will be covered with water [64, 67, 204, 224, 225]. Besides the smooth surface texture of the coating layer, this phenomenon facilitates the demolding quality (**Figure 108**).

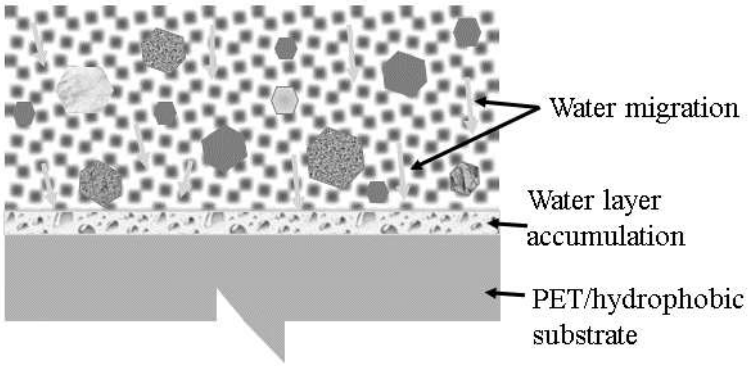

Figure 108 *accumulation of water layer at the polymeric substrate-cementitious materials*

For well understanding of the formwork surface morphology influence on the demolding force and to establish some correlation between studied properties, **Figure 109** illustrates the effect of surface roughness on formwork demolding quality in the pull-off demolding test graphically. It should be noted that the results were divided into groups based on the w/c ratio.

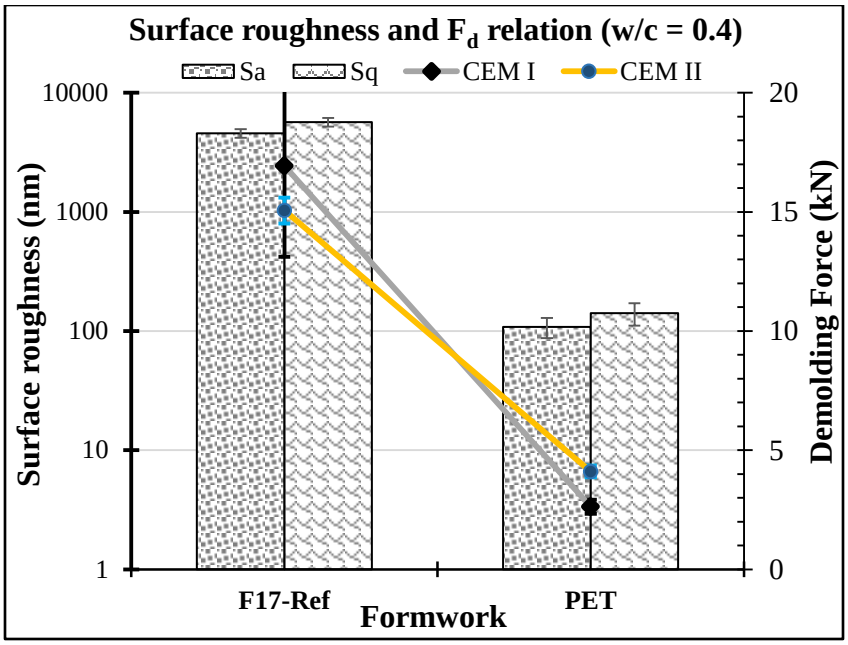
Surface roughness and F_d relation (w/c = 0.4)
Sa
Sq
CEM I
CEM II
10000
1000
100
10
1
20
15
10
5
0
Surface roughness (nm)
Demolding Force (kN)
F17-Ref
PET
Formwork

a)

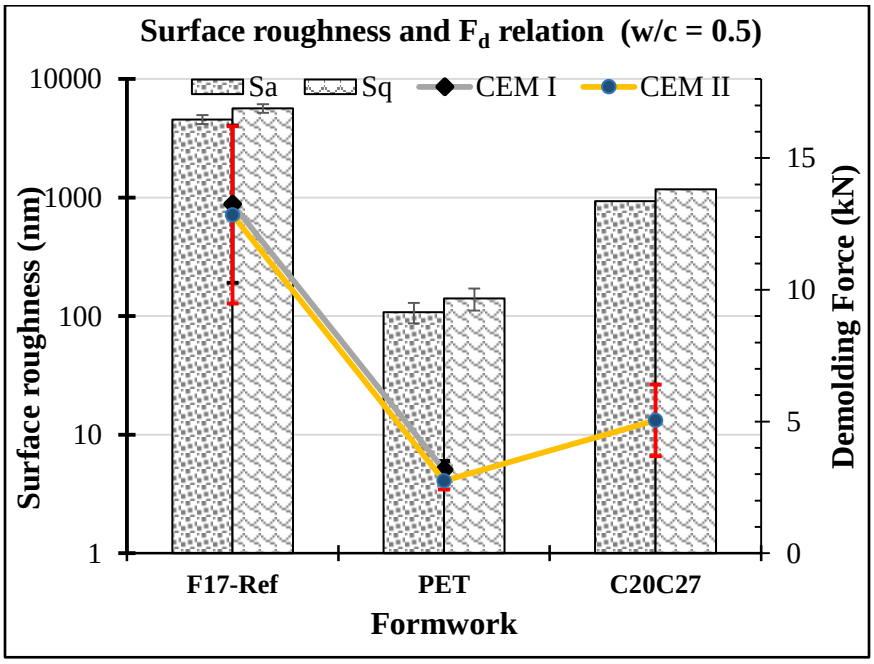
Surface roughness and F_d relation (w/c = 0.5)
Sa
Sq
CEM I
CEM II
10000
1000
100
10
1
15
10
5
0
Surface roughness (nm)
Demolding Force (kN)
F17-Ref
PET
C20C27
Formwork

b)

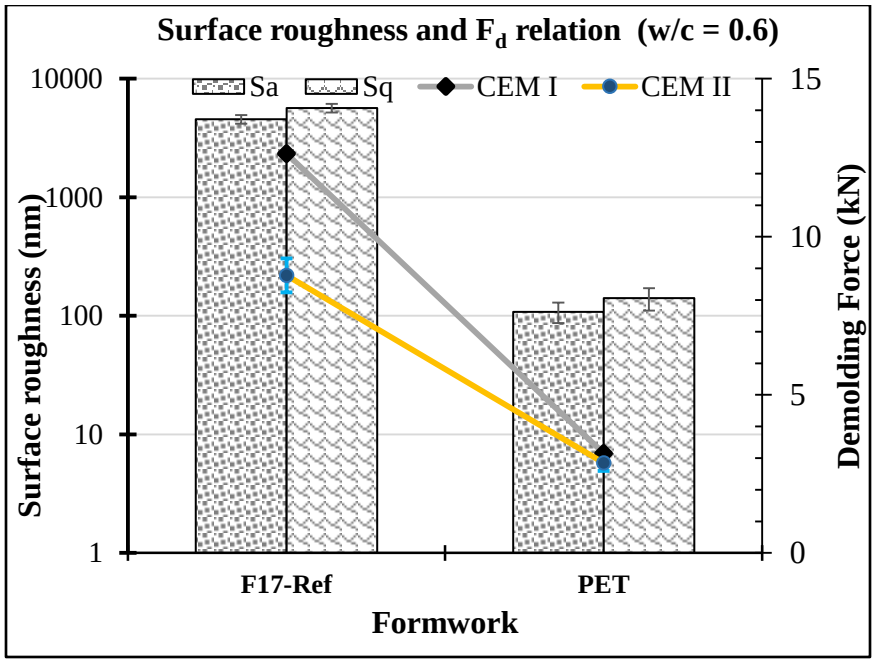

c)

Figure 109 *Formwork surface roughness parameters (Sa and Sq) influence on the demolding force (Fd) at mix fracture mode I & II: a) w/c = 0.4, b) w/c = 0.5, and c) w/c = 0.6*

The effect of surface morphology on adhesion behavior of concrete against various coated formworks is validated by the results obtained with cement paste by pre-crack demolding test. The F_d followed the same reduction path in all w/c ratios with the decrease of roughness parameters S_a and S_q from F17-Ref, C20C27, and PET (0.3, 0.4, and 0.5) (**Figure 109**). Moreover, **Table 37** shows the F_d reduction/improvement in percentage to better understand the progress in demolding force of concrete against different formworks. It should be noted that the average F_d was used for this calculation. In Con-PET/Con-Ref for all w/c ratios and cement types, the F_d value improved 70-80 %. Moreover, the ConC20C27/Con-Ref and Con-PET/Con-C20C27 exhibited 60.7 % and 45.5 % of F_d reduction, **Table 37**.

Table 37 *Fd improvement by comparing the formworks demolding force average values*

	Average Fd reduction development (%)					
Cement type	CEM I			CEM II/B		
w/c ratio / Formwork	0.4	0.5	0.6	0.4	0.5	0.6

ConC20C27/Con-Ref	-	-	-	-	60.7	-
Con-PET/Con-Ref	84.4	76.1	75	72.7	78.6	67.5
Con-PET/Con-C20C27	-	-	-	-	45.5	-

5. Visual aspects

Figure 110 shows the cement pastes cast in different formworks after pre-crack demolding tests. The surface of Cem-PET was shiny, while the other surfaces had opaque surfaces. The change in cement type and w/c ratio did not affect this feature in terms of shininess.

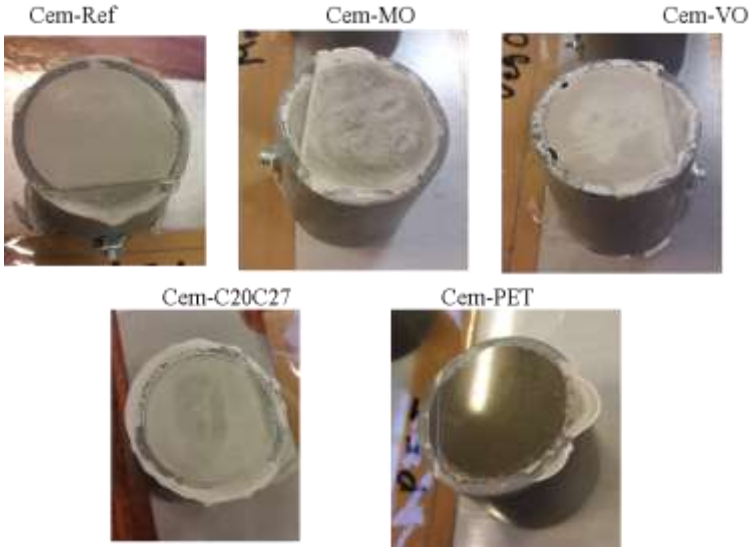

Figure 110 Cement paste surfaces cast in different formwork types

The visual analyzes for the plates and cement paste/concrete samples are summarized in **Table 38**. All coated formworks present adhesive failure behaviors during the demolding process except samples with reference formwork. However, the final appearance is different for the samples against the polymeric-coated compared to those of release agents.

Table 38: *failure types and surface aspects of concrete and cement samples regarding the formworks*

Concrete and Cement samples	Surface before test	Surface after test	Skin	Failure type
Cem-Ref & Con-Ref	Reference	- Rust - Concrete particles	Opaque	Cohesive
Cem-PET & Con-PET	0.19 mm of PET layer	- No corrosion or rust - Scratches appearance	Shiny	Adhesive
Cem-C20C27 & Con-C20C27	Laboratoire de Photochimie et d'Ingenierie			

	Macromoleculaires (LPIM) Product		
Cem-MO & Con-MO	Release agent coated	- No corrosion or rust	Opaque
Cem-VO & Con-VO		- No concrete particle	

The appearance of the facing surface is an important criterion and when the concrete is not covered with a coating, particular attention must be paid to the choice of the composition of the latter and to the quality of the formwork to obtain the aesthetic criteria. desired[207]. **Figure 111** demonstrates the effect of formwork coatings in the final surface color.

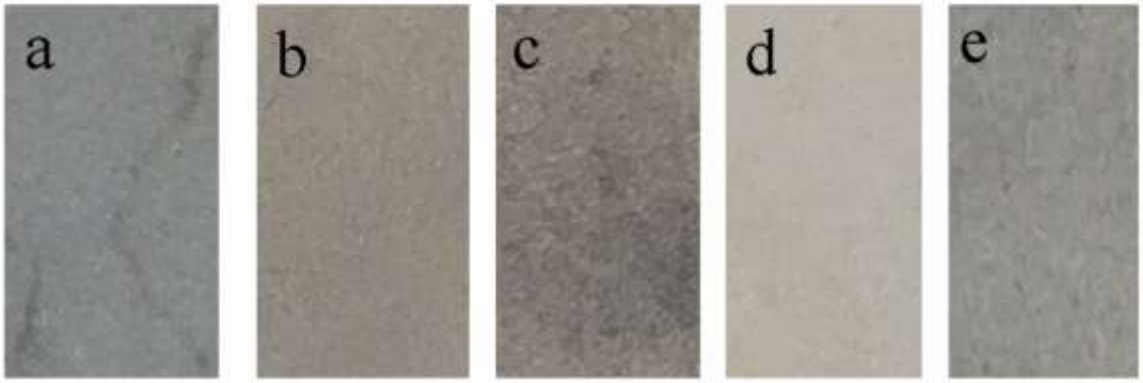

Figure 111 *cement paste color after 3 years: a)Cem-Ref, b)Cem-VO, c)Cem-MO, d)Cem-C20C27, and e)Cem-PET*

Beside vibration and formwork surface texture and porosity, each type of release agent have its own unique fingerprint, resulting in a varied concrete color [231- 232]. It can be seen that on the Cem-MO, the color uniformity was not kept. Moreover, the prints of release agent was observed in most of the samples (**Figure 111 a**). Cem-VO color was closer to green at the time of demolding, which decreased during the time. However, compared to other samples, Cem-VO had a green-gray color (**Figure 111 b**). The Cem-C20C27 resulted in a dry-looking color surface compared to others.

The effect of formwork morphology at the microscopic scale induces the facing surface aspect visually observed at macro scale. The concrete and cement samples that were prepared in different formwork types had a shiny or opaque surface. Regardless of cement type and w/c ratio variation, the Cem-PETs and Con-PETs had a smooth and shiny surface that reflected the light, even after

two years in laboratory environment. On the other hand, the rest of the samples had opaque surfaces. Similar results were reported by M. Marin [66].

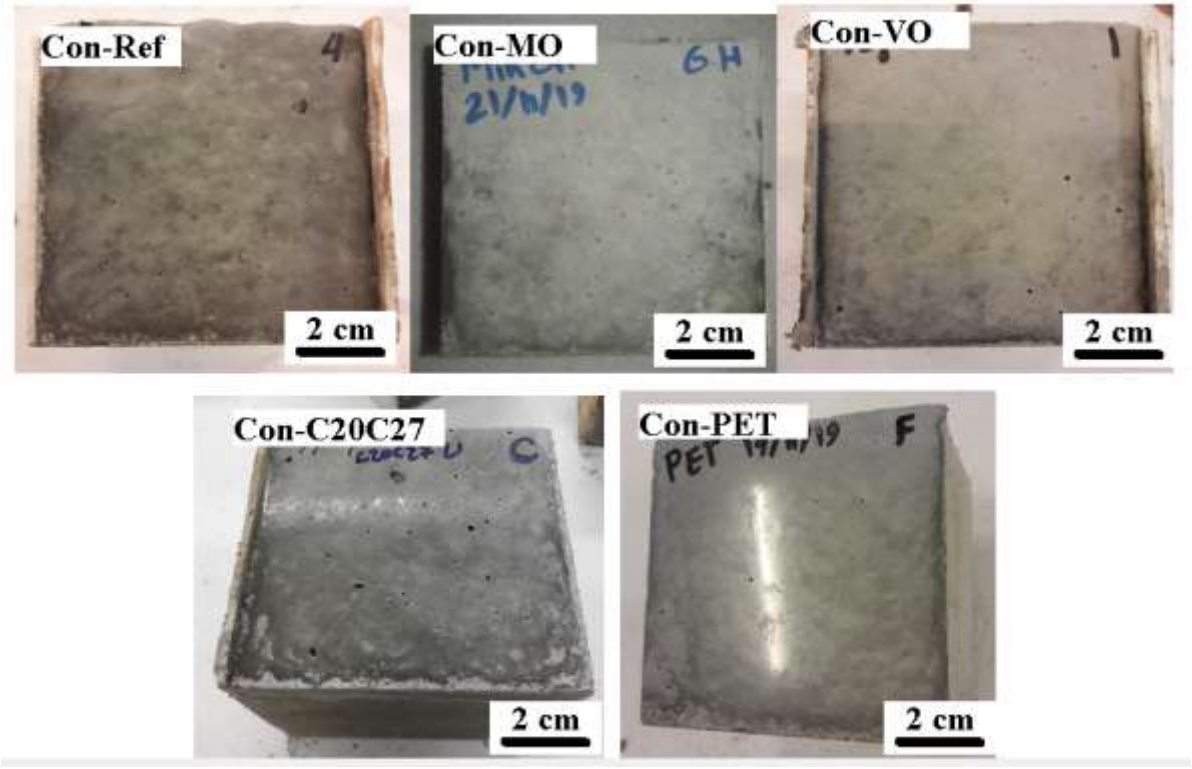

Figure 112 *Concrete samples after pull-off demolding test*

It is well known that w/c ration influences the color facing as illustrated by authors that made a two-layer concrete (Izoret, 2014) [209]. A lower layer with a w/c ratio of 0.45 and an upper layer with a w/c ratio of 0.40. The cement used was a CPA 55 PM cement. The total volume of the mixture was 60 liters with a weight of 400 Kg. We can observe that the lower layer is darker than the upper layer from these results. This means that the increase of water in the composition of the concrete can generate a darkening of the concrete surface.

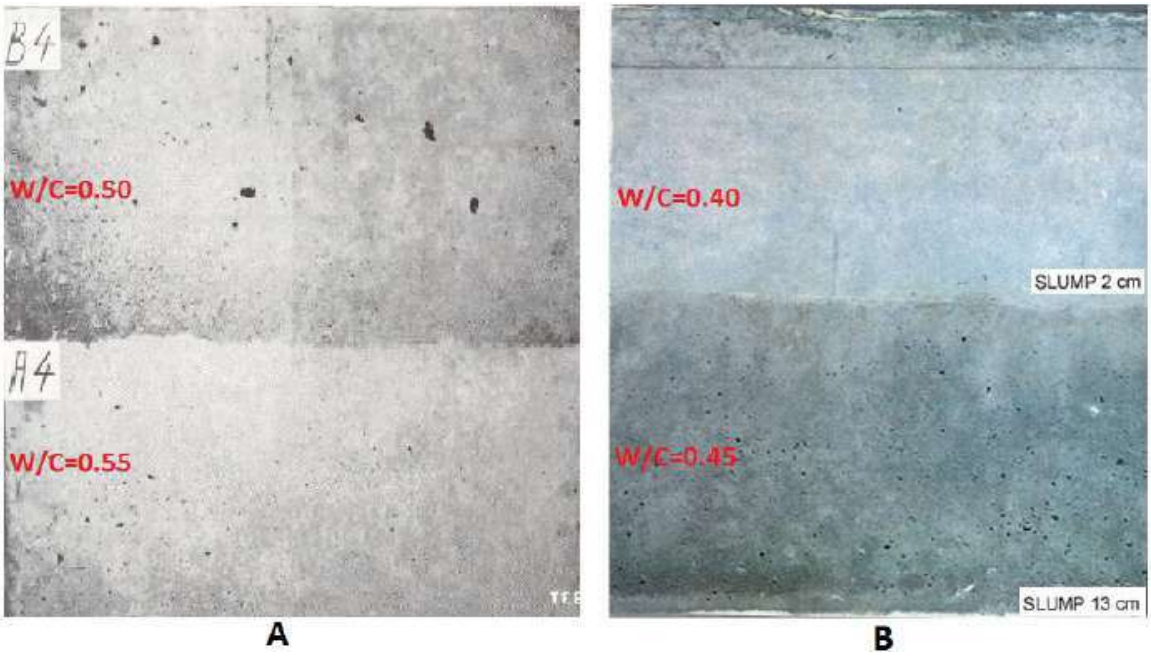

Figure 113 *Effect of the w/c ratio on the surface color: A) w/c=0.55 at bottom, and w/c=0.50 at the top (Trub, 1973) and B) w/c=0.45 at the bottom and w/c=0.40 at the top (Izoret, 2014)*

Consequently, an increase of water at the interface between formwork and concrete may change the facing color.

Conclusions

This experimental work was carried out to examine the effect of formwork's surface parameters on adhesion force between the formwork and concrete/cement paste. For this, various types of coating were used to explore their effect on microstructural properties and on demolding forces for two types of tests on cementitious materials after 24 hours of hydration. Therefore, the major concluding points drawn from the above experiments are as follows:

- The surface energy data show that coated plates, regardless of coating material type, have nearly similar surface energy. The highest surface energy was observed for the reference plate (F17-Ref) without any coating materials.
- Mechanical interlocking occurs at the microscopic scale in the absence of a releasing substrate due to irregularities on the formwork surface and the concrete. Furthermore, Van der Waals forces and hydrogen bonding improve concrete-metal formwork adhesion.
- The lowest surface roughness parameters were detected for cement paste samples subjected to polymeric-coated plates (Cem-PET and Cem-C20C27) compared to those with release agents. Here the highest value was recorded for Cem-VO.
- The microstructure analysis using E-SEM shows that the Cem-VO present a more porous surface with a lower degree of surface hydration compare to Cem-PET and Cem-C20C27. Therefore, its highest value of surface roughness subjected to the coated formworks can be linked to the existence of unhydrated cement particles and pores among the samples.
- Releasing agents exhibit variable separation tendencies depending on their chemical characterizations. These materials link to the formwork surface by Van der Waals forces and show a hydrodynamics characteristics. In comparison to mineral oil, vegetable oil demonstrated improved functionality in terms of demolding due to its higher viscosity qualities and creation of a thin monomolecular ester layer.
- Both pull-off and pre-crack demolding tests illustrated that the PET and F17-VO had better performance with a lower adhesion force.
- Cementitious surfaces subjected to polymeric-coated formwork produce shiny and smooth surfaces, whereas mineral and vegetable agents produce opaque and rougher surfaces.
- Overall the PET can be considered as an alternative for the replacing of used release agents due to its lower adhesion force and durability in terms of usage repeatability.

General conclusions

This work is carried out in the frame of ERGOFORM (Ergonomic Formwork) project which one of its objectives is to offer an alternative to used release agents by applying a polymer coating with high durability and low adhesion property. In addition, this project aims to reduce to decrease the harsh working conditions, increase the efficiency of the work by automatization of the system. As a scientific partner of ERGOFORM project, This study investigated the interaction between cementitious materials and different types of formworks at the early stage of hydration (24 hours) after the demolding procedure from the macro-scale to the micro-scale. Besides, this research work will develop the effect of mix design components by varying the w/c ratio and cement type against various types formwork on adhesion phenomenon.

The experimental tests were considered three w/c ratio (0.3, 0.4 and 0.5) for both types of cement (CEM I and CEM II) against the five variations of coated formwork: reference formwork (F17-Ref: without coated material), two oils release agent coated formworks (mineral and vegetable oil) and two polymeric coated fromworks (C20C27 and PET). The pre-crack demolding test was executed to investigate the adhesion between cement paste and formwork. To simulate the realistic scenario of site work in macro scale, an original test experiment called Pull-off demolding test was carried out on concrete samples in a mix fracture mode I & II. Moreover, the cement surface are analyzed through microstructure analysis of Interferometry Microscopy (IM), Scanning Electron Microscopic (SEM) and X-ray Diffractometry (XRD) analysis. Finally, the visual aspect of cement paste and concrete samples were compared.

Based on obtained experimental results, some conclusions can be drawn as following:

- The surface roughness of used formwork affect the demolding or adhesion force between formwork and cementitious materials. The highest demolding ($\boldsymbol{F_d}$) force was recorded for the cement paste/concrete samples against reference formwork (F17-Ref) without release agent.
- The demolding force doesn't affected by cement type with w/c ratios of 0.3 and 0.5, however, with w/c ratio of 0.4 an improvement of adhesion was illustrated for polymeric

coated surface through changing of CEM I by CEM II. In this parts, it can be concluded that more tests is necessary to highlight clearly the impact of cement type on adhesion.

- The effect of w/c ratio on demolding force is dependent of the type of formwork, wheareas, the demolding force doesn't change for cement samples against F-17, however, it can be seen that the F_d decreases proportionally with increase of water content for CEM I against PET formwork.
- The usage of release agents decrease the adhesion phenomenon of formwork/concrete. The experimental results revealed that the $\boldsymbol{F_d}$ decreased significantly by the introduction of mineral vegetable oil as release agents.
- The polymeric coated formwork improves the $\boldsymbol{F_d}$ compare to those from reference one. The obtained values of $\boldsymbol{F_d}$ are comparable to those against mineral and vegetable oil coated fromworks. It must be noted that the lowest adhesion was recorded for the cement samples against vegetable oil coated formworks (F17-VO).
- The Interferometry microscopic analysis (IM) indicate that the roughness of used formwork presents an impact on the surface in contact (cementitious surface). Whereas, the roughest surface of cement paste samples were recorded for those against reference formwork (F17-Ref) with high roughness parameters. The roughness of cement samples against oil coated formworks (F17-MO and F17-VO) are slightly similar to those against F17-Ref, however, the usage of oil release agents facilitates the $\boldsymbol{F_d}$.
- The smoother surface are shown for the cement samples against polymeric coated formworks (C20C27 and F17-PET), whereas, the lowest roughness parameters are observed for the cement samples against F17-PET and followed by C20C27.
- The Scanning Electron Microscopy analysis (SEM) confirm the findings by IM. In taking in account the the pore size, number of cavities, and surface roughness of the cement paste samples against F17-MO and F17-VO are similar to those against F17-Ref. However, the unhydrated cement particles are more visible on the surface of cement paste samples against oil coated formwork, independent of cement type and variations of w/c ratio.
- The form and placement of hydrated phases are related to the roughness of used formworks. The SEM images highlight that the cement surfaces against polymeric coated fromworks are smoother than those against F17-Ref, F17-MO and F17-VO which confirme the

obtained results by IM. It must be noted that the interne porosity of cementitious materials increases with the increase of w/c ratio, however, the findings by SEM indicate that the variation w/c ratio doesn't affect the surface porosity.

- The XRD analysis reveals that the presence of release agents blunts the hydration process compare to hydrated phases of cement samples against R17-Ref, regardless of cement type and w/c ratio.
- Moreover, the hydrated phases are more detectable on cement paste samples against polymeric coated formworks compare to those against F17-MO and F17-VO. It is due to the non-absorbent characteristics of polymeric layers, C20C27 and PET, which result in the formation of a thin water layer for hydration. Besides, among the polymeric coating layers, the cement pastes prepared in F17-PET showed higher hydration comparing to C20C27. It must be noted that obtained XRD results confirm the relationship between hydration levels and roughness of cementitious surfaces and the approaches via the SEM images.
- The 50 utilizations of the PET were intended, but due to the time restrictions, the PET coating in the pull-off demolding test with concrete was utilized not more than 13 times. The micro-scratches on the PET surface increased after the next utilization. However, the demolding force analyses of these test series on PET showed that using repetition does not significantly affect the stripping quality of the PET formwork. In this case, more investigations should be performed on the PET in terms of durability. Also, the obtained cementitious surfaces from PET formwork had the smoothest surface, among others. Besides, the proposed C20C27 polymer coating also improved the stripping quality by reducing the adhesion with the cement and constitutes a promising track to facilitate the stripping. Unfortunately, a study of the evolution of this adhesion over time reveals a weakness in the polymer, which tends to detach itself from the metal support after only 6 uses, maximum.
- From the visual observation of the obtained cement paste and concrete surfaces from different formworks with various w/c ratios and cement types indicate that the cementitious surfaces obtained from PET coatings are shiny and smooth which is not the case for the rest of the surfaces. Moreover, the color of the obtained surfaces is different from light gray

color (Cem-C20C27) to a darker color (Cem-Ref and Cem-MO). Moreover, the w/c ratio affects the surface color too.

Perspectives

This experimental work was focused on some parameters related to the adhesion between concrete and formworks. Some perspectives can be drawn as follows:

- For the well understanding, the effect of cement and w/c cement ratio on adhesion can be investigated in a large scale.
- The effect of studied parameters on adhesion can be clarified through the water penetration, capillarity and surface porosity by mercure tests on the surface of cement paste samples.

References

[1] UN environment, "Global status report 2017, Towards a zero-emission, efficient, and resilient buildings and construction sector," 2017.

[2] J. Radic, A. Kindij, and A. Mandic, "History of Concrete Application in Development of Concrete and Hybriad Arch Bridges," Chinese-Croatian Jt. Colloq. LONG ARCH Bridg., vol. LONG ARCH, p. 20, 2008.

[3] M. K. Hurd, Formwork for Concrete, 7th ed. American Concrete Institute, 2005.

[4] M. K. Hurd, Formwork for Concrete, 7th ed. ACI, 2005.

[5] F. A. Riveros and L. E. Llano, "Development and testing of a novel steel formwork for casting concrete slabs with different sizes Desarrollo y ensayo de un nuevo molde en acero para fundir losas de concreto con diferentes tamaños de concreto com diferentes tamanhos," vol. 26, no. 46, pp. 51–59, 2017.

[6] R. Schipper and B. Janssen, "MANUFACTURING DOUBLE-CURVED ELEMENTS IN PRECAST CONCRETE USING A FLEXIBLE MOULD -," pp. 1–11, 2011.

[7] C. C. Kuo and M. X. Wu, "Evaluation of service life of silicone rubber molds using vacuum casting," Int. J. Adv. Manuf. Technol., vol. 90, no. 9–12, pp. 3775–3781, 2017.

[8] Isabelle Lallemant, "Hétérogénéité de teinte des parements en béton : caractérisation et identification des mécanismes," Université de Cergy Pontoise, 2001.

[9] N. Kumar et al., "Design , Development and Experimental Assessment of a Robotic End-effector for Non-standard Concrete Applications," pp. 1707–1713, 2017.

[10] R. Lab H., "Think Formwork - Reduce Costs," Structure Magazine, no. April, pp. 14–16, 2007.

[11] C. Chadfeau, S. Omary, E. Belhaj, C. Fond, and F. Feugeas, "Characterization of the surface of formworks – Influence of the surface energy and surface texture parameters on the demolding forces," Constr. Build. Mater., vol. 272, 2021.

[12] W. R. L. Silva, D. S. Lucena, P. Štemberk, and L. R. P. Jr, "Evaluation of the effect of concrete compositional changes and the use of ethyl-alcohol and biodegradable-oil-based release agents on the final surface appearance of self-compacting concrete precast elements," Constr. Build. Mater., vol. 52, pp. 202–208, 2014.

[13] T. Lee, J. Lee, J. Kim, H. Choi, and D. Lee, "Effect of Formwork Removal Time Reduction on Construction Productivity Improvement by Mix Design of Early Strength Concrete," Appl. Sci., vol. 10, p. 7046, 2020.

[14] L. Libessart, C. Djelal, D. C. P., and I. Dubois-brugger, "The Effects of Release Agents on the Formwork / Concrete Interface," in Fédération Internationale du Béton Proceedings of the 2nd International Congress, 2006, no. June 2005.

[15] IEA/OECD, "Global Building sector Fuel type energy consumption," World Energy Statistics and Balances, IEA/OECD Paris, 2017. [Online]. Available: www.iea.org/statistics.

[16] S. Bouharoun, "CHARACTERIZATION OF THE INTERFACE BETWEEN FRESH CONCRETE AND FORMWORK," J. Civ. Eng. Manag., vol. 22, no. 1, pp. 26–37, 2016.

[17] N. Spitz, N. Coniglio, M. El Mansori, A. Montagne, and S. Mezghani, "Quantitative and representative adherence assessment of coated and uncoated concrete-formwork," Surf. Coatings Technol., vol. 352, no. July, pp. 247–256, 2018.

[18] N. Spitz, N. Coniglio, M. El Mansori, A. Montagne, and S. Mezghani, "On functional signatures of bare and coated formwork skin surfaces," Constr. Build. Mater., vol. 189, pp. 560–567, 2018.

[19] R. Das, I. Bhattacharya, and R. Saha, "Comparative Study between Different Types of Formwork," vol. 1, no. 4, pp. 173–175, 2016.

[20] L. Libessart, "Influence de la composition des agents de démoulage à l'interface coffrage/béton - Impact sur l'esthétique des parements en béton," Université d'Artois, 2006.

[21] C. R. Gagg, "Cement and concrete as an engineering material: An historic appraisal and case study analysis," Eng. Fail. Anal., vol. 40, pp. 114–140, 2014.

[22] SYNAD, "Syndicat National des Adjuvants pour Beton et Mortier. Classifiacation SYNAD des agents de demoulage," Paris, 2004.

[23] C. N. D. Cruickshank and J. R. Squire, "Skin Cancer In The Engineering Industry From The Use Of Mineral Oil," Br. J. Ind. Med., pp. 1–11, 1950.

[24] A. N. Gent and H. G. R., "Definition of Adhesion and Adhesive Joint," Encycl. Polym. Sci. Technol., vol. 1, pp. 218–256.

[25] R. Larsson, "Adhesion and surface energy," Surf. Charact. A User's Sourceb., pp. 565–569, 2007.

[26] A. Çolak, H. Wormeester, H. J. W. Zandvliet, and B. Poelsema, "Surface adhesion and its dependence on surface roughness and humidity measured with a flat tip," Appl. Surf. Sci. jou, vol. 258, pp. 6938–6942, 2012.
[27] H. R. Pakravan, M. Jamshidi, M. Latifi, and M. M. Chehimi, "Polymeric fibre adhesion to the cementitious matrix related to the fibres type , water to cement ratio and curing time," Int. J. Adhes. Adhes., vol. 35, pp. 102–107, 2012.
[28] R. A. Bowling, A Theoretical Review of Particle Adhesion, 1st ed. New York: Springer, Boston, MA., 1988.
[29] Jacob N. Israelachvili, Intermolecular and Surface Forces, 3rd ed., vol. 59. Elsevier, 2011.
[30] D. E. Packham, "THE ADHESION OF POLYMERS TO METALS: THE ROLE OF SURFACE TOPOGRAPHY," in Adhesion Aspects of Polymeric Coatings, Plenum press, New York, 1983, pp. 19–44.
[31] T. Craipeau, T. Lecompte, F. Toussaint, and A. Perrot, "Evolution of Concrete / Formwork Interface in Slipforming Process," in Digital Concrete, 2018, vol. 2, pp. 12–23.
[32] L. Nicoleau, "New Calcium Silicate Hydrate Network," Transp. Res. Rec., vol. 2142, no. 1, pp. 42–51, Jan. 2010.
[33] J. C. Berg, "Semi-empirical strategies for predicting adhesion," in Surfaces, Chemistry and Applications, Elsevier B.V., 2002, pp. 1–73.
[34] J. Henriques, "Modeling and simulation of intrinsically disordered proteins," 2016.
[35] The concrete Society, Formwork a guide to good practice, 2nd ed. Berkshire, UK: The concrete Society, 196AD.
[36] A. Mazkewitsch and A. Jaworski, "The Adhesion Between Concrete And Formwork," Adhes. between Polym. Concr. Adhes. entre Polym. Bet., pp. 67–72, 1986.
[37] Portland Cement Association, "Types and Causes of Concrete Deterioration," 2002.
[38] L. Libessart, P. De Caro, C. Djelal, and I. Dubois, "Correlation between adhesion energy of release agents on the formwork and demolding performances," Constr. Build. Mater., vol. 76, pp. 130–139, 2015.
[39] C. Chadfeau, "Caracterisations Multiechelles De Surfaces Cimentaires De Parement En Fonction De Differentes Surfaces Coffrantes," Strasbourg University, Ph.D. Thesis, 2020.
[40] D. Chafika, V. Yannick, and L. Libessart, "ANALYSIS OF FRICTION AND LUBRICATION CONDITIONS OF CONCRETE / FORMWORK INTERFACES," Int. J. Civ. Eng. Technol., vol. 7, no. 3, pp. 18–30, 2016.
[41] Y. Vanhove, C. Djelal-dantec, and H. Kada, "DEVELOPMENT OF A NEW DEMOLDING PROCESS BASED ON," in 15th International Conference on Experimental Mechanics, 2012, no. August.
[42] C. Djelal, P. De Caro, L. Libessart, I. Dubois, and N. Pebere, "Comprehension of demolding mechanisms at the formwork / oil / concrete interface," Mater. Struct., pp. 571–581, 2008.
[43] C. Djelal, Y. Vanhove, P. De Caro, and A. Magnin, "Role of demolding agents during self-compacting concrete casting in formwork," Mater. Struct. Constr., vol. 35, no. October, pp. 470–476, 2002.
[44] Philip G. Malone, "Use of Permeable Formwork in Placing and Curing Concrete," Washington DC, 1999.
[45] N. R. Andriamanantsilavo and S. Amziane, "Étude expérimentale sur l'évolution de la pression exercée par une pâte de ciment contre un coffrage pendant la prise," Rhéologie, vol. 3, pp. 12–21, 2003.
[46] M. A. U, "The effects of permeable formworks with sucker liners on the physical properties of concrete surfaces," Constr. Build. Mater., vol. 15, pp. 149–156, 2001.
[47] W. A. Megid and K. H. Khayat, "Variations in surface quality of self-consolidation and highly workable concretes with formwork material," Constr. Build. Mater., vol. 238, p. 117638, 2020.
[48] N. Spitz, N. Coniglio, L. Libessart, M. El Mansori, and C. Djelal, "Characterizing tribological behavior of fresh concrete against formwork surfaces," Constr. Build. Mater., vol. 303, no. April, p. 124233, 2021.
[49] F. Şebnem Kuloglu Yuksel, "Kendi kendini Temizleyen Betonlarda Kalip Tipinin Durabiliteye Etkisi," İSTANBUL TEKNİK ÜNiVERSiTESİ, Ph.D. Thesis, 2010.
[50] du coffrage et de l'étaiement Syndicat français de l'échafaudage, "Collection technique syndicat français de l'echafaudage, du coffrage et de l'etaiement," 2005.
[51] S. Bouharoun, "Comportement tribologique des huiles de décoffrage à l ' interface béton / coffrage - Influence de la formulation du béton Remerciements," UNIVERSITE D'ARTOIS, Ph.D. Thesis, 2011.
[52] Ł. Sadowski, Ż. Andrzej, and J. Ho, "ScienceDirect Multi-sensor evaluation of the concrete within the interlayer bond with regard to pull-off adhesion," ScienceDirect, vol. 8, pp. 573–582, 2018.
[53] Y. Vanhove, C. Djelal-dantec, and H. Kada, "Development of a new demolding process based on concrete polarization," in 15th International Conference on Experimental Mechanics, 2012, no. August, pp. 1–16.
[54] R. Goyal, A. Mukherjee, and S. Goyal, "An investigation on bond between FRP stay-in-place formwork and

concrete," Constr. Build. Mater., vol. 113, pp. 741–751, 2016.
[55] Paul G. Rouxhet, "Contact Angles and Surface Energy of Solids: Relevance and Limitations," WETTABILITY Surf. Free ENERGY, pp. 349–376, 2013.
[56] P. C. Hiemenz and R. Rajagopalan, "Surface Tension and Contact Angle: Application to Pure Substances," in Principles of cloid adn surface chemistry, 3rd ed., no. 1, New York: Marcel Dekker, Inc., 1997, pp. 248–293.
[57] R. J. Good, "Contact Angles and the Surface Free Energy of Solids," Plenum Press, 1979.
[58] O. Carrier and D. Bonn, Contact Angles and the Surface Free Energy of Solids. Elsevier Inc., 2015.
[59] A. Kozbial et al., "Study on the surface energy of graphene by contact angle measurements," Langmuir, vol. 30, no. 28, pp. 8598–8606, 2014.
[60] A. Gerschel, Liaisons intermoléculaires. Les forces en jeu dans la matière condensée, InterEditi. CNRS, 1995.
[61] D. K. Owens and R. C. Wendt, "Estimation of the surface free energy of polymers," Appl. Polym., 1969.
[62] NF EN 828:2013-02, "Adhesives — Wettability — Determination by measurement of contact angle and surface free energy of solid surface," French Stand., 2013.
[63] D. Maugis, Contact, Adhesion and Rupture of Elastic Solids, 1 st editi. New York: Springer, 2000.
[64] Clark S.L., "Release agents," Springer, Boston, MA, 1982.
[65] N. Migeotte and M. Martin, "Influence of the reuse of OSB and marine plywood formworks on concrete surface aesthetics," pp. 1331–1343, 2012.
[66] M. Martin, "Etude de la texture de la surface coffrée des parements verticaux en béton," Universite de LAVAL- Quebec, 2007.
[67] Y. Pan, Y. Zhang, D. Zhang, and H. Yang, "Effect of polymer and conventional molds on the aesthetical surface quality of concretes," Constr. Build. Mater., vol. 302, no. August, p. 124375, 2021.
[68] Y. Vanhove and C. Djelal, "Influence of the formwork removal by polarization on the facing aesthetics in reinforced concrete," Constr. Build. Mater., vol. 284, no. May, p. 122841, 2021.
[69] L. Libessart, C. Djelal, and P. De Caro, "Influence of the type of release oil on steel formwork corrosion and facing aesthetics," vol. 68, pp. 391–401, 2014.
[70] L. Libessart, C. Djelal, and P. De Caro, "Influence of the type of release oil on steel formwork corrosion and facing aesthetics," Constr. Build. Mater., vol. 68, pp. 391–401, 2014.
[71] AFNOR, "NF EN 13670: Exécution des structures en béton — Complément national," 2013.
[72] SYNAD+, "CLASSIFICATION DES AGENTS DE DÉMOULAGE," Paris, 2019.
[73] D. Brito, R. Santos, F. A. Branco, I. S. T, and R. Pais, "Evaluation of the technical performance of concrete vegetable oil based release agents," Mater. Struct. Constr., vol. 1, no. May, pp. 262–269, 2000.
[74] S. Bouharoun, "Influence of Paste Volume , Type of Release Agents , and Contact Pressure on the Quality of Concrete Surfaces," Arab J Sci Eng, no. Ea 4515, 2014.
[75] NF EN 197-1, "Cement Part 1: Composition, specifications and conformity criteria for common cements," Eur. Stand., 2012.
[76] K. L. Scrivener and A. Nonat, "Hydration of cementitious materials, present and future," Cem. Concr. Res., vol. 41, no. 7, pp. 651–665, 2011.
[77] J. Beaudoin and I. Odler, "Hydration, Setting and Hardening of Portland Cement," in Lea's Chemistry of Cement and Concrete, 4th ed., P. C. Hewlett, Ed. Butterworth-Heinemann, 1998, pp. 241–297.
[78] C. D. Lawrence, "The Constitution and Specification of Portland cements," Butterworth-Heinemann, 1998.
[79] A. Bazzoni, "Study of early hydration mechanisms of cement by means of electron microscopy," 2014.
[80] V. Baroghel-bouny, "Caractérisation microstructurale et hydrique des pâtes de ciment et des bétons ordinaires et à très hautes performance," Ph.D. thesis, Ecole Nationale des Ponts et Chaussées, 1994.
[81] A. N. Junior, R. D. T. Filho, E. De Moraes Rego Fairbairn, and J. Dweck, "Early stages hydration of high initial strength Portland cement: Part I. thermogravimetric analysis on calcined mass basis," J. Therm. Anal. Calorim., vol. 108, no. 2, pp. 725–731, 2012.
[82] E. M. J. BERODIER, "Impact of the Supplementary Cementitious Materials on the kinetics and microstructural development of cement hydration," ÉCOLE POLYTECHNIQUE FÉDÉRALE DE LAUSANNE, Ph.D. Thesis, 2015.
[83] M. A. Haque, B. Chen, and Y. Maierdan, "Influence of supplementary materials on the early age hydration reactions and microstructural progress of magnesium phosphate cement matrices," J. Clean. Prod., vol. 333, no. December 2021, 2022.

[84] A. R. Barron and D. Johnson, "Portland cement in the energy industry," p. 7, 2008.
[85] R. Rumman, M. R. Kamal, T. Manzur, and M. A. Noor, "Comparison of Cem I and Cem II Cement Concretes in Terms of Water Permeability," Proc. 3rd Int. Conf. Civ. Eng. Sustain. Dev. (ICCESD 2016), 12~14 Febr. 2016, KUET, Khulna, Bangladesh, no. February, pp. 1–7, 2016.
[86] S. Goñi et al., "Quantitative Study of Hydration of C3S and C2S by Thermal Analysis," J. Therm. Anal. Calorim., vol. 102, Dec. 2010.
[87] D. Kong, S. Huang, D. Corr, Y. Yang, and S. P. Shah, "Whether do nano-particles act as nucleation sites for C-S-H gel growth during cement hydration?," Cem. Concr. Compos., vol. 87, pp. 98–109, 2018.
[88] T. Conte, "Impact des nano-particules sur le comportement au jeune âge et à l'état frais des matériaux à base de ciment," Doctorate thesis, Ecole Normale Supérieure Paris Saclay, Cachan, 2017.
[89] J.L. Granju, "tude des propri t s m caniques des pfites pures de ciment durcies," Mater. Constr., vol. 7, no. 37, 1974.
[90] J. W. Bullard et al., "Mechanisms of cement hydration," Cem. Concr. Res., vol. 41, no. 12, pp. 1208–1223, 2011.
[91] S. J. Preece, J. Billingham, and A. C. King, "On the initial stages of cement hydration," J. Eng. Math., vol. 40, no. 1, pp. 43–58, 2001.
[92] P. M. Dove, N. Han, and J. J. De Yoreo, "Mechanisms of classical crystal growth theory explain quartz and silicate dissolution behavior," Proc. Natl. Acad. Sci. U. S. A., vol. 102, no. 43, pp. 15357–15362, 2005.
[93] and V. M. M. L. Mills, R. (Reginald), "Self-Diffusion in Electrolyte Solutions : a Critical Examination of Data Compiled from the Literature," Elsevier, 1989.
[94] W. K. Burton, N. Cabrera, and F. C. Frank, "The growth of crystals and the equilibrium structure of their surfaces," Philos. Trans. R. Soc. London. Ser. A, Math. Phys. Sci., vol. 243, no. 866, pp. 299–358, 1951.
[95] D. Kashchiev and G. M. Van Rosmalen, "Review: Nucleation in solutions revisited," Cryst. Res. Technol., vol. 38, no. 7–8, pp. 555–574, 2003.
[96] M. M. C. Fernandez, "Effect of Particle Size on the Hydration Kinetics and Microstructural Development of Tricalcium Silicate," PhD Thesis, ÉCOLE POLyTECHNIQUE FÉDÉRALE DE LAUSANNE, 2008.
[97] K. L. Scrivener and A. Nonat, "Hydration of cementitious materials , present and future," Cem. Concr. Res., vol. 41, no. 7, pp. 651–665, 2011.
[98] V. Rheinheimer, "Sulphate attack and the role of thaumasite in historical constructions," Master thesis, CZECH TECHNICAL UNIVERSITY IN PRAGUE, CZECH REPUBLIC TECHNICAL UNIVERSITY OF CATALONIA, SPAIN, 2008.
[99] K. L. Scrivener, "THE DEVELOPMENT OF MICROSTRUCTURE DURING THE HYDRATION OF PORTLAND CEMENT," PhD Thesis, Imperial College of Science and Technology University of London, 1984.
[100] ACI, "228.1R-95: In-Place Methods for Determination of Strength of Concrete," 1995.
[101] Afnor, "Équipement de chantier — Coffrages verticaux industrialisés pour parois planes en béton," 2021.
[102] J. M. D'Aloia Schwartzentruber, L., and Torrenti, Le grand livre des bétons, Edition le. IFSTTAR/MAST - Département Matériaux et Structures, 2014.
[103] Portland Cement Association, "WHITE CEMENT CONCRETE AND COLORED CONCRETE CONSTRUCTION," Washington DC.
[104] Nestor Perez, Fracture mechanics, Second. Springer International Publishing, 2017.
[105] D. Beer, F, Johnston, R, Dewolf, J, & Mazurek, Mechanics of materials, Forth. Mc Graw Hill, 2006.
[106] A.A. Griffith, "The Phenomena of Rupture and Flow in Solids," JSTOR, vol. 221, pp. 163–198, 1921.
[107] Jean Lemaitre & Rodrigue Desmorat, Engineering Damage Mechanics Ductile, Creep, Fatigue and Brittle Failures. Springer Berlin Heidelberg, 2005.
[108] T. H. Huxley, "Fracture : To Crack or Not to Crack . That Is the Question," pp. 215–242, 1895.
[109] H. D. Bui, Fracture Mechanics. Springer, 2006.
[110] ALAN T. ZEHNDER, "Modes of Fracture," in Encyclopedia ofTribology, no. 2001, Y.-W. C. (eds. . Q.J. Wang, Ed. Springer Science+Business Media New York, 2013, pp. 2292–2295.
[111] H. D. BUI, Fracture Mechanics Inverse Problems and Solutions, vol. 139, no. 2. Springer, 2006.
[112] I. E. Dzyaloshinskii, E. M. Lifshitz, and L. P. Pitaevskii, "General Theory of Van Der Waals' Forces," Sov. Phys. Uspekhi, vol. 4, no. 2, pp. 153–176, 1961.
[113] K. Allaer, I. De Baere, S. Jacques, W. Van Paepegem, and J. Degrieck, "Experimental Assesment of Infrared Welded Bonds Using Lapshear , Double Cantilever Beam and End Notch Flexure Tests for a

Carbon Fabric," no. 2012, pp. 1–9, 2012.
[114] T. Vilhelmsen and G. A. Webster, "Creep Crack Growth and Constraints in Weldments," Adv. Fract. Res., no. August 1996, pp. 555–562, 2013.
[115] D. Yavas, X. Shang, and A. Bastawros, "Contamination-Induced Degradation/Enhancement of Interfacial Toughness and Strength in Polymer-Matrix Composite Interfaces," 2018, pp. 73–78.
[116] P. C. Kreijger, "The skin of concrete composition and properties," Matériaux Constr., vol. 17, no. 4, pp. 275–283, 1984.
[117] R. N. WENZEL, "RESISTANCE OF SOLID SURFACES," Ind. Eng. Chem., vol. 28, NO. 8, pp. 988–994, 1936.
[118] R. Wilson, D. Dini, and B. Van Wachem, "The influence of surface roughness and adhesion on particle rolling," Powder Technol., vol. 312, pp. 321–333, 2017.
[119] B. N. J. Persson and M. Scaraggi, "Theory of adhesion : Role of surface roughness Theory of adhesion : Role of surface roughness," vol. 124701, 2014.
[120] K. Meine, K. Kloß, T. Schneider, and D. Spaltmann, "The influence of surface roughness on the adhesion force," pp. 694–697, 2004.
[121] NF EN ISO 4287, "Spécification géométrique des produits (GPS) État de surface : Méthode du profil," Afnor, vol. 2nd 2009, 1998.
[122] V. Rodriguez, J. Sukumaran, M. Ando, and P. De Baets, "ROUGHNESS MEASUREMENT PROBLEMS IN TRIBOLOGICAL TESTING," Sustain. Constr. Des., pp. 115–121, 2011.
[123] AFNOR, "ISO 25178-2: Geometrical product specifications (GPS) - Surface texture: Areal - Part 2: Terms, definitions and surface texture parameters," Afnor, vol. 1st, 2012.
[124] G. A. Rao and B. K. R. Prasad, "Inf luence of the roughness of aggregate surface on the interface bond strength," Cem. Concr. Res., vol. 32, pp. 253–257, 2002.
[125] Ł. Sadowski, A. Żak, and J. Hoła, "Multi-sensor evaluation of the concrete within the interlayer bond with regard to pull-off adhesion," Arch. Civ. Mech. Eng., vol. 18, no. 2, pp. 573–582, 2018.
[126] C. Liu, J. Gao, Y. Tang, and Y. Zhao, "Early hydration and microstructure of gypsum plaster revealed by environment scanning electron microscope," Mater. Lett., vol. 234, pp. 49–52, 2019.
[127] Eqiom, "CEM I 52.5 N CE CP2 NF," 2017.
[128] Eqiom, "CEM II/B-S 42.5 N CE CP1 NF," 2017.
[129] Afnor, "NF EN 933-1: Tests for geometrical properties of aggregates Part 1: Determination of particle size distribution —Sieving method," 2012.
[130] Afnor NF EN 934-2, "Admixtures for concrete, mortar and grout - Part 2 : concrete admixtures - Definitions, requirements, conformity, marking and labelling," 2009.
[131] Sika Decoffre Mineral, "Sika ® decoffre mineral," Sika, pp. 1–2, 2011.
[132] L. S. P. S.A., "57 Lankodem veg," parexlanko.com, p. 531, 2020.
[133] NF EN 10088-2 Décembre 2014, "Aciers inoxydables - Partie 2 : conditions techniques de livraison des tôles et bandes en acier de résistance à la corrosion pour usage général," Afnor, 2014.
[134] Agnès Rannee, "Developpement De Revetements Photopolymeres Pour Le Demoulage De Coffrages De Beton," Thesis, Universite de Haute-Alsace, Ph.D. Thesis, 2018.
[135] ASTM, "ASTM C188-17. Standard Test Method for Density of Hydraulic Cement," 2017.
[136] NF EN 196-3, "Methods of testing cement - Part 3 : determination of setting times and soundness," French Stand., 2017.
[137] D. P. Bentz, E. J. Garboczi, C. J. Haecker, and O. M. Jensen, "Effects of cement particle size distribution on performance properties of Portland cement-based materials," vol. 29, pp. 1663–1671, 1999.
[138] Haimei Zhang, Ed., Building materials in civil engineering. Woodhead Publishing Limited and CRC Press LLC, 2011.
[139] "Mastersizer 3000," Malvern Panalytical, 2019.
[140] European Standard, "EN 1097-6. Tests to determine the mechanical and physical characteristics of aggregates - Part 6: determination of the actual density and the water absorption coefficien," 2014.
[141] NF P18-404, "Concretes. Study, suitability and control tests. Manufacture and storage of test specimens.," Afnor, 1981.
[142] AFNOR, "NF EN 206-1, Concrete - Part 1 : specification, performance, production and conformity," 2013.
[143] AFNOR, "NF EN 12350-2 Testing fresh concrete - Part 2 : slump test," 2019.
[144] E. C. for Standardization, "EN 12390-3:2009; Testing hardened concrete - Part 3: Compressive strength of

test specimens," 2005.
[145] S. Bahafid, "A multi-technique investigation of the effect of hydration temperature on the microstructure and mechanical properties of cement paste," l'Université Paris-Est, 2019.
[146] N. C. Collier, J. H. Sharp, N. B. Milestone, J. Hill, and I. H. Godfrey, "Cement and Concrete Research The in fl uence of water removal techniques on the composition and microstructure of hardened cement pastes," vol. 38, pp. 737–744, 2008.
[147] V. Antonovic, "Investigation of early hydration of high aluminate cement-based binder at different ambient temperatures," pp. 717–726, 2012.
[148] J. Zhang and G. W. Scherer, "Comparison of methods for arresting hydration of cement," Cem. Concr. Res., vol. 41, no. 10, pp. 1024–1036, 2011.
[149] A. Korpa and R. Trettin, "The influence of different drying methods on cement paste microstructures as reflected by gas adsorption : Comparison between freeze-drying (F-drying), D-drying , P-drying and oven-drying methods," vol. 36, pp. 634–649, 2006.
[150] M. Moukwa and P. Attcin, "THE EFFECT OF DRYING ON CEMENT PASTES PORE STRUCTURE AS DETERMINED BY MERCURY POROSIMETRY," vol. 18, no. c, pp. 745–752, 1988.
[151] Kalliopi K. Aligizaki, Pore Structure of Cement-Based Materials, vol. 66. 2012.
[152] R. L. Day, B. K. Marsh, and C. C. D. Pomeroy, "MEASUREMENT OF POROSITY IN BLENDED CEMENT PASTES," vol. 18, no. c, pp. 63–73, 1988.
[153] J. J. Beaudoin, B. Tamtsia, J. Marchand, and H. R. Myers, "Solvent exchange in partially saturated and saturated microporous systems Length change anomalies," vol. c, pp. 359–370, 2000.
[154] S. Diamond, "A discussion of the paper 'Effect of drying on cement-based materials pore structure as identified by mercury porosimetry—a comparative study between oven-, vacuum-, and freeze-drying' by C. Gallé," Cem. Concr. Res., vol. 33, pp. 169–170, Jan. 2003.
[155] T. Emeritus, Cement chemistry, 2nd ed. Thomas Telford Publishing, 1997.
[156] C. Munzer, "Université de strasbourg," 2016.
[157] R. Leach, L. Brown, X. Jiang, R. Blunt, M. Conroy, and D. Mauger, "Measurement Good Practice Guide No. 108; Guide for the Measurement of Smooth Surface Topography using Coherence Scanning Interferometry," 2008.
[158] ASTM C188-17, "Standard Test Method for Density of Hydraulic Cement," Am. Soc. Test. Mater., 2017.
[159] NF EN 196-3, "Cement test methods - Part 3: determination of setting time and stability," Eur. Stand., 2017.
[160] EN 1097-6, "Tests to determine the mechanical and physical characteristics of aggregates - Part 6: determination of the actual density and the water absorption coefficien," Eur. Stand., 2014.
[161] EN 933-1, "Tests for determining the geometrical characteristics of aggregates - Part 1: determination of granularity - Particle size analysis by sieving," Eur. Stand., 2012.
[162] EN 1015-3, "Test methods for masonry mortars - Part 3: determination of the consistency of fresh mortar," Eur. Stand., 1999.
[163] EN 1015-6/A1, "Test methods for masonry mortars - Part 6: determination of the apparent density of fresh mortar," Eur. Stand., 2007.
[164] EN 1015-11, "Test methods for masonry mortars - Part 11: determination of the flexural and compressive strength of hardened mortar," Eur. Stand., 2019.
[165] EN 12390-6, "Tests for hardened concrete - Part 6: determination of the tensile strength by splitting of test pieces," Eur. Stand., 2012.
[166] d'EQIOM, "produits/ciments." [Online]. Available: https://www.eqiom.com/produits/ciments.
[167] D. Snelson, S. Wild, and M. O. Farrell, "Setting times of portland cement-metakaolin-fly ash blends," J. Civ. Eng. Manag., vol. 17, no. 1, pp. 55–62, 2011.
[168] Cement.org, "American cement manufacturer." [Online]. Available: https://www.cement.org/.
[169] Civil and Structural Engineering, "4- cement," in Building Materials in Civil Engineering, Haimei Zhang, Ed. Woodhead Publishing Limited and CRC Press LLC, 2011, pp. 46–80.
[170] ASTM C33/ C33M-18, "Standard Specification for Concrete Aggregates," ASTM, 2018.
[171] AFNOR, "EN 12620+A1: Aggregates for concrete," 2008.
[172] A. MAZKEWITSCH and A. JAWORSKI, "The adhesion between concrete and formwork," Adhes. between Polym. Concr., pp. 67–72, 1986.
[173] W. Piasta and B. Zarzycki, "The effect of cement paste volume and w/c ratio on shrinkage strain, water

absorption and compressive strength of high performance concrete," Constr. Build. Mater., vol. 140, pp. 395–402, 2017.

[174] C. Albano, N. Camacho, M. Hernández, A. Matheus, and A. Gutiérrez, "Influence of content and particle size of waste pet bottles on concrete behavior at different w/c ratios," Waste Manag., vol. 29, no. 10, pp. 2707–2716, 2009.

[175] Y. Y. Kim, K. M. Lee, J. W. Bang, and S. J. Kwon, "Effect of W/C ratio on durability and porosity in cement mortar with constant cement amount," Adv. Mater. Sci. Eng., vol. 2014, 2014.

[176] S. Czarnecki and Ł. Sadowski, "Morphological Properties of the Cement Skin: understanding the effect of contact with formwork," Case Stud. Constr. Mater., no. March, p. e01007, 2022.

[177] D. Ahmad, I. Van Den Boogaert, J. Miller, and R. Presswell, "Hydrophilic and hydrophobic materials and their applications," Energy Sources, Part A Recover. Util. Environ. Eff., vol. 40, no. 22, pp. 2686–2725, 2018.

[178] F. A. Hartmann and J. Plank, "New insights into the effects of aging on Portland cement hydration and on retarder performance," Constr. Build. Mater., vol. 274, 2021.

[179] A. Peled, J. Castro, and W. J. Weiss, "Atomic force and lateral force microscopy (AFM and LFM) examinations of cement and cement hydration products," Cem. Concr. Compos., vol. 36, no. 1, pp. 48–55, 2013.

[180] Bruker AXS GmbH, "Bruker D8 Produktbroschüre," 2010.

[181] R. Lachaud, "Données de la diffraction des rayons X sur l'hydration à court terme de ciments dans la gamme 20°-60°C," Matériaux Constr., vol. 2, no. 6, pp. 453–460, 1969.

[182] A. Morandeau, M. Thiéry, and P. Dangla, "Investigation of the carbonation mechanism of CH and C-S-H in terms of kinetics, microstructure changes and moisture properties," Cem. Concr. Res., vol. 56, pp. 153–170, 2014.

[183] J. Kittnerová et al., "Comparative study of radium and strontium behaviour in contact with cementitious materials," Appl. Geochemistry, vol. 122, 2020.

[184] V. Baroghel-bouny, "Caractérisation microstructurale et hydrique des pâtes de ciment et des bétons ordinaires et à très hautes performance," L'ECOLE NATIONALE DES PONTS ET CHAUSSEES, 1994.

[185] P. Gu and J. J. Beaudoin, "A conduction calorimetric study of early hydration of ordinary Portland cement/high alumina cement pastes," J. Mater. Sci., vol. 32, no. 14, pp. 3875–3881, 1997.

[186] C. Y and I. Odler, "On the origin of Portland cement setting," Cem. Concr. Res., vol. 22, pp. 1130–1140, 1992.

[187] R. Ylmén, U. Jäglid, B. M. Steenari, and I. Panas, "Early hydration and setting of Portland cement monitored by IR, SEM and Vicat techniques," Cem. Concr. Res., vol. 39, no. 5, pp. 433–439, 2009.

[188] E. T. Stepkowska, J. L. Perez-Rodriguez, M. J. Sayagues, and J. M. Martinez-Blanes, "Calcite, vaterite and aragonite formong on cement hydrtion from liquid and gaseous phase," J. Therm. Anal. Calorim., vol. 73, pp. 247–269, 2003.

[189] C. D. Æ. P. D. C. Æ. L. L. Æ, "Comprehension of demolding mechanisms at the formwork / oil / concrete interface," pp. 571–581, 2008.

[190] P. D. Todorov et al., "Kinetics of triglyceride solubilization by micellar solutions of nonionic surfactant and triblock copolymer. 3. Experiments with single drops," Langmuir, vol. 18, no. 21, pp. 7896–7905, 2002.

[191] J.-L. Salager, "SURFACTIFS types et usages," 2002.

[192] R. N. Wenzel, "Resistance of solid surfaces to wetting by water," Ind. Eng. Chem., vol. 28, no. 8, pp. 988–994, 1936.

[193] D. Kim, J. G. Kim, and C. N. Chu, "Aging effect on the wettability of stainless steel," Mater. Lett., vol. 170, pp. 18–20, 2016.

[194] M. Mantel and J. P. Wightman, "Influence of the surface chemistry on the wettability of stainless steel," Surf. Interface Anal., vol. 21, no. 9, pp. 595–605, 1994.

[195] Y. Hedberg, M. E. Karlsson, E. Blomberg, I. Odnevall Wallinder, and J. Hedberg, "Correlation between surface physicochemical properties and the release of iron from stainless steel AISI 304 in biological media," Colloids Surfaces B Biointerfaces, vol. 122, pp. 216–222, 2014.

[196] Y. VANHOVE, "Contribution à l'étude du frottement d'un béton autoplaçant contre une surface métallique - Application aux poussées contre les coffrages," Université d'Artois, 2001.

[197] H. Biscaia, N. Franco, and C. Chastre, "Stainless Steel Bonded to Concrete: An Experimental Assessment using the DIC Technique," Int. J. Concr. Struct. Mater., vol. 12, no. 1, 2018.

[198] C. . Deng, Z.C.; Jumbe, R.D.; Yuan, "Bonding between high strength rebar and reactive powder concrete," China Civ. Eng. J., vol. 47, pp. 69–78, 2014.
[199] Y. Song et al., "Rebar corrosion and its interaction with concrete degradation in reinforced concrete sewers," Water Res., vol. 182, p. 115961, 2020.
[200] F.M. Leo-Martinez, E. F. Abad-Zarate, L. L., and C.-B. P.F. de J., "Laboratory and field performance of biodegradable release agents for hydraulic concrete," Mater. Struct., no. 1003, pp. 2731–2748, 2016.
[201] G. Baty et R. Reynolds, "Release agents- how they work," Concr. Int., pp. 52–54, 1997.
[202] D. Barnat-Hunek and M. Szafraniec, "Influence of biodegradable release oils on the physical and mechanical properties of light-colored architectural concrete," Materials (Basel)., vol. 14, no. 16, 2021.
[203] E. B. Rabinovitch, E. Lacatus, and J. W. Summers, "The lubrication mechanism of calcium stearate/paraffin wax systems in PVC compounds," J. Vinyl Technol., vol. 6, no. 3, pp. 98–103, 1984.
[204] J. Crawford, A. Psaila, and S. T. Orszulik, Chemistry and Technology of Lubricants. 2010.
[205] N. GOUDJIL, "Développement d ' un nouveau procédé de décoffrage basé sur la polarisation du béton – Etude de l ' a spect des parements en béton," UNIVERSITE D'ARTOIS, 2011.
[206] S. Bouharoun, P. De Caro, I. Dubois, C. Djelal, and Y. Vanhove, "Effect of a superplasticizer on the properties of the concrete / oil / formwork interface," Constr. Build. Mater., vol. 47, pp. 1137–1144, 2013.
[207] ACI 303R-12, "Guide to cast-in-place architectural concrete practice," 2012.
[208] PERI Group, "Best practice for architectural concrete," 2018.
[209] L. Izoret, "Paramètres physiques du contrôle de la qualité des parements : une approche phénoménologique," 2014.

Annex 1

Cement paste sample images of Cem-Ref against reference formwork (F17-Ref), ***(CEM I with w/c=0.3)***

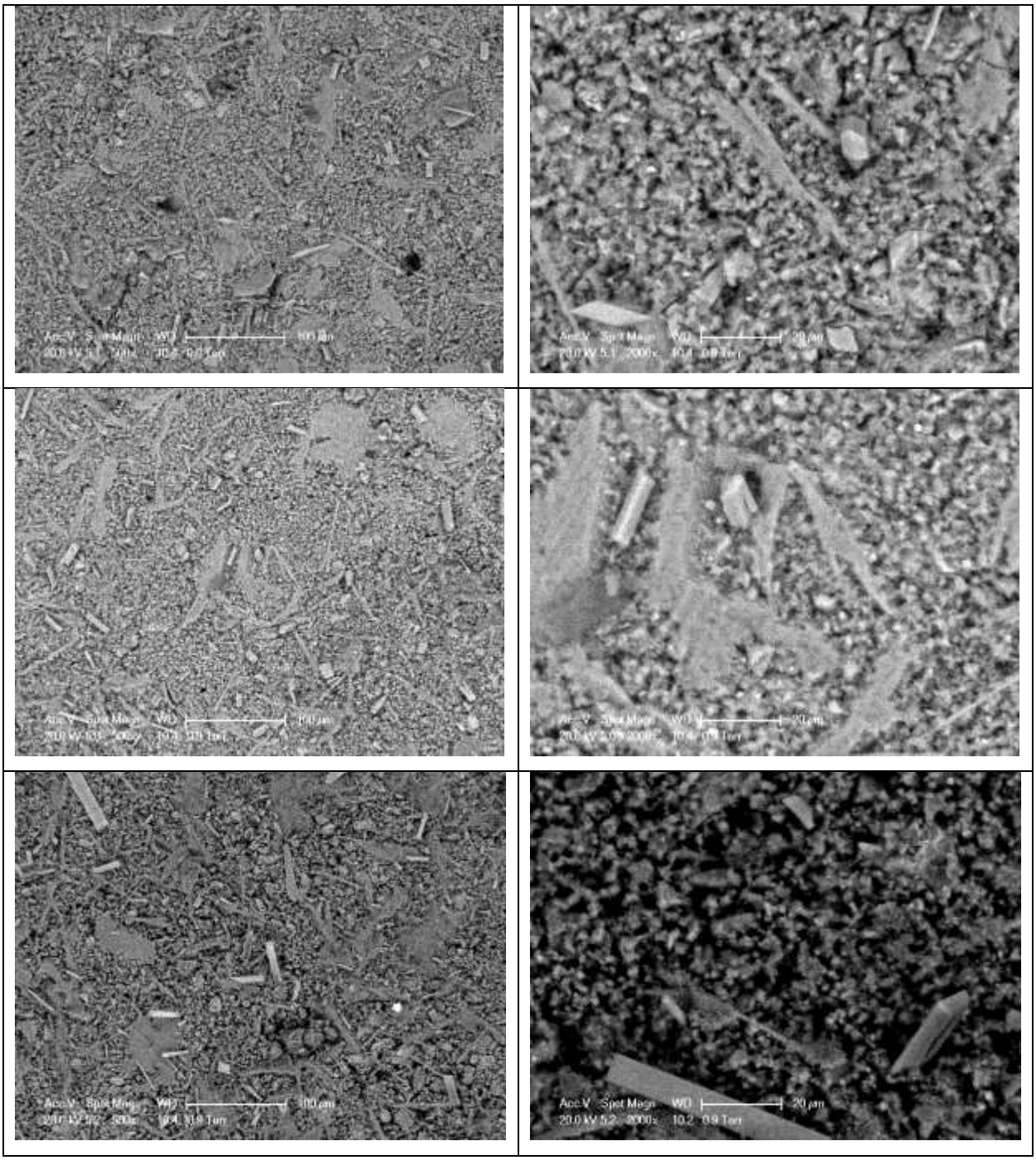

Cement paste sample images of Cem-PET against PET coated formwork, ***(CEM I with w/c=0.3)***

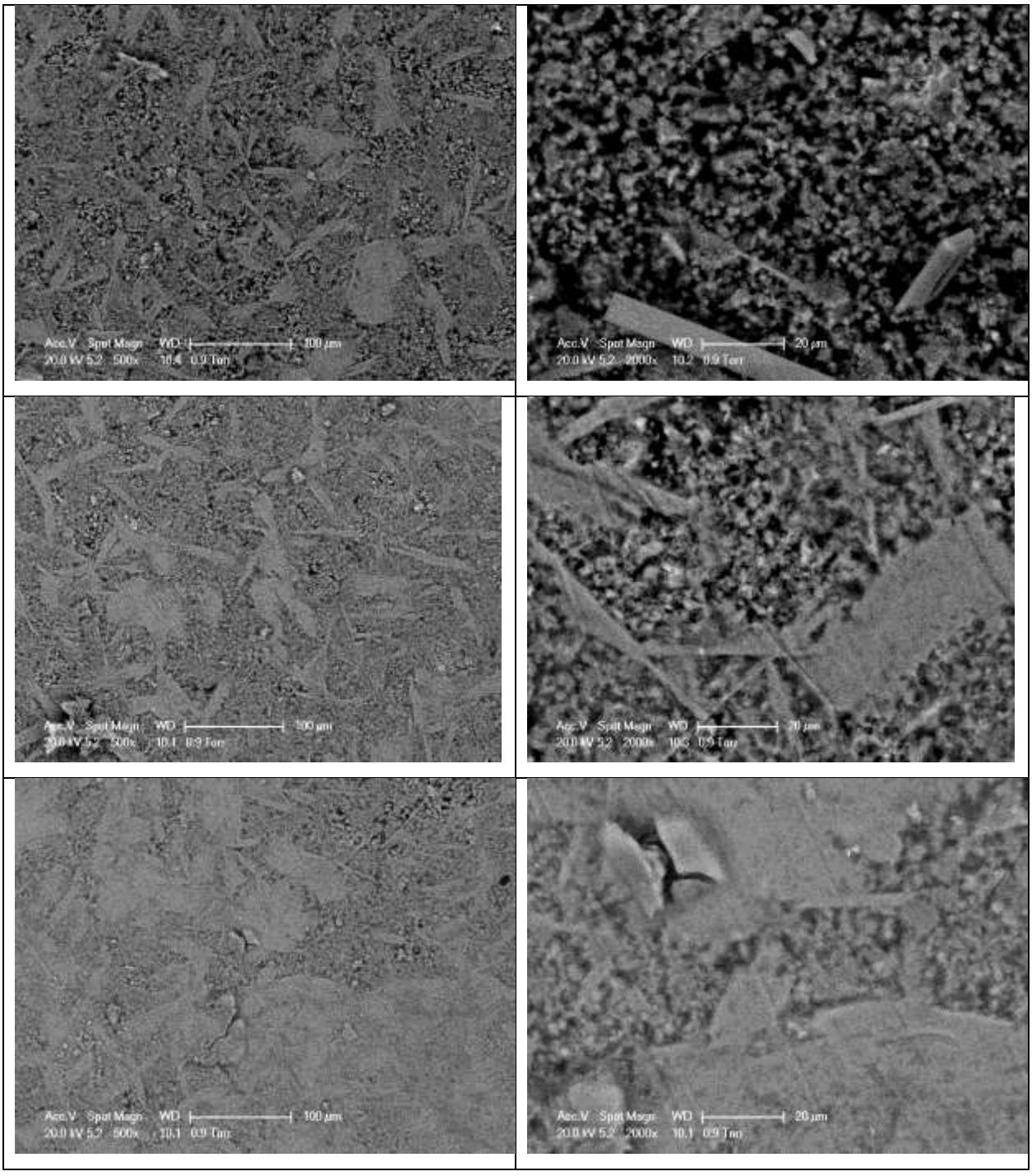

Cement paste sample images of Cem-C20C27 against C20C27 coated formwork, ***(CEM I with w/c=0.3)***

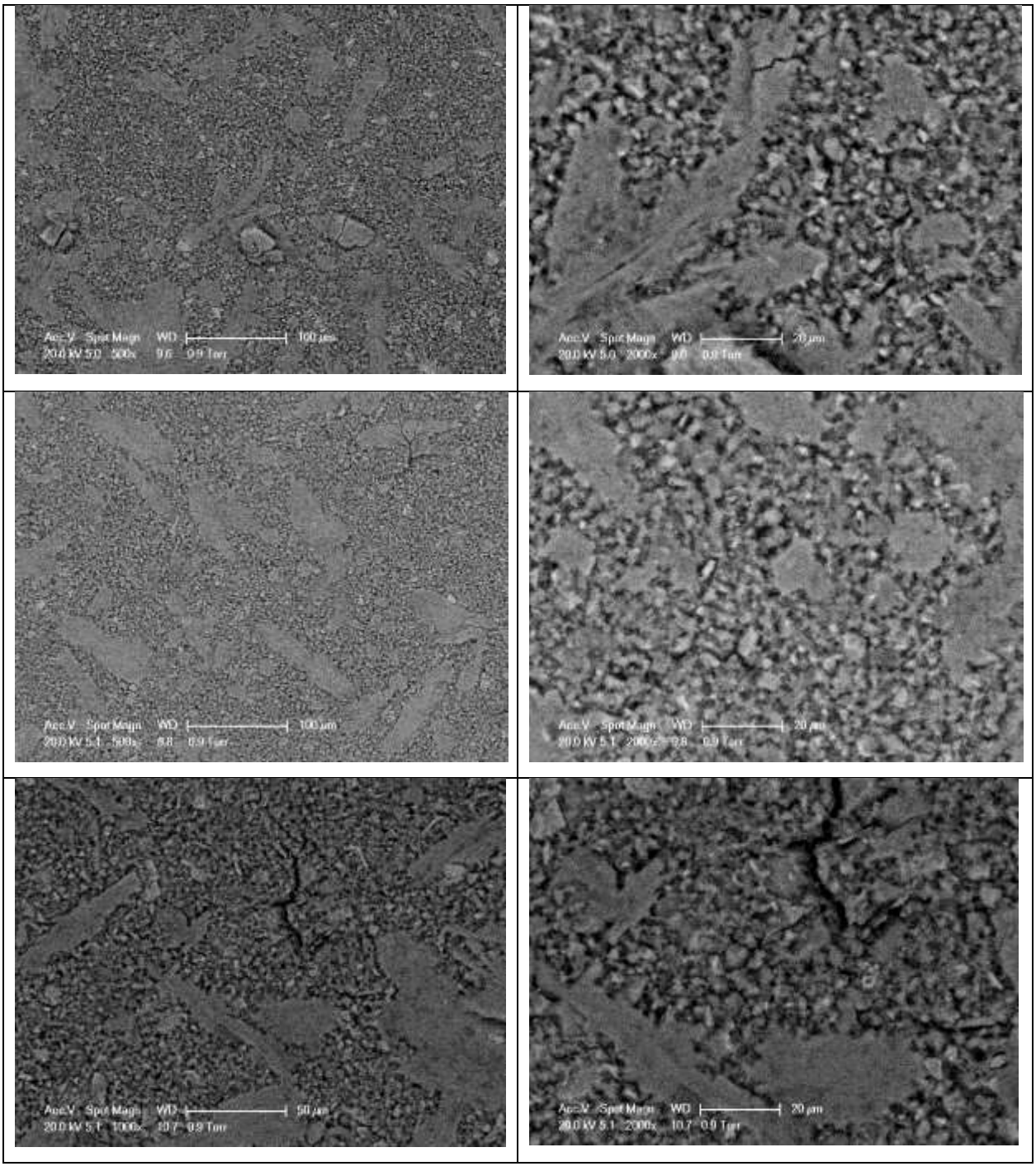

Cement paste sample images of Cem-MO against mineral oil coated formwork (F17-MO),

(CEM I with w/c=0.3)

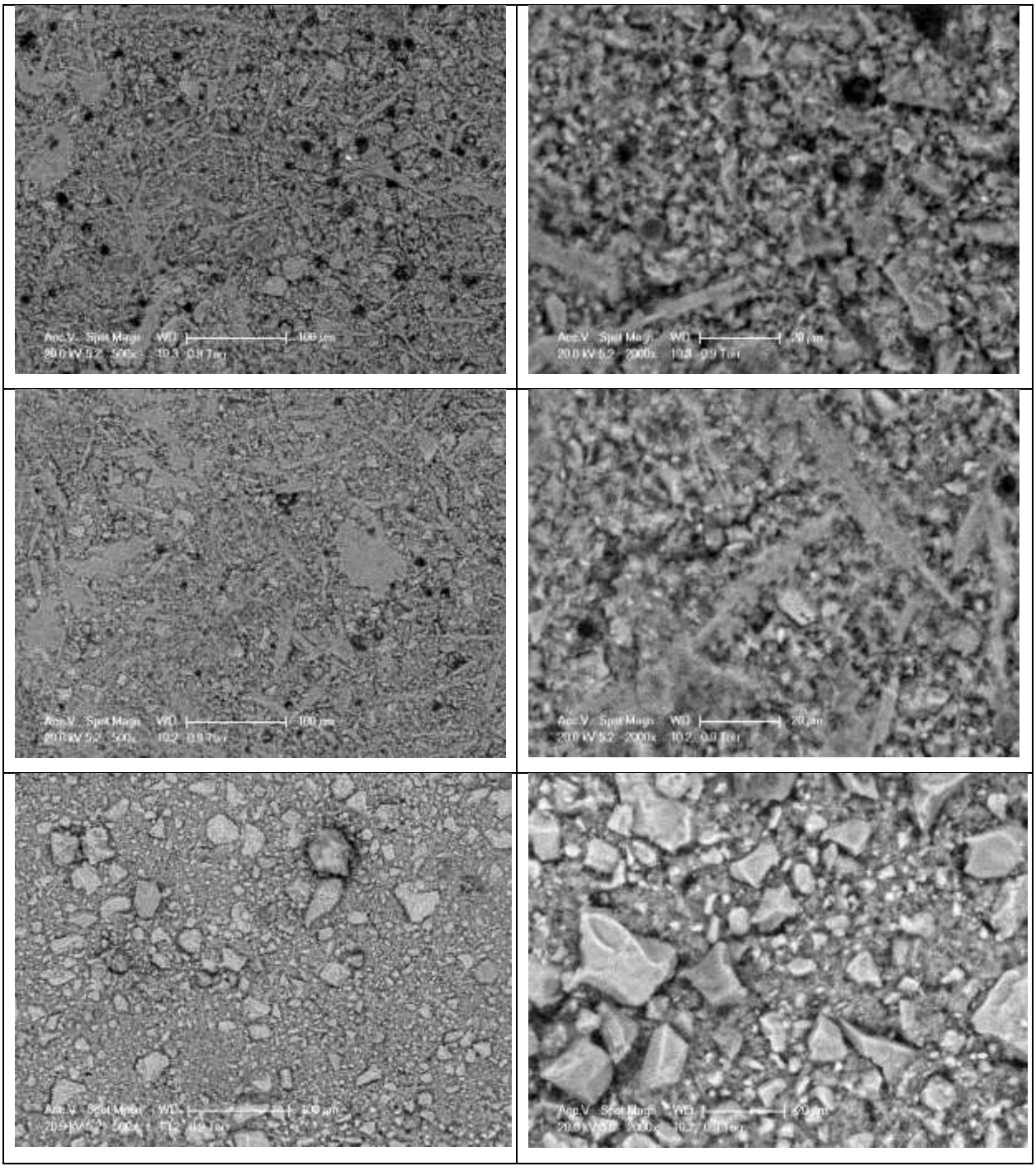

Cement paste sample images of Cem-VO against vegetable oil coated formwork (F17-VO),

(CEM I with w/c=0.3)

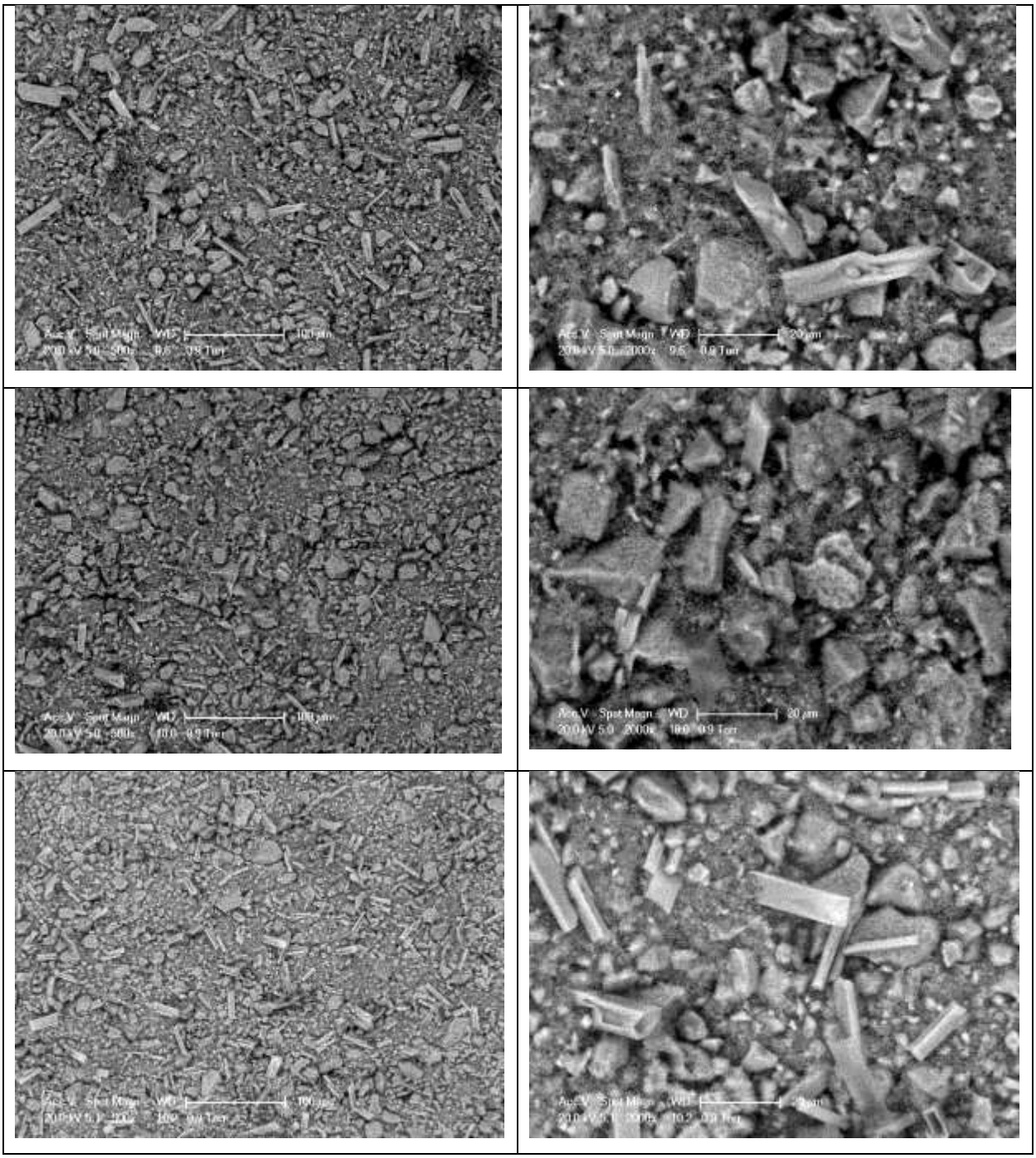

Cement paste sample images of Cem-Ref against reference formwork (F17-Ref), ***(CEM I with w/c=0.4)***

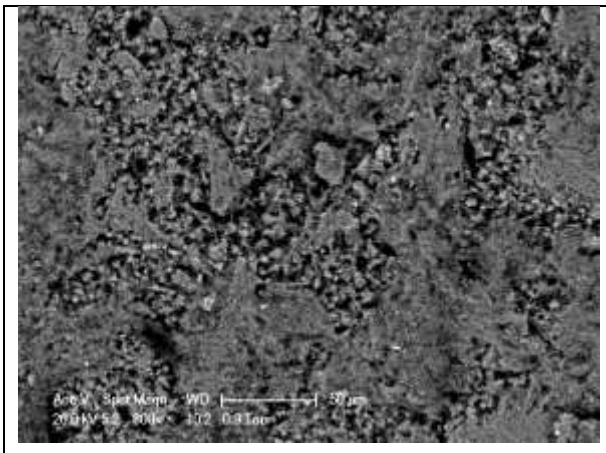

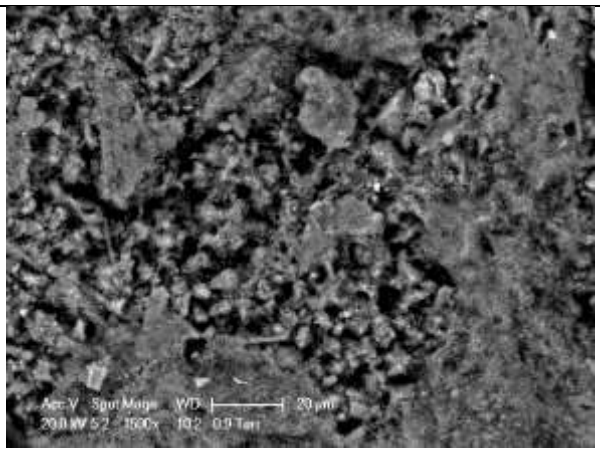

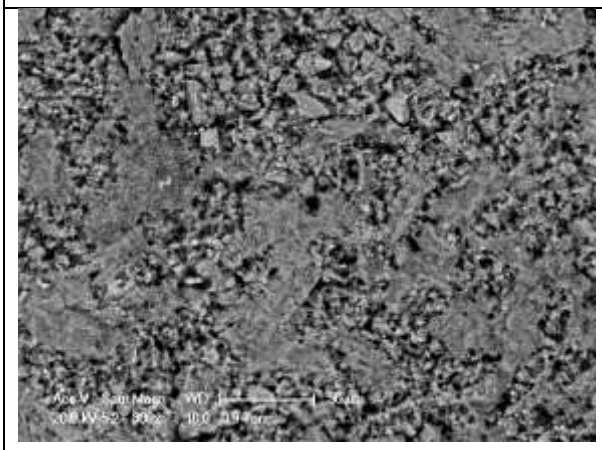

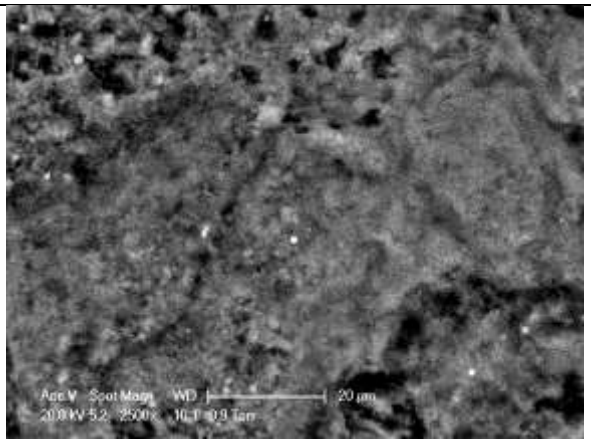

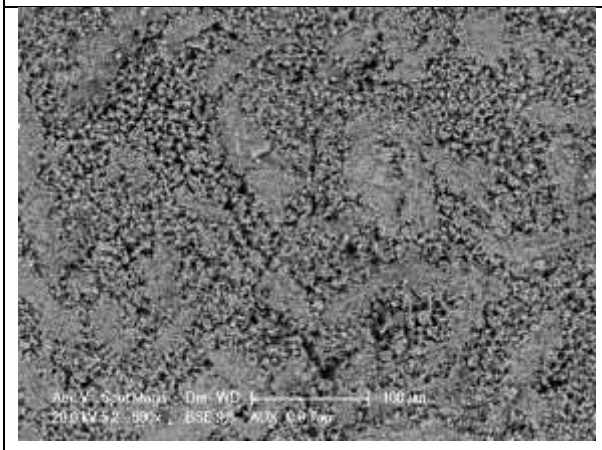

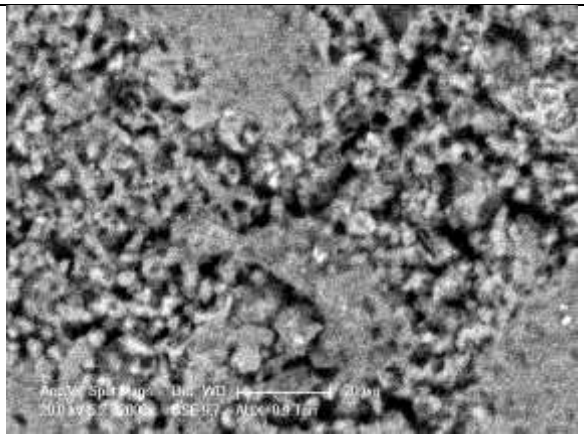

Cement paste sample images of Cem-PET against PET coated formwork, ***(CEM I with w/c=0.4)***

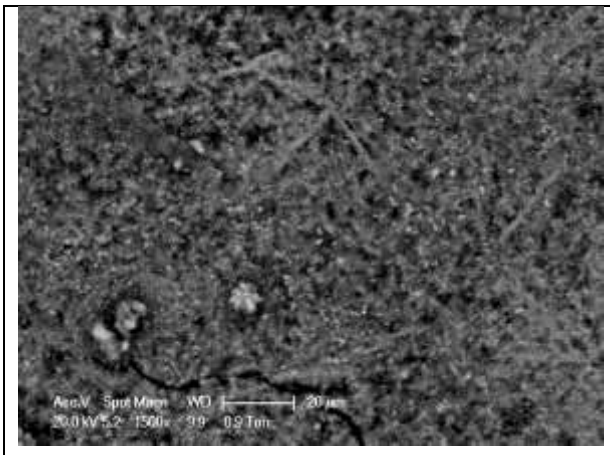

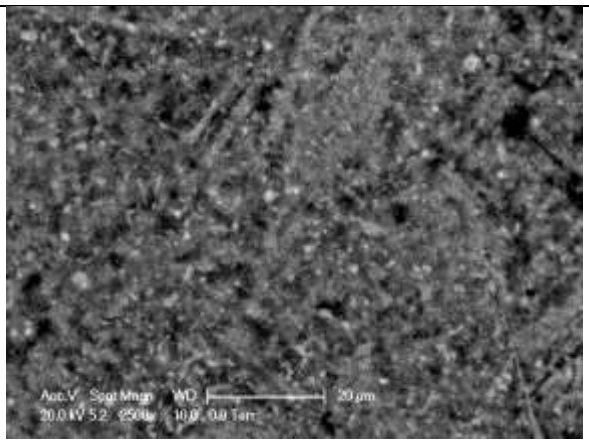

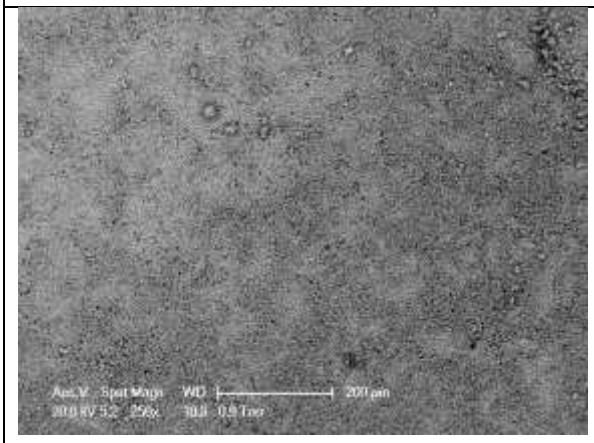

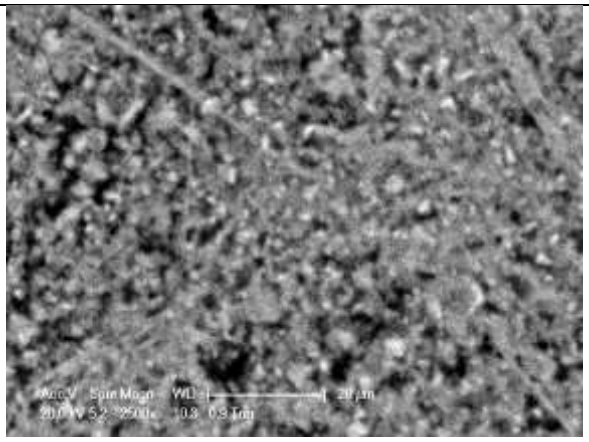

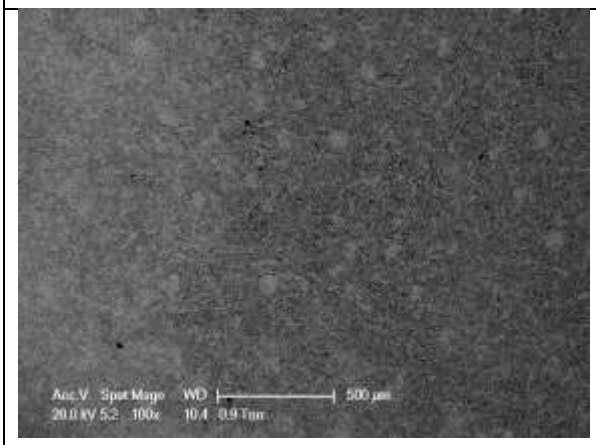

Cement paste sample images of Cem-C20C27 against C20C27 coated formwork, ***(CEM I with w/c=0.4)***

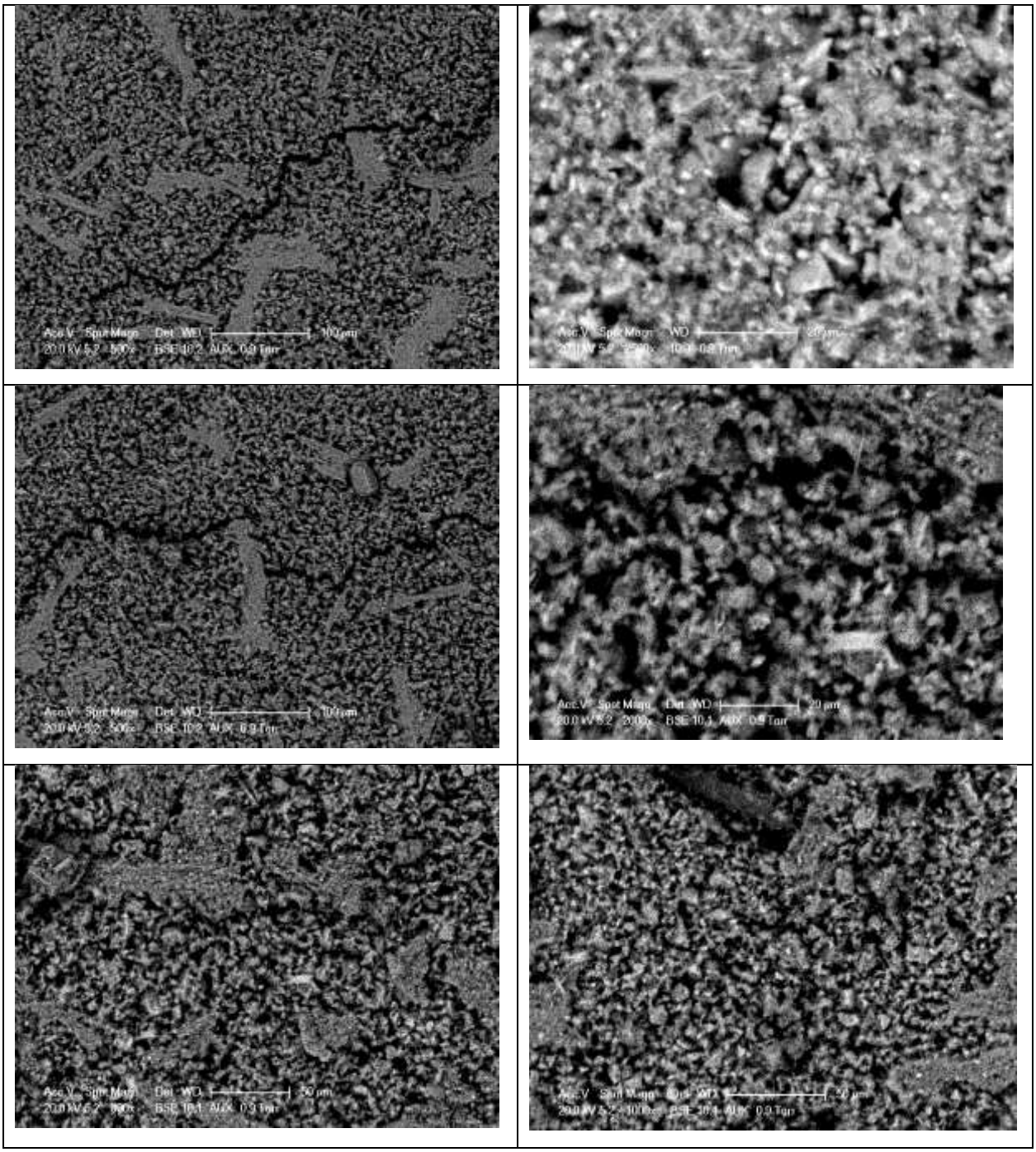

Cement paste sample images of Cem-MO against mineral oil coated formwork (F17-MO),

(CEM I with w/c=0.4)

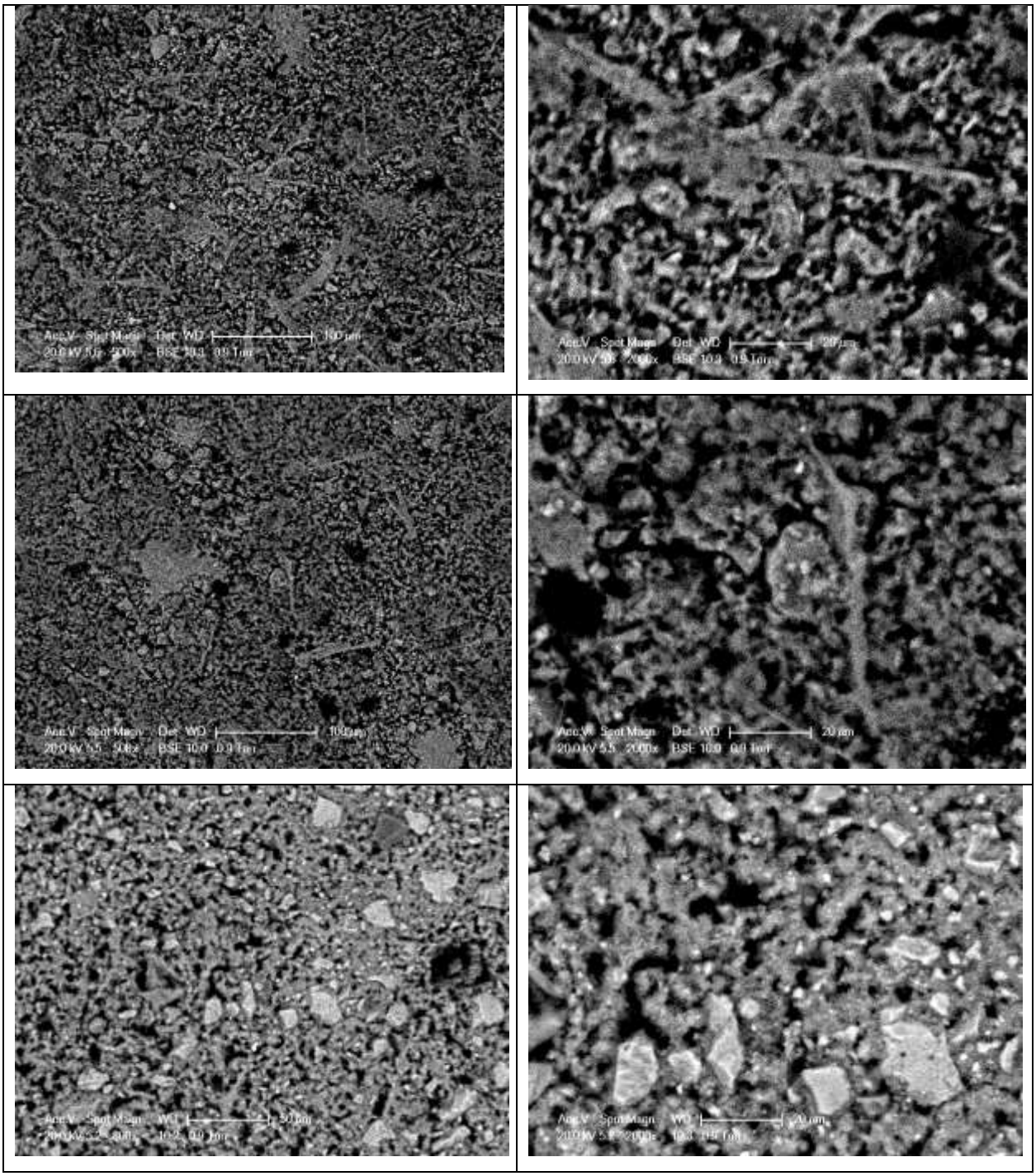

Cement paste sample images of Cem-VO against vegetable oil coated formwork (F17-VO),

(CEM I with w/c=0.4)

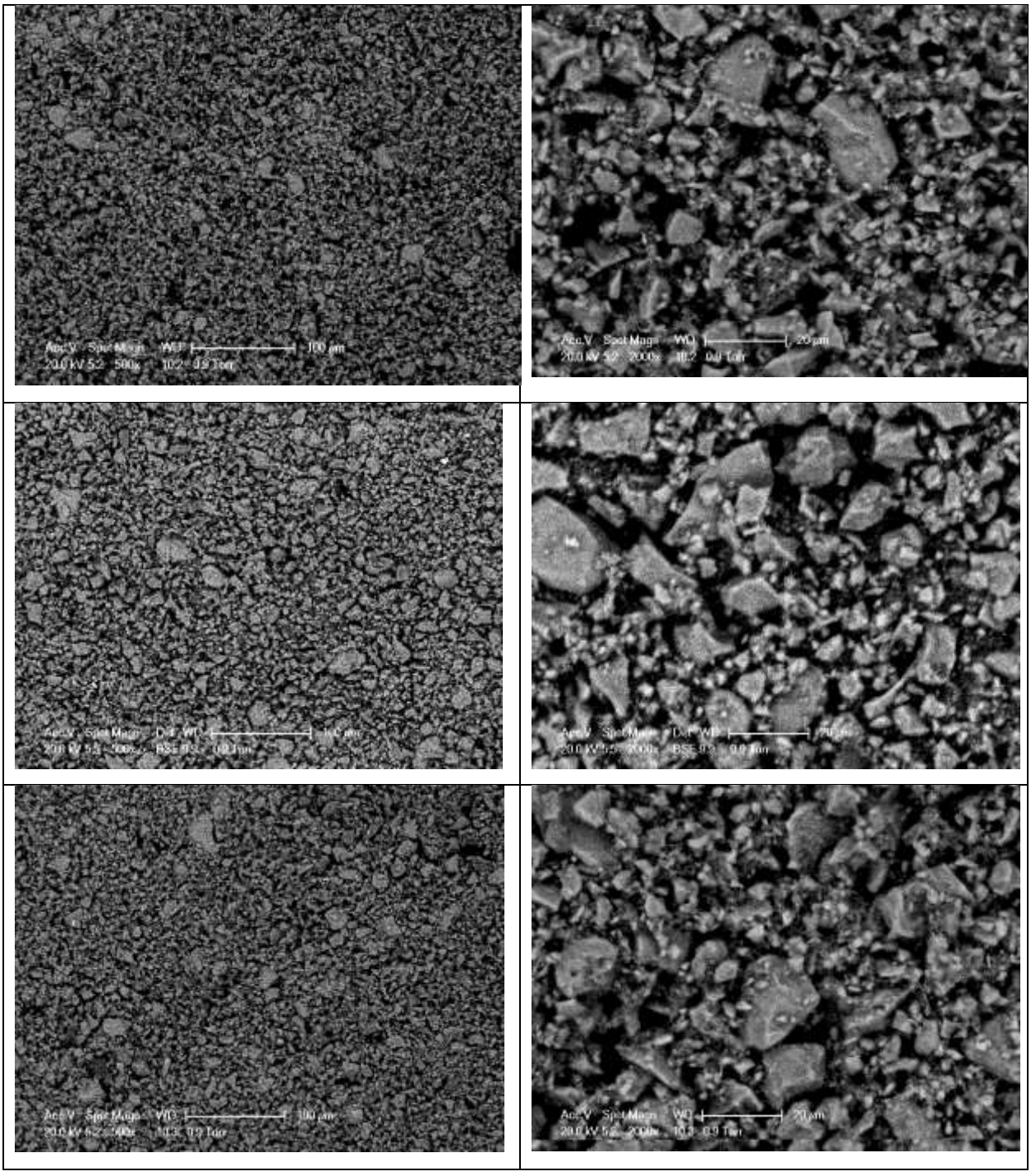

Cement paste sample images of Cem-Ref against reference formwork (F17-Ref), ***(CEM I with w/c=0.5)***

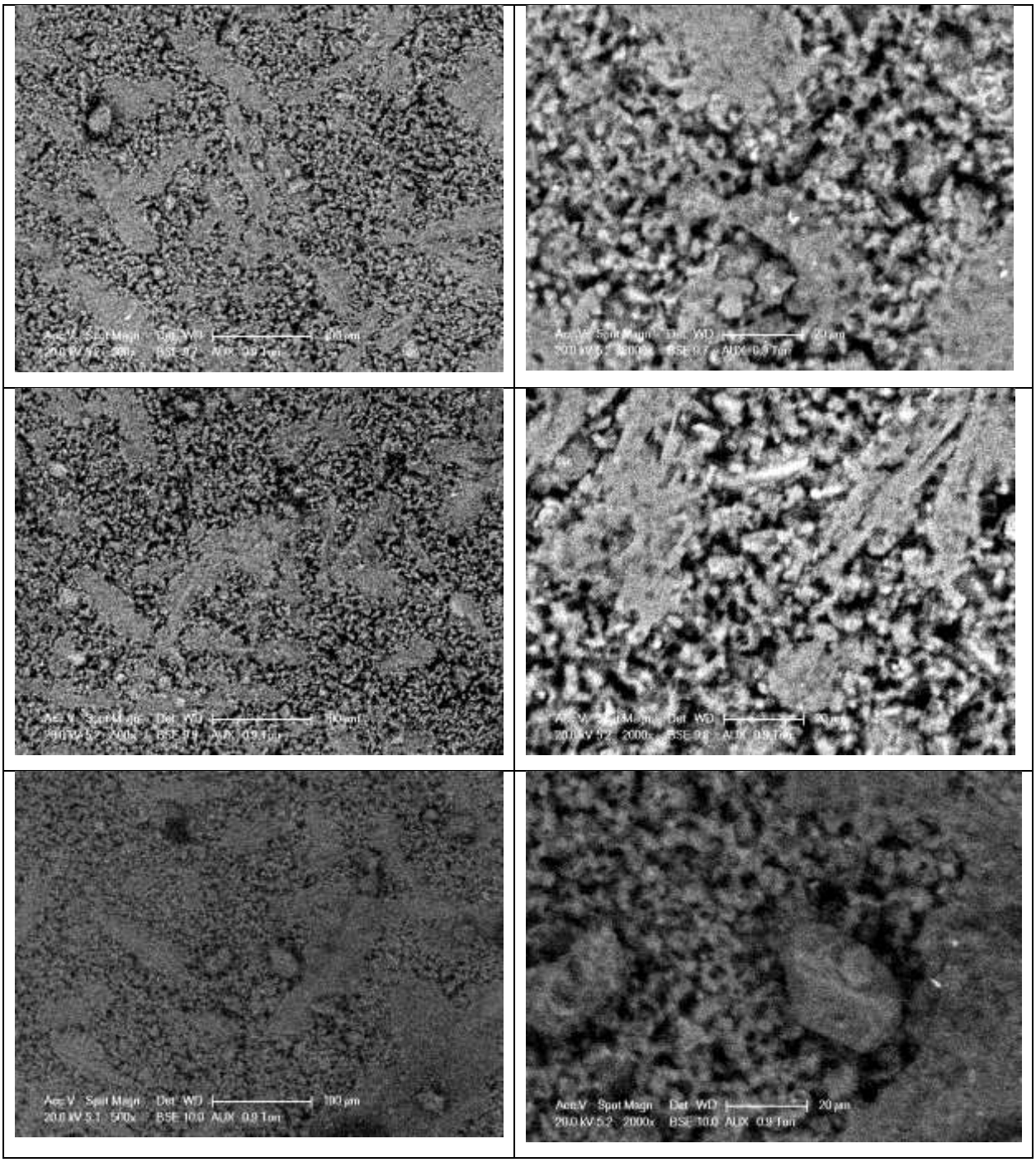

Cement paste sample images of Cem-PET against PET coated formwork, ***(CEM I with w/c=0.5)***

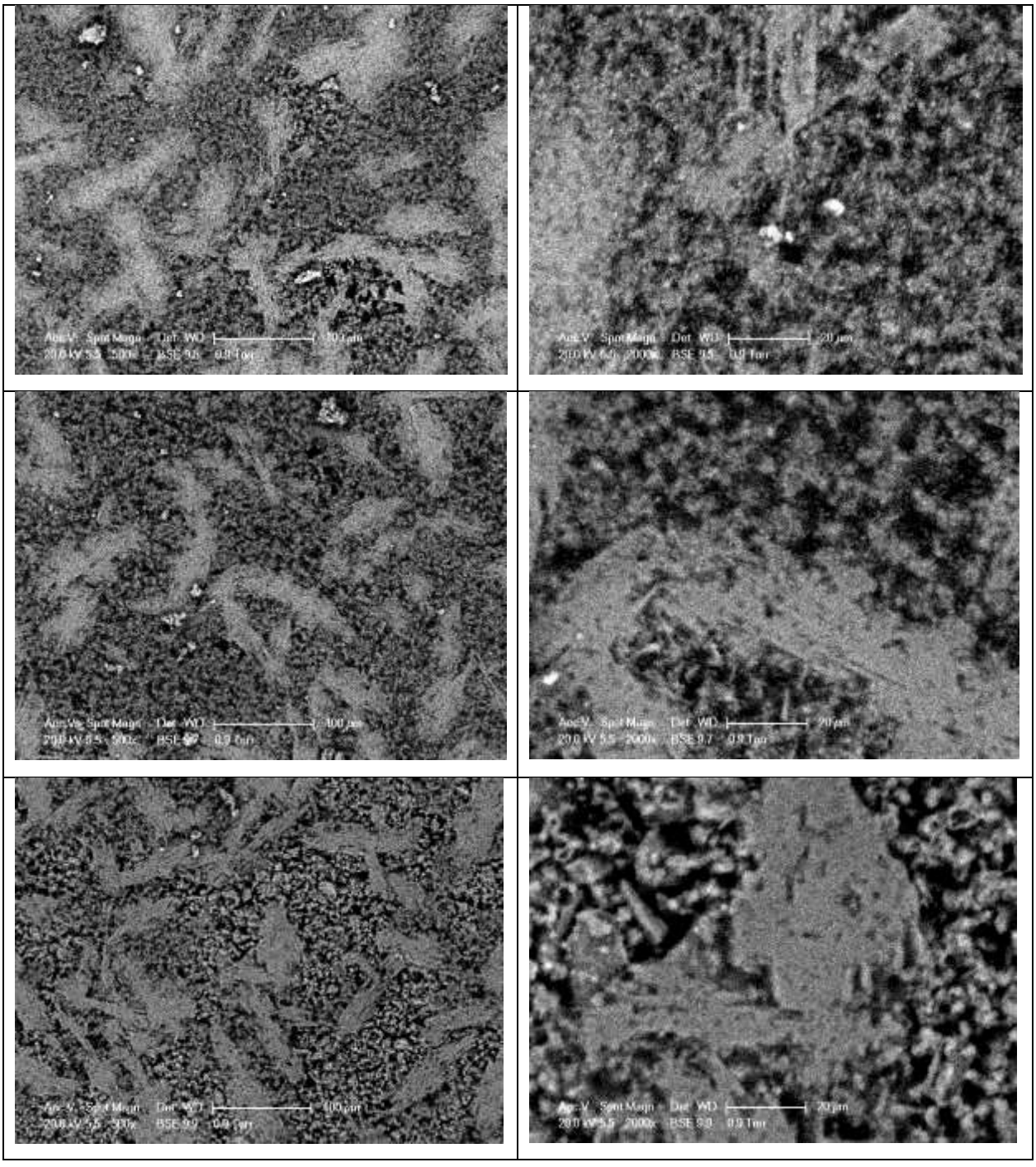

Cement paste sample images of Cem-C20C27 against C20C27 coated formwork, ***(CEM I with w/c=0.5)***

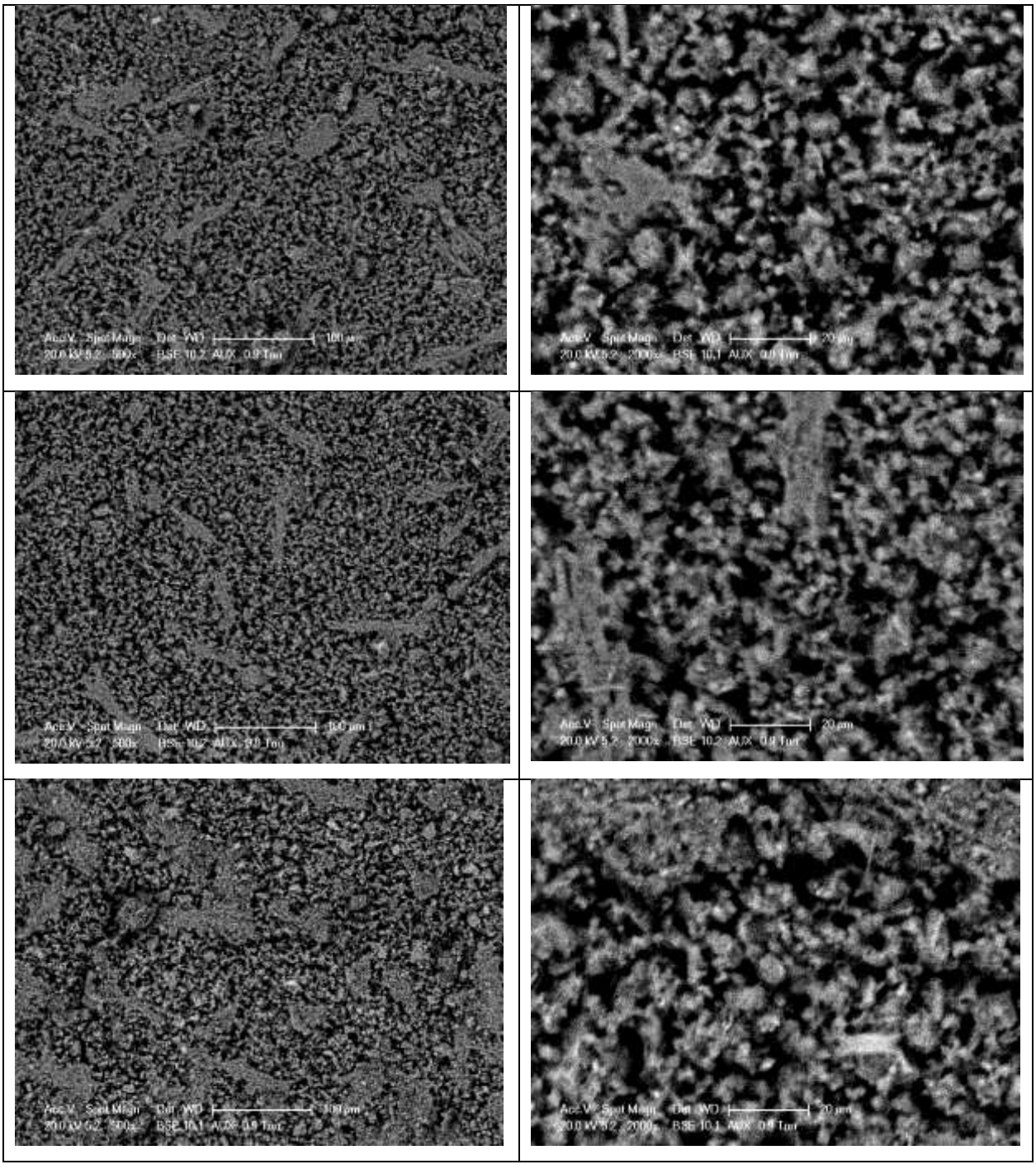

Cement paste sample images of Cem-MO against mineral oil coated formwork (F17-MO),

(CEM I with w/c=0.5)

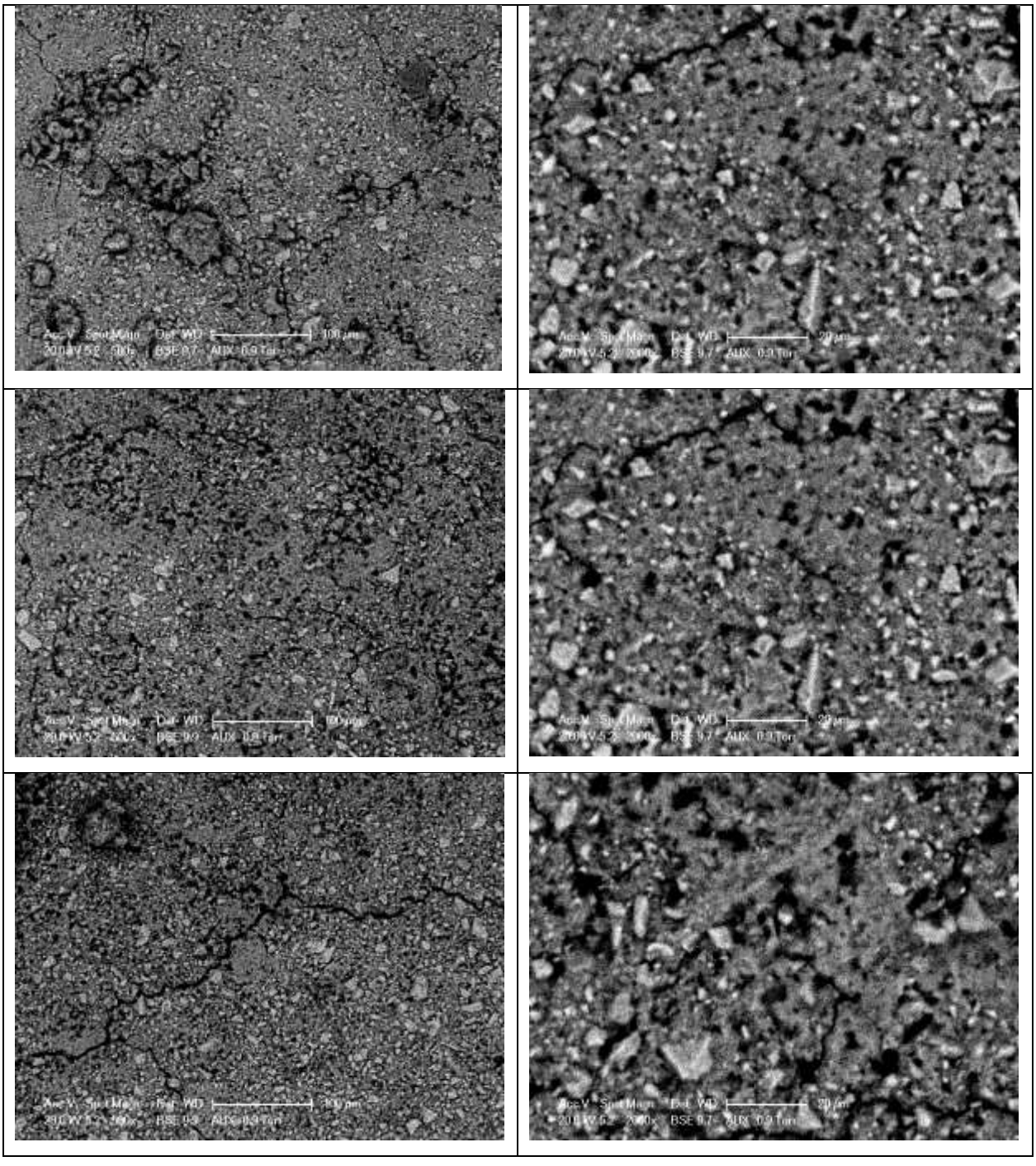

Cement paste sample images of Cem-VO against vegetable oil coated formwork (F17-VO),

(CEM I with w/c=0.5)

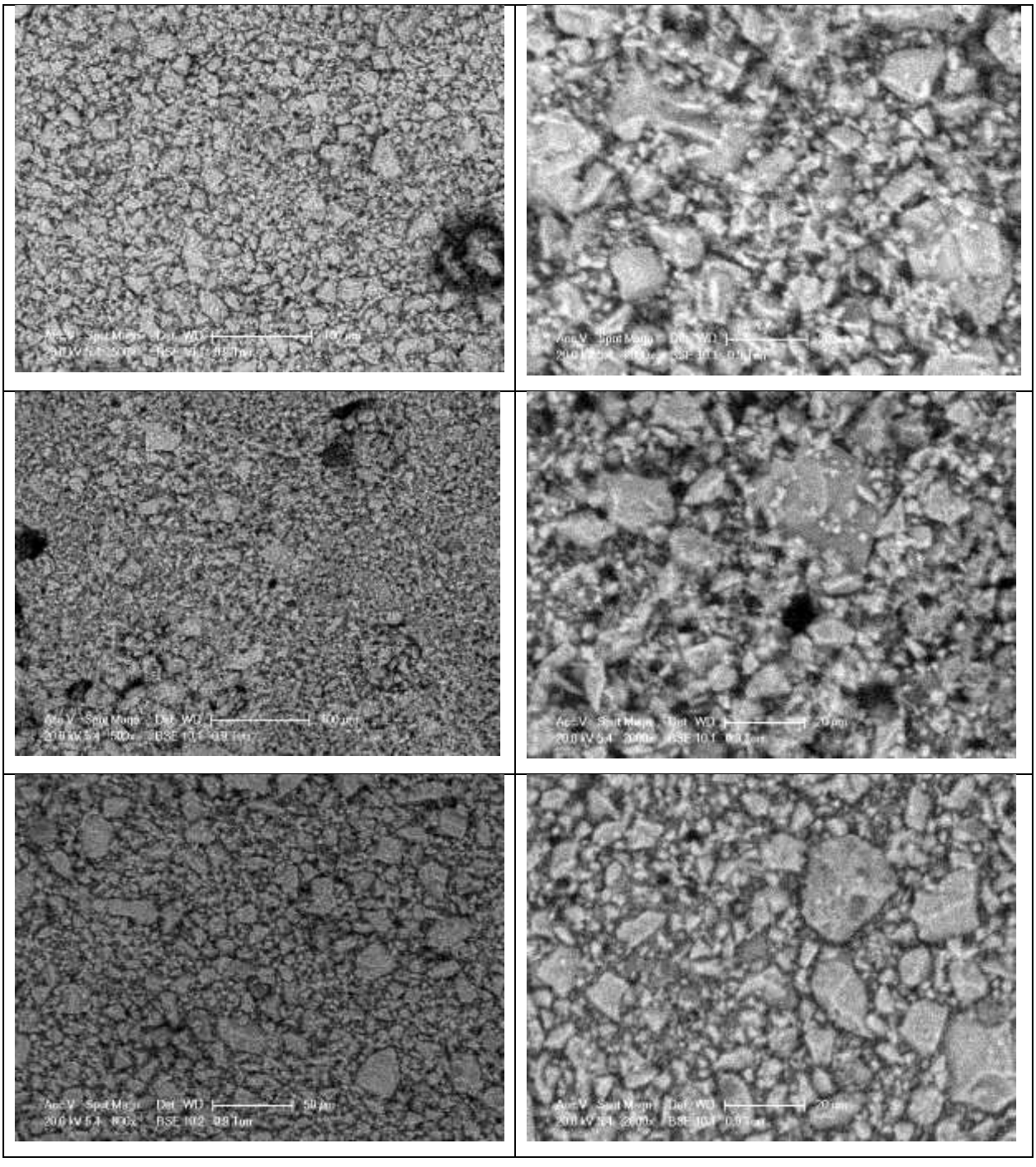

Cement paste sample images of Cem-Ref against reference formwork (F17-Ref), ***(CEM II/B with w/c=0.3)***

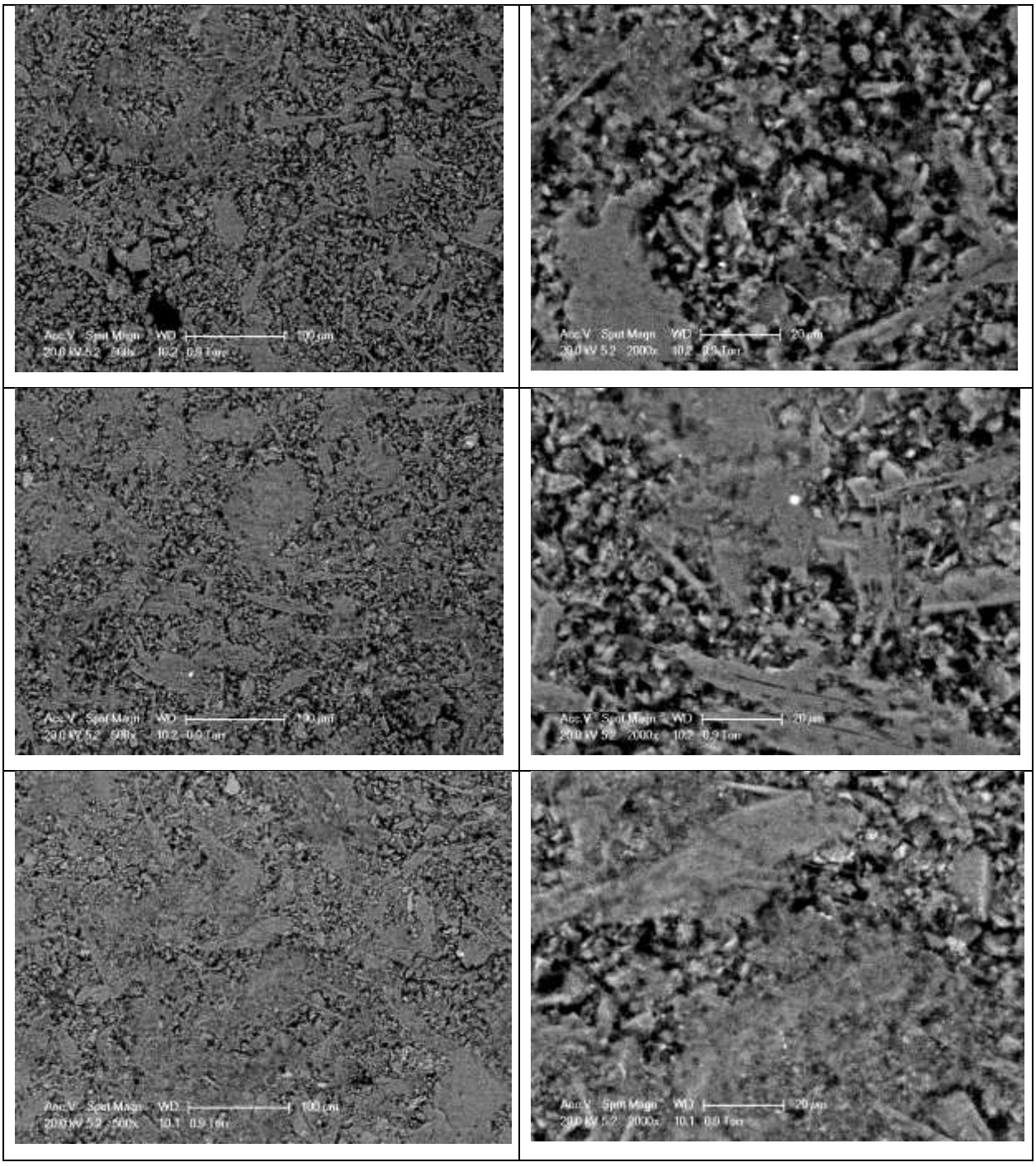

Cement paste sample images of Cem-PET against PET coated formwork, ***(CEM II/B with w/c=0.3)***

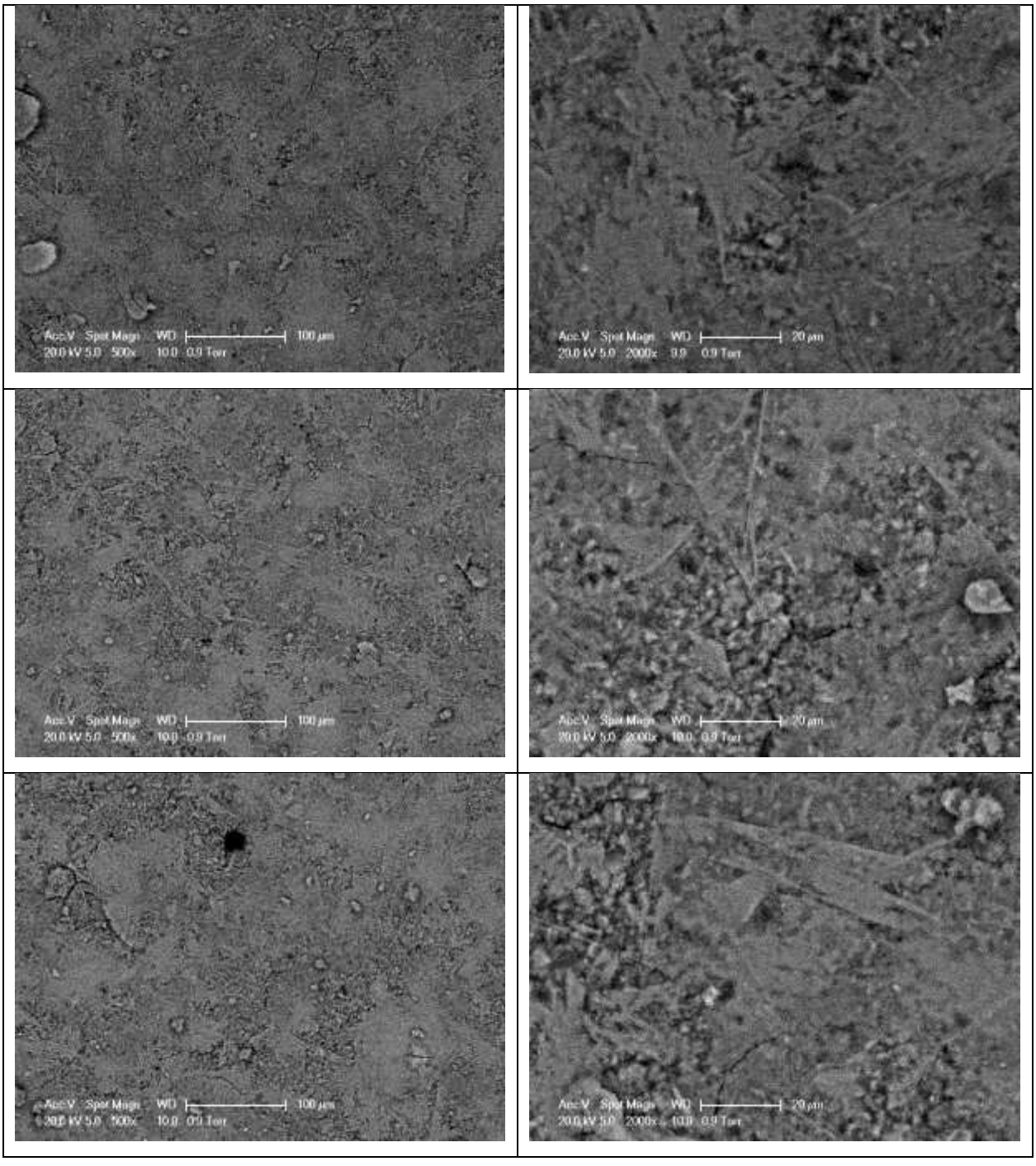

Cement paste sample images of Cem-C20C27 against C20C27 coated formwork, ***(CEM II/B with w/c=0.3)***

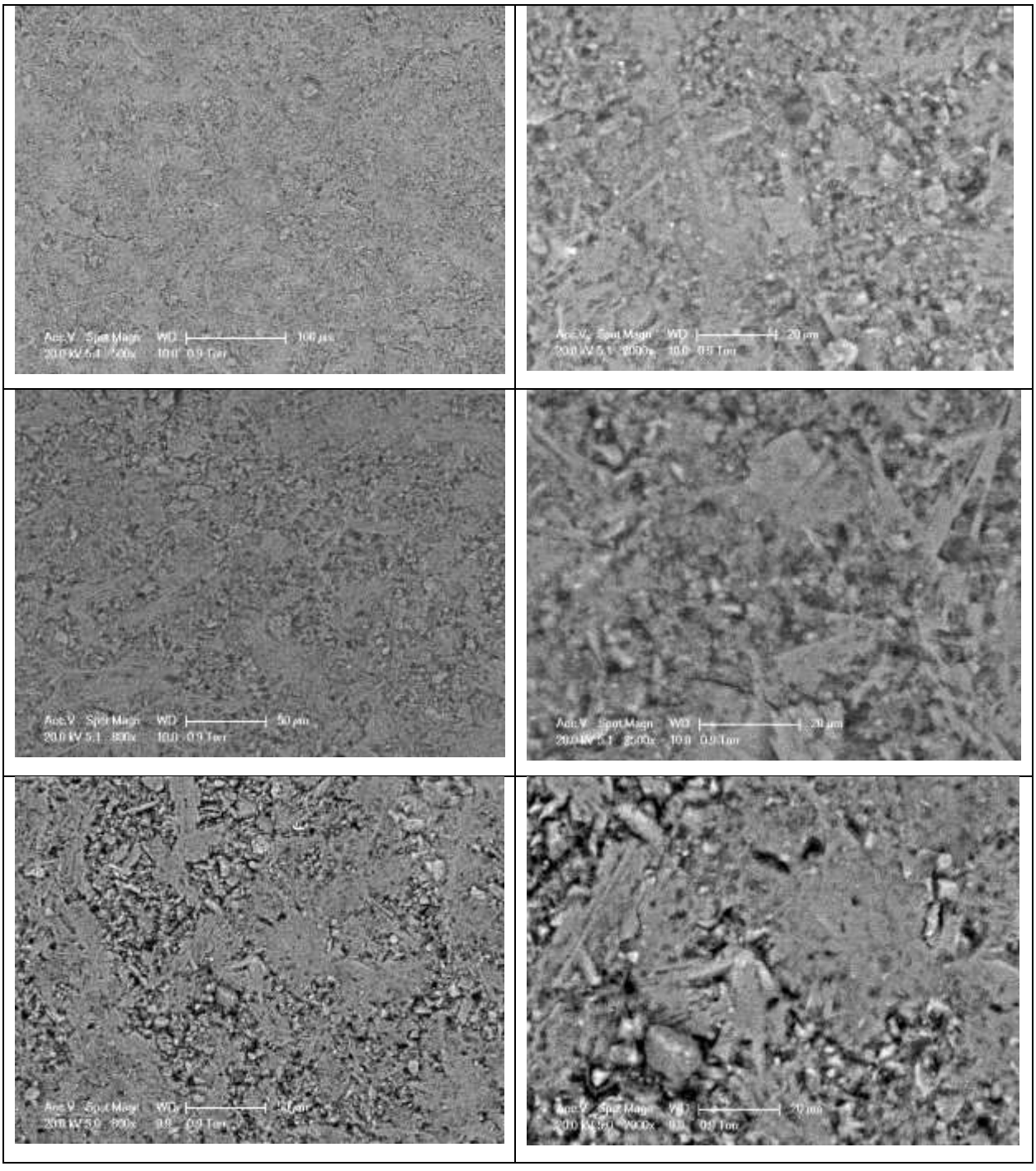

Cement paste sample images of Cem-MO against mineral oil coated formwork (F17-MO), ***(CEM II/B with w/c=0.3)***

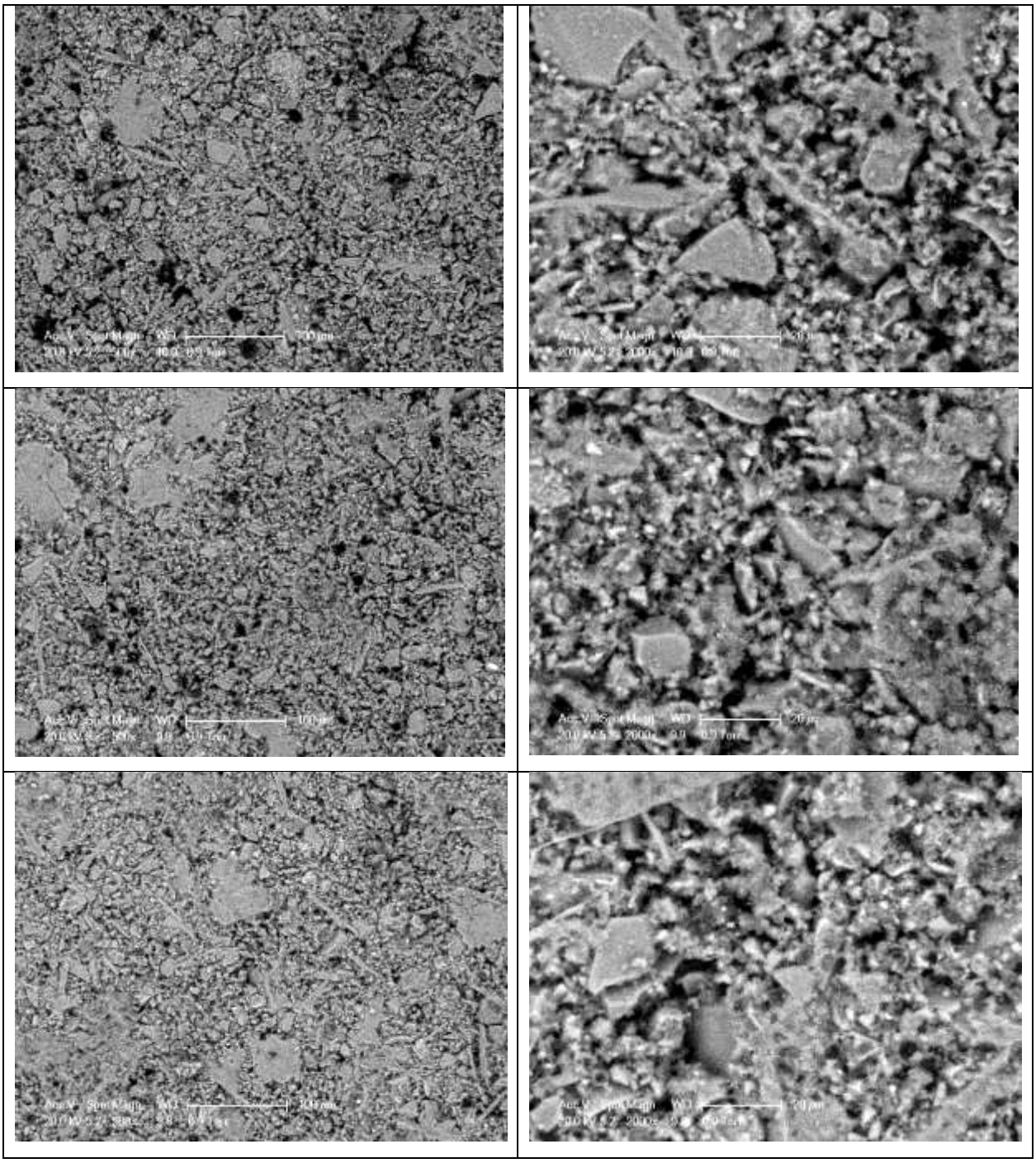

Cement paste sample images of Cem-VO against vegetable oil coated formwork (F17-VO),

(CEM II/B with w/c=0.3)

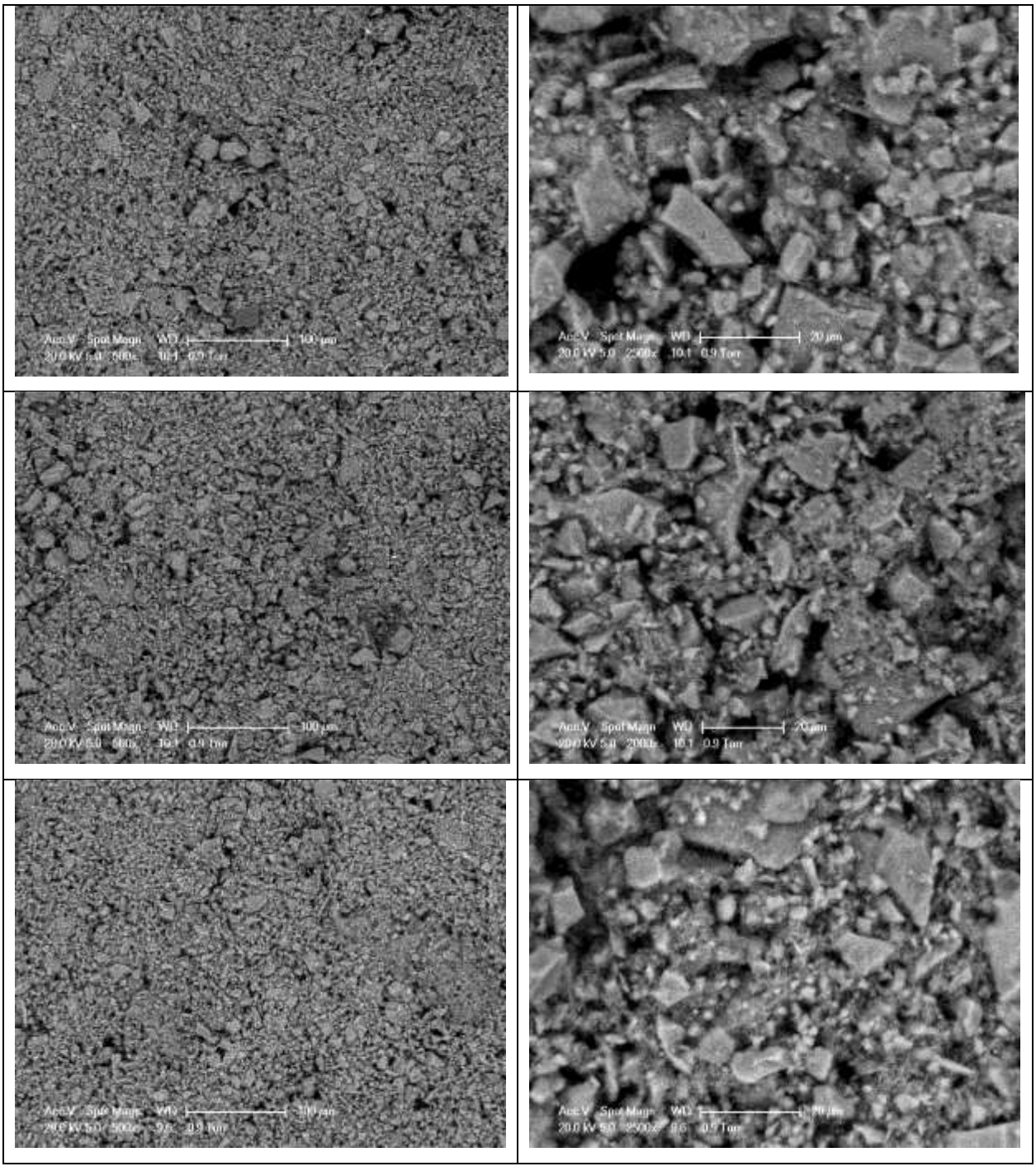

Cement paste sample images of Cem-Ref against reference formwork (F17-Ref), ***(CEM II/B with w/c=0.4)***

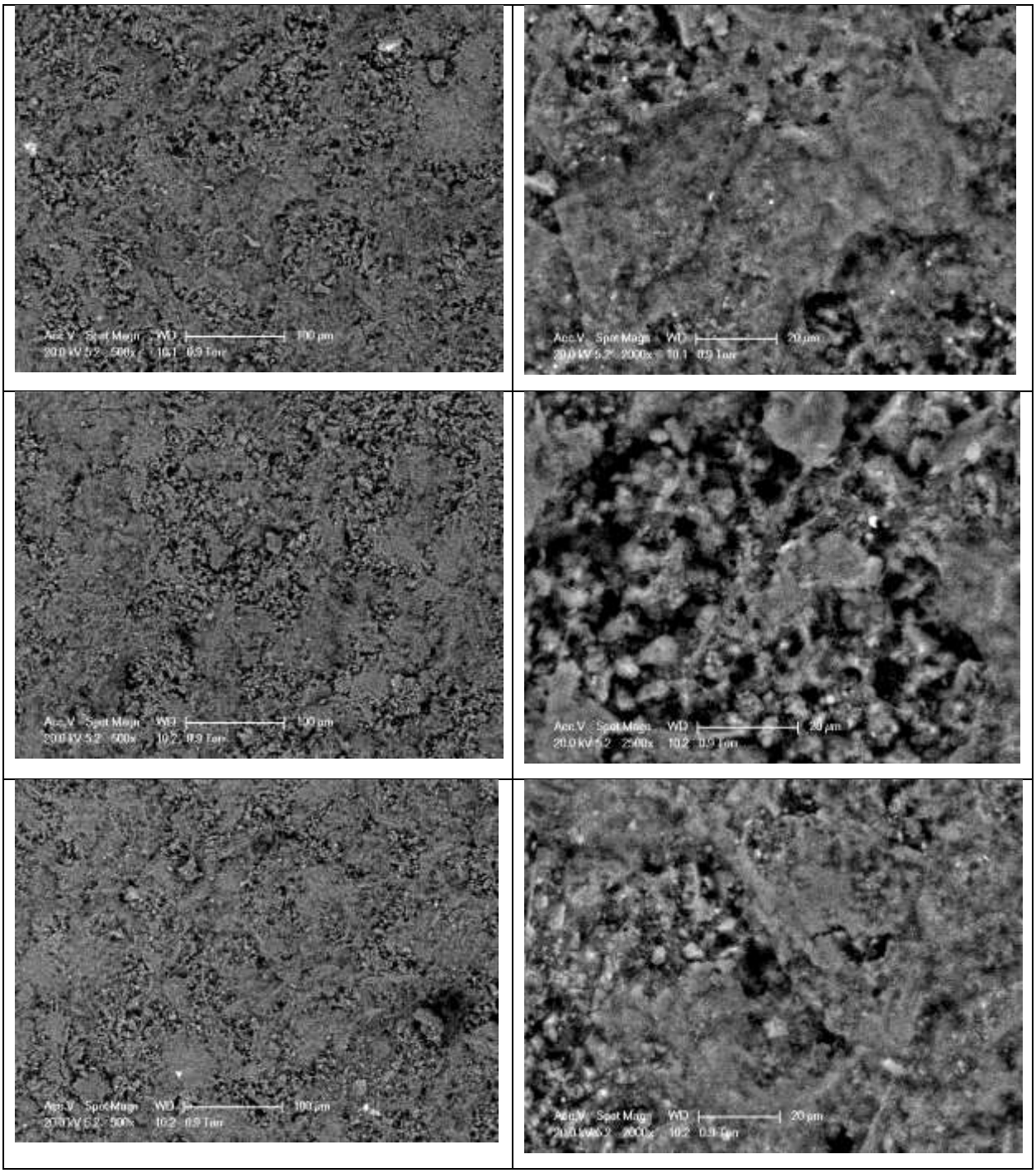

Cement paste sample images of Cem-PET against PET coated formwork, ***(CEM II/B with w/c=0.4)***

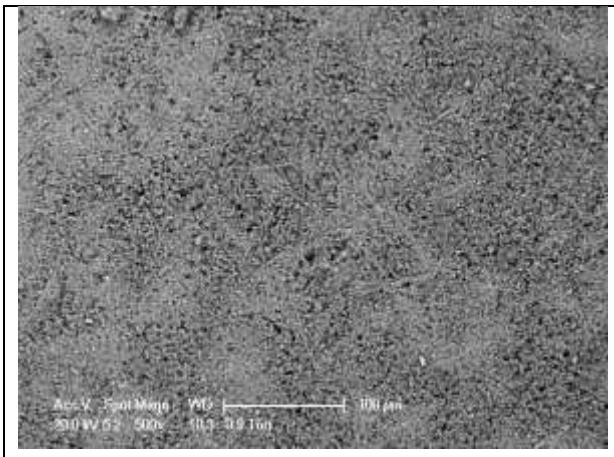

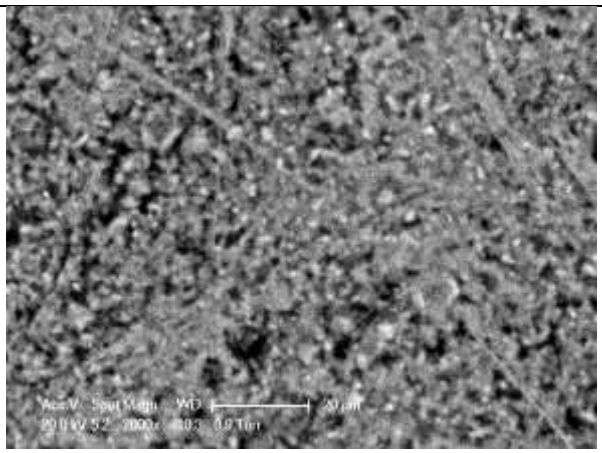

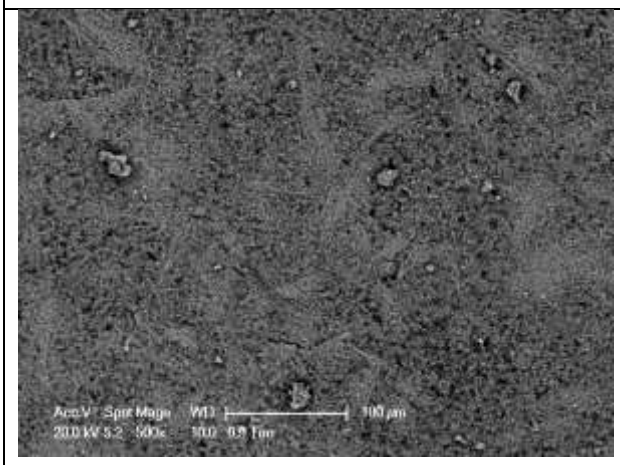

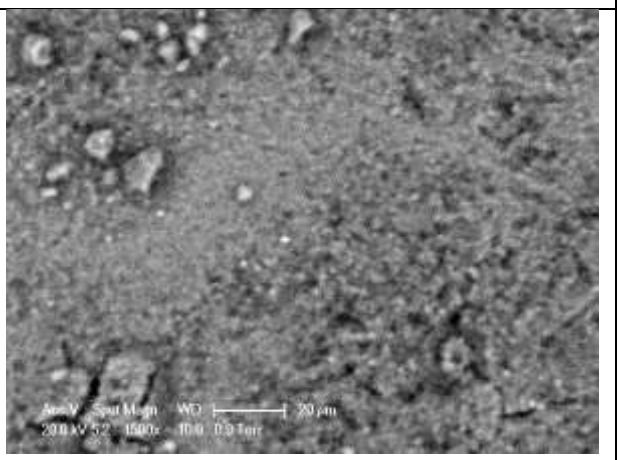

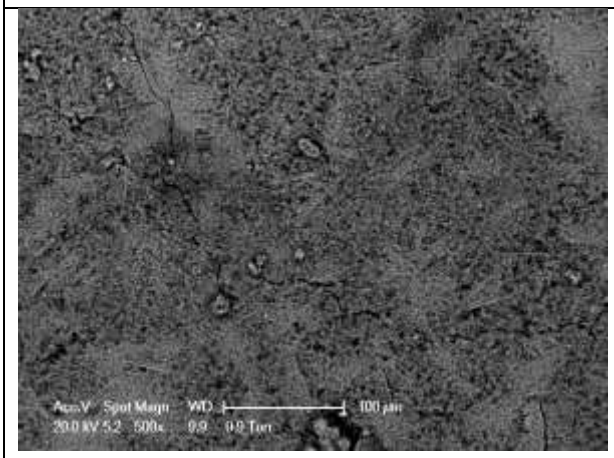

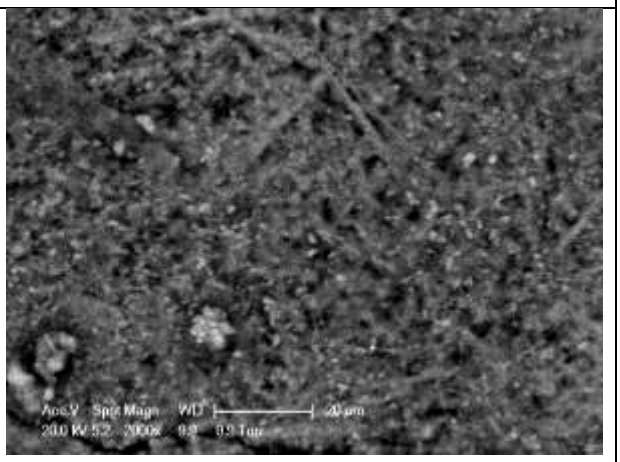

Cement paste sample images of Cem-C20C27 against C20C27 coated formwork, ***(CEM II/B with w/c=0.4)***

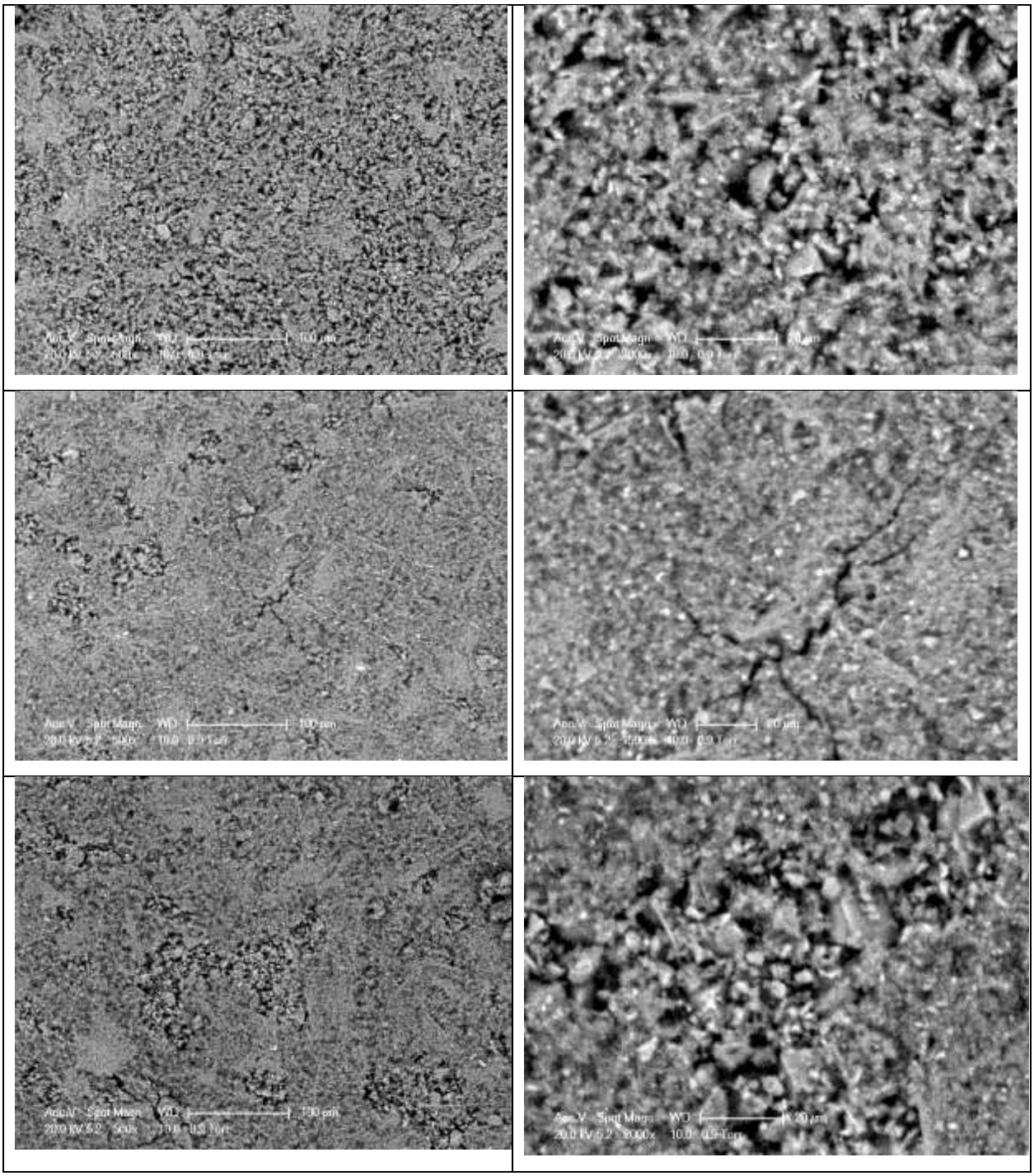

Cement paste sample images of Cem-MO against mineral oil coated formwork (F17-MO),

(CEM II/B with w/c=0.4)

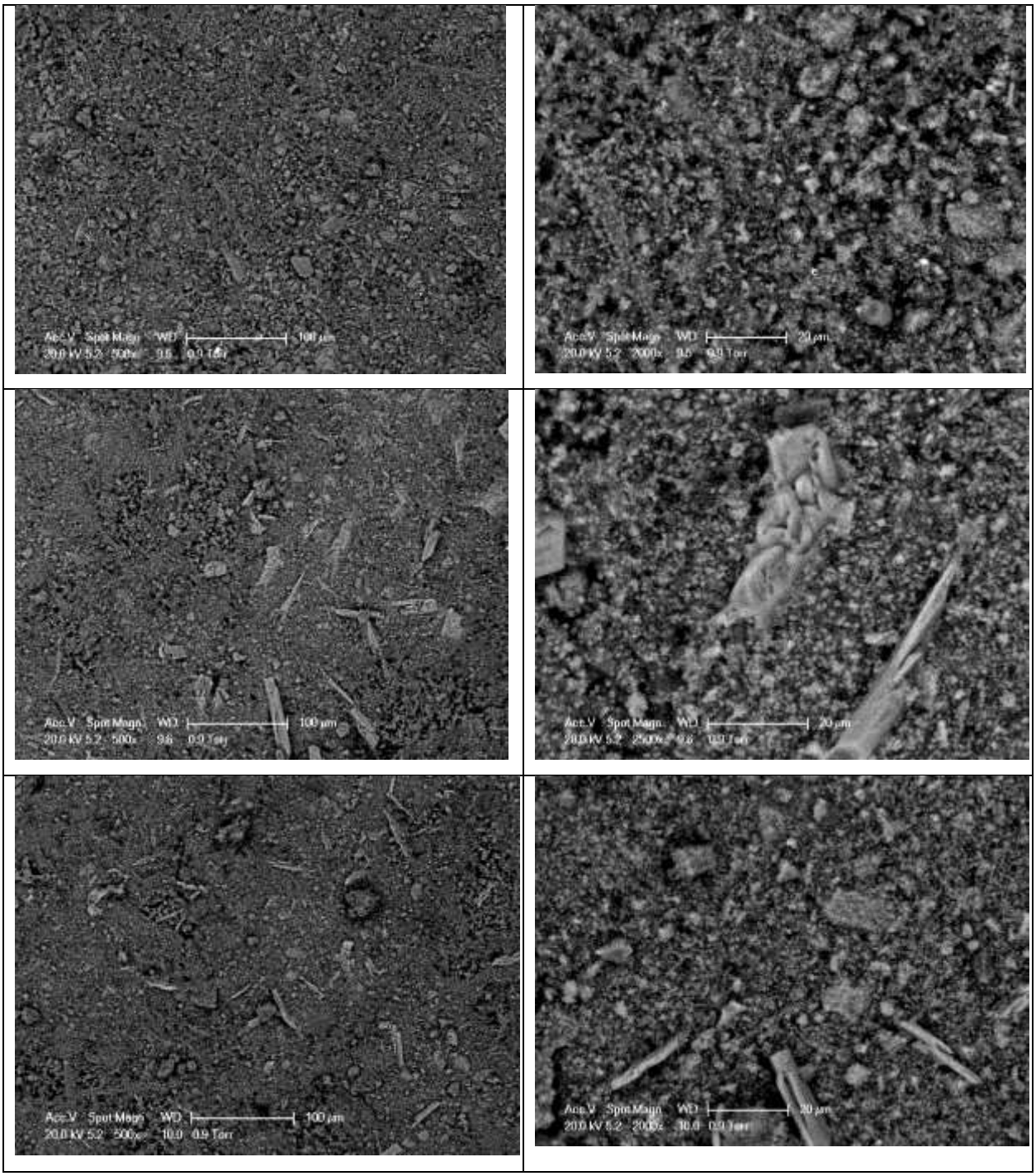

Cement paste sample images of Cem-VO against vegetable oil coated formwork (F17-VO),

(CEM II/B with w/c=0.4)

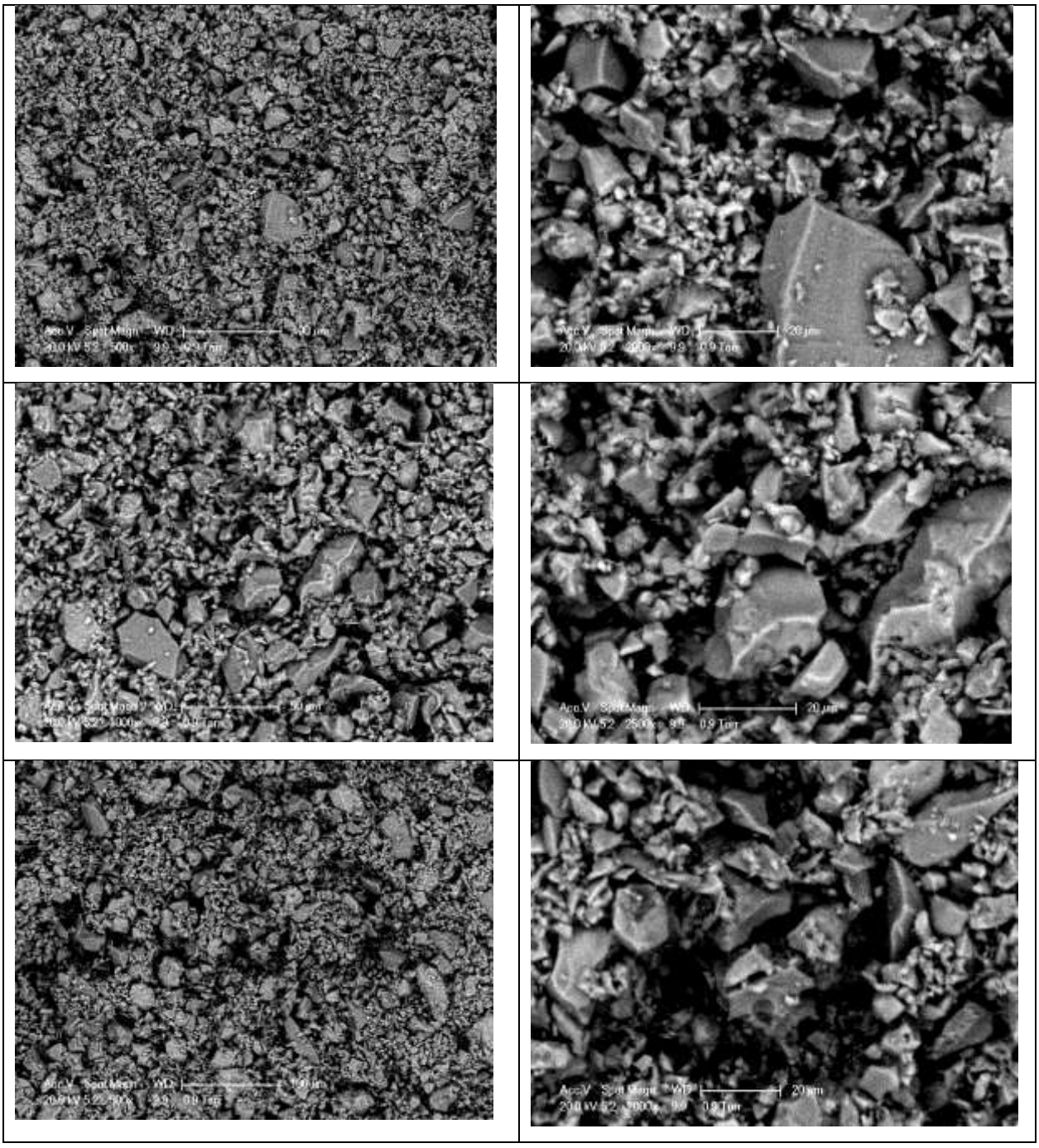

Cement paste sample images of Cem-Ref against reference formwork (F17-Ref), ***(CEM II/B with w/c=0.5)***

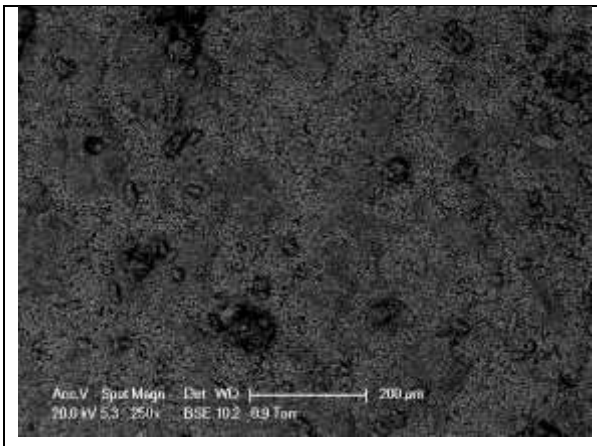

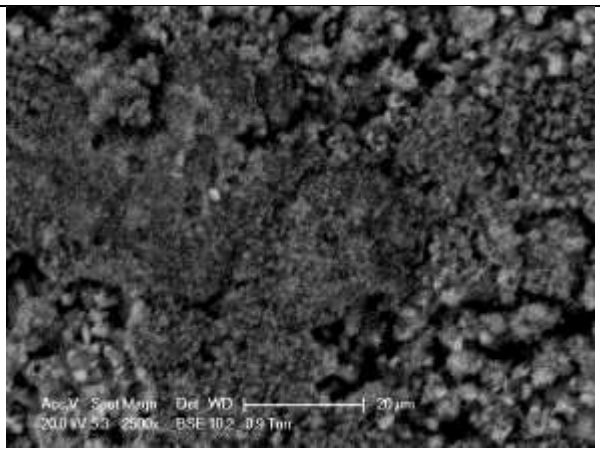

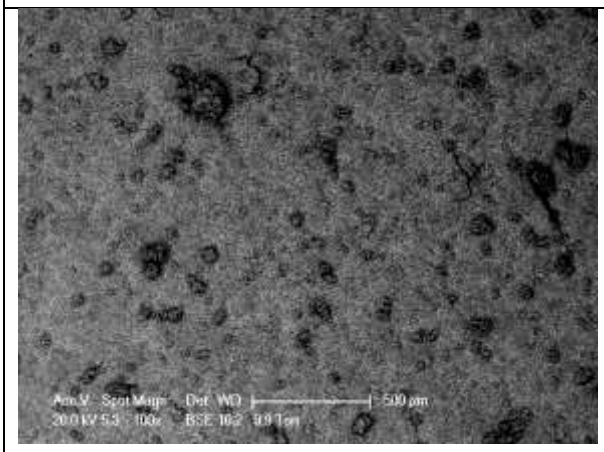

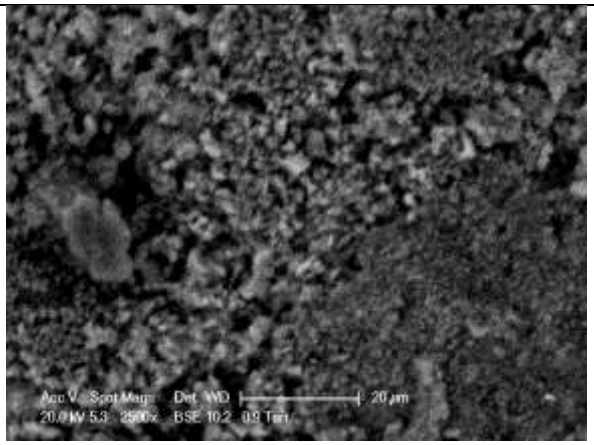

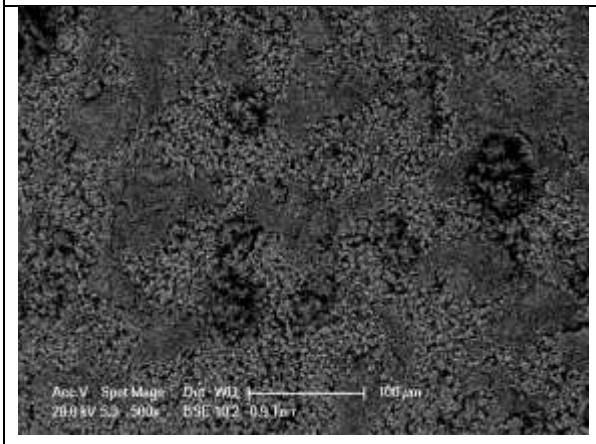

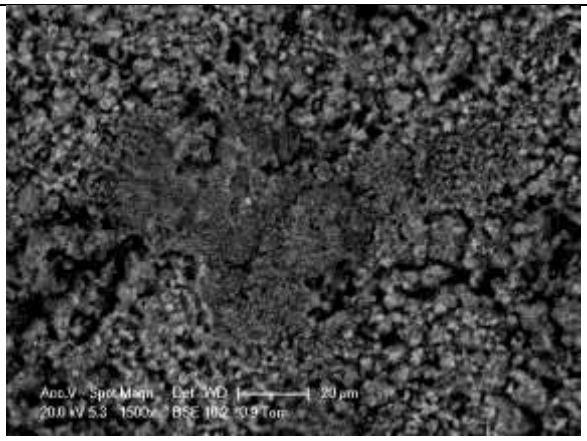

Cement paste sample images of Cem-PET against PET coated formwork, ***(CEM II/B with w/c=0.5)***

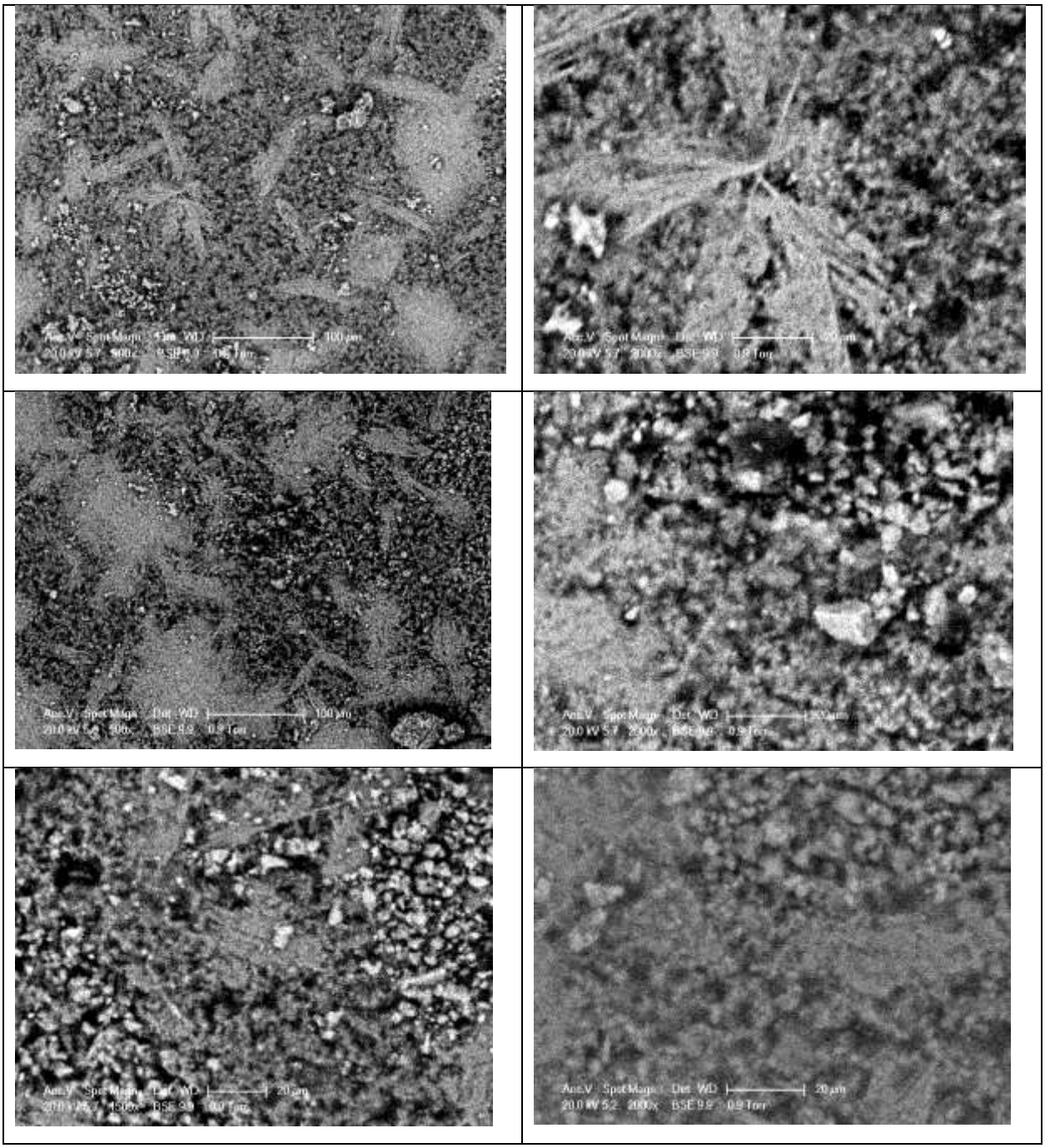

Cement paste sample images of Cem-C20C27 against C20C27 coated formwork, ***(CEM II/B with w/c=0.5)***

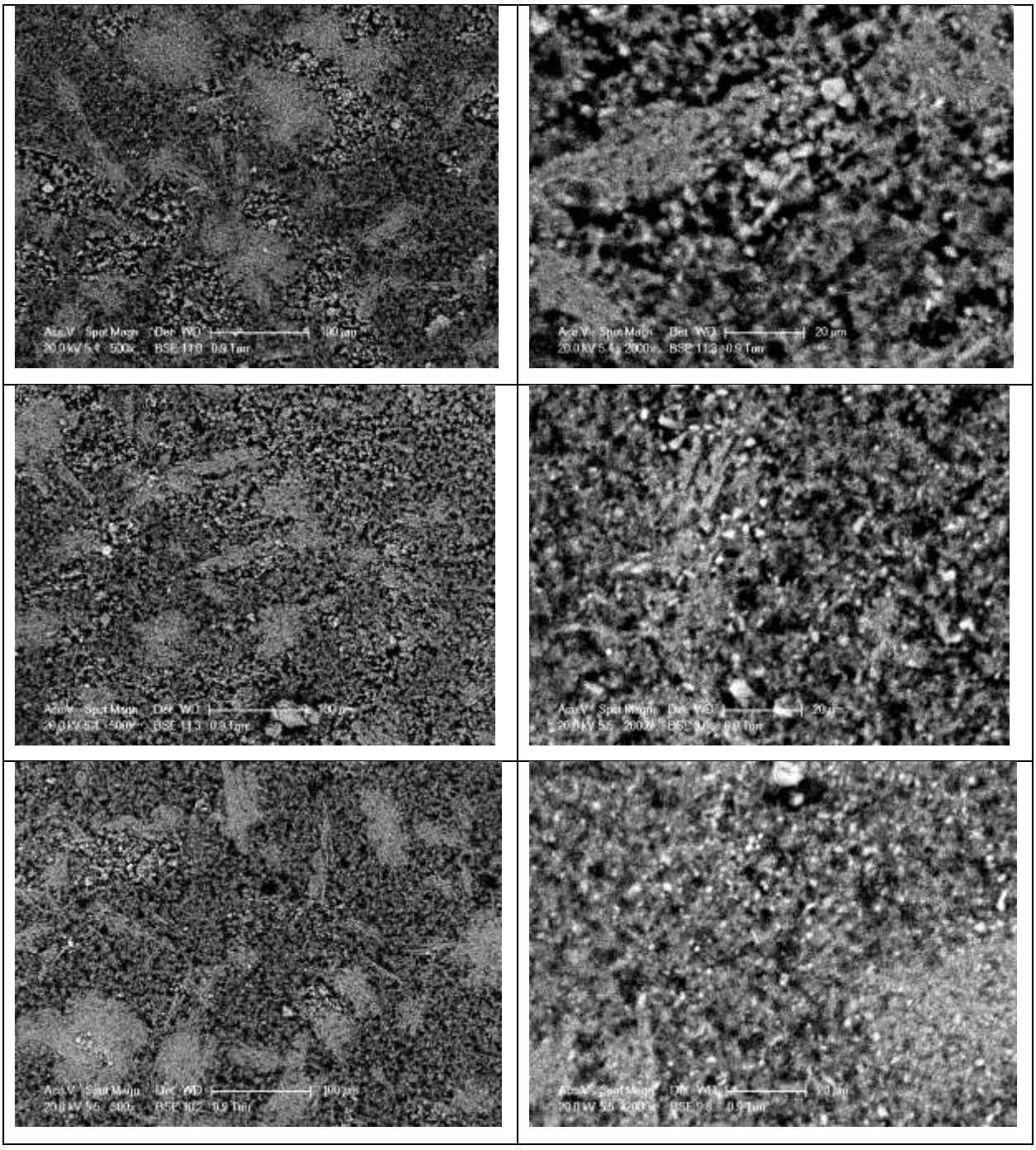

Cement paste sample images of Cem-MO against mineral oil coated formwork (F17-MO),

(CEM II/B with w/c=0.5)

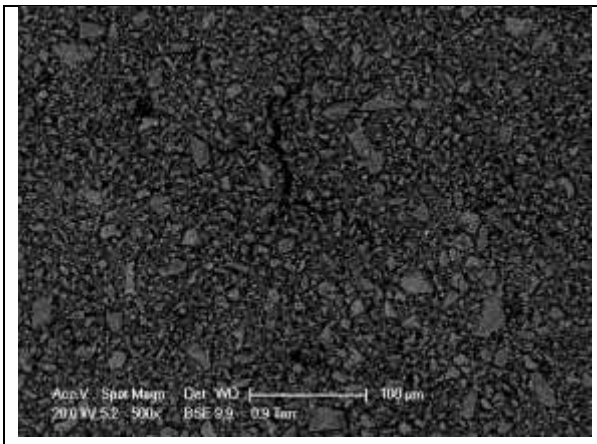

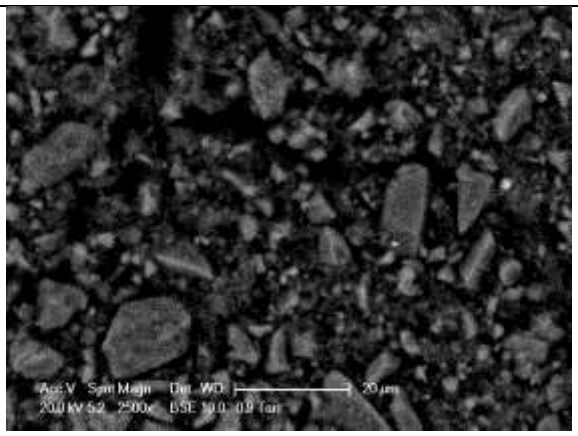

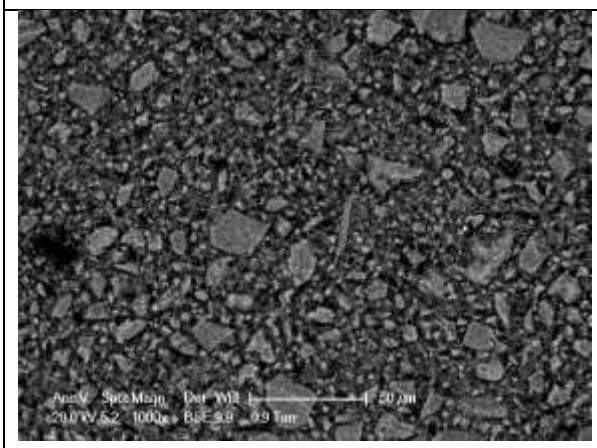

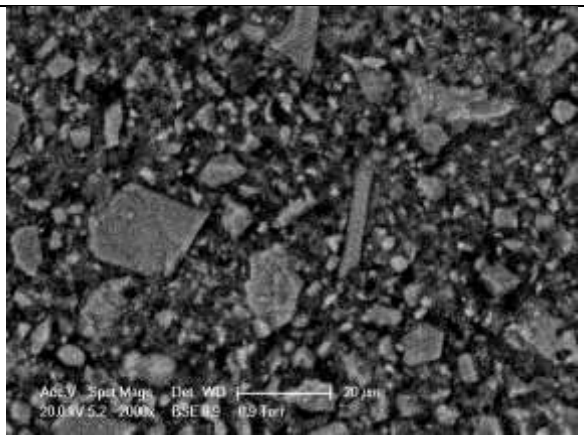

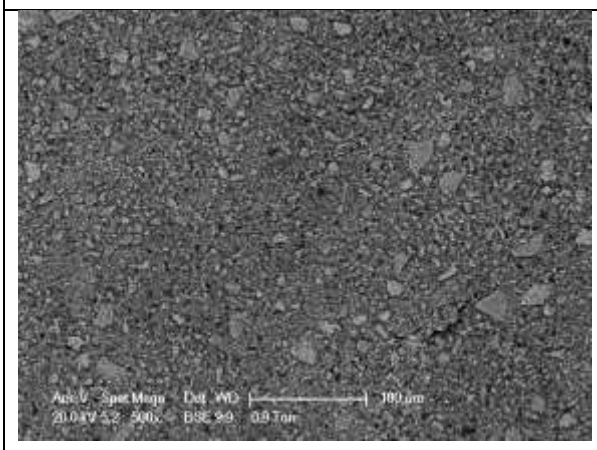

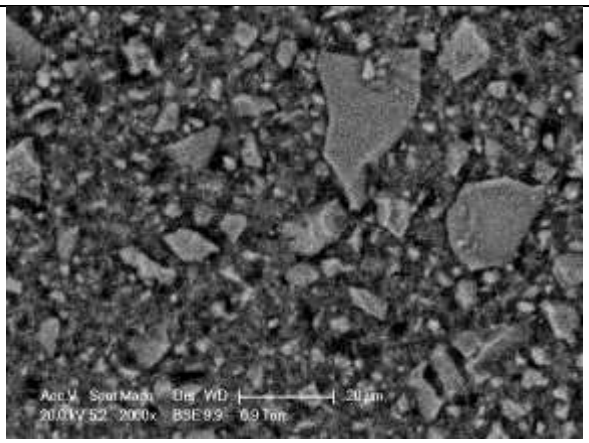

Cement paste sample images of Cem-VO against vegetable oil coated formwork (F17-VO),

(CEM II/B with w/c=0.5)

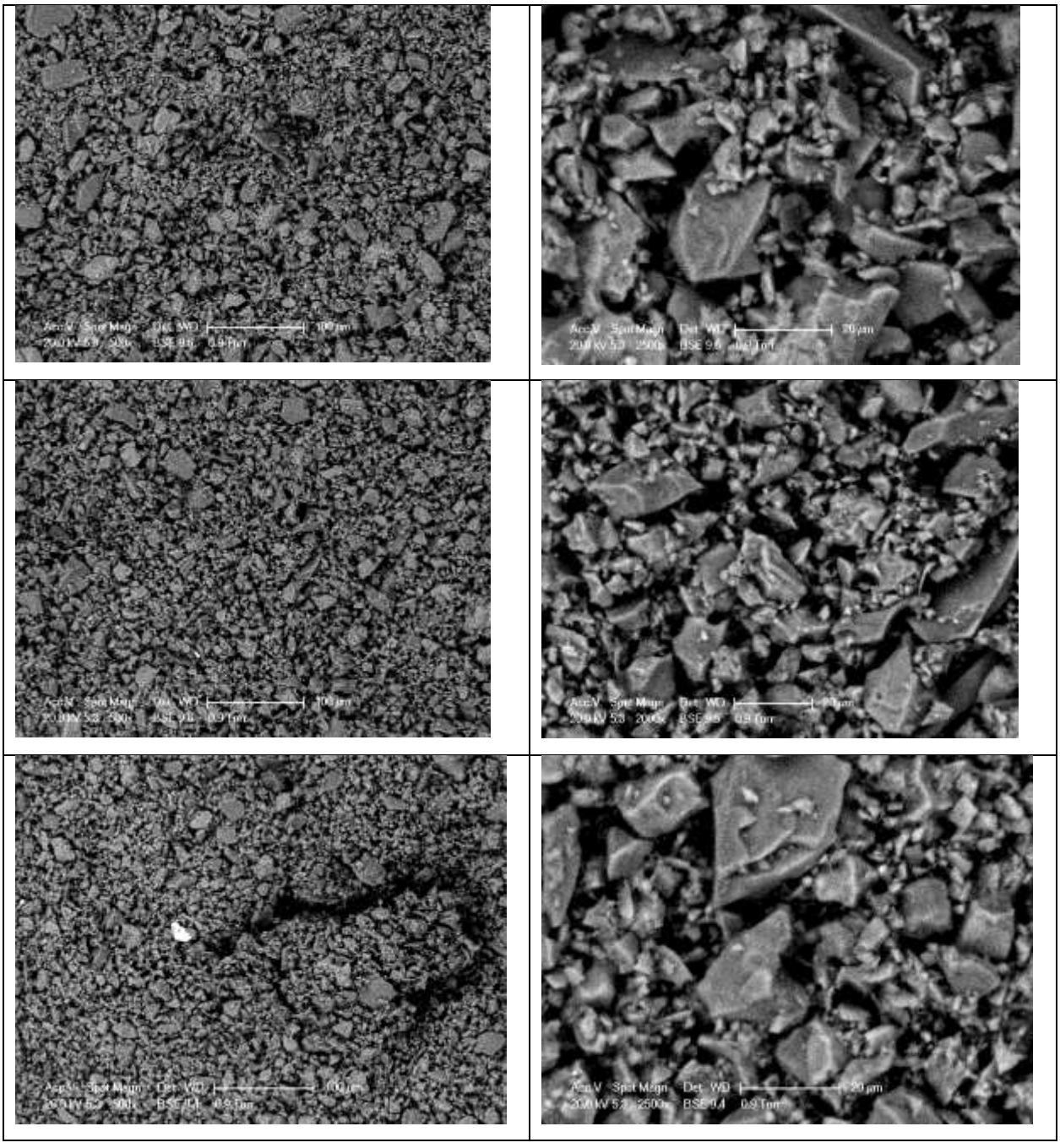

Cement pastes' surface roughness, CEM I, w/c = 0.3

Cem-Ref

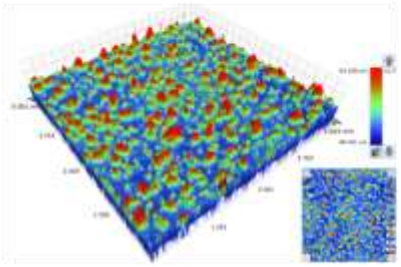

Cem-MO

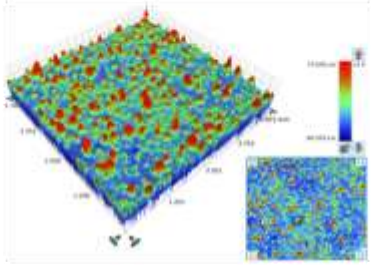

Cem-VO

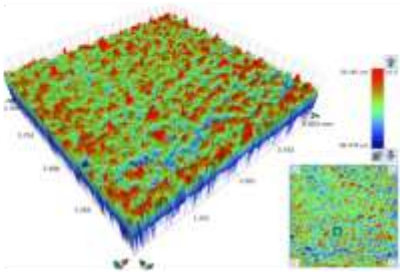

Cem-C20C27

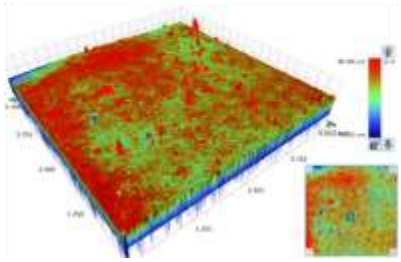

Cem-PET

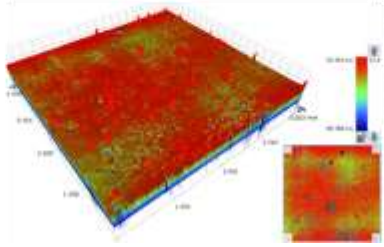

Cement pastes' surface roughness, CEM I, w/c = 0.4

Cem-Ref

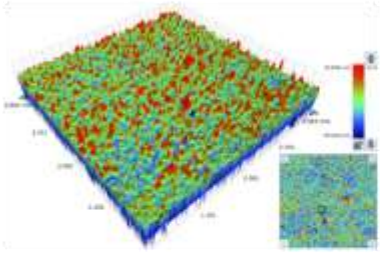

Cem-MO

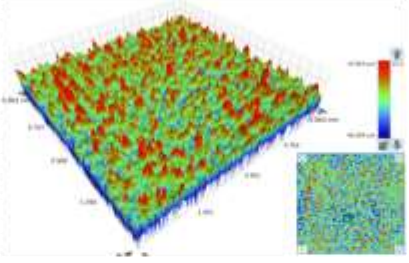

Cem-VO

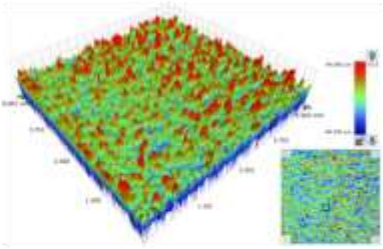

Cem-C20C27

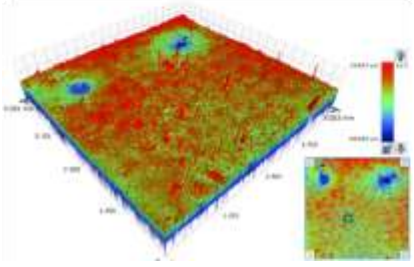

Cem-PET

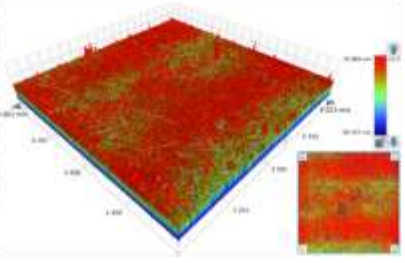

Cement pastes' surface roughness, CEM I, w/c = 0.5

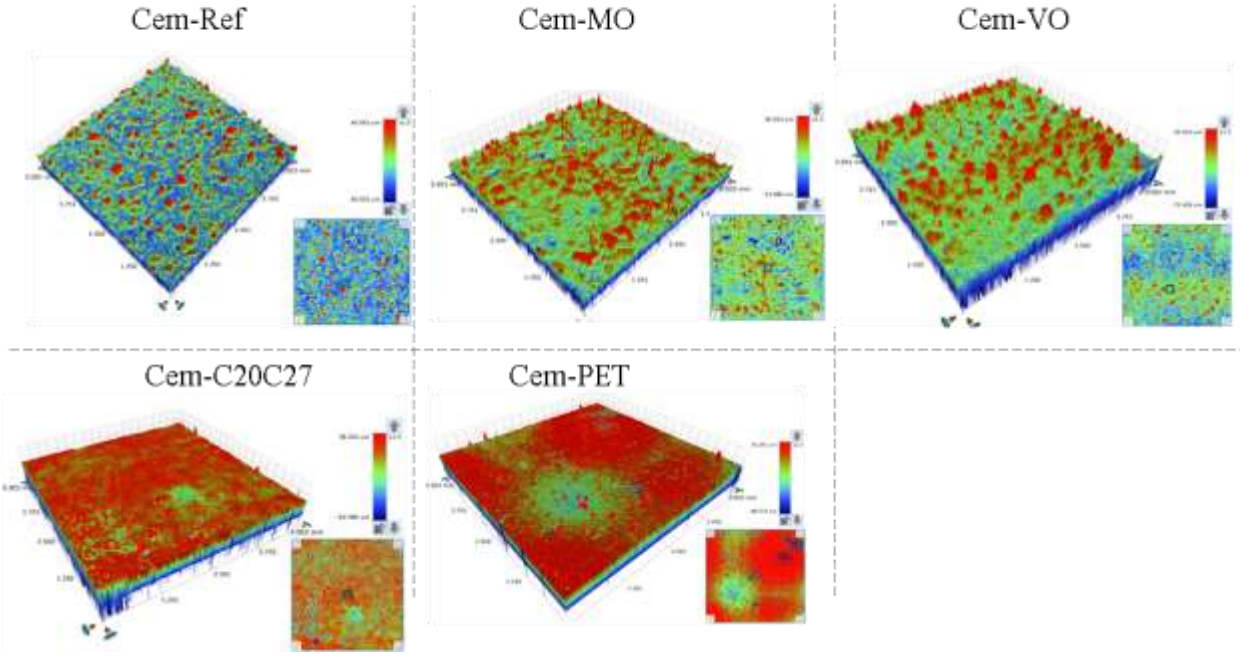

Cement pastes' surface roughness, CEM II, w/c = 0.3

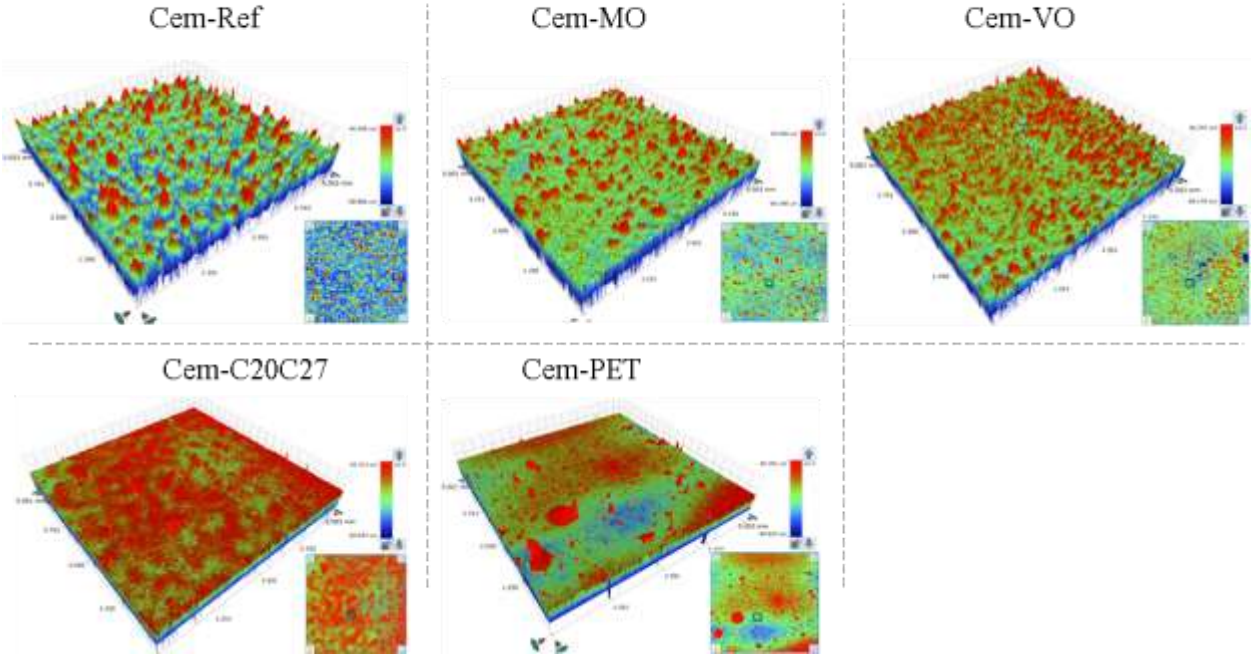

Cement pastes' surface roughness, CEM II, w/c = 0.4

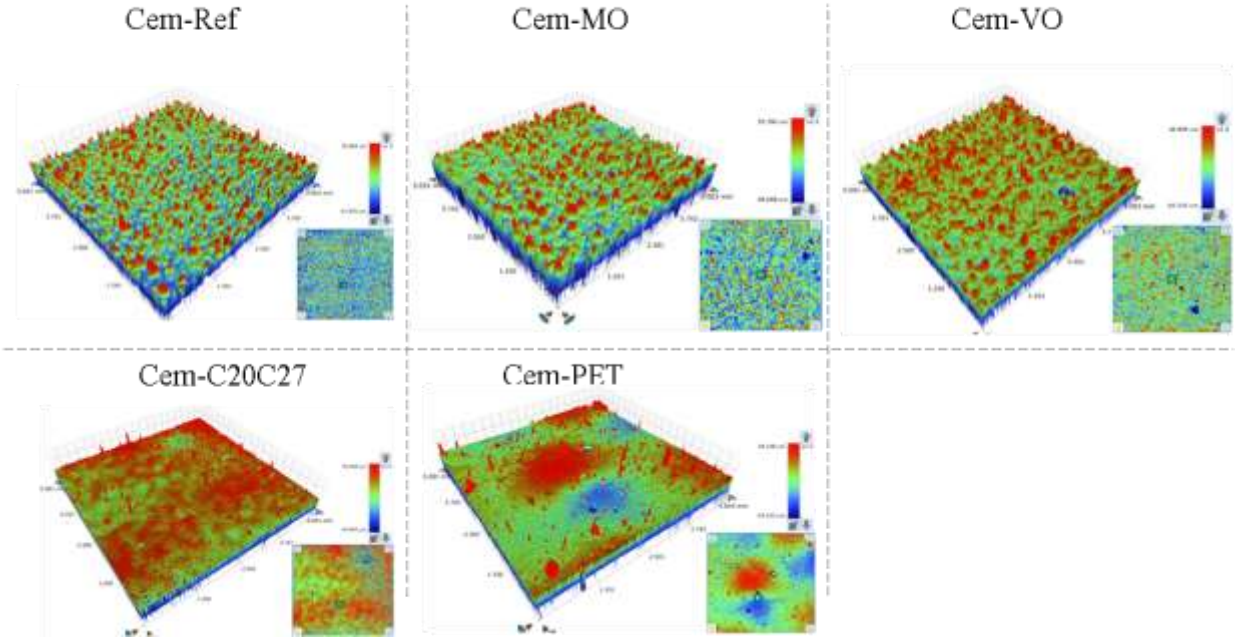

Cement pastes' surface roughness, CEM II, w/c = 0.5

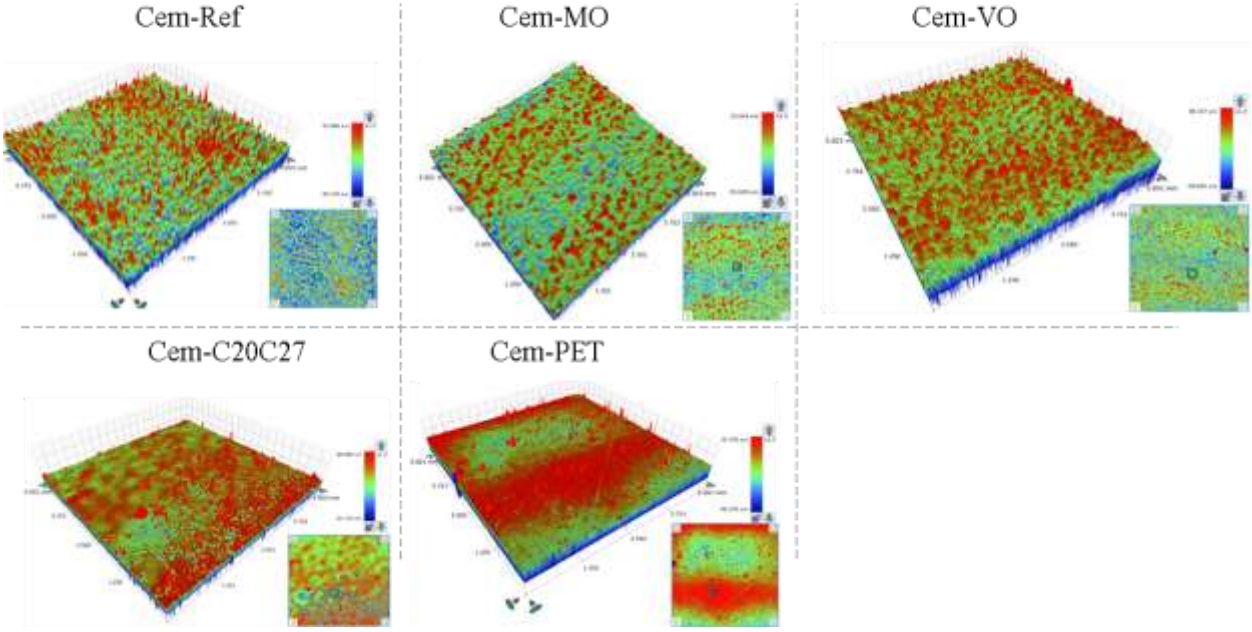

Annex 2

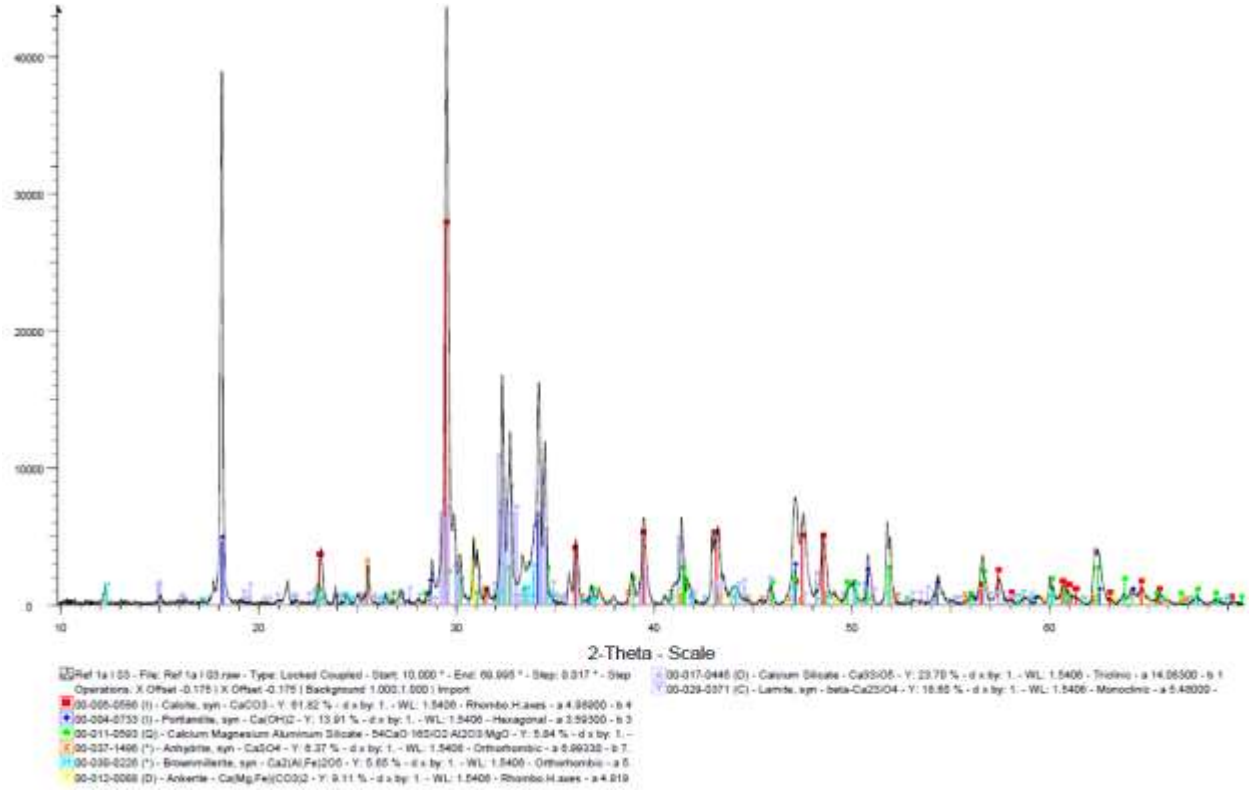

Cem-Ref (w/c=0.3, CEM I)

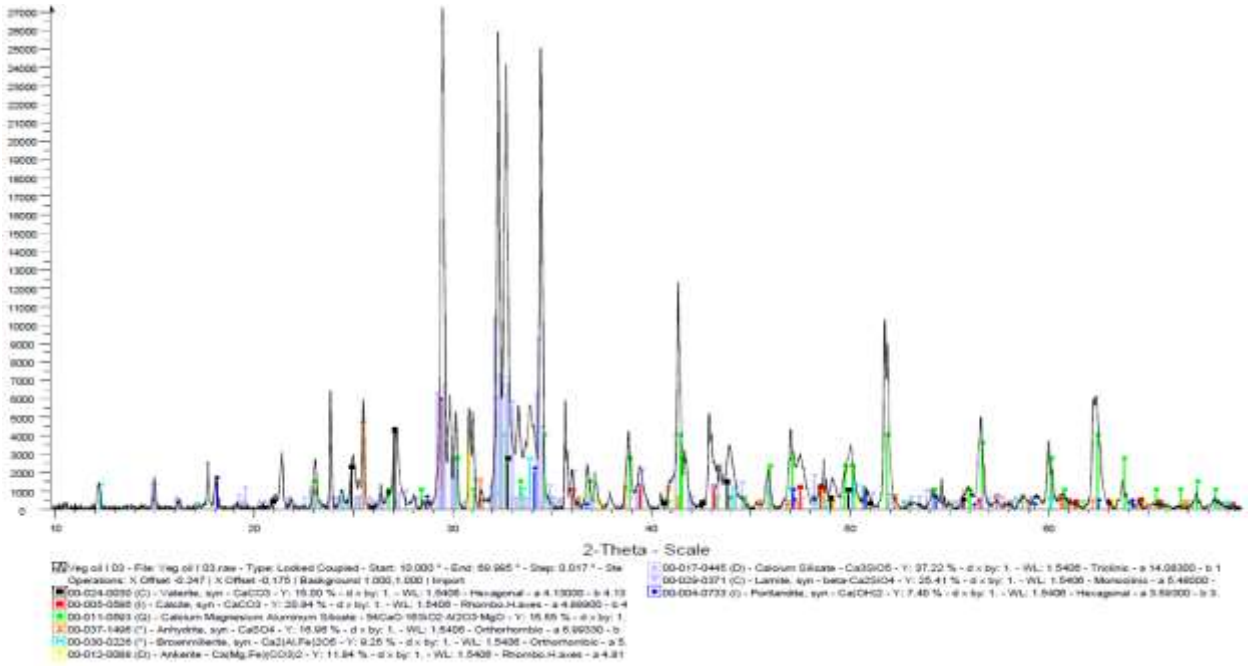

Cem-VO (w/c=0.3, CEM I)

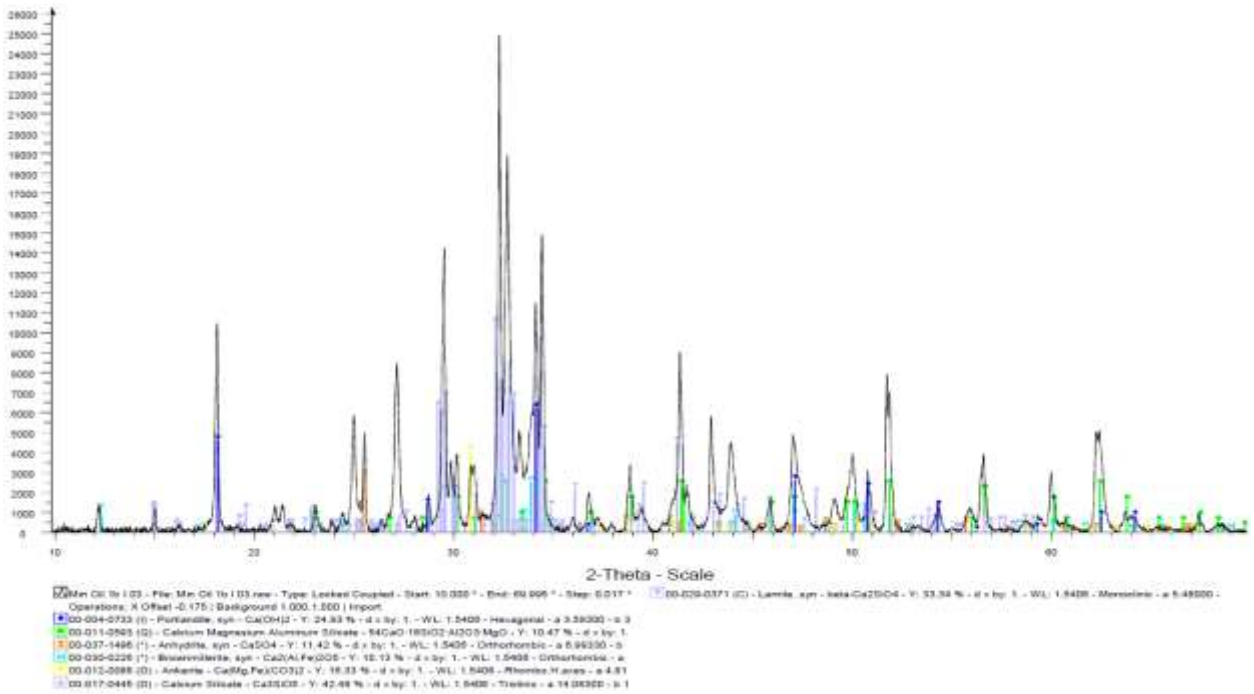

Cem-MO (w/c=0.3, CEM I)

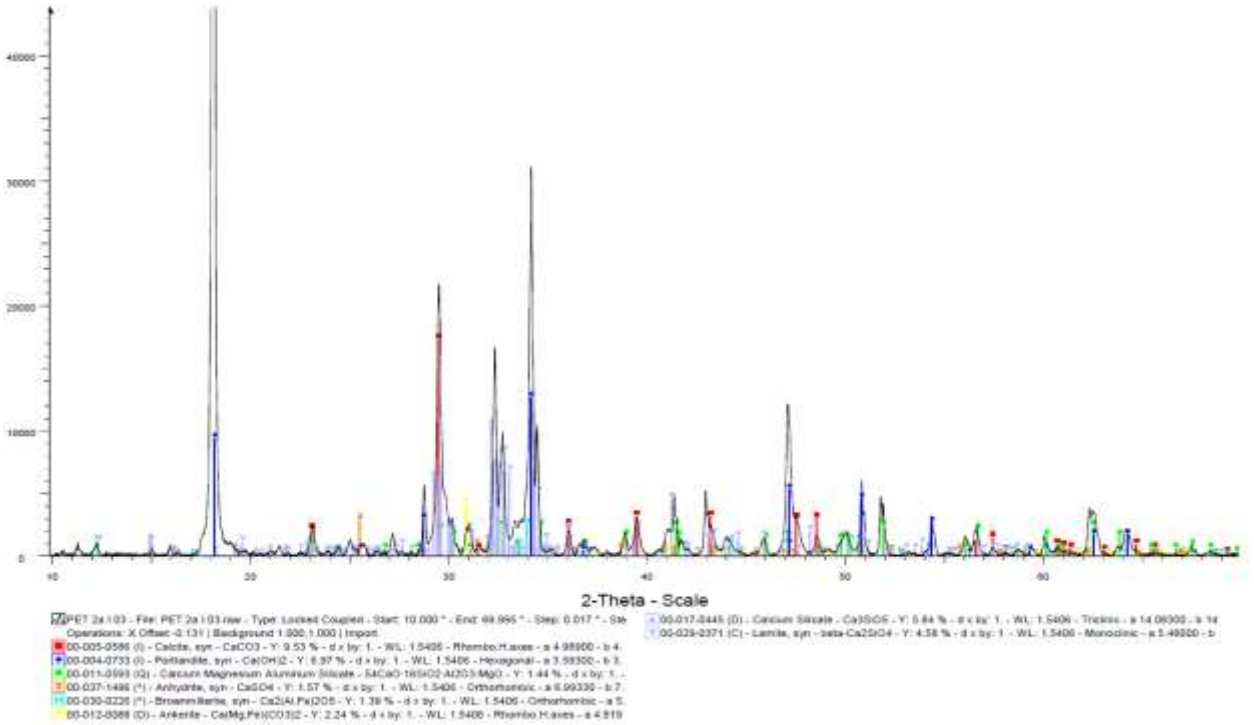

Cem-PET (w/c=0.3, CEM I)

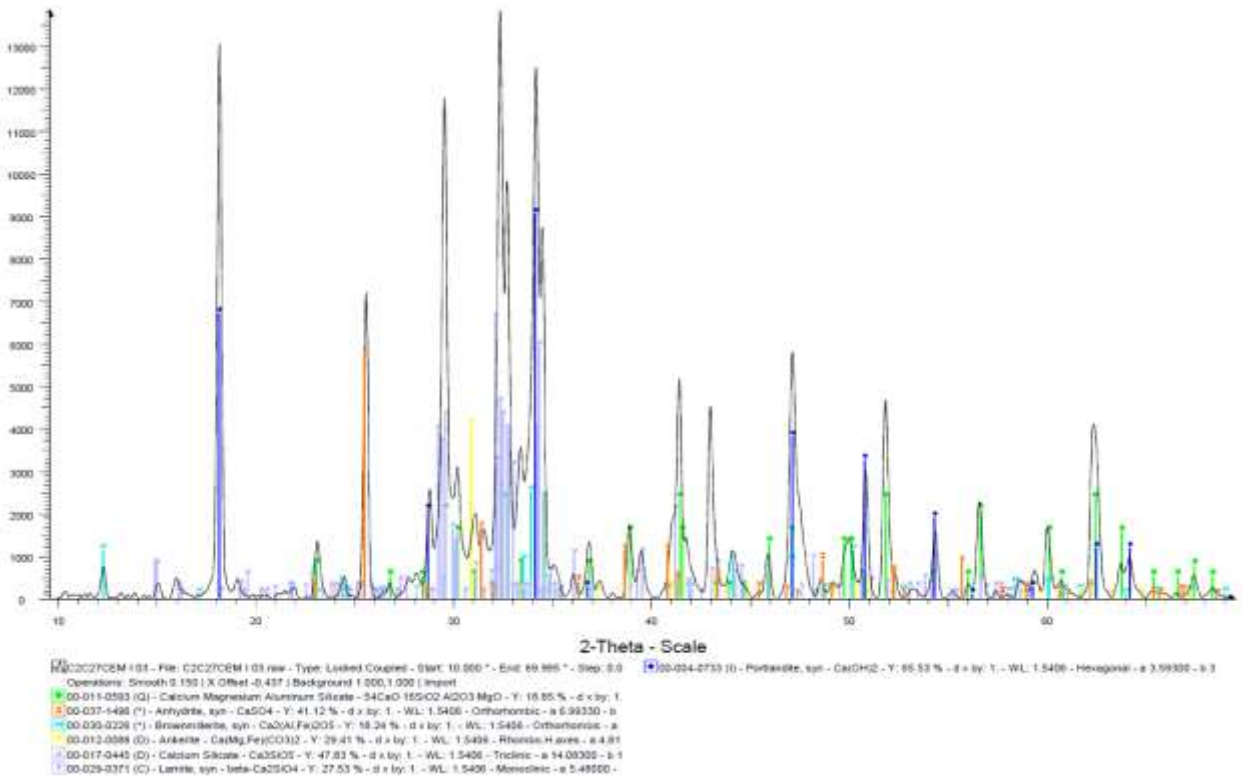

Cem-C20C27 (w/c=0.3, CEM I)

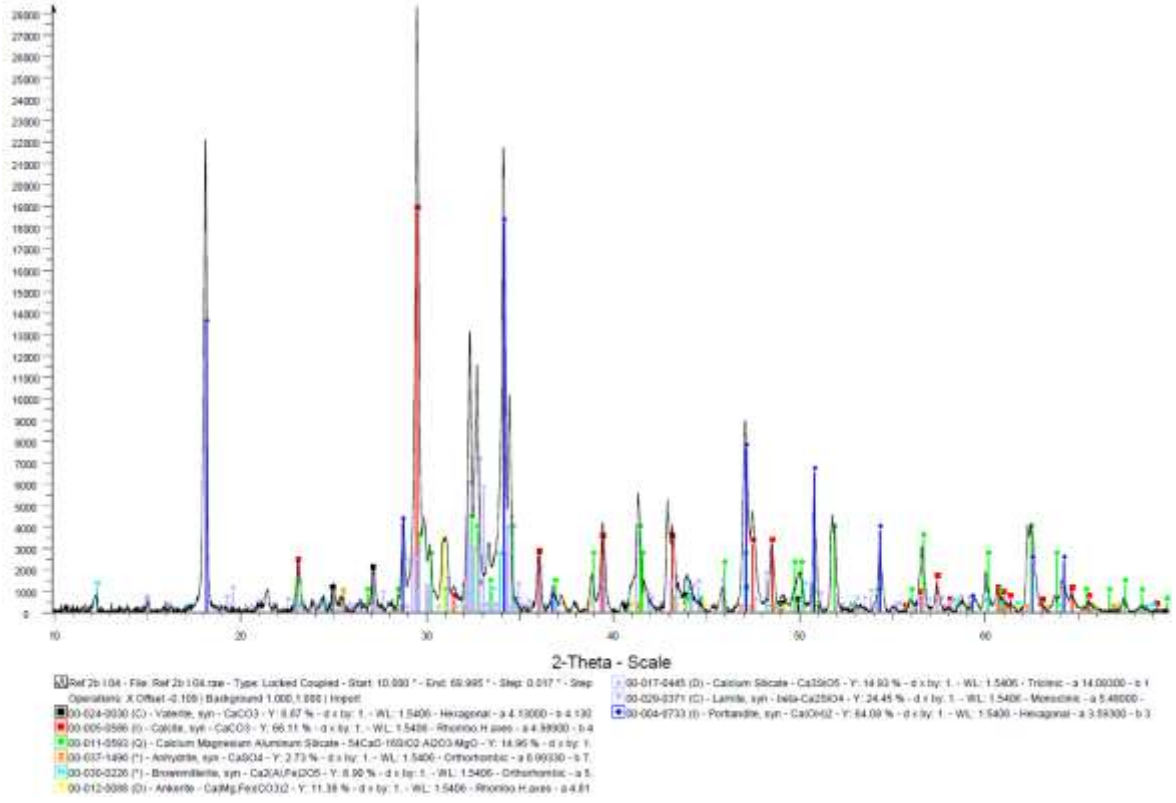

Cem-Ref (w/c=0.4, CEM I)

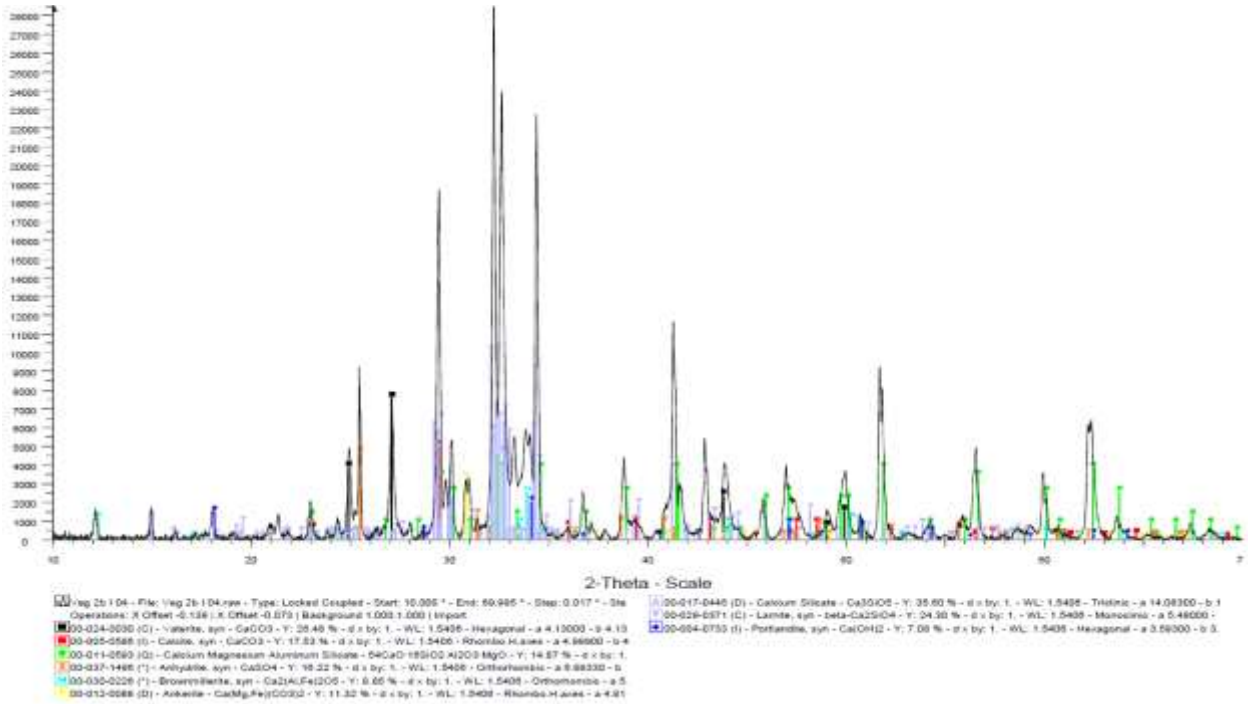

Cem-VO (w/c=0.4, CEM I)

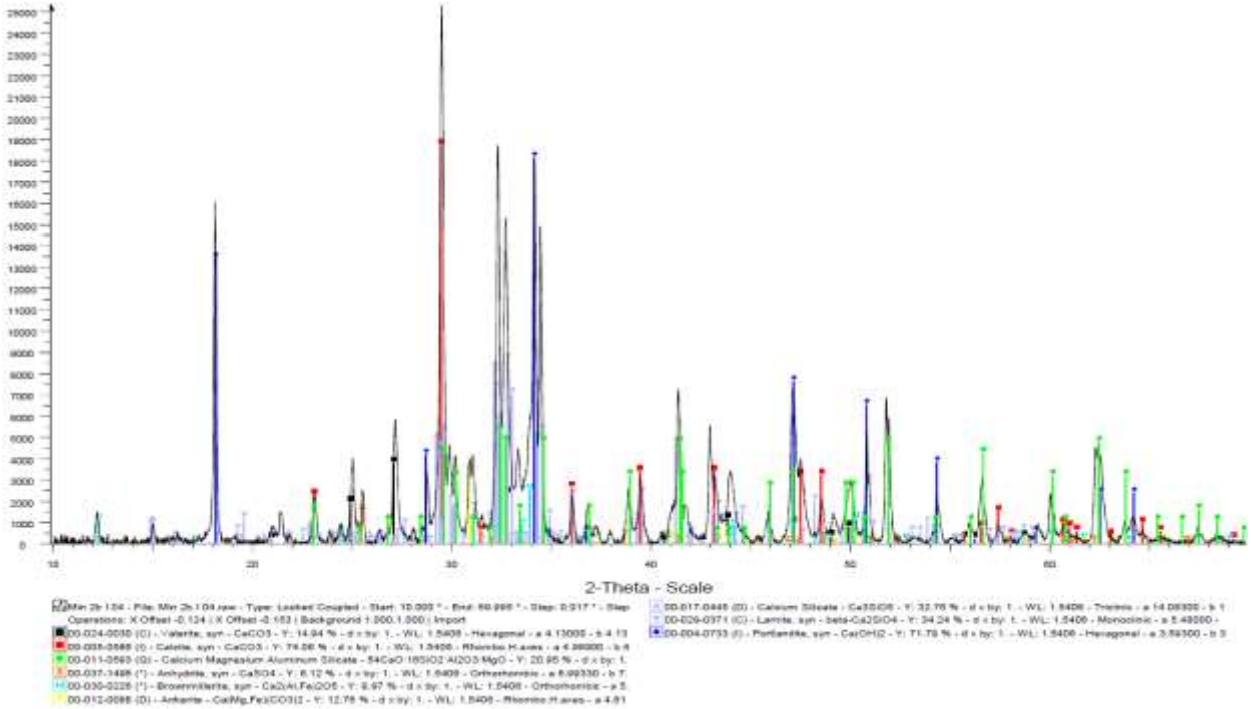

Cem-MO (w/c=0.4, CEM I)

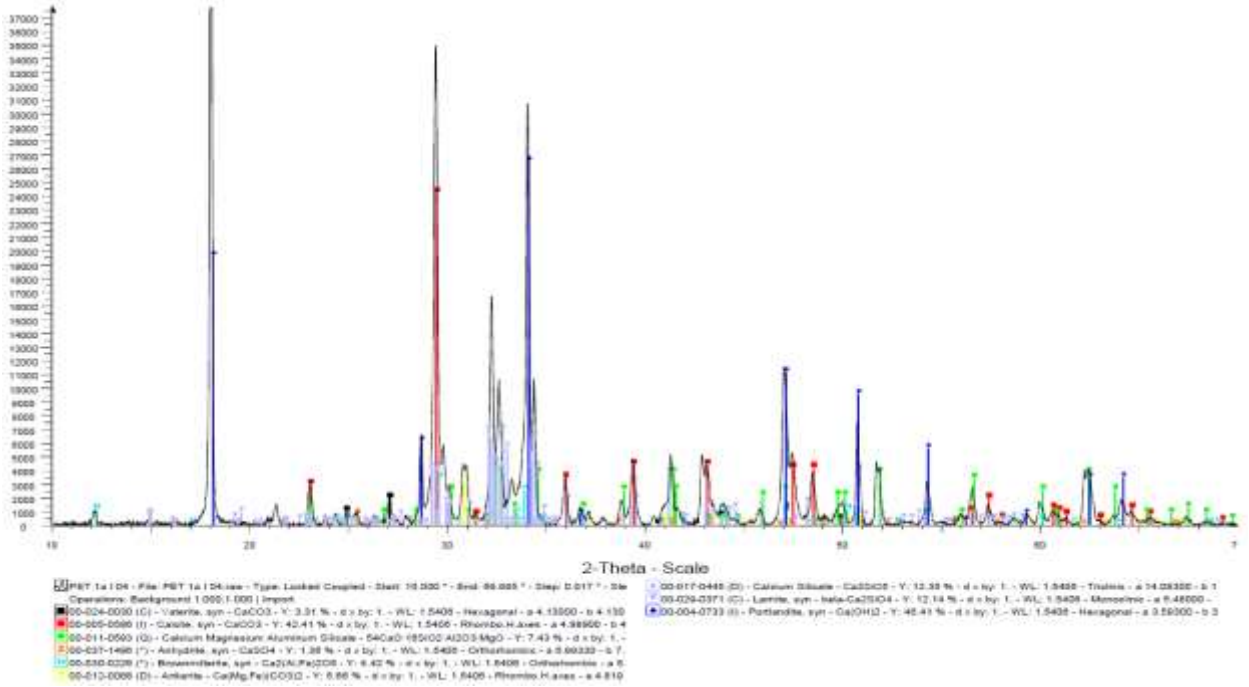

Cem-PET (w/c=0.4, CEM I)

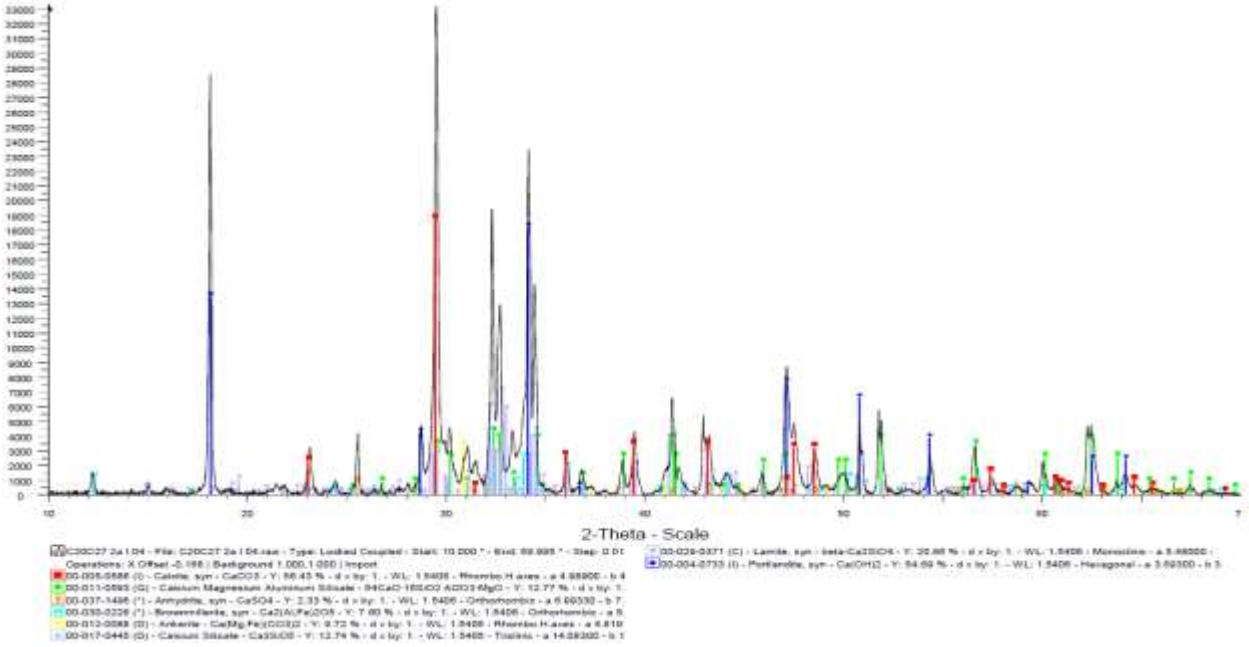

Cem-C20C27 (w/c=0.4, CEM I)

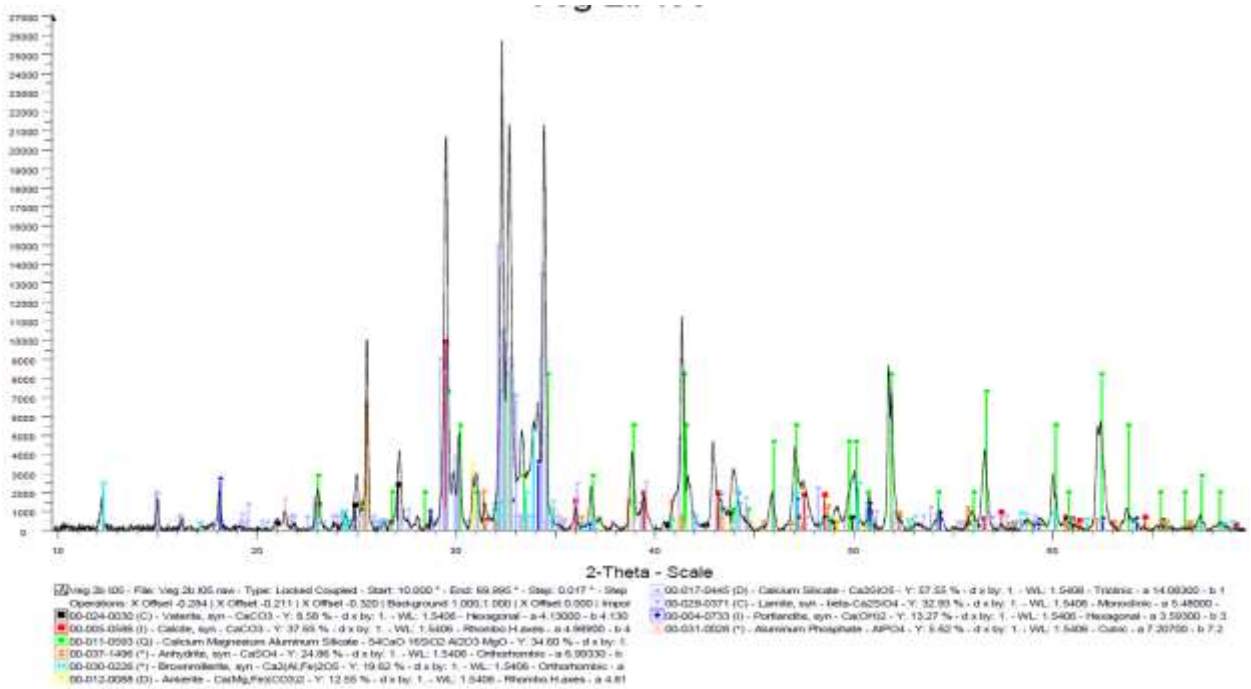

Cem-VO (w/c=0.5, CEM I)

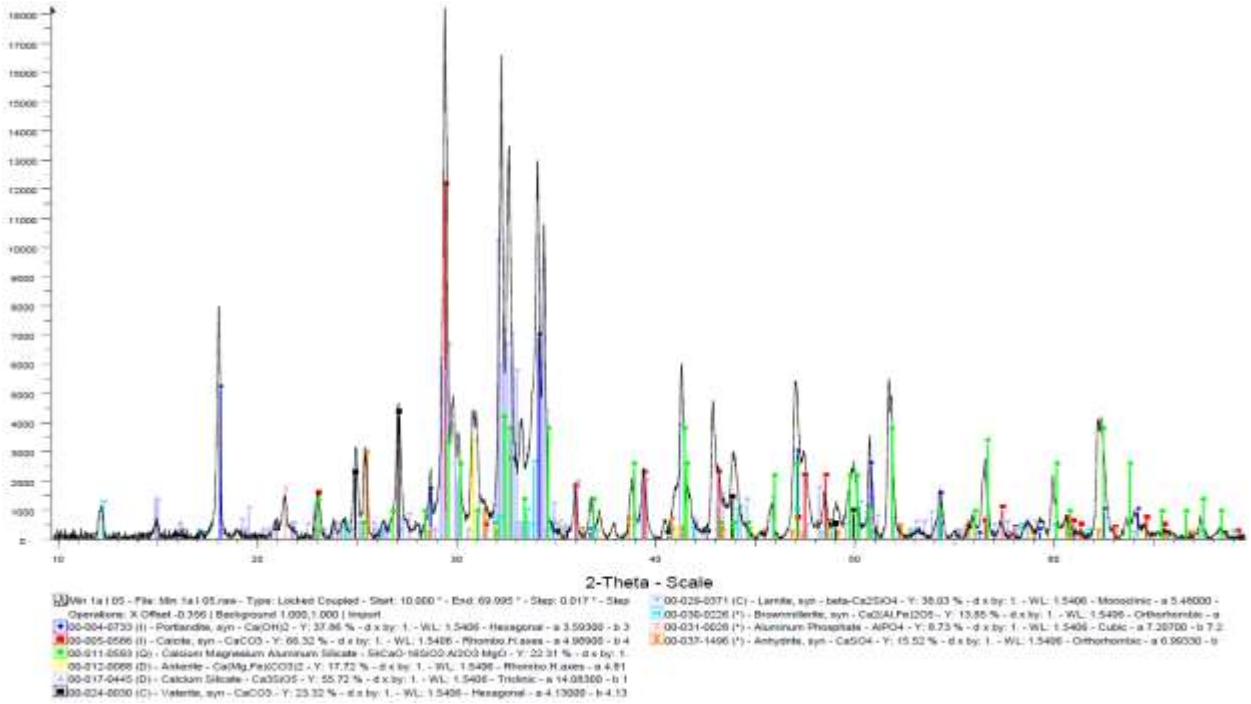

Cem-MO (w/c=0.5, CEM I)

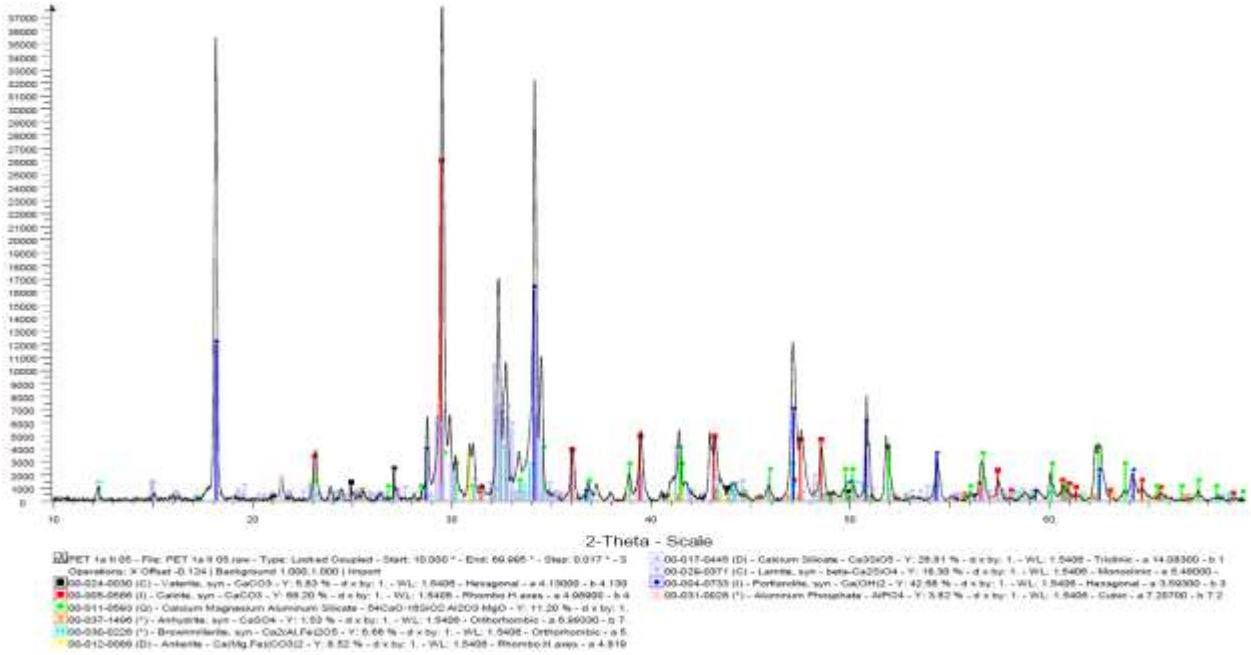

Cem-PET (w/c=0.5, CEM I)

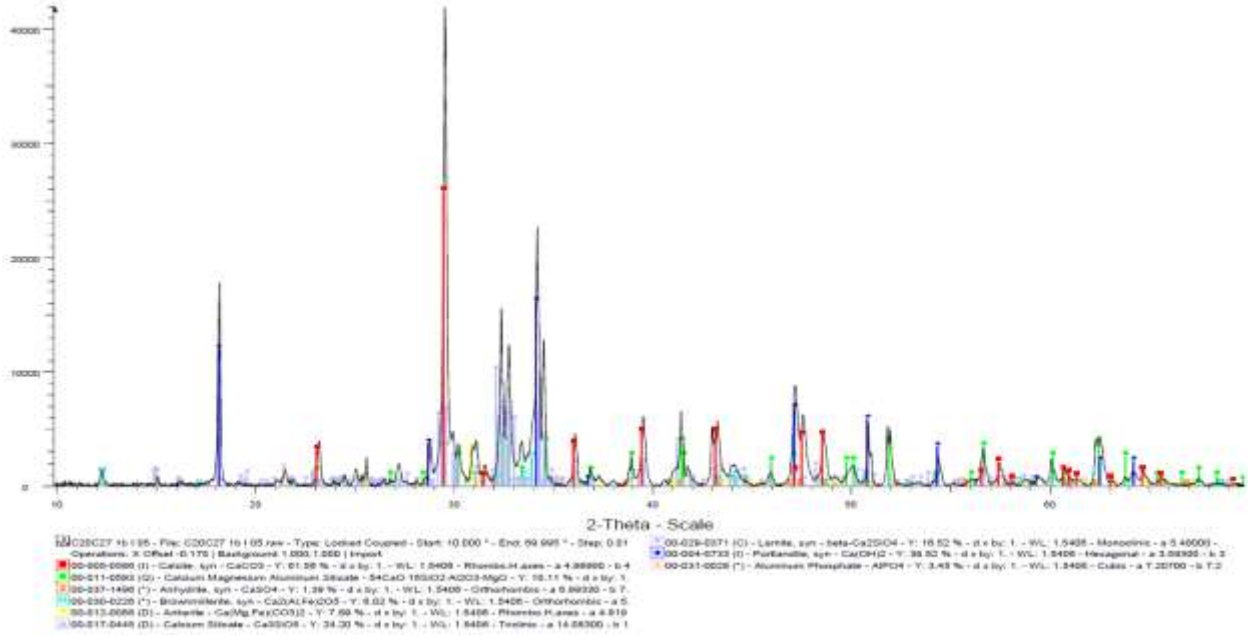

Cem-C20C27 (w/c=0.5, CEM I)

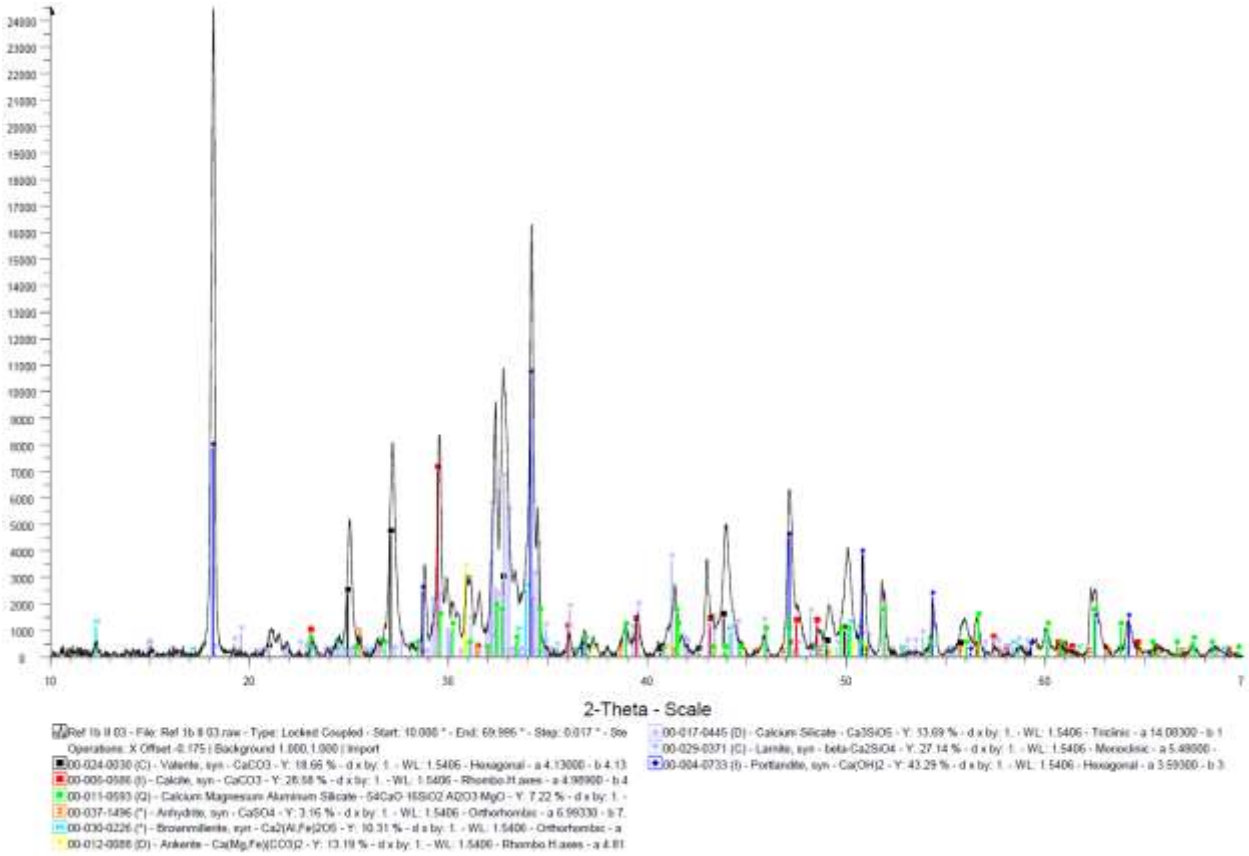

Cem-Ref (w/c=0.3, CEM II/B)

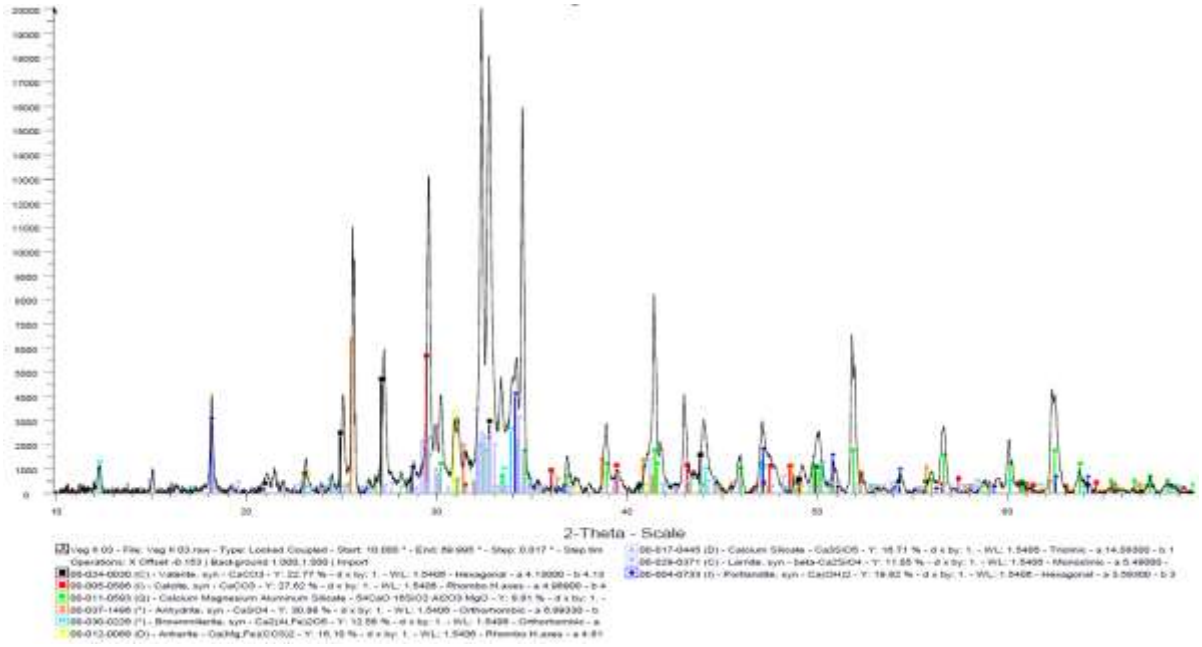

Cem-VO (w/c=0.3, CEM II/B)

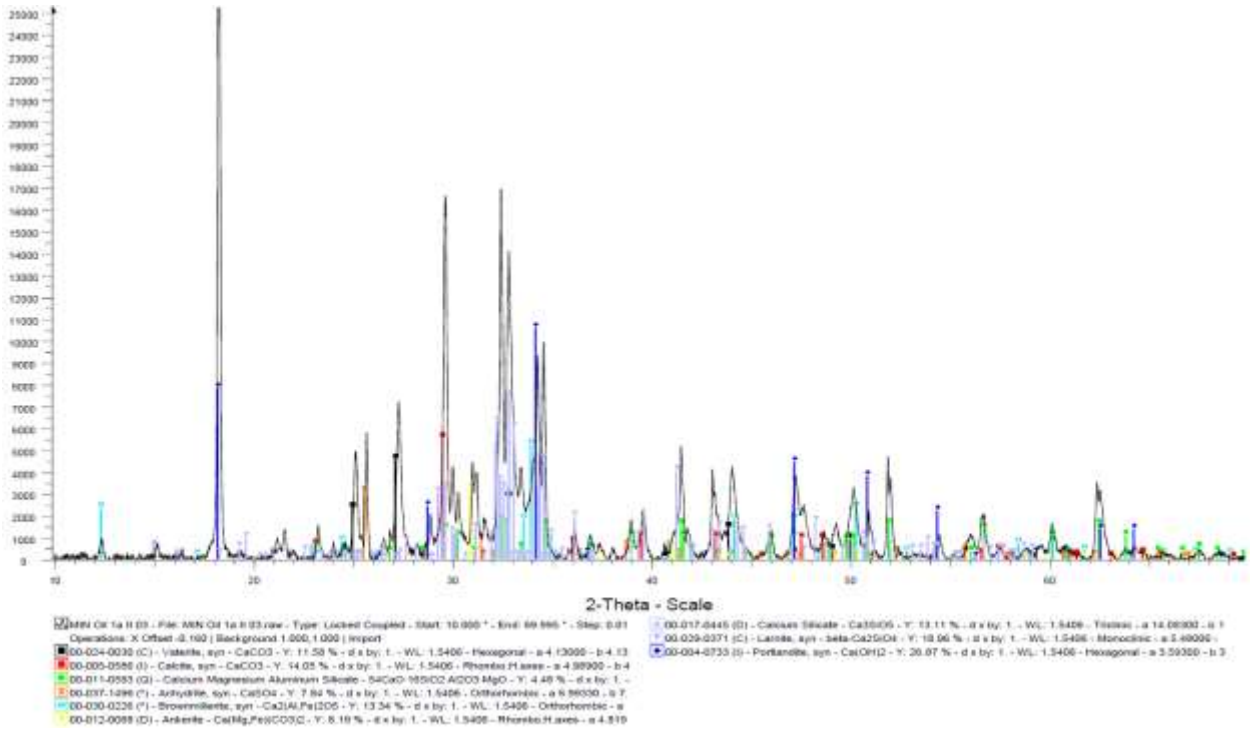

Cem-MO (w/c=0.3, CEM II/B)

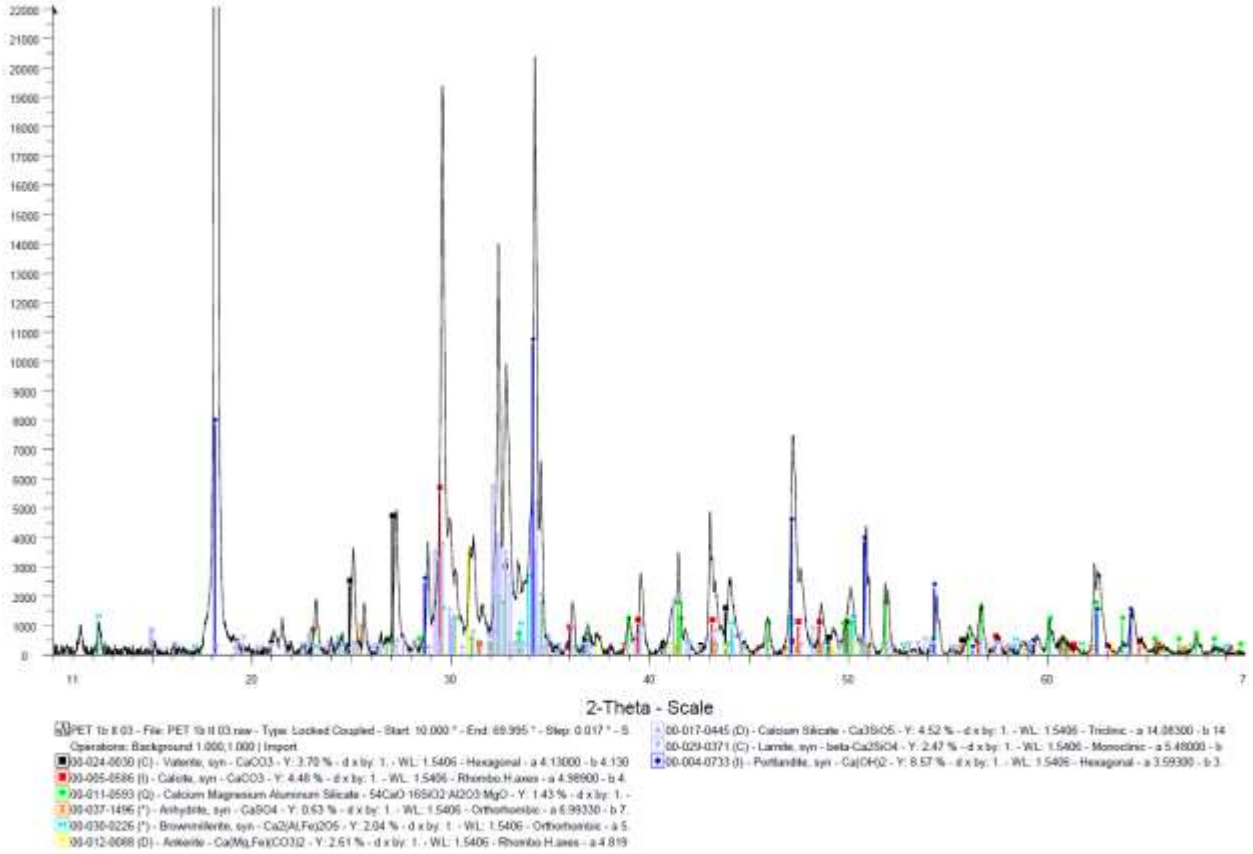

Cem-PET (w/c=0.3, CEM II/B)

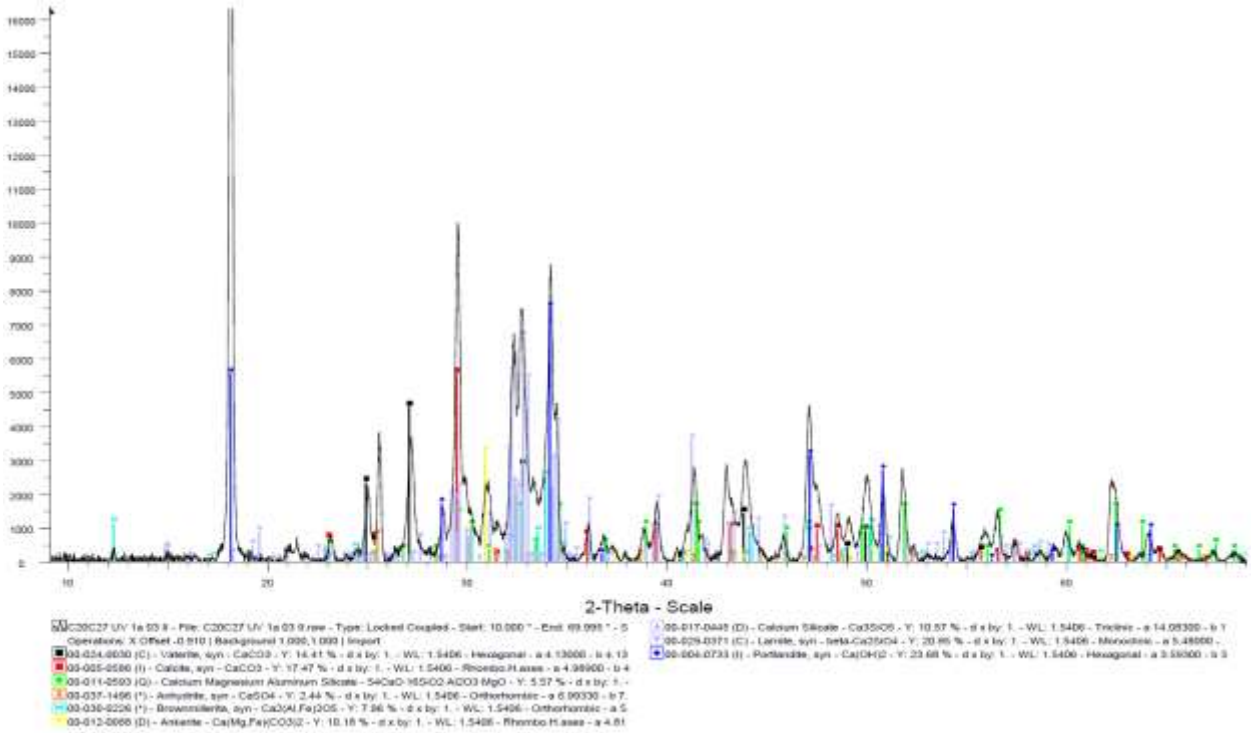

Cem-C20C27 (w/c=0.3, CEM II/B)

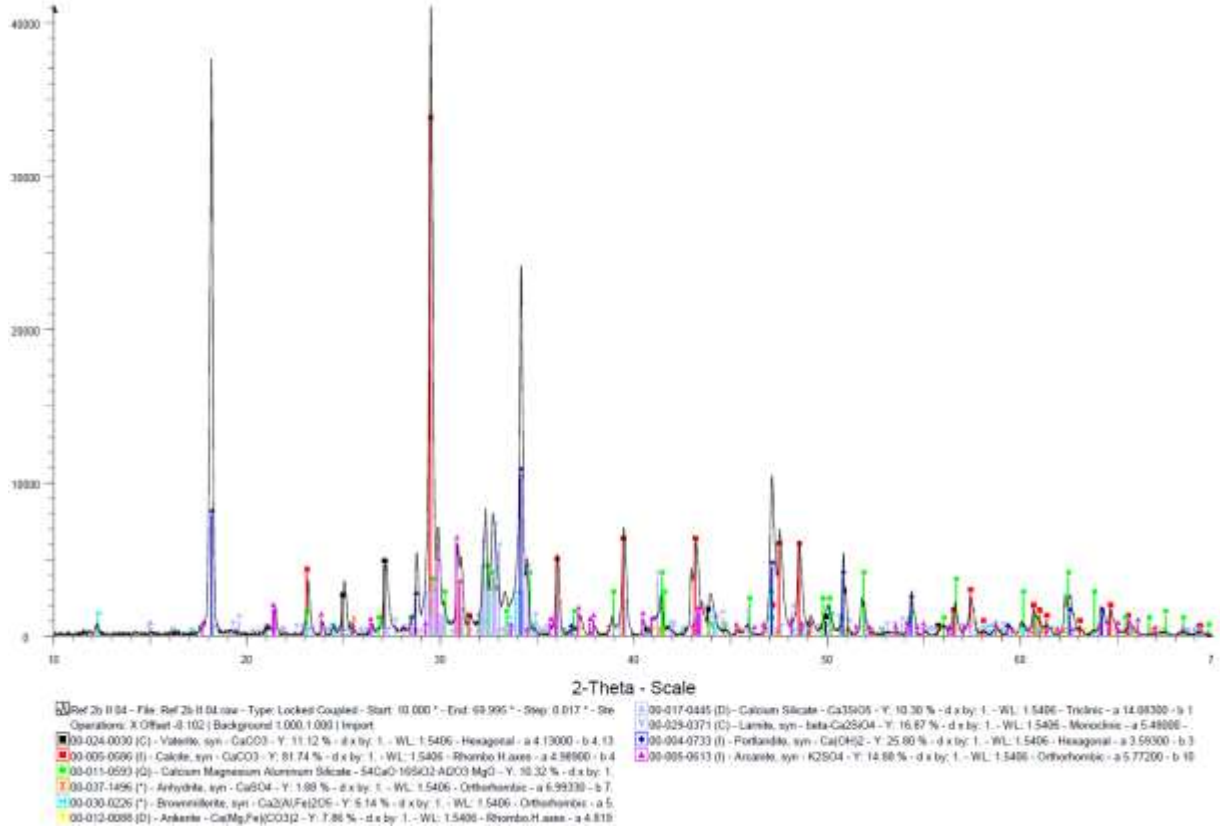

Cem-Ref (w/c=0.4, CEM II/B)

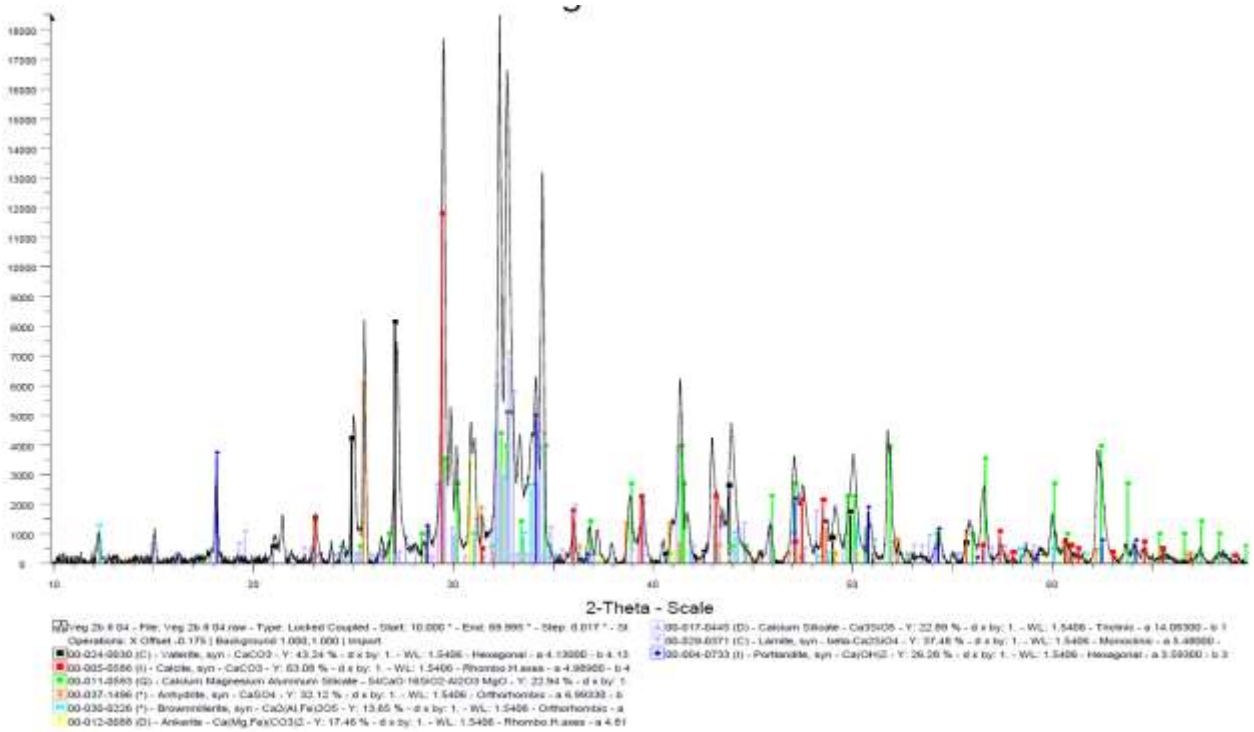

Cem-VO (w/c=0.4, CEM II/B)

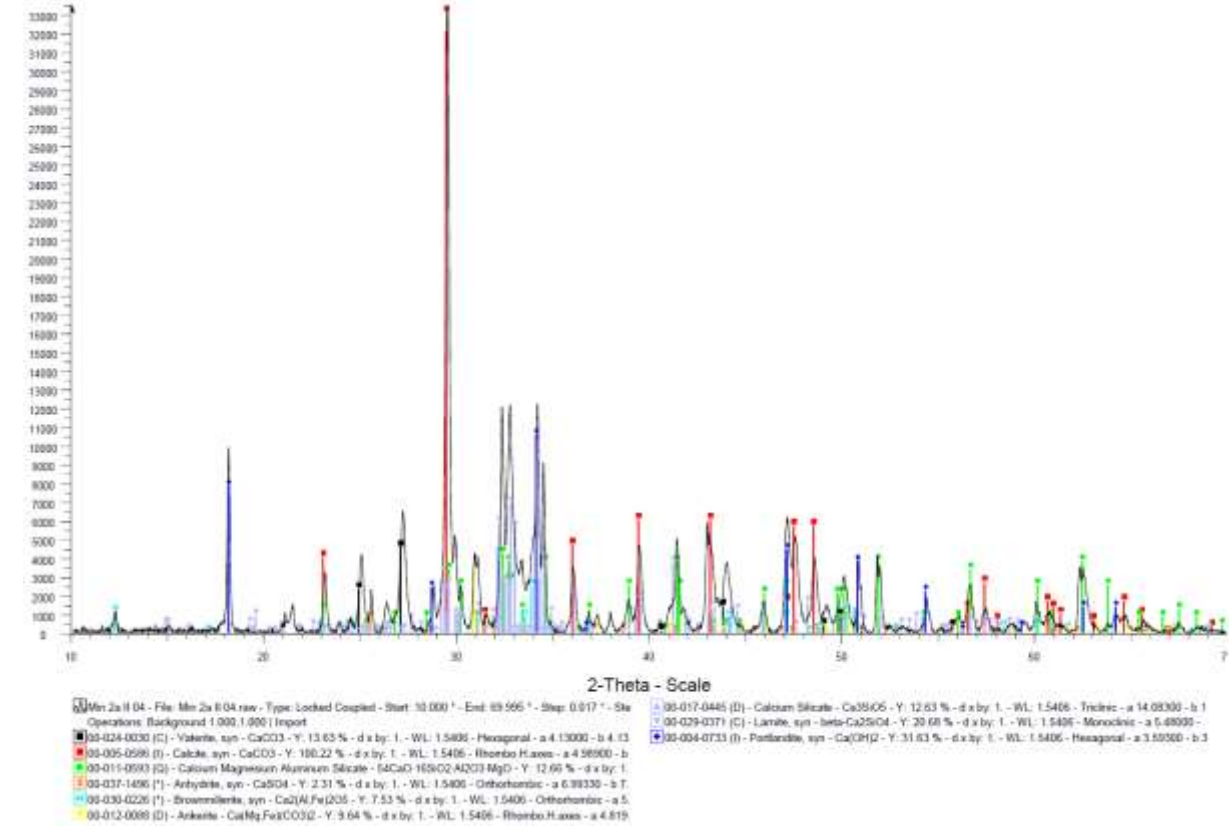

Cem-MO (w/c=0.4, CEM II/B)

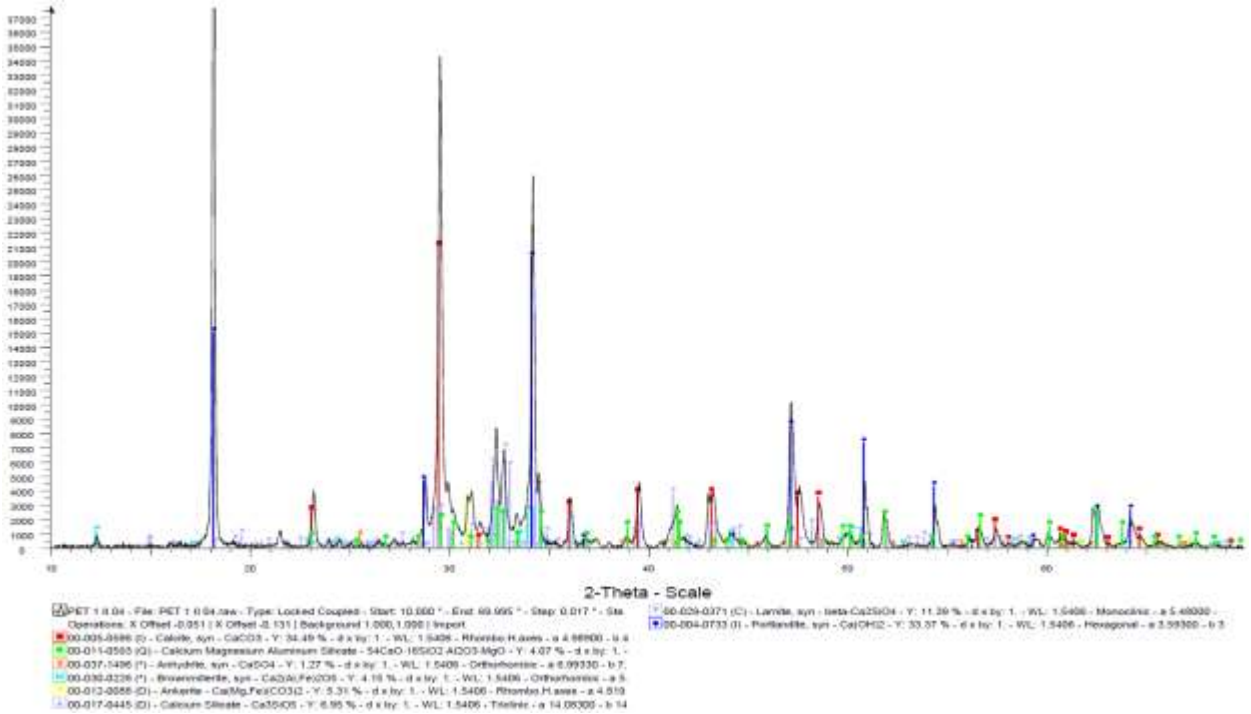

Cem-PET (w/c=0.4, CEM II/B)

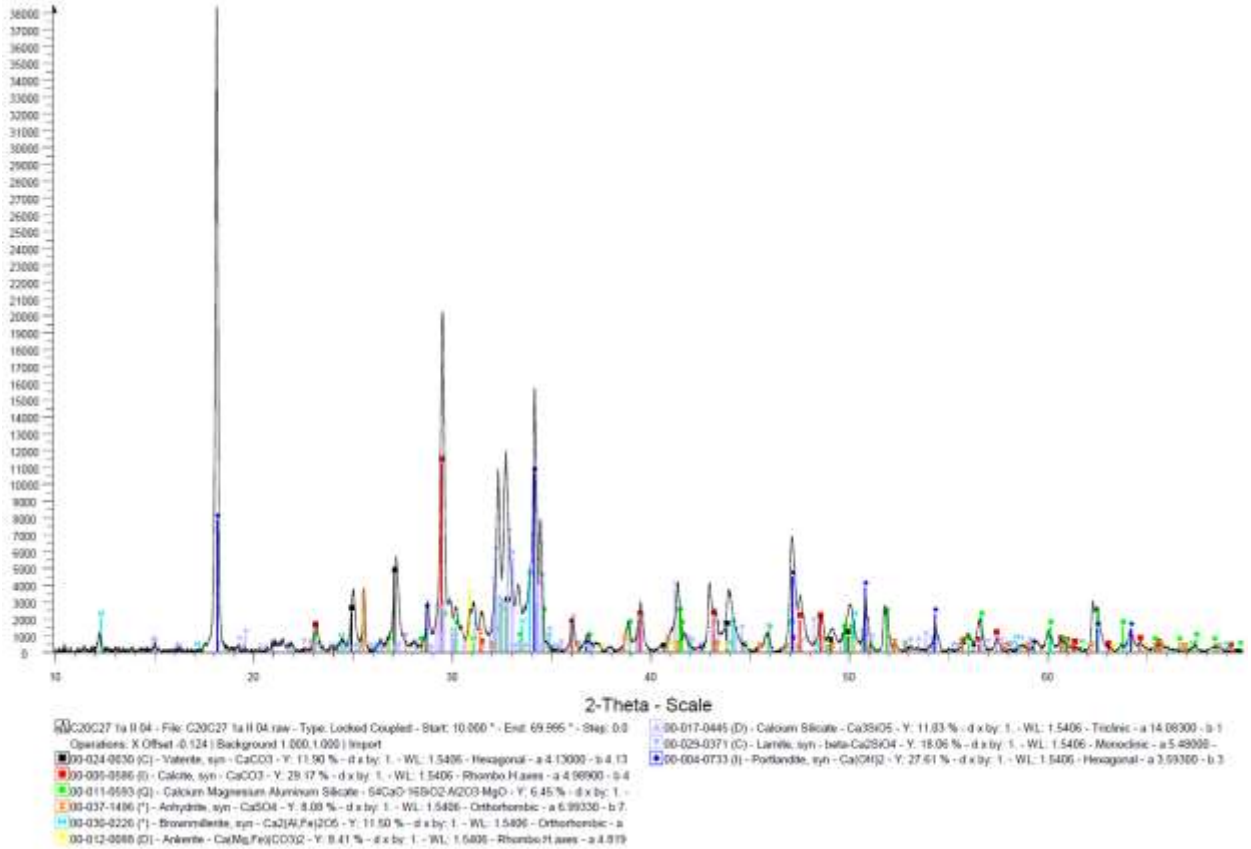

Cem-C20C27 (w/c=0.4, CEM II/B)

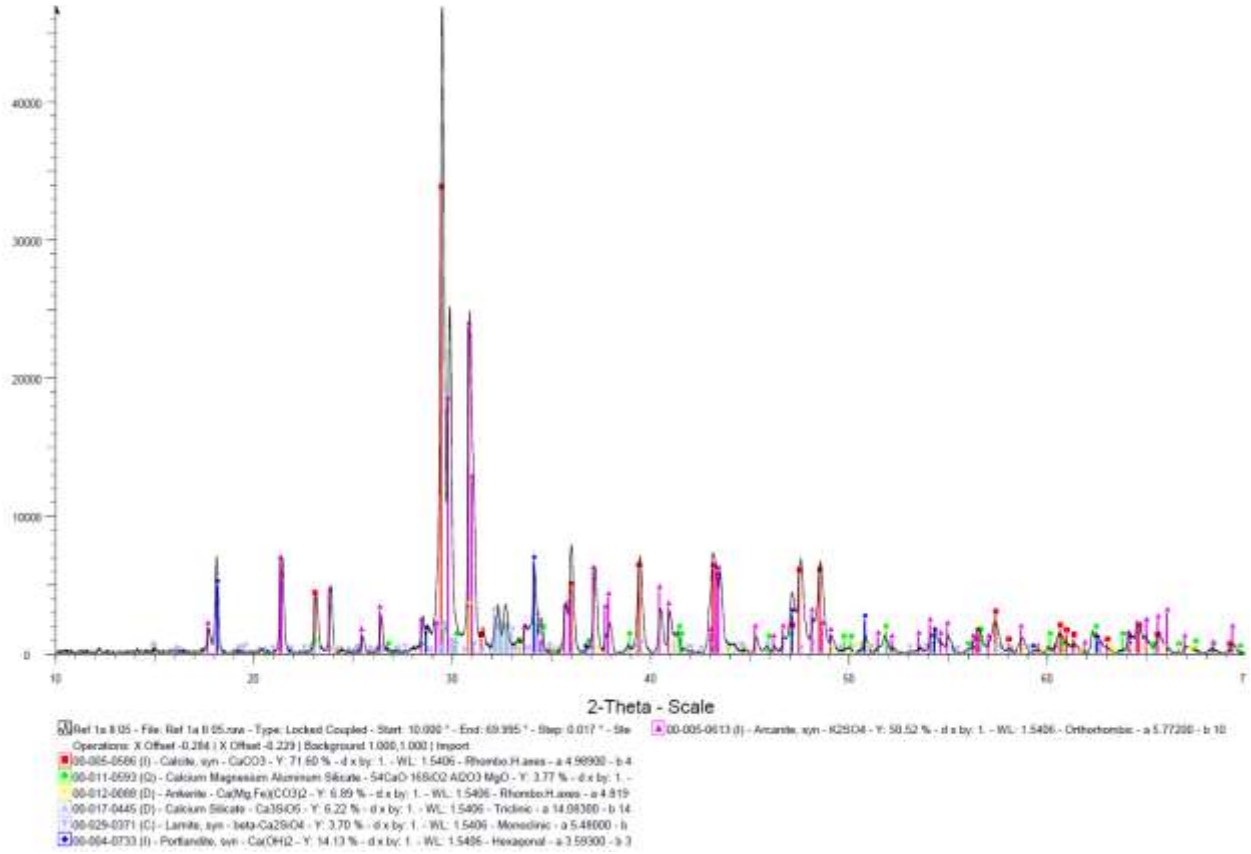

Cem-Ref (w/c=0.5, CEM II/B)

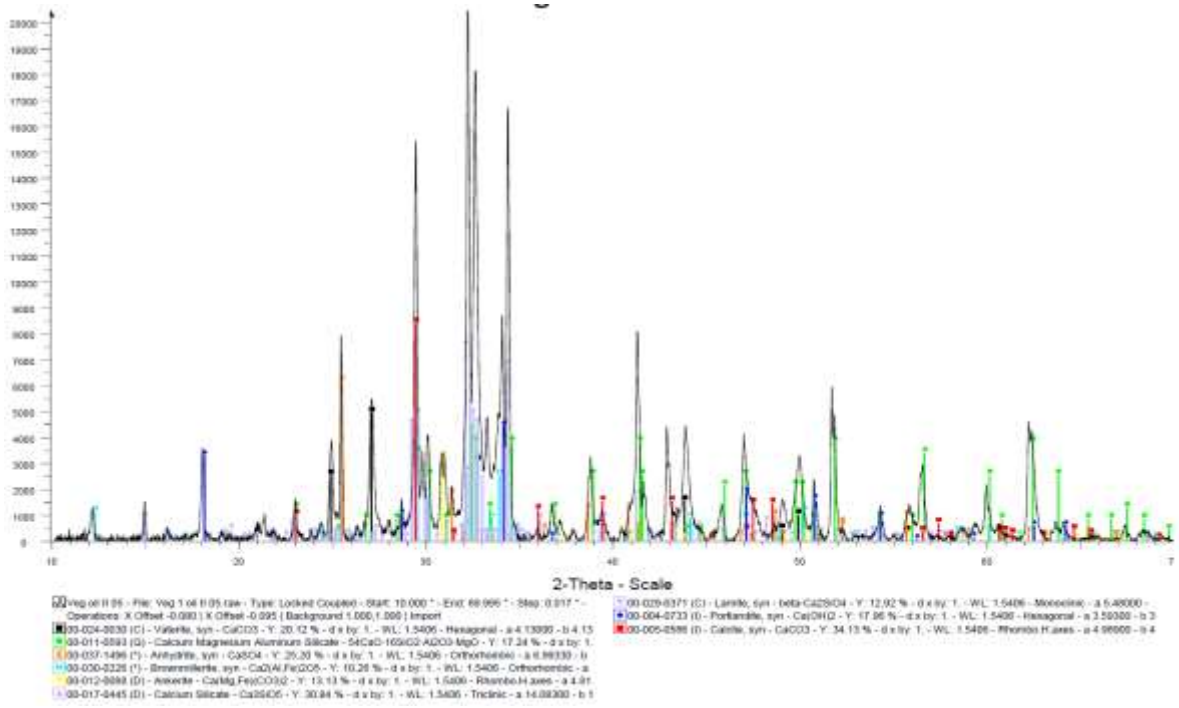

Cem-VO (w/c=0.5, CEM II/B)

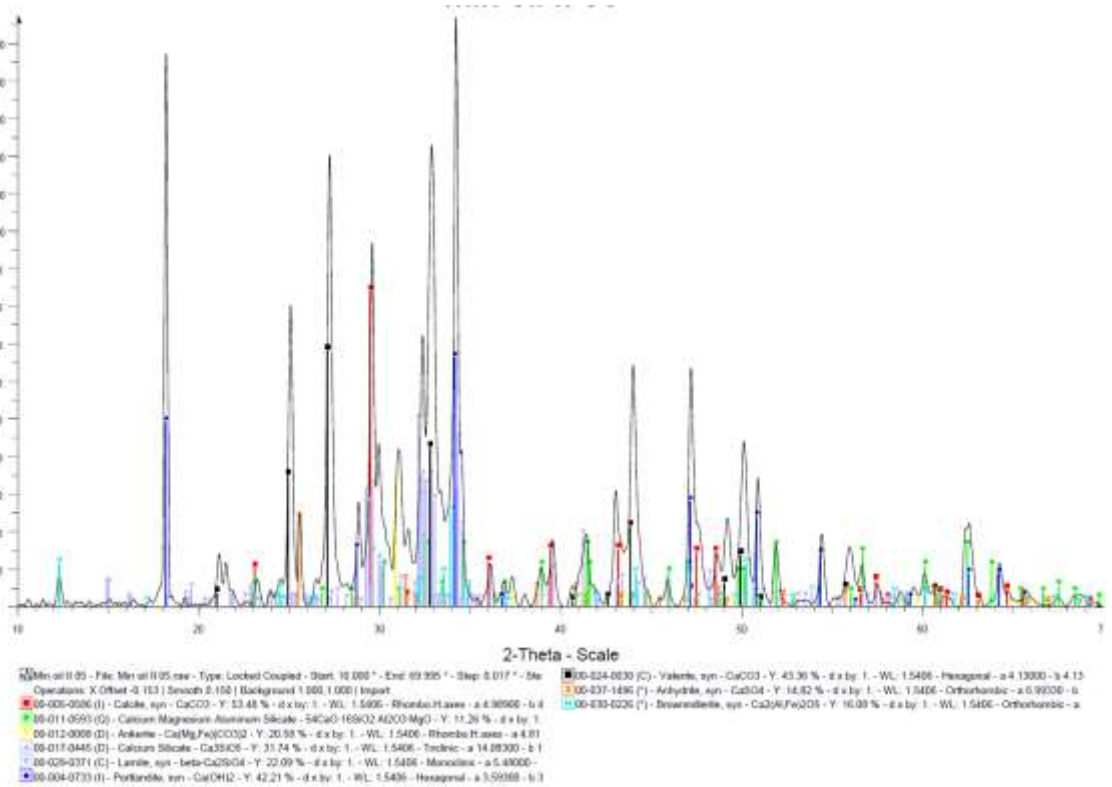

Cem-MO (w/c=0.5, CEM II/B)

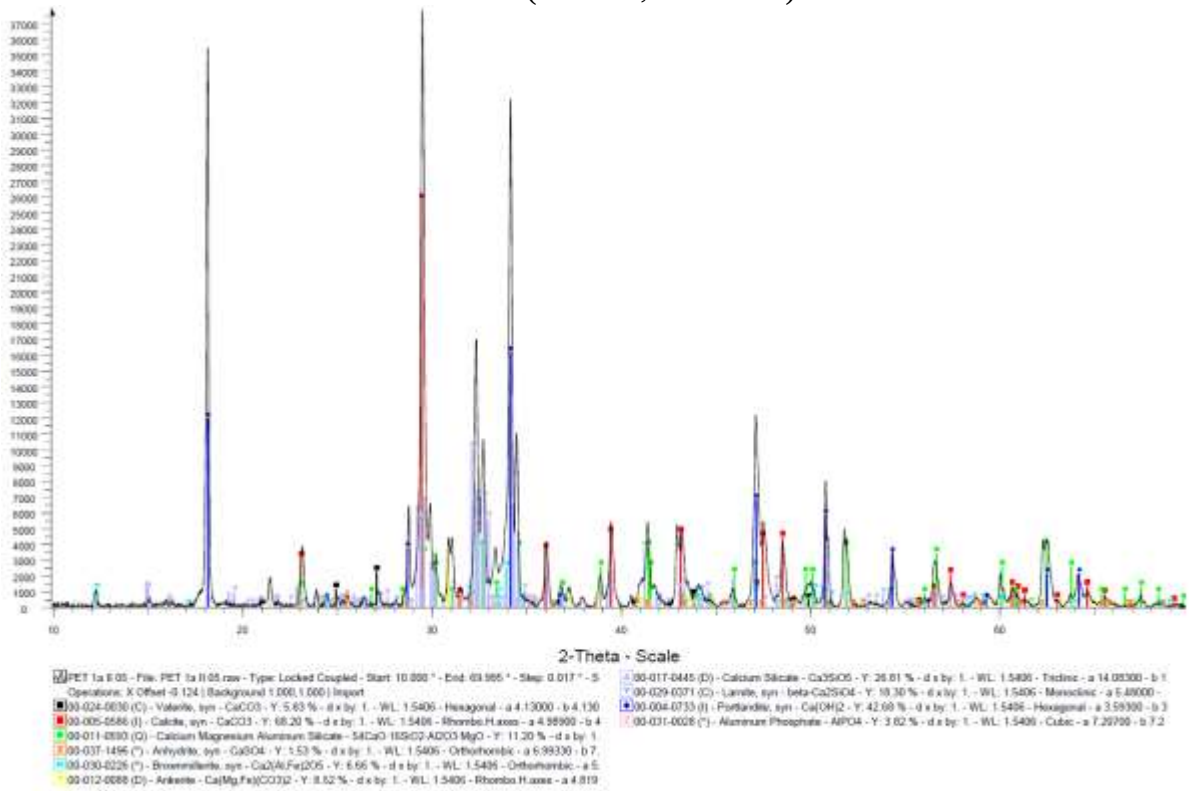

Cem-PET (w/c=0.5, CEM II/B)

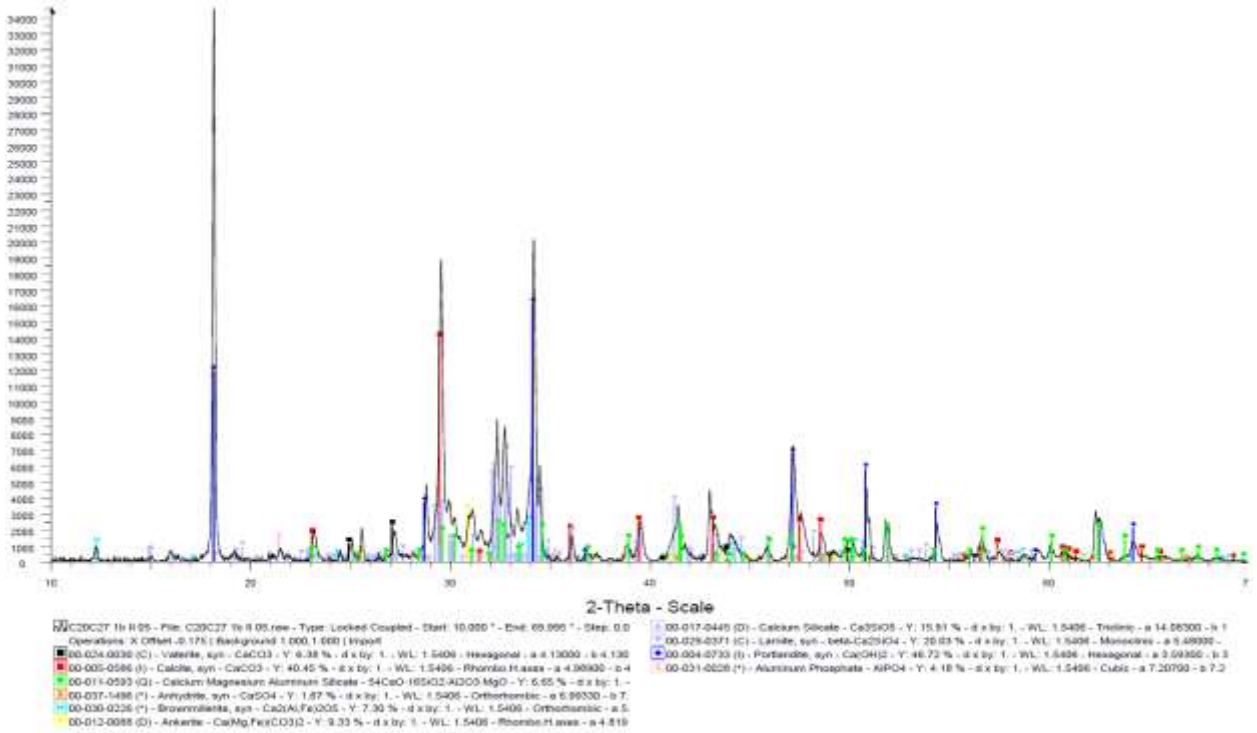

Cem-C20C27 (w/c=0.5, CEM II/B)

Résumé :

Le secteur de la construction connaît une croissance rapide à l'échelle mondiale. En tant que l'un des principaux composants utilisés, le béton joue un rôle important dans le secteur de la construction. En outre, le béton à l'état frais est éprouvé dans le coffrage pour lui donner la forme voulue. Donc, le coffrage est un élément essentiel dans le secteur de la construction. Ils sont utilisés comme un dispositif destiné à maintenir le béton frais en attendant sa prise et son durcissement pour lui conférer sa forme définitive [1-3]. En général, les projets de construction utilisent différents coffrages tels que le bois, l'acier, le contreplaqué et l'aluminium [4-6]. Le choix du système de coffrage et les traitements appliqués conditionnent la qualité de parement finale. En effet, le parement qui constitue la peau de l'élément structural visible après décoffrage, est principalement composé de ciment [2,3] et doit répondre à la fois aux exigences techniques : résister aux diverses agressions extérieures, conserver son état le temps de la vie de l'ouvrage, tout en assurant le respect des exigences esthétiques prédéfinies.

Le parement final des surfaces cimentaires en contact avec coffrage est directement lié à la conception du mélange, aux méthodes de mise en place, aux méthodes de vibration, au durcissement, au démoulage et au type de coffrage [4]-[7]. Principalement, le type de coffrage peut être considéré comme un paramètre important qui affecte les propriétés des surfaces cimentaires telles que la durabilité surfacique et l'aspect esthétique. Outre le coffrage, l'utilisation des agents de démoulage et les différentes couches de revêtement sont les médiateurs qui diminue le phénomène d'adhésion entre coffrage et matériaux cimentaire et facilitent le processus de démoulage. De plus, les agents de démoulage vont influencer l'aspect final du parement [6-8].

L'adhésion regroupe les phénomènes physico-chimiques qui se manifestent entre deux surfaces en contact et l'adhérence représente la force de démoulage nécessaire pour séparer deux matériaux réunis par une surface commune [7,8]. L'environnement physico-chimique à l'interface coffrage/ciment crée des conditions particulières où peuvent se manifester des forces intra et interparticulaires entre les deux surfaces. De plus, la compatibilité des morphologies de surface peut favoriser l'ancrage mécanique, l'adhésion mécanique [9]. L'adhésion entre le coffrage et le béton se manifeste ainsi à différentes échelles : macro, micro et submicrométrique [6-9].

Déterminant dans la construction et toujours optimisé, le procédé de coffrage conserve des faiblesses : la pénibilité de sa mise en œuvre et l'impact environnemental associé à l'utilisation d'agents de démoulage [6-8]. Effectivement, malgré leur efficacité et leur amélioration concernant la sécurité sanitaire et environnementale, l'application de ces

produits reste la source de situations à risque pour le personnel de chantier et l'environnement [10]. Donc, la solution développée dans le projet ERGOFORM consiste ainsi en un revêtement à base de polymères photopolymérisables appliqué sur les coffrages et devant conserver ses propriétés d'aide au décoffrage sur 50 cycles de coffrage/décoffrage. Afin de mettre au point une solution de décoffrage pertinente, il est indispensable d'analyser les paramètres influençant l'adhésion entre les surfaces après 24h de contact ainsi que leurs influences respectives l'une sur l'autre à différentes échelles.

L'objectif de cette étude est donc de lever certaines barrières scientifiques afin de comprendre l'effet des propriétés de la surface du coffrage sur la surface cimentaire brute de décoffrage à différentes échelles, en analysant l'état de surface de la pâte cimentaire ainsi que leur adhésion et force de démoulage au décoffrage. Ces caractérisations multiéchelles (macro-échelle et micro-échelle) permettent d'étudier l'influence des paramètres de des coffrages sur les propriétés morphologiques, chimiques et mécaniques des surfaces cimentaires. La surface cimentaire brute de décoffrage a été caractérisés par différents technique d'analyses en utilisant la microscopie interférométrique (IM), la microscopie électronique à balayage environnemental (ESEM), la diffractométrie des rayons X (XRD), De plus, pour répondre aux enjeux industriels, ce travail est concentré sur l'étude d'une solution alternative durable et respectueuse de l'environnement, proposés par les partenaires de projet ERGOFORM, en remplaçant les agents de démoulage [9-10]. En outre, ce travail de recherche développera l'effet des composants de la conception de la formulation de béton sur l'adhésion ou force de démoulage, en faisant varier le rapport e/c et le type de ciment (CEM I et CEM II) au contact avec différents types coffrages.

Ce manuscrit s'articule autour de quatre chapitres suivantes :

- Le premier chapitre est consacré à une revue bibliographique concernant les travaux antérieurs portant sur l'étude de l'adhésion. Dans une première étape, quelques notions théoriques concernant les mécanismes d'adhésion sont abordées. Un intérêt particulier est porté sur les travaux consacrés à l'étude des paramètres influençant sur le phénomène d'adhésion entre le coffrage et matériaux cimentaire. Une synthèse concernant les constituants du ciment et leur mécanisme d'hydratation est suivie de celle sur les travaux ayant été effectués.
- Le deuxième chapitre est dédié à la présentation des matériaux étudiés et des procédures mises au point utilisés dans le cadre de ce travail. Les matériaux qui ont été utilisés dans l'élaboration de pâte cimentaire et béton ont été caractérisés pour s'assurer de leur qualité selon les normes. La caractérisation des propriétés physiques des granulats (gravillons et sable) ont été détaillée. De plus, la caractérisation du

ciment a été présenté en utilisant l'analyse granulométrique au laser, la mesure de densité, de module de finesse et de temps de prise. Les méthodes microstructurales tels que la microscopie interférométrique (IM), la microscopie électronique à balayage environnemental (ESEM) et la diffractométrie des rayons X (XRD) ont été présenté pour analyser les surfaces cimentaires. Ces techniques concernent les caractérisation morphologique, chimique et thermodynamique des surfaces. Le protocole mise en place pour l'étude du phénomène d'adhésion et la force de démoulage est également abordé. Deux méthodes expérimentales, pre-crack sur la pâte cimentaire et pull-off sur les échantillons de béton, ont été détaillés.

- Le troisième chapitre présente, dans un premier temps, les résultats expérimentaux concernant la caractérisation des deux types de ciment (CEM I and CEM II/B) en utilisant l'analyse granulométrique au laser, la mesure de densité, de module de finesse et de temps de prise. Les résultats expérimentaux ont été présentés. Ainsi que les résultats concernant les propriétés physiques des gravillons et sable ont été présenté par des mesures de masse volumique et de coefficient d'absorption d'eau. Finalement, une analyse microstructurale par la microscopie électronique à balayage (MEB) ainsi qu'une microanalyse chimique élémentaire des ciments par la méthode Energy Dispersive X-ray (EDX) a été réalisée.
- L'étude, réalisée et présentée au quatrième chapitre, vise à déterminer l'influence des différents coffrages sur la force de démoulage ainsi que la morphologie des surfaces cimentaires. Finalement, une analyse microstructurale des surfaces cimentaires brutes de décoffrage et âgées de 24 heures aux échelles macrométrique et micrométrique réalisés par la microscopie interférométrique (IM), la microscopie électronique à balayage environnemental (MEB) et la diffractométrie des rayons X (XRD) ont été effectuées. Les résultats obtenus par ces techniques concernent les caractérisation morphologique, chimique et thermodynamique des surfaces. Finalement, la force de démoulage à macro échelle a été présenté en utilisant la méthode de démoulage de pull-off sur le béton.

Une conclusion générale et des perspectives clôturent ce mémoire en synthétisant les principaux résultats obtenus. La conclusion met en avant les principaux résultats obtenus permettant ainsi de proposer des pistes de modifications des surfaces coffrantes pour améliorer le décoffrage des bétons et la qualité des parements. Les perspectives du travail sont présentées et les résultats resitués dans le contexte du projet ERGOFORM.

Résultats

Les méthodes expérimentales réalisées dans le cadre de ce travail ont été regroupées dans le Table 1. Les méthodes utilisées pour la caractérisation des matériaux, de la pâte de ciment et du béton ont été réalisées conformément aux normes.

Table 1 *Les tests effectués et leurs méthodes*

Type of property			Standard/equipment
Materials characterization	Cement	Specific gravity	ASTM C188-17 [158]
		Bulk density	
		Laser granulometry	Mastersizer 3000E
		Normal consistency and setting times	NF EN 196-3 [159]
		SEM and EDs analysis	E-SEM based Philips XL30
	Aggregates	Bulk density	NF EN 1097-6 [160]
		Specific gravity and water absorption	
		Size distribution	NF EN 933-1 [161]
	Water	pH value	pHM210
Concrete	Fresh properties	Workability	EN 1015-3 [162]
		Fresh density	EN 1015-6/A1 [163]
	Mechanical properties	Compressive strength	EN 1015-11 [164] EN 12390-6 [165]
Microstructure analysis	Surface energy	Contact angle and surface energy	DROP SHAPE ANALYSER – DSA30 equipped with an ALLIED camera
	Surface roughness	Interferometric microscopy (IM)	Bruker® Contour GT-K interferometer
	Surface microstructure	Scanning Electron Microscopy (SEM)	E-SEM based Philips XL30
	Crystalline phases	X-ray Diffractometry analysis (XRD)	D8 Advance Bruker®
Adhesion or demolding force	Demolding force	Pre-crack demolding test	Universal test bench- BED 100
		Pull-off demolding test	Shimadzu 100 kN machine

Les nomenclatures des plaques de coffrage, de la pâte de ciment et des échantillons de béton pour tous les coffrages utilisés dans les expériences sont présentées dans le**Table 2**.

Table 2: *la nomenclature des coffrages, de la pâte de ciment et des échantillons de béton*

Variations	**Coffrage**	**Pâte de ciment**	**Beton**
			
Plaque de référence	F17-Ref	Cem-Ref	Con-Ref
Enduit d'huile minérale	F17-MO	Cem-MO	Con-MO
Enduit d'huile végétale	F17-VO	Cem-VO	Con-VO

Enduit de PET	PET	Cem-PET	Con-PET
Enduit de C20C27 (LPIM)	C20C27	Cem-C20C27	Con-C20C27

Les résultats obtenus concernant la rugosité des surfaces de coffrage sont résumés dans le **Table 3**. Les résultats révèlent que la surface la plus rugueuse est enregistrée pour le coffrage de référence (F17-Ref), (Sa = 4,56 ± 0,39 µm, Sq = 5,663 ± 0,467 µm). Il faut noter qu'aucun traitement de surface n'a été appliqué aux plaques de référence. En outre, pour comparer la surface du coffrage revêtu de polymère, la couche de PET avait la valeur de rugosité la plus faible par rapport au C20C27 de Sa = 0,11 ± 0,02 µm, Sq = 0,14 ± 0,03 µm, et Sa = 0,93 ± 0,23 µm, Sq = 1,17 ± 0,37 µm, respectivement.

Table 3: *Obtained roughness parameters of formworks through Interferometry microscopy*

Formwork surface	**S_a (nm)**	**S_q (nm)**	**Remarks**
F17-Ref	4563 ± 389	5663 ± 467	No treatment
C20C27	931 ± 235	1176 ± 370	Metalized (gold)
PET	108 ± 21	141 ± 30	Metalized (gold)

Les variables qui ont été prises en compte dans les expériences sont présentées dans la **Figure 1**.

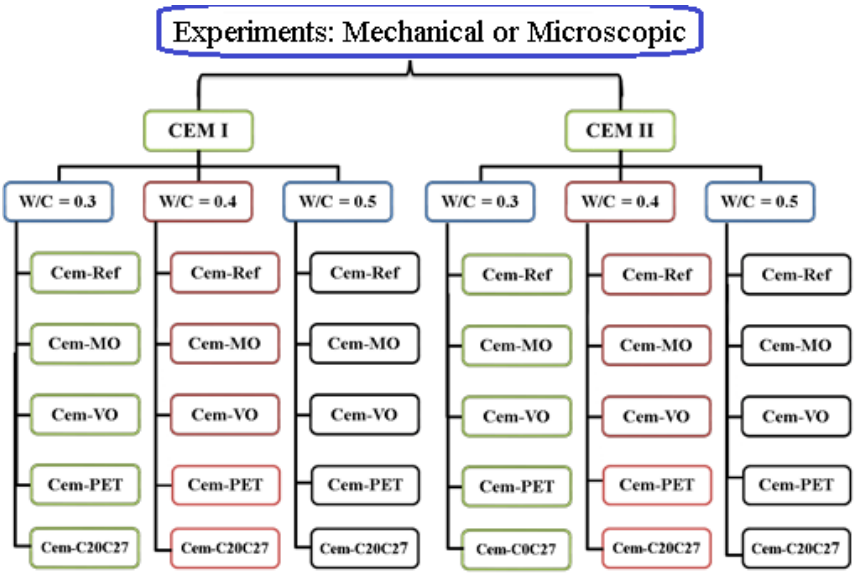

Figure 1 *Variables de l'expérience*

Après avoir effectué les séries de tests et les avoir analysés, les résultats suivants ont été extraits :

- **Performance de démoulage :**

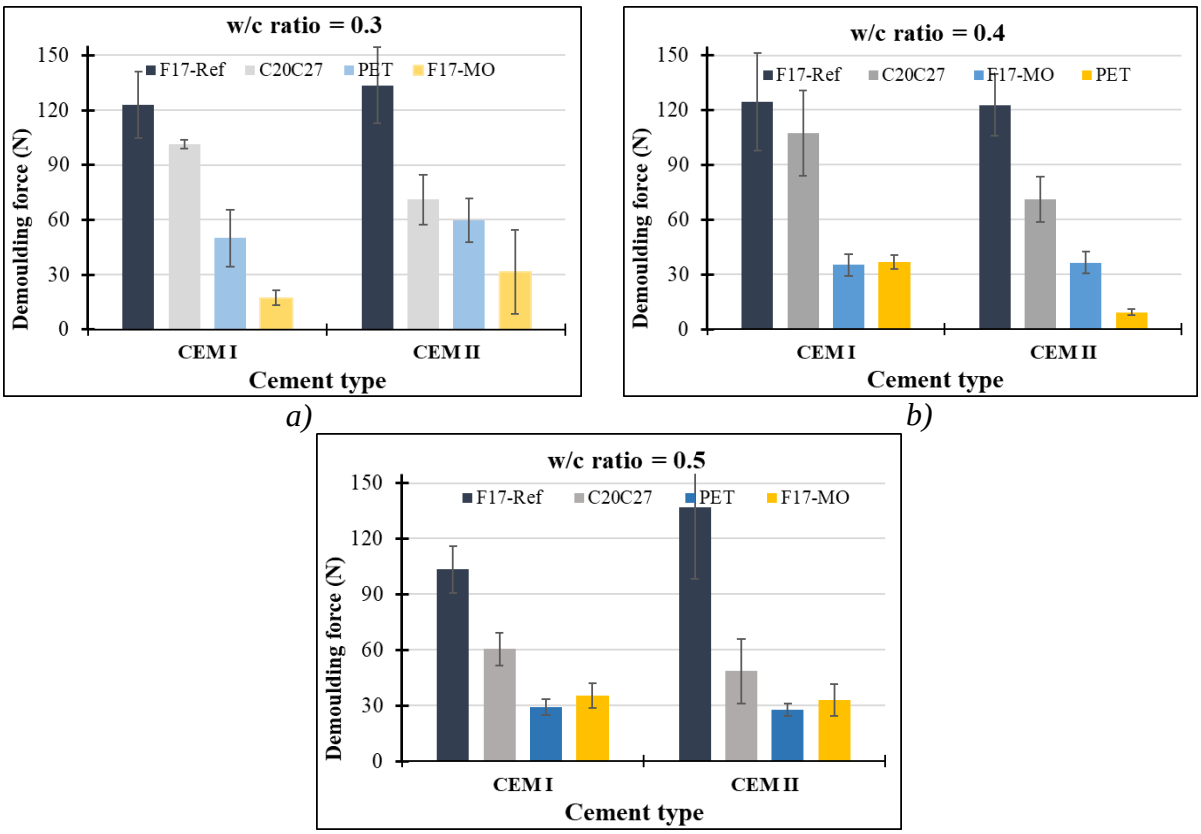

Figure 2 *Résultats des essais de démoulage avant fissure classés en fonction des différents rapports e/c : a) e/c = 0,3, b) e/c = 0,4, et c) e/c = 0,5.*

Dans la **Figure 1**:

- Globalement, en raison de la dispersion de la force de démoulage (F_d), les résultats expérimentaux montrent que le type de ciment ne présent pas un effet sur la force de démoulage. Une analyse plus approfondie d'un plus grand nombre de tests est nécessaire pour conclure.
- L'augmentation du rapport E/C de 0,4 à 0,5 sur les essais de pâte de ciment a provoqué une baisse de la F_d qui a été réalisée sur le C20C27 et le PET pour les deux types de ciment. Cependant, les autres coffrages ont montré une fonctionnalité similaire lors de la variation du rapport E/C.
- L'utilisation des agents de démoulage diminue la force de démoulage. Ça peut-être expliquer par l'application d'agents de démoulage sur la surface du coffrage entraîne une modification de la rugosité de la surface [10] ; elle remplit les vides de la surface du coffrage, ce qui permet un meilleur démoulage. Cependant, sur une surface lisse, l'effet de l'agent de démoulage est différent, il crée une barrière d'épaisseur variable entre le coffrage et le béton, ce qui augmente la micro-rugosité de la surface du coffrage et, par conséquent, de la surface du béton.

- En général, les performances de décoffrage des revêtements en PET et en polymère C20C27 étaient meilleures que celles du revêtement de référence. Cela pourrait être dû à la morphologie de la surface des revêtements et à leurs caractéristiques de mouillabilité. Malgré cela, le PET avait une propriété de favorable de démoulage à celle du C20C27.
- Quantitativement, en termes de performance de décoffrage, de la plus faible à la plus élevée, la valeur moyenne de F_d obtenue peut être présentée comme suit :
    - échantillons contre des coffrages enduits d'huile végétale (F17-VO)
    - échantillons contre l'huile minérale (F17-MO)
    - échantillons contre un revêtement polymère PET (PET)
    - échantillons contre le polymère C20C27 (C20C27)
    - Echantillons contre le coffrage de référence (F17-Ref)

Ces résultats ont été confirmés par l'analyse microstructural d'ESEM des surfaces de ciment. Il convient de mentionner que les surfaces les plus rugueuses présentaient davantage de zones sombres et de cavités. De plus, des grains plus gros et des phases anhydres ont été observés sur leurs surfaces.

- En termes de durabilité, les revêtements C20C27 ont été utilisés 6 fois maximum. En revanche, le revêtement PET a été utilisé 13 fois sans dégradation majore de revêtement (**Figure 3**).

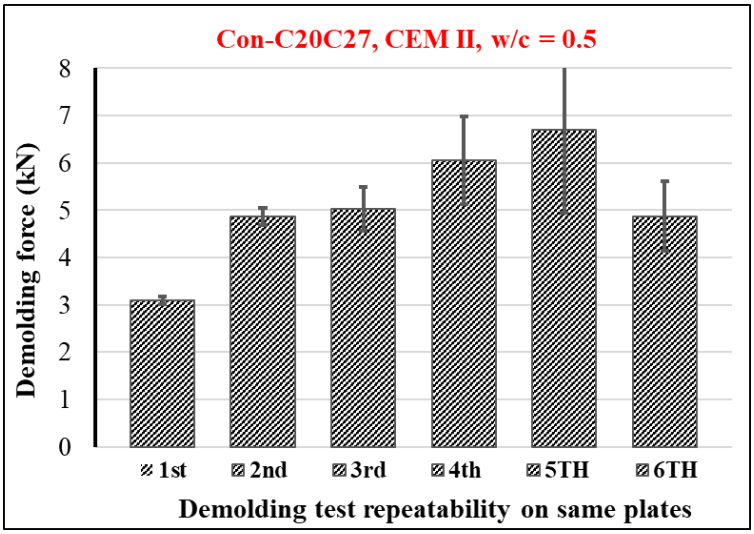

a)

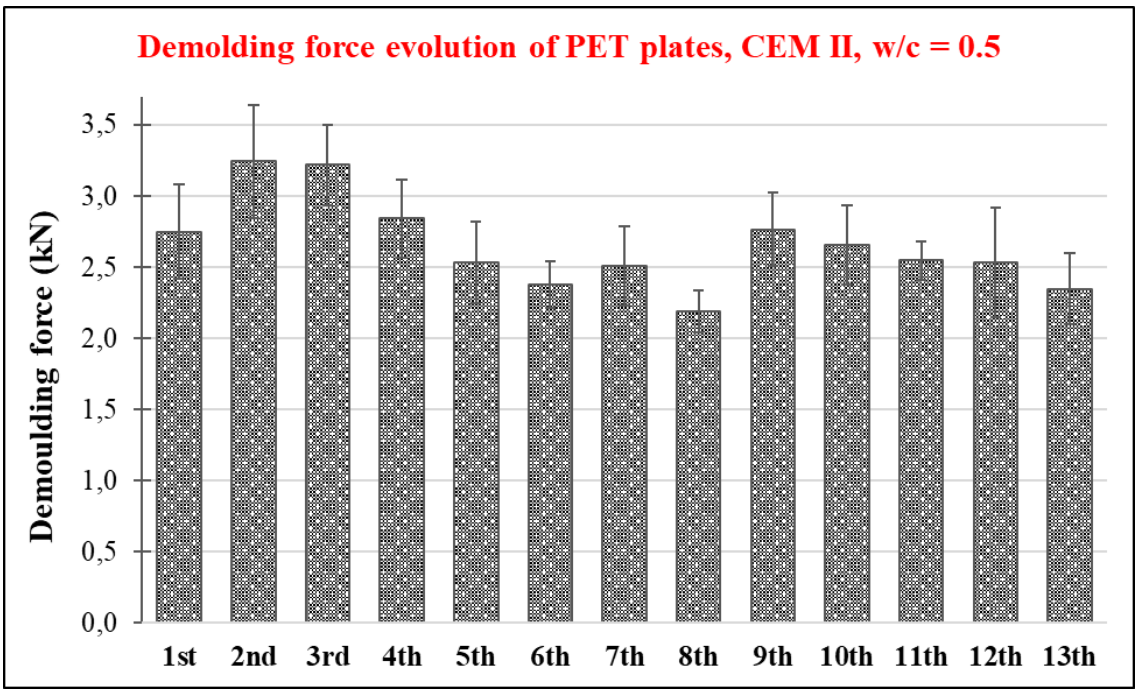

b)

Figure 3 *Essai de répétabilité d'un coffrage revêtu de polymère via la répétition de l'essai de démoulage par arrachage: a)C20C27, b)PET*

- **Analyses de la rugosité de surface :**

Table 4 *rugosité de surface des pâtes de ciment (Sa et Sq) avec leurs valeurs de dispersion obtenues par microscopie interférométrique*

Cement type / Parameters		CEM I (nm)		CEM II	
		S_a (nm)	S_q (nm)	S_a (nm)	S_q (nm)
w/c = 0.3	Cem-Ref	5385 ± 837	7062 ± 766	6086 ± 509	7742 ± 485
	Cem-MO	4307 ± 475	5751 ± 280	4686 ± 202	6543 ± 344
	Cem-VO	4008 ± 887	5852 ± 1529	4139 ± 241	3247 ± 3698
	Cem-C20C27	1453 ± 288	2802 ± 1185	1111 ± 127	2014 ± 66
	Cem-PET	531 ± 126	1570 ± 213	468 ± 123	1416 ± 427
w/c = 0.4	Cem-Ref	4871 ± 745	6239 ± 980	3795 ± 154	4962 ± 258
	Cem-MO	4346 ± 242	5462 ± 323	3152 ± 917	4187 ± 1136
	Cem-VO	4528 ± 314	5661 ± 168	6284 ± 115	8080 ± 226
	Cem-C20C28	1739 ± 210	2616 ± 326	2570 ± 1739	3505 ± 1973
	Cem-PET	400 ± 62	942 ± 577	1456 ± 346	2447 ± 259
w/c = 0.5	Cem-Ref	4774 ± 523	6399 ± 607	4759 ± 302	6019 ± 425
	Cem-MO	2467 ±420	3707 ± 1028	2790 ± 167	3766 ± 186
	Cem-VO	5013 ± 160	6825 ± 361	4465 ± 434	5925 ± 548
	Cem-C20C29	1722 ± 213	2519 ± 168	1229 ± 107	2055 ± 325
	Cem-PET	546 ± 75	1476 ± 38	499 ± 34	1218 ± 158

Du **Table 4**:

- Les échantillons cimentaires contre le coffrage de référence (sans traitement de surface) présentaient les paramètres de surface les plus rugueux. Il était suivi par les échantillons en contact avec revêtements en utilisant les agents de démoulage (VO et MO) et C20C27. Cependant, la surface cimentaire obtenue du PET était la plus lisse avec faible rugosité de surface.
- La comparaison des paramètres a montré que la morphologie de la surface du coffrage, le type de ciment et le rapport E/C modifient la rugosité finale de la surface des échantillons cimentaire.
- L'effet de la morphologie de la surface sur le comportement d'adhésion du béton contre divers coffrages revêtus est validé par les résultats obtenus avec la pâte de ciment par le test de démoulage avant fissure. Le Fd a suivi la même trajectoire de réduction dans tous les rapports w/c avec la diminution des paramètres de rugosité Sa et Sq de F17-Ref, C20C27, et PET (0.3, 0.4, et 0.5) (**Figure 5**). De plus, le tableau 36 montre la réduction/amélioration de Fd en pourcentage pour mieux comprendre la progression de la force de démoulage du béton contre différents coffrages. Il convient de noter que la Fd moyenne a été utilisée pour ce calcul. Dans le cas du Con-PET/Con-Ref, pour tous les rapports E/C et types de ciment, la valeur Fd s'est améliorée de 70 à 80 %. De plus, le ConC20C27/Con-Ref et le Con-PET/Con-C20C27 ont présenté une réduction de 60,7 % et 45,5 % de la Fd, **Table 5**.

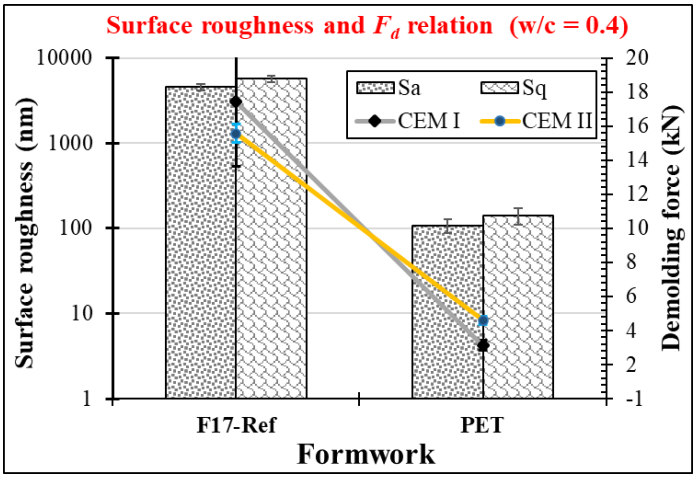

a)

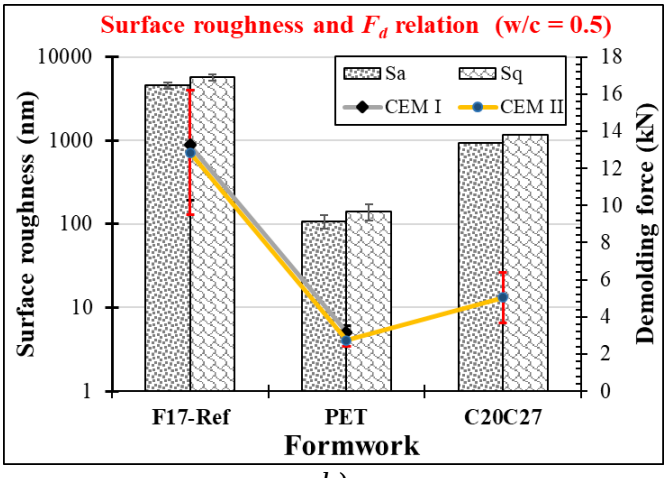

b)

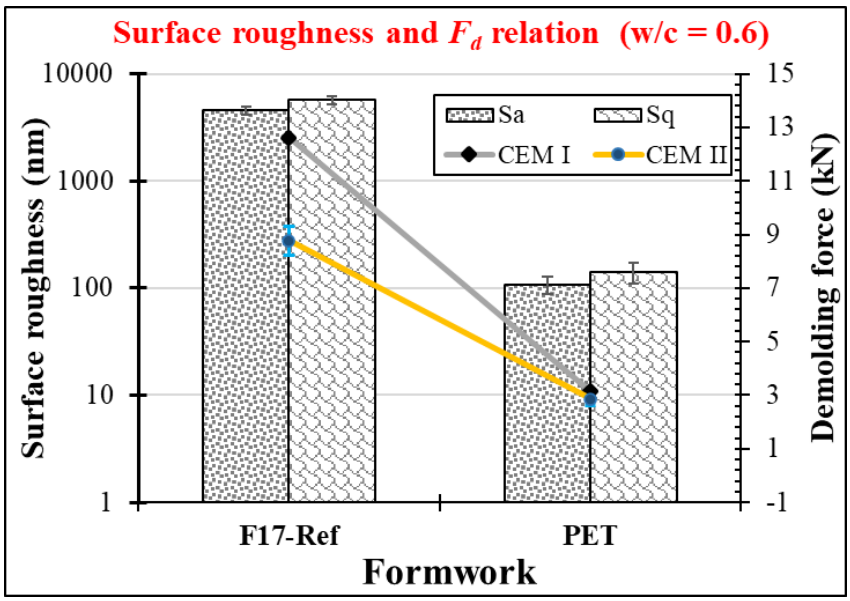

c)

Figure 4 *Les paramètres de rugosité de la surface du coffrage (Sa et Sq) influencent la force de démoulage (Fd) au mode de rupture du mélange I & II : a) w/c = 0.4, b) w/c = 0.5, and c) w/c = 0.6*

Table 5 *Amélioration de la force de démoulage en comparant les valeurs moyennes de la force de démoulage des coffrages*

	Average Fd reduction development (%)					
Cement type	CEM I			CEM II/B		
w/c ratio / Formwork	0.4	0.5	0.6	0.4	0.5	0.6
ConC20C27/Con-Ref	-	-	-	-	60.7	-
Con-PET/Con-Ref	84.4	76.1	75	72.7	78.6	67.5
Con-PET/Con-C20C27	-	-	-	-	45.5	-

- D'après les résultats de XRD sur les échantillons de ciment à 24 heures d'hydratation, il a été détecté que les échantillons obtenus à partir de PET avaient le niveau le plus élevé de phases hydratées. Néanmoins, il a été confirmé que la présence d'huiles de démoulage a ralenti le processus d'hydratation.

➢ **Aspects visuels :**

Au final, à partir de l'observation visuelle des surfaces de pâte de ciment et de béton obtenues à partir de différents coffrages avec divers rapports E/C et types de ciment, les conclusions suivantes peuvent être extraites (**Figure 5**):

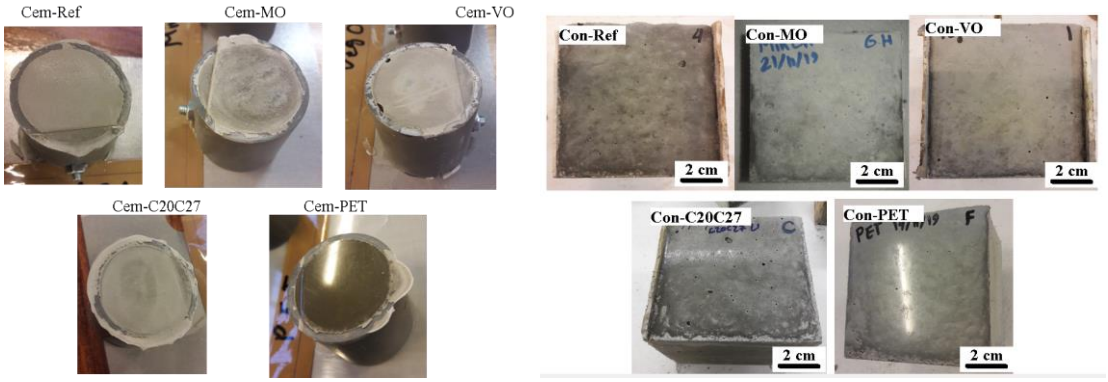

a) *b)*

Figure 5 *Surfaces en pâte de ciment coulées dans différents types de coffrages : a) Échantillons de pâte de ciment b)Echantillons de béton*

- Les surfaces cimentaires obtenues à partir des revêtements PET sont brillantes et lisses, ce qui n'est pas le cas pour le reste des surfaces.
- La couleur des surfaces obtenues est différente, allant du gris clair (Cem-C20C27) à une couleur plus foncée (Cem-Ref et Cem-MO). De plus, le rapport eau/carburant affecte également la couleur de la surface (**Figure 6**).

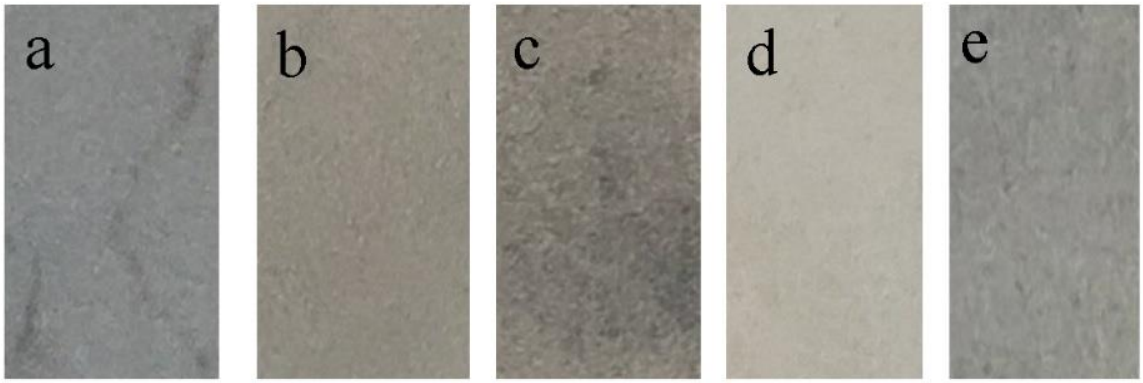

Figure 6 *couleur de la pâte de ciment après 3 ans : a)Cem-Ref, b)Cem-VO, c)Cem-MO, d)Cem-C20C27, and e)Cem-PET*

Perspectives

Bien qu'il y ait eu des études qui incluent certains éléments contribuant à la qualité du démoulage, aucun travail n'a été fait pour considérer tous ces facteurs ensemble en raison de la complexité de le faire. La prochaine étape peut être d'inclure plus des paramètres tels que les additifs et les méthodes de mise en place du béton afin d'analyser plus en profondeur le phénomène d'adhésion à l'interface coffrage-ouvrage et d'étudier de la même manière la durabilité des revêtements alternatifs proposés pour les coffrages au lieu des méthodes traditionnelles. En outre, de nombreux paramètres de surface, en particulier les paramètres mécaniques, doivent encore être explorés sur ces surfaces hétérogènes et poreuses.

La recherche sur les matériaux polymères est une alternative prometteuse pour éviter les impacts environnementaux engendraient par les agents de démoulage et de contribuer à la gestion des déchets plastiques peut-être une piste intéressante.

Valorisation scientifique

- **Sayed H. MOHSENI,** Safiullah OMARY, Francoise FEUGEAS, and Fahri BIRINCI: "Effect of formwork surface texture features on surface morphology, roughness parameters, and the demolding force of cementitious materials", Accepted (13/05/2022): Journal of Civil & Environmental Engineering
- **Sayed Hashim MOHSENI,** Safiullah OMARY, Francoise FEUGEAS, and Fahri BIRINCI: "Effect of cement type, w/c ratio, and formwork type on adhesion between concrete and formwork", 10th Annual International Conference on Civil Engineering, 22-25 June 2020, Athens, Greece
- C. Chadfeau, **S. Mohseni**, S. Omary, V. Steiner, E. Belhaj, C. Fond, F. Feugeas « Influence d'un bioadjuvant sur l'adhésion du ciment sur parois coffrantes et évaluation de l'effet de la rugosité des parois coffrantes » Matériaux & Techniques, EDP Sciences (SNIP : 0.27, SJR : 0.201), page 18, 2020. DOI : 10.1051/mattech/2020031

Références

[1] S. Bouharoun, “Characterization Of The Interface Between Fresh Concrete And Formwork,” *J. Civ. Eng. Manag.*, vol. 22, no. 1, pp. 26–37, 2016.

[2] N. Spitz, N. Coniglio, M. El Mansori, A. Montagne, and S. Mezghani, “Quantitative and representative adherence assessment of coated and uncoated concrete-formwork,” *Surf. Coatings Technol.*, vol. 352, no. July, pp. 247–256, 2018.

[3] N. Spitz, N. Coniglio, M. El Mansori, A. Montagne, and S. Mezghani, “On functional signatures of bare and coated formwork skin surfaces,” *Constr. Build. Mater.*, vol. 189, pp. 560–567, 2018.

[4] L. Libessart, C. Djelal, P. De Caro, and I. Laiymani, “Comparative study of the tribological behaviour of emulsions and demoulding oils at the concrete / formwork interface,” vol. 239, 2020.

[5] “Effects of formwork on concrete,” *Aberdeen group*, 1973.

[6] Philip G. Malone, “Use of Permeable Formwork in Placing and Curing Concrete,” Washington DC, 1999.

[7] A. Mazkewitsch And A. Jaworski, “The adhesion between concrete and formwork,” *Adhes. between Polym. Concr.*, pp. 67–72, 1986.

[8] S. Bouharoun, “Comportement tribologique des huiles de décoffrage à l ’ interface béton / coffrage - Influence de la formulation du béton Remerciements,” Universite D’artois, Ph.D. Thesis, 2011.

[9] C. N. D. Cruickshank and J. R. Squire, “Skin Cancer In The Engineering Industry From The Use Of Mineral Oil,” *Br. J. Ind. Med.*, pp. 1–11, 1950.

[10] M. Martin, “Etude de la texture de la surface coffrée des parements verticaux en béton,” Universite de LAVAL- Quebec, 2007.

Université de Strasbourg

INSA INSTITUT NATIONAL DES SCIENCES APPLIQUÉES STRASBOURG

Sayed Hashim MOHSENI

Effect of Formwork's Parameters on Surface Properties of Different Concrete Mix Designs

Résumé

Ce travail étudie l'interaction entre les matériaux cimentaires et différents types de coffrages au stade précoce de l'hydratation (24 heures). Le phénomène d'adhésion entre le béton et le coffrage est étudié en modifiant des facteurs tels que le rapport eau/ciment et le type de ciment par rapport à différents coffrages. L'utilisation d'analyses à micro-échelle (SEM, XRD et interférométrie) et d'expériences à macro-échelle (essais de démoulage avant fissuration et par arrachement) a permis d'étudier l'effet des caractéristiques physiochimiques des coffrages sur la force de démoulage et la morphologie de la surface du matériau cimentaire. Et, on peut conclure qu'en fonction du type de coffrage une modification des paramètres de surface de la pâte cimentaire apparaît.

En termes de démoulage, l'agent de démoulage à base d'huile végétale crée la condition la plus favorable pour réduire les forces de démoulage par rapport à tous les autres types de coffrage de cette étude. De même, la modification du rapport eau/consistance et du type de ciment n'a pas donné lieu à une corrélation. Cependant, l'augmentation de la teneur en eau de la conception du mélange entraîne l'apparition de plus de pores à la surface de l'échantillon et l'amélioration de la qualité du décoffrage. Enfin, il a également été démontré que le niveau d'hydratation est influencé par les propriétés de surface du coffrage.

Mots clés : Ouvrage en béton Adhésion, Surface du ciment, Agents de démoulage, PET, Hydratation du ciment, Force de démoulage

Résumé en anglais

This work investigates the interaction between cementitious materials and different types of formworks at the early stage of hydration (24 hrs). The concrete-formwork adhesion phenomenon is studied by changing factors such as water/cement ratio and cement type against different formworks. Using micro-scale analysis (SEM, XRD, and Interferometry) and macro-scale (pre-crack and pull-off demolding tests) experiments allowed for studying the effect of formwork physio-chemical characteristics on the demolding force and con cementitious material's surface morphology. And, it can be concluded that according to the type of formwork a modification of the surface parameters of the cementitious paste appears.

In terms of demolding, the vegetable oil release agent creates the most favorable condition to reduce the demolding forces compared to all other formwork types in this study. Also, the change in the w/c ratio and cement type did not result in a correlation. However, the increase in the water content of the mix design results in the appearance of more pores on the sample surface and the betterment of the stripping quality. Finally, the hydration level was also shown to be influenced by the formwork surface properties.

Keywords : Concrete-formwork Adhesion, Cement surface, Release agents, PET, Cement hydration, Demolding force